MIT-2344-13
MITNE-84

STUDIES OF TWO-REGION SUBCRITICAL URANIUM HEAVY WATER LATTICES

by

J. W. Gosnell, M. J. Driscoll, T. J. Thompson

February, 1969

Department of Nuclear Engineering
Massachusetts Institute of Technology
Cambridge, Massachusetts 02139

Contract AT(30-1)-2344
United States Atomic Energy Commission

MASSACHUSETTS INSTITUTE OF TECHNOLOGY

DEPARTMENT OF NUCLEAR ENGINEERING

Cambridge, Massachusetts

STUDIES OF TWO-REGION SUBCRITICAL URANIUM HEAVY WATER LATTICES

by

J. W. Gosnell, M. J. Driscoll, T. J. Thompson

February, 1969

MIT - 2344 - 13

MITNE - 84

AEC Research and Development Report
UC - 34 Physics
(TID-4500, 47th Edition)

Contract AT(30-1) 2344
U. S. Atomic Energy Commission

ABSTRACT

Reactor physics parameters were measured in eleven two-region subcritical assemblies moderated by heavy water. The regions of the assemblies consisted of nine different lattices of various fuel rod size, U^{235} enrichment, and spacing. The following parameters were measured in the assemblies: bare and cadmium-covered gold foil radial traverses; bare gold foil axial traverses; the ratio of epicadmium to subcadmium capture rates in U^{238} (ρ_{28}); and the ratio of fissions in U^{238} to fissions in U^{235} (δ_{28}).

From analysis of axial traverses at various radial positions, it was determined that the axial buckling was independent of radial position in the assemblies.

A method was developed to apply the age equation to the experimental gold foil traverses. This analysis yielded the quantity $k_\infty \Sigma_a / p$ for each region of the assemblies. Calculated values of Σ_a and p were used to obtain values of the infinite multiplication factor from this parameter. For assemblies of sufficiently large inner regions, the values of k_∞ so found agreed within experimental uncertainty with independent determinations.

The slowing-down spectra arising from the age theory analysis were used to extrapolate two-region assembly measurements of ρ_{28} to critical assembly values. General agreement was found between these extrapolated values and the results of measurements made in full, single region lattices.

The heterogeneous expressions for uncollided flux derived by Pilat were extended to two-region assemblies and used to determine single rod values of δ_{28} from two-region assembly measurements. The theory was also used to predict values of δ_{28} for each of the lattices composing the two-region assemblies. Both the single rod values and the full lattice predictions agreed within experimental error with previously reported results.

The determination of material buckling from two-region subcritical assemblies is also discussed. Because of the nature of the assemblies investigated, satisfactory measurements of the material buckling could not be made.

ACKNOWLEDGMENTS

The success of this work, and of the M. I. T. Heavy Water Lattice Project as a whole, has been due to the contributions of a number of individuals. Overall direction of the Lattice Project during the period when this research was done was shared by Professors I. Kaplan, D. D. Lanning, T. J. Thompson and M. J. Driscoll. The results reported here are due primarily to the work of its principal author, J. W. Gosnell, who has submitted substantially the same report in partial fulfillment of the requirements for the Ph. D. degree at M. I. T. He would particularly like to thank Professors Thompson and Driscoll for the valuable assistance given during the project.

Discussions with former members of the Lattice Project have been very helpful. In particular, the suggestions of Dr. E. Pilat, Dr. L. Papay and Dr. W. D'Ardenne are gratefully acknowledged. Miss Barbara Kelly has helped in the weighing of foils and analysis of data. Messrs. Joseph Barch, Norman Berube and Albert Supple have been of invaluable assistance in the experimental work. Mrs. Mary Bosco has ably prepared the final manuscript.

The patience, encouragement, and support of the author's wife were instrumental to the completion of this work.

All computer calculations were done at the M. I. T. Computation Center.

TABLE OF CONTENTS

TABLE OF CONTENTS (continued)

TABLE OF CONTENTS (concluded)

LIST OF FIGURES

LIST OF FIGURES (concluded)

LIST OF TABLES

Chapter I

INTRODUCTION

1.1 Discussion of Reactor Physics Measurements

The Nuclear Engineering Department at M. I. T. has concluded a research program, the Heavy Water Lattice Project, on the physics of D_2O-moderated lattices of natural or slightly enriched uranium rods. The program was supported by the United States Atomic Energy Commission with the purpose of extending the understanding of fundamental reactor physics in the area of heavy water moderated, slightly enriched uranium lattices.

Reports from this project have examined techniques for the determination of material buckling (P1, C5), neutron capture in U^{238} (W2, D1), and the fast fission effect (W1, P2). The spatial behavior of thermal neutrons (S2) and of fast neutrons (W3) in subcritical lattices have also been investigated. All of these reports applied to large, single region subcritical lattices.

An appreciable fraction of the latter part of the work on the project has centered on methods of obtaining reactor physics parameters from experiments using less fuel than that required for single region lattices. The methods investigated were use of miniature lattices (S1, P4), single rod and few rod clusters (P3), and two region subcritical assemblies. The reason for developing such approaches can be seen from consideration of the objectives of reactor physics

measurements and the degree to which these objectives can be most economically attained by the alternative experimental facilities available.

The ultimate goal of reactor physics as an engineering tool is to aid in the design and construction of nuclear power reactors. Measurement of reactor physics parameters for this purpose would ideally be performed on the operating power reactor core itself. Since this is obviously impossible, various degrees of approximation to the final operating core can be considered. The criterion to be applied for a choice among the alternative facilities and methods must be to obtain results that are accurate and reliable enough, using the least amount of fuel and at the lowest expense. A principal consideration must then be to evaluate the ultimate usefulness of the results considering the accuracy with which they can be obtained.

For all the experimental assemblies, regardless of size and subcriticality or criticality, substantial corrections are required to extrapolate the experimental measurements made in cold, clean lattices to conditions existing in an operating reactor core. Effects produced by the operating temperature, pressure, fission product poisons, control rod gaps, etc. are, in many cases, larger than spectral adjustments for measurements made in even very small samples of core material. Consideration of such effects is beyond the scope of this report, but it should be realized that even exact spectral matching of the experimental conditions with that of a cold, clean reactor will still do nothing about possible subsequent errors introduced by extrapolation to operating conditions. A cold, clean reactor

can only be considered as the initial state of a series of states through which an operating reactor passes on its way to power. Reactor parameters characteristic of this initial state, whether derived from lattices, large or small, critical or subcritical, can only constitute one point of reference, one core condition -- i.e. clean, room temperature -- for the reactor designer, to be used primarily as checks of the calculational methods which he employs. Therefore, the accuracy with which subcritical or critical reactor lattice parameters must be measured need only to be comparable in magnitude to that of the method of extrapolation to reactor operating conditions. For example, measurements of k_∞ for lattice cores at M. I. T. have been done with accuracies of 2 to 3 percent in k_∞ using the best techniques available, including many developed by the Lattice Project. On the basis of this experience, members of the project believe that no method of measurement will lead to results with better than one percent accuracy. On the other hand, the effective multiplication factor of duplicate cores for naval reactors made to the same specifications have been said to vary among themselves by as much as one percent. For reliable core lifetime estimates for commercial power reactors, improved accuracy is an economic necessity. There appears to be little hope of achieving that level of accuracy with <u>any</u> techniques presently available. Still, measurements of reactor physics parameters in experimental facilities do give guidance to the reactor designer and do, therefore, have important usefulness.

There is, however, another type of measurement, useful to the power reactor designer, that can be made. Comparison measurements

of the nuclear effect of small changes in the core design can be done accurately and with a basic validity which allows results to be more easily translated to the operating reactor. Such core changes might involve substitution of one type of stainless steel for another, or of zircalloy for aluminum as cladding materials, or small changes in fuel rod size or enrichment, or slight variations in the composition of the moderator. If these changes do not drastically alter the overall behavior of the system, their effects can be measured accurately by what is virtually differential or perturbation techniques. Accumulated experience with power reactor design and operation has generated accurate knowledge of the nuclear behavior of basic power reactor cores during operation. Much of the interest is now concentrated on the effects of modifications to these already existing and well understood cores. Thus the studies undertaken at M. I. T. to reduce the fuel requirements for lattice parameter measurements have a significant practical importance.

The amount of fuel to be used for the measurement can be the dominant consideration since some fuels, such as U^{233}, may be available in only small quantities when needed, regardless of cost. Even for more readily available U^{235} fuels, expensive fabrication costs or the desire to study differential changes in fuel construction, such as the effect of changes in cladding material, size of cooling gap, etc., may make a small facility advantageous.

The two most common facilities for lattice parameter measurements are the critical and subcritical assemblies. If the subcritical system is large enough, the spectrum attained in a region reasonably

far from the source is essentially identical with that of the critical system. The size of the system required for source effects to be negligible depends on the type of source and the nature of the lattice involved. Typical studies in the M. I. T. lattice facility have been conducted on core volumes of about half that required for the critical system. This substantial fraction of a critical core ensures the correct spectrum with the use of considerably less fuel, giving the subcritical facility an inherent advantage over the larger critical assemblies.

The heavy water, slightly enriched lattices studied at M. I. T. are well adapted to subcritical measurements. The single region lattices in the Heavy Water Lattice Facility have been far subcritical, but the results have been shown to be consistent with the critical and subcritical results obtained elsewhere and have become well accepted throughout the world. A large fraction of all the world's measurements of heavy water moderated, slightly enriched uranium reactor physics parameters for uniform lattices published to date have been made in this subcritical assembly system.

In an effort to further find ways to reduce the quantity of fuel required for meaningful lattice parameter measurements, the M. I. T. Heavy Water Lattice Project began concurrent studies of three alternate approaches to reactor physics measurements. These approaches included a study of the usefulness of measurements in miniature lattices, where the equilibrium spectrum is not attained, a study of single rod and few rod clusters, and a study of two region subcritical assemblies. All of these methods require considerably less fuel than

critical or large subcritical assemblies. The results of the studies of the first two approaches have been previously reported (S1, P4, P3). It was found that both methods yielded values for the rod integral parameters (defined in terms of the ratios of capture rates inside fuel elements and called microscopic parameters in some M. I. T. Lattice Project reports) in substantial agreement with those from large subcritical lattices and with comparable accuracy. However, neither approach could be used to directly determine the material buckling.

The third approach is the topic of this report and consists of measurements in two region subcritical assemblies, produced by forming a test region in the center of a surrounding lattice which acts as a neutron feeding assembly. Conservation of fuel and loading time is thereby achieved at the expense of spectral deformation. This document details the studies made in various two region assemblies. The components of these assemblies were chosen to test the advantages and the limitations of this third possible means of obtaining meaningful lattice physics parameters with reduced quantities of fuel.

1.2 Previous Work on Two Region Assemblies

The advantages of small fuel requirements possessed by two region assemblies were recognized some years ago. Extensive work has been conducted on the determination of material buckling of the test region from critical two region experiments. This work has been done chiefly at Savannah River (G4), Saclay (N1), and Sweden (P5). Bucklings have also been obtained from two region subcritical assemblies (L1).

These experiments were generally performed by the method of progressive substitution. This method consists of a series of critical height measurements on assemblies with various sizes of test region. The effect of the variation of test region size on the critical height of the assembly is analyzed to obtain the test region material buckling. The results of such experiments have, in general, been good. However, it was found that meaningful results, particularly for D_2O lattices, could only be obtained if the regions of the assembly were quite similar in nuclear characteristics and if very small test regions were avoided.

Spectral corrections to rod integral measurements have not received as much attention. Some work has been done using a few-group computer code to define a volume of the test region of a light water assembly where necessary corrections to a critical assembly spectrum would be small (V2). Such assemblies can be constructed fairly easily for H_2O-moderated lattices, since the slowing-down and diffusion lengths are relatively short; but D_2O lattice test regions must be considerably larger in order to approach an equilibrium spectrum. In most practical size D_2O test regions, relatively large corrections are required for many of the lattice parameters.

1.3 Purpose of This Work

The primary purpose of this investigation is to determine the usefulness of two region subcritical assemblies for lattice parameter measurements and to compare this usefulness with that of alternate approaches such as a miniature lattice experiment of single rod measurements. To attain this primary objective, methods must be

developed which will describe the spatial and energy behaviors of the neutron population in a two region assembly. Sufficient knowledge of this behavior is necessary to extrapolate with validity measurements of rod integral parameters made in a two region assembly to critical assembly values with which comparisons may be made.

In order to determine the validity of the theoretical analyses by experimental measurements, two region assemblies were formed from lattices which had been previously extensively investigated in single region experiments by the Heavy Water Lattice Project. It was then possible to compare measurements of the lattice parameters of each region made in the two region assemblies with those done in the more appropriate spectrum of the large, single region lattices, testing the validity of the extrapolation methods and, at the same time, lending additional confidence to the single region measurements. A total of eleven assemblies were used in the study. The composition of these assemblies afforded a quite severe test of the theoretical analyses.

Measurements were made of the following parameters in the two region assemblies:

1. ρ_{28} = the ratio of the epicadmium to subcadmium capture rates in U^{238} averaged over the fuel,
2. δ_{28} = the ratio of fast fissions in U^{238} to the total number of fissions in U^{235},
3. Axial activity distributions of bare gold foils,
4. Radial activity distributions of both bare and cadmium-covered gold foils.

1.4 Contents of the Report

Chapter II presents the theory used to describe the neutron distributions. A discussion of material buckling determination is also included. The experimental facilities and techniques and the two region assemblies used in the study are described in Chapter III. Reduction of experimental data to commonly measured lattice parameters is described in Chapter IV. Chapter V gives the results of the application of the theoretical analyses to the experimental measurements. The conclusions reached on the basis of these results are given in Chapter V together with recommendations for future work.

A method for calculating the effective resonance integral for U^{238} rods is presented in Appendix A. Appendix B contains descriptions of computer programs developed for the assembly analyses. Derivations of formulae for evaluating functions required for an uncollided flux kernel are given in Appendix C. Appendix D shows the methods used for calculating necessary lattice parameters. Appendix E contains the bibliography.

Chapter II

THEORY OF TWO REGION ASSEMBLIES

2.1 Introduction

The usual primary objective of carrying out experiments with a two region assembly is to determine the nuclear properties of the inner or test region, knowing those of the outer or reference region. The properties considered in this report include the ratio of epithermal absorptions to thermal absorptions in U^{238} (ρ_{28}), the ratio of fissions in U^{238} to those in U^{235} (δ_{28}), the infinite multiplication constant (k_∞), and the material buckling (B_m^2).

An approximation to the neutron spectrum as a function of radius in the assembly can be generated using a slowing down theory together with the experimental distribution of thermal and epicadmium activities of gold foils. This analysis also results in a value of $\frac{k_\infty \Sigma_a}{p}$ for each of the regions. The resulting spectra can then be used to correct ratios of measured values of resonance to thermal foil activities, such as ρ_{28}, to full lattice values. This treatment has particular advantages over diffusion theory when the thermal diffusion characteristics of the two regions are greatly different.

In addition, the results of measurements of fast neutron effects such as those measured by δ_{28} are explained by a heterogeneous method similar to those used by Pilat (P3) and Higgins (H3).

Finally, a two-group diffusion treatment has been developed which will allow calculation of the material buckling of the test region from the measured axial buckling.

2.2 Application of Age Theory to Two Region Assemblies

Many of the two region assemblies investigated in this study showed large differences in thermal diffusion characteristics between the two regions. Attempts to fit the radial distributions to two-group diffusion theory were unsuccessful, especially near the boundary between regions. Since the thermal diffusion lengths of neutrons in the lattices studied were large (10 to 20 cm) in comparison with the test region sizes, this boundary difficulty could not be easily overcome.

In the following treatment, age theory together with the measured thermal flux distribution are used to predict the shape of the gold resonance activity distribution. Fitting the experimental data for the slowing down densities to the theoretical distribution yields a value of $\frac{k_\infty \Sigma_a}{p}$ for each region.

For the assemblies investigated, the slowing down properties do not differ greatly between regions. The Fermi age varies only from 123 cm^2 to 129 cm^2. The error introduced in the slowing down density by assuming the age to be that of pure D_2O (125 cm^2) is less than one percent for a material buckling of 0.001, typical of the lattices involved in this study. It is therefore assumed that the slowing down properties are the same in each region. Then the age equation, valid in both regions, may be written for the whole assembly as:

$$\nabla^2 q = \frac{\partial q}{\partial \tau} . \qquad (2.1)$$

If it is assumed that the axial buckling is constant across both regions, then:

$$\left(\nabla_r^2+\gamma^2\right)q = \frac{\partial q}{\partial \tau} , \tag{2.2}$$

where γ^2 is the measured axial buckling. The solution of Eq. 2.2 may be written as:

$$q(r, \tau) = q(r, 0)\, e^{+\left(\nabla_r^2 q+\gamma^2\right)\tau} \tag{2.3}$$

In order to evaluate Eq. 2.3, the initial condition of the source at zero age must be specified. From age theory:

$$q(r, 0) = \frac{k_\infty \Sigma_a}{p}\, \phi_t(r) , \tag{2.4}$$

where ϕ_t is the thermal flux.

The quantity $\frac{k_\infty \Sigma_a}{p}$ is taken to be constant in each region separately; this approximation can be motivated by the following considerations.

If

$$\eta \simeq \left(\Sigma_f/\Sigma_a\right)_{fuel}$$

and

$$f = \Sigma_{a_{fuel}} \Big/ \Sigma_{a_{cell}} ,$$

then use of the four-factor definition for k_∞ gives:

$$\frac{k_\infty \Sigma_a}{p} \simeq \Sigma_f \nu \epsilon . \tag{2.5}$$

The fast fission factor ϵ shows a very small variation within a region (see results of δ_{28} measurements, section 4.3.2). The macroscopic fission cross section, Σ_f, depends on the microscopic properties of

the cell materials (constant throughout the assemblies) and on the ratio of fuel volume to moderator volume. This ratio shows a step change at the boundary between the regions.

The thermal flux distribution can be measured by foil activation, and the source is then known as a function of radius and $\frac{k_\infty \Sigma_a}{p}$ of each region.

In order to use this source in the age equation (Eq. 2.2), it is convenient to expand the distribution in terms of Bessel functions:

$$q(r, 0) = \sum_{i=1}^{\infty} a_i J_o(\alpha_i r) , \tag{2.6}$$

where α_i satisfies the boundary condition:

$$J_o(\alpha_i R_{ex}) = 0 ,$$

giving:

$$\alpha_i = j_i / R_{ex} , \tag{2.7}$$

where j_i is the i^{th} zero of the Bessel function and R_{ex} is the extrapolated radius of the assembly. Since the extrapolated radius depends primarily on the material properties of the outer region, the extrapolated radius measured in a single region experiment on the outer lattice or calculated from its properties may be used.

The orthogonal properties of the Bessel function together with Eq. 2.4 are used to evaluate the coefficients of the series.

$$a_i = \frac{2}{[R_{ex} J_1(\alpha_i R_{ex})]^2} \int_0^{R_{ex}} \frac{k_\infty \Sigma_a}{p} \phi_t(r)\, r\, J_o(\alpha_i r)\, dr$$

$$= \frac{2}{[R_{ex} J_1(\alpha_i R_{ex})]^2} \left[\int_0^{R} \left(\frac{k_\infty \Sigma_a}{p}\right)_1 \phi_t(r)\, r\, J_o(\alpha_i r)\, dr \right.$$

$$\left. + \int_R^{R_{ex}} \left(\frac{k_\infty \Sigma_a}{p}\right)_2 \phi_t(r)\, r\, J_o(\alpha_i r)\, dr \right] , \tag{2.8}$$

where the subscripts 1 and 2 refer to the inner and outer regions, respectively, and R is the radius of the inner region. The coefficients may be written as:

$$a_i = \left(\frac{k_\infty \Sigma_a}{p}\right)_1 b_i + \left(\frac{k_\infty \Sigma_a}{p}\right)_2 d_i \,, \tag{2.9}$$

where

$$b_i = 2 \int_0^R \phi_t(r) J_o(\alpha_i r)\, dr \Big/ \left[R_{ex} J_1(\alpha_i R_{ex})\right]^2 \,, \tag{2.10}$$

and

$$d_i = 2 \int_R^{R_{ex}} \phi_t(r) J_o(\alpha_i r)\, dr \Big/ \left[R_{ex} J_1(\alpha_i R_{ex})\right]^2 \,. \tag{2.11}$$

2.2.1 Slowing Down Density with Equal Resonance Escape Probabilities

For illustration of the method, consider a simplified case in which the resonance escape probabilities in the two regions are equal ($p_1 = p_2 = p$). A more realistic case will be treated in the next section. In the present case, the fractional number of neutrons lost at each resonance is constant across the assembly and the shape of the slowing down density radial distribution is unchanged by such absorption.

If Eq. 2.6 is inserted into Eq. 2.3, an expression for the slowing down density is obtained.

$$q(r,\tau) = \left(\frac{k_\infty \Sigma_a}{p}\right)_1 \sum_{i=1}^{\infty} b_i\, e^{\left(\gamma^2 - \alpha_i^2\right)\tau} \cdot J_o(\alpha_i r) + \left(\frac{k_\infty \Sigma_a}{p}\right)_2 \sum_{i=1}^{\infty} d_i\, e^{\left(\gamma^2 - \alpha_i^2\right)\tau} J_o(\alpha_i r) \,. \tag{2.12}$$

Below the U^{238} resonances, absorption in the resonances will decrease

the neutron density by a factor p, the resonance escape probability. The neutron density at ages below the U^{238} resonances is then:

$$Q(r,\tau) = pq(r,\tau)$$
$$= \sum_{i=1}^{\infty} [(k_\infty \Sigma_a)_1 b_i + (k_\infty \Sigma_a)_2 d_i] e^{\left(\gamma^2 - \alpha_i^2\right)\tau} J_o(\alpha_i r). \qquad (2.13)$$

If the radial distribution of the neutron density at a particular age is measured, a least squares fit of the data to Eq. 2.13 will yield $k_\infty \Sigma_a$ for each region.

2.2.2 Slowing Down Density with Unequal Resonance Escape Probabilities

When unequal resonance escape probabilities exist in the two regions, the treatment of the slowing down process is considerably more complex. Because of the continuous neutron interchange between assembly regions during the slowing down process, the resonance absorption cannot be lumped into a single effective resonance as is done successfully in many single region applications. To treat the resonance absorption more realistically, the statistical resonance region is divided into a number of hypothetical resolved resonances, and these, together with the actual resolved resonances, are treated singly. The mathematics involved will be illustrated with the effect of the highest hypothetical resonance. In the actual calculations, the number of actual and hypothetical resonances is reduced to 38 to save computation time. Resonances whose contributions are small are consolidated to produce "lumped" resonances having a minimum fractional

resonance escape probability of about two percent. (The energies of the lumped resonances are taken as the average of the composite resonances weighted with their fractional effective resonance integrals.) The process illustrated below for a single resonance is therefore repeated 38 times.

The slowing down density above the highest hypothetical resonance is given by Eq. 2.12. Absorption in this resonance will decrease the density by a factor p_1^1, the partial resonance escape probability for this resonance. In the inner region:

$$Q(r,\tau_1) = p_1^1 q(r,\tau) = p_1^1\left(\frac{k_\infty \Sigma_a}{p}\right)_1 \sum_{i=1}^{\infty} b_i\, e^{\left(\gamma^2 - \alpha_i^2\right)\tau} J_o(\alpha_i r)$$

$$+ p_1^1 \left(\frac{k_\infty \Sigma_a}{p}\right)_2 \sum_{i=1}^{\infty} d_i\, e^{\left(\gamma^2 - \alpha_i^2\right)\tau} J_o(\alpha_i r)\,. \qquad (2.14)$$

A similar expression with p_2^1 describes the distribution in the outer region.

Again, an expansion in terms of Bessel functions will make the total distribution amenable to the age equation. Equation 2.14 can be written as:

$$Q(r,\tau) = \Sigma C_i J_o(\alpha_i r)\, e^{\left(\gamma^2 - \alpha_i^2\right)\tau} \qquad \text{for } r \leq R,$$

and

$$Q(r,\tau) = 0 \qquad \text{for } r > R.$$

We wish to express Q in a new series:

$$Q = \Sigma g_j J_o(\alpha_j r)\, e^{\gamma^2 - \alpha_j^2 \tau},$$

where $$g_j = 2 \int_0^{R_{ex}} rQJ_o(\alpha_j r)\, dr \Big/ \left[R_{ex} J_1(\alpha_j R_{ex})\right]^2.$$

Again, using the orthogonality of the Bessel functions:

$$\frac{[R_{ex} J_1(\alpha_i R_{ex})]^2}{2} g_j = C_j \int_0^R r\, J_o^2(\alpha_j r)\, dr + \sum_{i \neq j} C_i \int_0^R r\, J_o(\alpha_i r)\, J_o(\alpha_j r)\, dr \,. \tag{2.15}$$

If the Bessel function integrals are denoted by B_{ij}, then Eq. 2.15 becomes:

$$g_j = \sum_{i=1}^{\infty} C_i B_{ij} = \sum_{i=1}^{\infty} \left[p_1^1 \left(\frac{k_\infty \Sigma_a}{p}\right)_1 b_i B_{ij} + p_1^1 \left(\frac{k_\infty \Sigma_a}{p}\right)_2 d_i B_{ij} \right]. \tag{2.16}$$

The Bessel function integrals are:

$$B_{jj} = R^2 [J_o(\alpha_j R) + J_1(\alpha_j R)] / [R_{ex} J_1(\alpha_j R_{ex})]^2 \,,$$

$$B_{ij} = \frac{2R[\alpha_i J_1(\alpha_i R) J_o(\alpha_j R) - \alpha_j J_1(\alpha_j R) J_o(\alpha_i R)]}{(\alpha_i^2 - \alpha_j^2)[R_{ex} J_1(\alpha_j R_{ex})]^2} \,.$$

Similar operations on the expression for the slowing down density distribution in the outer region involve Bessel function integrals from R to R_{ex} which will be denoted by D_{ij}.

$$D_{jj} = \int_R^{R_{ex}} r\, J_o^2(\alpha_j r)\, dr = 1 - B_{jj} \,,$$

$$D_{ij} = \int_R^{R_{ex}} r\, J_o(\alpha_i r)\, J_o(\alpha_j r)\, dr = -B_{ij} \,.$$

The final expression for the slowing down density below the resonance becomes:

$$Q(r, \tau_1 \rightarrow \tau_2) = \sum_{j=1}^{\infty} \left\{ \left(\frac{k_\infty \Sigma_a}{p}\right)_1 \left[p_1^1 \sum_{i=1}^{\infty} b_i B_{ij} + p_2^1 \sum_{i=1}^{\infty} b_i D_{ij} \right] + \left(\frac{k_\infty \Sigma_a}{p}\right)_2 \left[p_1^1 \sum_{i=1}^{\infty} d_i B_{ij} + p_2^1 \sum_{i=1}^{\infty} d_i D_{ij} \right] \right\} e^{\left(\gamma^2 - \alpha_j^2\right)\tau} J_o(\alpha_j r) . \tag{2.17}$$

Repetition of this process for each U^{238} resonance will produce a set of expressions for the slowing down density at any age. Partial resonance escape probabilities can be calculated (see Appendix A) and if the slowing down density distribution is measured at a particular age, a least squares fit of the data to the appropriate expression will yield $\frac{k_\infty \Sigma_a}{p}$ for each region.

2.2.3 Determination of the Slowing Down Densities from Gold Foil Activation

In order to determine the slowing down density and thermal flux distributions in the assemblies, bare and cadmium-covered traverses with gold foils were made in each assembly as described in section 3.4. Gold has proven particularly convenient for this measurement because of its single natural isotope, its comparatively large cross section and moderate half-life. In addition, a prominent resonance at 4.9 ev makes it suitable for resonance flux measurements.

Contributions to the activity of the gold foils may be considered to be of three types: thermal, epithermal 1/v, and epithermal resonance. The thermal flux is assumed to have a Maxwellian energy distribution, M(E). The epithermal flux is closely approximated by:

$$\phi(r, E) = \frac{Q(r, \tau)}{\xi \Sigma_s E} , \tag{2.18}$$

where $Q(r,\tau)$ is the neutron slowing down density at an age corresponding to the energy E and is given by Eq. 2.13 or 2.17 or a similar expression. The epithermal flux is assumed to join the Maxwellian distribution at an energy of $5\,kT$ (~ 0.12 ev).

The activation cross section for gold varies as $1/v$ throughout the thermal energy range while in the epithermal energy range, resonance contributions must be added to the $1/v$ response. Under these assumptions, the total activity, A_t, of a gold foil may be written as:

$$A_t = \int_0^{0.12\ \text{ev}} \sigma_{1/v}\,\phi_t(r)M(E)\,dE + \int_{.12\ \text{ev}}^{.4\ \text{ev}} \sigma_{1/v}\,\frac{Q(r,\tau)}{\xi\Sigma_s}\,\frac{dE}{E}$$

$$+ \int_{.4}^{\infty} \sigma_{1/v}\,\frac{Q(r,\tau)}{\xi\Sigma_s}\,\frac{dE}{E} + \int_{.4}^{\infty} \sigma_{res}(E)\,\frac{Q(r,\tau)}{\xi\Sigma_s}\,\frac{dE}{E}\,, \qquad (2.19)$$

where $\sigma_{1/v}$ is the $1/v$ cross section and σ_{res} is the resonance cross section. Here the epithermal activation has been separated into subcadmium and epicadmium activities with an assumed cadmium cutoff energy of 0.4 ev.

It is convenient to normalize the epithermal activities to the slowing down density at the major resonance of Au^{198} (4.9 ev). τ_{Au} will represent the age of neutrons at this energy.

Integration over the Maxwellian distribution is performed and the resonance integral replaced by a summation of partial effective resonance integrals. The result is:

$$A_t = 0.886\ \sigma_o \phi_t(r) + \frac{Q(r,\tau_{Au})}{\Sigma_s \xi}\ \sigma_o \int_{.12}^{.4} \frac{Q(r,\tau)}{Q(r,\tau_{Au})}\ \frac{dE}{E^{1.5}}$$

$$+ \frac{Q(r,\tau_{Au})}{\xi \Sigma_s}\ \sigma_o \int_{.4}^{\infty} \frac{Q(r,\tau)}{Q(r,\tau_{Au})}\ \frac{dE}{E^{1.5}}$$

$$+ \frac{Q(r,\tau_{Au})}{\xi \Sigma_s} \sum_{\substack{\text{Gold} \\ \text{Resonances}}} ERI_k\ \frac{Q(r,\tau_k)}{Q(r,\tau_{Au})}\ , \qquad (2.20)$$

where

$$ERI_k = \int_{k^{th}\ \text{resonance}} \sigma_{res}\ \frac{dE}{E}$$

and τ_k is the age to the k^{th} resonance of gold.

Finally, non-1/v indexes are defined as follows:

$$C_{SC} = \int_{.12}^{.4} \frac{Q(r,\tau)}{Q(r,\tau_{Au})}\ \frac{dE}{E^{1.5}}\ ,$$

(2.21)

and $$C_{EC} = \int_{.4}^{\infty} \frac{Q(r,\tau)}{Q(r,\tau_{Au})}\ \frac{dE}{E^{1.5}}\ .$$

In a pure 1/v spectrum the neutron densities are independent of age and the integration of Eq. 2.21 can be performed directly, giving $C_{SC} = 0.414$ and $C_{EC} = 0.500$.

The ratio of subcadmium to epicadmium activities is the cadmium ratio R_{Cd} minus one. From Eqs. 2.20 and 2.21:

$$R_{Cd} - 1 = \frac{.886\ \sigma_o\ \phi_t(r) + \frac{Q(r,\tau_{Au})}{\xi \Sigma_s}\ \sigma_o\ C_{SC}}{\frac{Q(r,\tau_{Au})}{\xi \Sigma_s}\ ERI_{Au} + \frac{Q(r,\tau_{Au})}{\xi \Sigma_s}\ \sigma_o\ C_{EC}}\ , \qquad (2.22)$$

where

$$ERI_{Au} = \sum_{\substack{\text{Gold} \\ \text{Resonances}}} ERI_k \frac{Q(r, \tau_k)}{Q(r, \tau_{Au})} .$$

A slowing down function is now defined as:

$$\psi(r,\tau) \equiv \frac{Q(r, \tau)}{\xi \Sigma_s \phi_t(r)} . \tag{2.23}$$

Solving Eq. 2.22 for ψ gives:

$$\psi(r, \tau) = \frac{0.886}{(R_{Cd}-1)\left(\frac{ERI}{\sigma_o} + C_{EC}\right) - C_{SC}} . \tag{2.24}$$

Using the new definitions, Eq. 2.20 for the total thermal activation may be rewritten as:

$$A_t(r) = \left[0.886 + \psi(r, \tau_{Au})\left(C_{SC} + C_{EC} + \frac{ERI}{\sigma_o}\right)\right] \phi_t(r) , \tag{2.25}$$

and ϕ_t, defined as the total thermal flux, is then given by:

$$\phi_t(r) = \frac{A_t(r)}{\left[.886 + \psi(r, \tau_{Au})\left(C_{SC} + C_{EC} + \frac{ERI}{\sigma_o}\right)\right]} . \tag{2.26}$$

Algebraic manipulations will produce alternate expressions for ψ and ϕ_t as functions of the epicadmium and subcadmium activities.

$$\phi_t(r) = \frac{\text{subcadmium activation per nuclide}}{0.886 + C_{EC}\, \psi(r, \tau_{Au})} , \tag{2.27}$$

and

$$\psi(r, \tau_{Au}) = \frac{\text{epicadmium activation per nuclide}}{\left(\frac{ERI}{\sigma_o} + C_{EC}\right) \phi_t(r)} . \tag{2.28}$$

The experimental quantity obtained from simple counting of gold foils is proportional to the actual activation, the proportionality constant being the efficiency of the counter. However, if the bare and cadmium-covered foils are counted on the same equipment or otherwise suitably normalized, the cadmium ratio and hence the slowing down function ψ will be absolute values. Use of the relative activities in Eq. 2.26 or Eq. 2.27 yields a quantity proportional to the thermal flux. This proportionality is incorporated in the expansion coefficients calculated with Eq. 2.8. Since, from the definition of ψ,

$$Q(r, \tau) = \xi \Sigma_s \phi_t(r) \psi(r, \tau), \tag{2.29}$$

the proportionality constant will appear on both sides of Eq. 2.17 and will not affect the values of $\frac{k_\infty \Sigma_a}{p}$.

The steps in the use of the activation traverses to determine $\frac{k_\infty \Sigma_a}{p}$ for each region of the assembly are:

1. An axial buckling is found from axial gold traverses (see section 4.2.3).
2. Gold-cadmium ratios are calculated from bare and cadmium-covered radial traverses and their monitor foils (see section 4.2.2).
3. The spectrum is everywhere assumed to be 1/E and the 1/E values of C_{SC}, C_{EC} and ERI/σ_o are used.
4. Partial resonance escape probabilities are calculated for each region.
5. The radial distribution of $\psi(r,\tau_{Au})$ and $\phi(r)$ are calculated with Eqs. 2.24 and 2.27.
6. Expansion coefficients are calculated by use of Eq. 2.8.

7. The results of these calculations are fitted to Eq. 2.17 to give $k_\infty \Sigma_a / p$ for each region.

8. The slowing down spectra thus found are used to re-evaluate C_{SC}, C_{EC} and ERI/σ_o at each point, and steps 5 through 8 are repeated until a convergence limit is reached.

A computer program has been developed to perform these calculations and is described in Appendix B.

2.2.4 Correction of Assembly Values of ρ_{28} to Full Lattice Values

The ratio ρ_{28} of the epicadmium to subcadmium capture rates in U^{238} is related to the cadmium ratio of U^{238} inside a fuel rod by (D1):

$$\rho_{28} = \frac{1}{R_{28} - 1} , \tag{2.30}$$

where R_{28} is the cadmium ratio of U^{238}. It is also directly related to p, the resonance escape probability. The simplest equation used to relate p to ρ_{28} is:

$$p = \frac{1}{1 + \rho_{28} fG} , \tag{2.31}$$

where f is the thermal utilization factor and G is the ratio of the sub-cadmium-U^{238} capture rate to the total thermal absorption rate in the fuel. This relationship represents a very simple approach, and many corrections have been applied to the basic equation to include the effects of fast U^{238} capture, 1/v capture above cadmium cutoff, and leakage of neutrons in the fast, resonance and thermal energy groups (K2). Thus the measurement of ρ_{28} is of considerable interest as an

easily measured and meaningful parameter in lattice experiments. In a two region assembly, however, the cadmium ratio of U^{238} inside a fuel rod varies as a function of radial position and is, in general, considerably different from that found in a full lattice of the same composition. The results of the preceding analysis can be used to correct these values to the full lattice or critical assembly value. Similar corrections have been successfully applied by previous workers to subcritical measurements (S1, P4).

Equation 2.22 has been derived in the previous section for the gold-cadmium ratio. By defining the effective resonance integral for U^{238} as:

$$ERI_{28} = \sum_{\substack{U^{238} \\ \text{resonances}}} ERI_k \frac{Q(r,\tau_k)}{Q(r,\tau_{Au})},$$

the same expression may be written for the U^{238} cadmium ratio.

In a critical, single region assembly and in a large subcritical lattice, the slowing down density is given by standard age theory (G3) as:

$$q^c(\tau) = \frac{k_\infty \Sigma_a}{p} \phi\, e^{-B_m^2 \tau},$$

leading to:

$$\psi^c(\tau) = \frac{p(\tau)}{\xi \Sigma_s} \frac{k_\infty \Sigma_a}{p} e^{-B_m^2 \tau}, \qquad (2.32)$$

where B_m^2 is the material buckling and the superscript c refers to critical assembly values. Note that the slowing down function, $\psi^c(\tau)$, is independent of position.

Using this expression for the critical assembly and Eq. 2.22 with the ERI for U^{238} and the definition of ψ (Eq. 2.23), a correction factor is obtained.

$$\rho_{28}^{c} = \frac{1}{R_{Cd}^{c} - 1}$$

$$= \left[\frac{0.886 + \psi(r,\tau_{Au})C_{SC}}{\psi(r,\tau_{Au})\left(\frac{ERI_{28}}{\sigma_o} + C_{EC}\right)} \right] \left[\frac{\psi^{c}(\tau_{Au})\left(\frac{ERI_{28}^{c}}{\sigma_o} + C_{EC}^{c}\right)}{0.886 + \psi^{c}(\tau_{Au})C_{SC}^{c}} \right] \rho_{28} \cdot \qquad (2.33)$$

Equation 2.22 does not strictly apply within a fuel rod, since the spectrum inside the rod is greatly hardened by uranium absorptions and fissions. Also, a true Maxwellian spectrum does not exist. For this reason, agreement between the U^{238}-cadmium ratio given by Eq. 2.22 and experiment is not to be expected. However, if it is assumed that the ratio of neutrons of a given energy in the moderator to those in the fuel is the same in a cell of a two region assembly as it is in a critical cell, i. e. the disadvantage factors are equal, then the expression can be used to derive the correction factor given by Eq. 2.33.

2.3 Fast Neutron Distribution and δ_{28}

The fast neutron fission ratio, δ_{28}, is defined as the ratio of the average total U^{238} fission rate to the average total U^{235} fission rate in the fuel. It is related to the fast fission factor, ϵ, of the four-factor formula by:

$$\epsilon = \frac{\text{net number of neutrons produced by all fissions}}{\text{number of neutrons produced by fissions in } U^{235}}$$

$$= 1 + \delta_{28}^{\infty} \frac{\nu_{28} - 1 - \alpha_{28}}{\nu_{25}} , \qquad (2.34)$$

where ν_{28} and ν_{25} are the number of neutrons produced per fission in U^{238} and U^{235}, respectively, and α_{28} is the ratio of capture to fission cross sections of U^{238}.

It has been shown (W3, P3) that the neutrons responsible for fast fissions may be considered as those neutrons which have not suffered a collision since birth. A collision, then, is assumed to decrease the neutron's energy below the threshold value necessary for fission of U^{238}. To calculate the uncollided flux at some point, the contributions of each single rod in the assembly to the flux at that point is summed over the entire core. Using this heterogeneous principle, the uncollided flux ϕ_j^f at a point within the j^{th} fuel rod may be written as:

$$\phi_j^f = K_{jj} S_j + \sum_{\substack{i=1 \\ i \neq j}}^{N} S_i K_{ij} , \qquad (2.35)$$

where K_{ij} is a removal kernel which relates the source of fast neutrons within rod i to the uncollided flux in the j^{th} rod. The above equation neglects the effect of finite volume of the fuel rods. The total uncollided flux in the j^{th} rod can be found by integrating the previous expression across the rod:

$$\int_0^{R_o} 2\pi \phi_j^f r \, dr = \int_0^{R_o} K_{jj} S_j(r) \, 2\pi r \, dr + \pi R_o^2 \sum_{\substack{i=1 \\ i \neq j}}^{N} S_i K_{ij} , \qquad (2.36)$$

where R_o is the radius of the rod. Here it is assumed that the contribution from neighboring rods is constant across the subject rod. The actual variation of this contribution is very close to linear across the fuel rod, since the rod diameters considered are small in comparison to the relaxation length for uncollided neutrons in uranium (~10 cm). Thus, integration across the rod using a constant flux equal to that at the center of the rod introduces little error. The equation is next normalized to a single fission neutron in rod j:

$$H = \frac{\int_0^{R_o} 2\pi \phi_j^f r\, dr}{\int_0^{R_o} S(r)\, 2\pi r\, dr}$$

$$= \frac{\int_0^{R_o} K_{jj} S_j(r)\, 2\pi r\, dr}{\int_0^{R_o} S_j(r)\, 2\pi r\, dr} + \pi R_o^2 \sum_{\substack{i=1 \\ i\neq j}}^{N} \frac{S_i K_{ij}}{\int_0^{R_o} S_j(r)\, 2\pi r\, dr} . \qquad (2.37)$$

Assume that the first n rods in the assembly are identical with rod j. Then:

$$S_i = \frac{\phi_i^s}{\phi_j^s} \int_0^{R_o} S_j(r)\, 2\pi r\, dr , \quad i < n , \qquad (2.38)$$

since the source in each rod is proportional to ϕ^s, the thermal flux. Rods above n are assumed to have a different radius, R_2.

$$S_i = \frac{\phi_i^s}{\phi_j^s} \int_0^{R_2} S_i(r)\, 2\pi r\, dr , \quad n < i < N$$

$$= \frac{\phi_i^s}{\phi_j^s} P \int_0^{R_o} S_j(r)\, 2\pi r\, dr , \quad \text{where } P = \frac{\int_0^{R_2} S_i(r)\, 2\pi r\, dr}{\int_0^{R_o} S_j(r)\, 2\pi r\, dr} ,$$

(2.39)

and since the value of H for a single rod in an infinite sea of moderator must be:

$$H_j^{SR} = \frac{\int_0^{R_o} K_{jj} S_j(r)\, 2\pi r\, dr}{\int_0^{R_o} S_j(r)\, 2\pi r\, dr}, \tag{2.40}$$

Equation 2.37 becomes:

$$H = H_j^{SR} + \pi R_o^2 \left[\sum_{\substack{i=1 \\ i\neq j}}^{n} \frac{\phi_i^s}{\phi_j^s} K_{ij} + \sum_{i=n}^{N} \frac{\phi_i^s}{\phi_j^s} P K_{ij} \right]. \tag{2.41}$$

Pilat (P3) has shown that:

$$\delta_{28} = \frac{\nu_{25}\Sigma_f H}{1 - \nu_{28}\Sigma_f H}. \tag{2.42}$$

The denominator is quite close to unity, so that δ_{28} may be considered proportional to H and:

$$\delta_{28}^j = \delta_{28}^{SR} \left[1 + \frac{\pi R_o^2}{H_j^{SR}} \left(\sum_{\substack{i=1 \\ i\neq j}}^{n} \frac{\phi_i^s}{\phi_j^s} K_{ij} + \sum_{i=n}^{N} \frac{\phi_i^s}{\phi_j^s} P K_{ij} \right) \right]. \tag{2.43}$$

A single collision transport kernel has been used successfully to evaluate the interaction effects in heavy water lattices. Woodruff (W3) assumed a parabolic distribution of fission sources within the fuel rod,

$$S(r) = 1.0 + b r^2, \tag{2.44}$$

using experimental distributions to determine the value of b. A computer program was developed to numerically integrate the kernel for a series of cylindrical sources to obtain the uncollided flux distribution

within the fuel rod. Pilat, using the same basic kernel and source distribution, developed semi-analytic expressions for the integrated kernel. His expressions have been used in the present study.

Outside a single fuel rod of radius R_o, the uncollided flux is given by:

$$\phi^f_{SR}(r, R_o, \Sigma_R) = \phi^A(r, R_o, \Sigma_R) = \frac{1}{r}\left\{ C_2(\Sigma_R r)S_2(\Sigma_R, R_o) + \frac{C_3(\Sigma_R r)S_3(\Sigma_R, R_o)}{r} + \frac{C_4(\Sigma_R r)S_4(\Sigma_R, R_o)}{r^2} + \ldots \right\}, \tag{2.45}$$

where:

$$C_n(z) \equiv \int_1^\infty \frac{e^{-zt}}{t^{n-1}\sqrt{1-t^2}}\, dt, \qquad n = 2, 3, 4, \ldots, \tag{2.46}$$

$$S_n(\Sigma, R) \equiv \int_0^R t^{j-1} I_o^{(j-2)}(\Sigma t)\, S(t)\, dt, \tag{2.47}$$

and $I_o^{(i)}(x)$ is the i^{th} derivative of the Bessel function. At quite small distances from the rod, smaller than the closest pitch of the lattices investigated, a line source description suffices for the flux distribution:

$$\phi^f_{SR}(r, R_o, \Sigma_R) \simeq \frac{C_2(\Sigma_R r)}{2\pi r} \int_0^{R_o} I_o(\Sigma_R R)\, 2\pi R\, S(R)\, dR, \tag{2.48}$$

and

$$K_{ij} = \frac{C_2\left(\Sigma_R(|\bar{r}_i - \bar{r}_j|)\right)}{2\pi(|\bar{r}_i - \bar{r}_j|)} \frac{\int_0^{R_o^i} I_o(\Sigma_R R)\, 2\pi R S_i(R)\, dR}{\int_0^{R_o^i} 2\pi R\, S_i(R)\, dR}. \tag{2.49}$$

Since $I_o(\Sigma_R R)$ is very close to unity in the rods considered, the ratio of the integrals in the above expression is also close to one.

Inside the rod, Pilat has shown that:

$$\phi^{f}_{SR}(r, R_o, \Sigma_R) = \phi^{A}_{SR}(r, r, \Sigma_R) + \phi^{C}_{SR}(r, R_o, \Sigma_R) \ , \tag{2.50}$$

where:

$$\phi^{C}_{SR}(r, R_o, \Sigma_R) = I_o(\Sigma r)\, f_2(r, R_o) + r\, I_o^{(1)}(\Sigma r)\, f_3(r, R_o) + r^2\, I_o^{(2)}\, f_4(r, R_o) + \ . \ . \ . \ , \tag{2.51}$$

and:

$$f_n(r, R_o) = \int_r^{R_o} C_n(\Sigma R)\, S(R)\, \frac{dR}{R^{n-2}} \ . \tag{2.52}$$

Evaluation of the various integrals involved in these expressions is described in Appendix C.

Using Eq. 2.50 for the uncollided flux inside the rod, H^{SR} can be evaluated by numerical integration, and having defined K_{ij}, a measurement of δ_{28} in a two region lattice will then yield δ^{SR}_{28} from Eq. 2.43. The same equation and the value of δ^{SR}_{28} can be used to predict δ_{28} values for full lattices composed of the same type of fuel rods.

2.4 Determination of Test Region Material Buckling

In work on critical two region experiments, several methods have been developed for the determination of the material buckling, B^2_m, of the inner test region (G4). Most of these theories depend on a series of experiments in which the test region is successively enlarged and the results of the series of experiments are analyzed for the difference in buckling between the regions. The experiments in the present study were not designed as progressive substitution

experiments, and so attention is restricted here to theories which might provide results from experiments on a single two region assembly. The following sections describe algebraic manipulations of the basic diffusion equations to produce expressions amenable to solution for the test region buckling. Similar expressions have been derived by others for critical two region facilities (B3).

It will be shown in section 4.3.1 that the axial flux distributions in the assemblies fit a simple hyperbolic sine distribution over a considerable portion of the assembly height. Since no evidence of higher harmonics is evident in the axial component of the flux, higher harmonics must also make only a small contribution to the radial distribution. Therefore, in the diffusion theory treatments to follow, the flux distribution in the assemblies is expressed by the lowest mode solution of the diffusion equation.

2.4.1 One Group Diffusion Theory

The one group diffusion equation is:

$$\nabla^2 \phi + B_m^2 \phi = 0 . \tag{2.53}$$

This equation has the solution for cylindrical coordinates:

$$\phi_n(r,z) = C_n[J_o(\alpha_n r) + E_n Y_o(\alpha_n r)] \sinh(\gamma(H-z)) . \tag{2.54}$$

If the assembly is subcritical:

$$\alpha_n^2 = B_{m,n}^2 + \gamma^2 . \tag{2.55}$$

In these equations, and subsequent ones in this chapter, n is 1 in the inner region and 2 in the outer region of the assembly.

In the inner region, E_1 must be zero since the flux is finite at the assembly center, and since the flux is zero at the extrapolated radius of the assembly, E_2 must equal $-J_o(\alpha_2 R_{ex})/Y_o(\alpha_2 R_{ex})$. The usual boundary conditions of continuity of flux and current at the boundary interface give two equations:

$$J_o(\alpha_1 R) = C_2 H_o(\alpha_2 R) , \tag{2.56}$$

and

$$\alpha_1 D_1 J_1(\alpha_1 R) = \alpha_2 C_2 D_2 H_1(\alpha_2 R) , \tag{2.57}$$

where

$$H_o(\alpha_2 R) = J_o(\alpha_2 R) + E_2 Y_o(\alpha_2 R) , \tag{2.58}$$

$$H_1(\alpha_2 R) = J_1(\alpha_2 R) + E_2 Y_1(\alpha_2 R) , \tag{2.59}$$

and D_n is the thermal diffusion coefficient. Division of Eq. 2.56 by Eq. 2.57 and rearrangement gives:

$$\Lambda = D\Pi , \tag{2.60}$$

where

$$\Lambda \equiv J_o(\alpha_1 R)/\alpha_1 J_1(\alpha_1 R) , \tag{2.61}$$

$$\Pi = H_o(\alpha_2 R)/\alpha_2 H_1(\alpha_2 R) , \tag{2.62}$$

and

$$D = D_2/D_1 . \tag{2.63}$$

The quantity Π depends on the values of R, γ^2 and $B^2_{m,2}$. If these quantities and the ratio of the diffusion coefficients are known, Eq. 2.60 can be solved by iteration techniques for α_1, which will give the material buckling of the test region by Eq. 2.55.

2.4.2 Two Group Diffusion Theory

One group theory is obviously only a poor approximation to the processes which take place in a two region assembly. A better

description should be given by two group theory. The two group diffusion equations are (G3):

$$\nabla^2\phi_{f,n} - \frac{1}{L_{f,n}^2}\phi_{f,n} + \frac{k_{\infty,n}\Sigma_{s,n}}{p_n D_{f,n}}\phi_{s,n} = 0 , \tag{2.64}$$

$$\nabla^2\phi_{s,n} - \frac{1}{L_{s,n}^2}\phi_{s,n} + \frac{p_n\Sigma_{f,n}}{D_{s,n}}\phi_{f,n} = 0 . \tag{2.65}$$

The subscripts s and f are here employed to denote the slow and fast energy neutron groups, respectively. These equations have the general solution in cylindrical coordinates (G3):

$$\phi_{f,n}(r) = C_n[J_o(\alpha r)+E_n Y_o(\alpha_n r)] + A_n[I_o(\beta_n r)+F_n K_o(\beta_n r)], \tag{2.66}$$

and

$$\phi_{s,n}(r) = S_{1,n}C_n[J_o(\alpha_n r)+E_n Y_o(\alpha_n r)] + S_{2,n}A_n[I_o(\beta_n r)+F_n K_o(\beta_n r)], \tag{2.67}$$

where $$\alpha_n^2 = B_{m,n}^2 + \gamma^2 , \tag{2.68}$$

and $$\beta_n^2 = B_{m,n}^2 - \gamma^2 + 1/(L_{s,n}^2 + L_{f,n}^2) . \tag{2.69}$$

Since both the fast and slow flux are finite at the assembly centerline, $E_1 = F_1 = 0$ and the zero fluxes at the extrapolated radius require $E_2 = -J_o(\alpha_2 R_{ex})/Y_o(\alpha_2 R_{ex})$ and $F_2 = -I_o(\beta_2 R_{ex})/K_o(\beta_2 R_{ex})$. In addition to the functions defined by Eq. 2.58 and Eq. 2.59, two new functions are defined:

$$M_o(\beta_2 R) = I_o(\beta_2 R) + F_2 K_o(\beta_2 R) , \tag{2.70}$$

and $$M_1(\beta_2 R) = I_1(\beta_2 R) - F_2 K_o(\beta_2 R) . \tag{2.71}$$

To further condense the equations, the following ratios are defined:

$D_f = D_{f,2}/D_{f,1}$, $D_s = D_{s,2}/D_{s,1}$, $y_n = S_{2,n}/S_{1,n}$, and $V = S_{1,2}/S_{1,1}$. The continuity of the fluxes and currents at the region interface can now be written as:

$$\begin{aligned} J_o + A_1 I_o &= C_2 H_o + A_2 M_o , \\ VJ_o + y_1 VA_1 I_o &= C_2 H_o + y_2 A_2 M_o , \\ \alpha_1 J_1 - \beta_1 A_1 I_1 &= D_f C_2 \alpha_2 H_1 - D_f \beta_2 A_2 M_1 , \\ \alpha_1 VJ_1 - \beta_1 y_1 VA_1 I_1 &= D_s C_2 \alpha_2 H_1 - D_s \beta_2 y_2 A_2 M_1 . \end{aligned} \tag{2.72}$$

The arguments of the functions have been omitted, it being understood that they are evaluated at the region boundary. Algebraic manipulation of these four equations and the further substitution of $z = D_s/D_f$ will reduce them to a single transcendental equation:

$$\begin{aligned} \frac{(y_1 V-1)(V-y_2)}{(y_1 V-y_2)(V-1)} = & \frac{\left[1 - \frac{y_1(z-1)}{y_1 V-y_2}\right]\Pi + D_s\Lambda_1}{\left[1 - \frac{z-1}{y_1 V-1}\right]\Pi_1 - D_s\Lambda_1} \\ & \times \frac{\left[1 - \frac{z-1}{V-1}\right]\Pi_1 + D_s\Lambda}{\left[1 - \frac{y_2(z-1)}{V-y_2}\right]\Pi - D_s\Lambda} , \end{aligned} \tag{2.73}$$

where Λ and Π are given by Eqs. 2.61 and 2.62, and

$$\Lambda_1 = I_o(\beta_1 R)/\beta_1 I_1(\beta_1 R) \tag{2.74}$$

and

$$\Pi_1 = M_o(\beta_2 R)/\beta_2 M_1(\beta_2 R) . \tag{2.75}$$

Note that in the case of equal diffusion coefficients in the two regions

(i.e. $z = D_s = 1$), the right-hand side of Eq. 2.73 becomes a function of the material bucklings of the two regions and the geometry of the assembly only, while the left-hand side is determined solely by the material properties of the lattices involved.

In substitution experiments, it is common practice to regard the left-hand side of Eq. 2.73 as an experimental unknown (B3). It is helpful to define this expression as a separate quantity.

$$S = (y_1 V-1)(V-y_2)/(y_1 V-y_2)(V-1) . \tag{2.76}$$

If the diffusion coefficients can be considered equal in the two regions, S can be eliminated from the calculations if a series of assemblies is investigated, each with a different size test region. If only one assembly is available, S must be evaluated theoretically. Expressions for the coupling coefficients are readily derived from two group theory (G3):

$$S_{1,n} = \frac{\frac{1}{L^2_{f,n}} + B^2_{m,n}}{\frac{k_{\infty,n}\Sigma_{s,n}}{D_{f,n}p_n}} \quad \text{or} \quad \frac{\frac{p_n\Sigma_{f,n}}{D_{s,n}}}{B^2_{m,n} + \frac{1}{L^2_{s,n}}} ; \tag{2.77}$$

$$S_{2,n} = -\frac{\frac{1}{L^2_{s,n}} + B^2_{m,n}}{\frac{k_{\infty,n}\Sigma_{s,n}}{D_{f,n}p_n}} \quad \text{or} \quad -\frac{\frac{p_n\Sigma_{f,n}}{D_{s,n}}}{B^2_{m,n} + \frac{1}{L^2_{f,n}}} . \tag{2.78}$$

These equations lead directly to:

$$y_n = \frac{S_{2,n}}{S_{1,n}} = -\frac{\frac{1}{L^2_{s,n}} + B^2_{m,n}}{\frac{1}{L^2_{f,n}} + B^2_{m,n}} . \tag{2.79}$$

Since $L^2_{f,n} = D_{f,n}/\Sigma_{f,n}$, the ratio V may be written as:

$$V = \frac{p_2}{p_1} \frac{L^2_{f,1}}{L^2_{f,2}} \frac{1}{z} \frac{\left(B^2_{m,1} + \frac{1}{L^2_{s,1}}\right)}{\left(B^2_{m,2} + \frac{1}{L^2_{s,2}}\right)} . \qquad (2.80)$$

Equations 2.79 and 2.80 can then be used to evaluate the ratios necessary for the calculation of S by Eq. 2.76, for any value of the test region buckling. An iteration process can then be used to solve Eq. 2.73 for the proper value of α_1^2 and hence the material buckling of the test region.

2.5 Summary

This chapter has presented methods of interpreting two region assembly measurements to obtain lattice parameters characteristic of the individual regions comprising the assembly. The remainder of this report will be concerned with the experimental verification of the usefulness of these theories.

Chapter III

EXPERIMENTAL APPARATUS AND METHODS

3.1 The M. I. T. Lattice Facility

The two region assemblies were studied in the M. I. T. Heavy Water Lattice Facility. This facility has been described in previous reports (e. g. H1).

The subcritical facility uses the thermal column of the M. I. T. Reactor as a primary source of neutrons. During the present work, the reactor operated at thermal power levels of two or five megawatts. Figure 3.1 shows the relationship of the lattice facility to the reactor.

Figures 3.2 and 3.3 are vertical and plan views of the lattice facility. Neutrons from the reactor thermal column enter a graphite-lined cavity or hohlraum and a considerable fraction of them are reflected upward into the bottom of the exponential tank. A graphite pedestal directly below the tank is designed to shape the flux entering the tank to an approximate J_o radial distribution (P1).

The exponential tank is 67-1/4 inches high and either 36 inches or 48 inches in diameter, depending on the assembly being studied. The side of the tank is covered with 0.020-inch-thick cadmium, and the tank is in turn contained in a 72-inch-diameter outer tank.

Fuel rods are supported in the tank from double girders at the top. The rods are positioned at the desired spacing by tabs on the upper adapters which fit into notches in the support girders. Lower

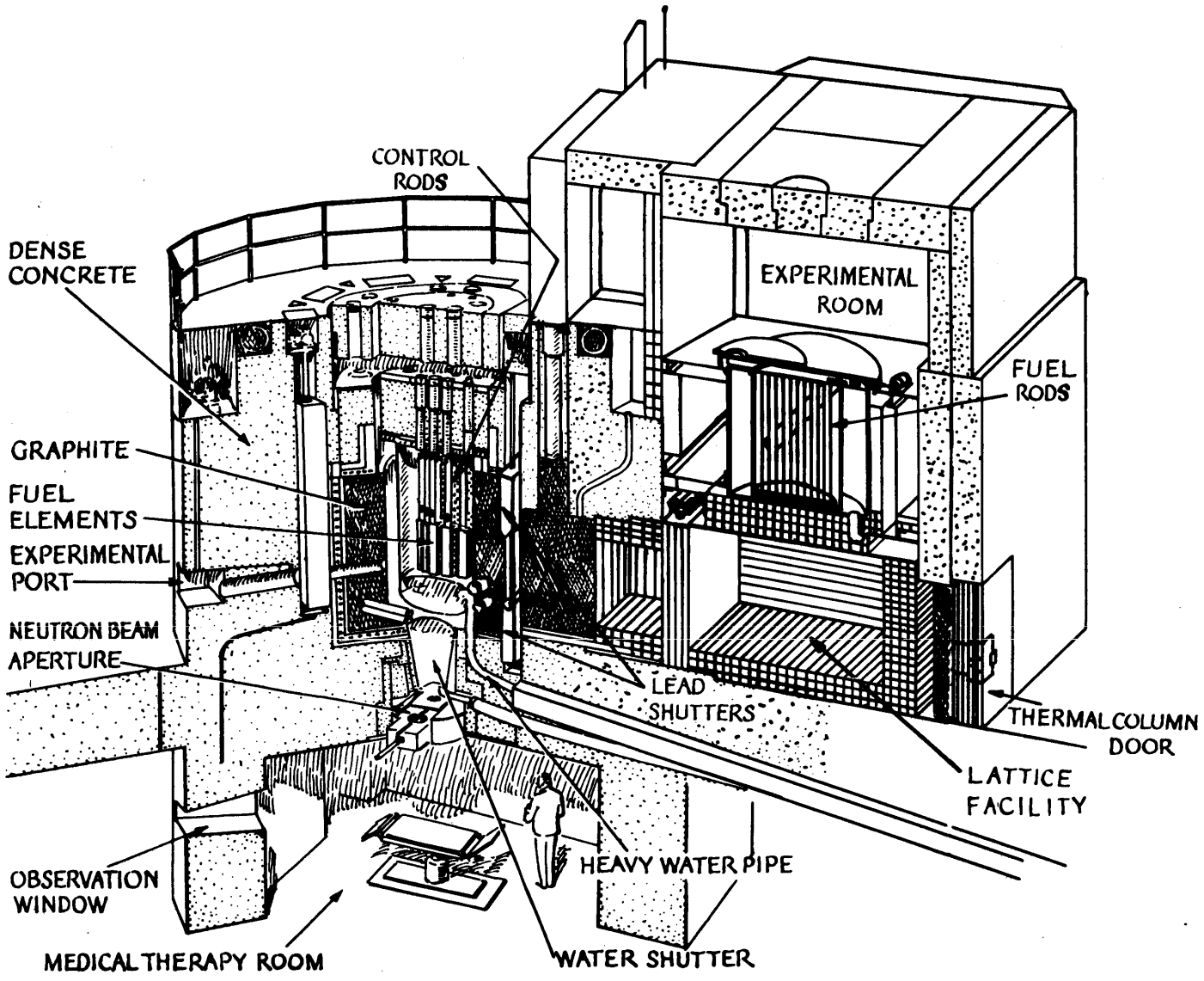

FIG. 3.1
CUT-AWAY VIEW OF THE MIT RESEARCH REACTOR

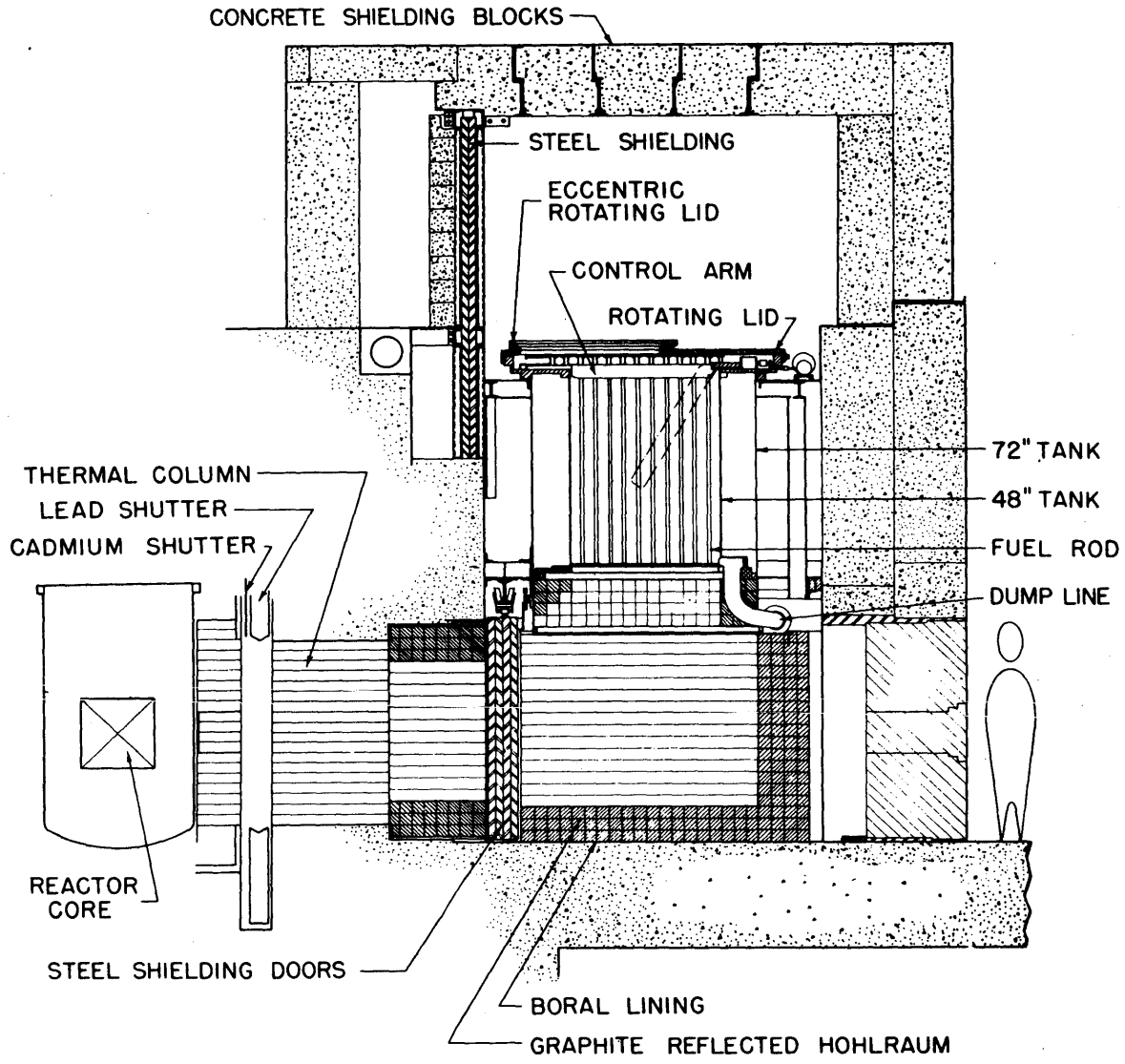

FIG. 3.2 VERTICAL SECTION OF THE SUBCRITICAL ASSEMBLY

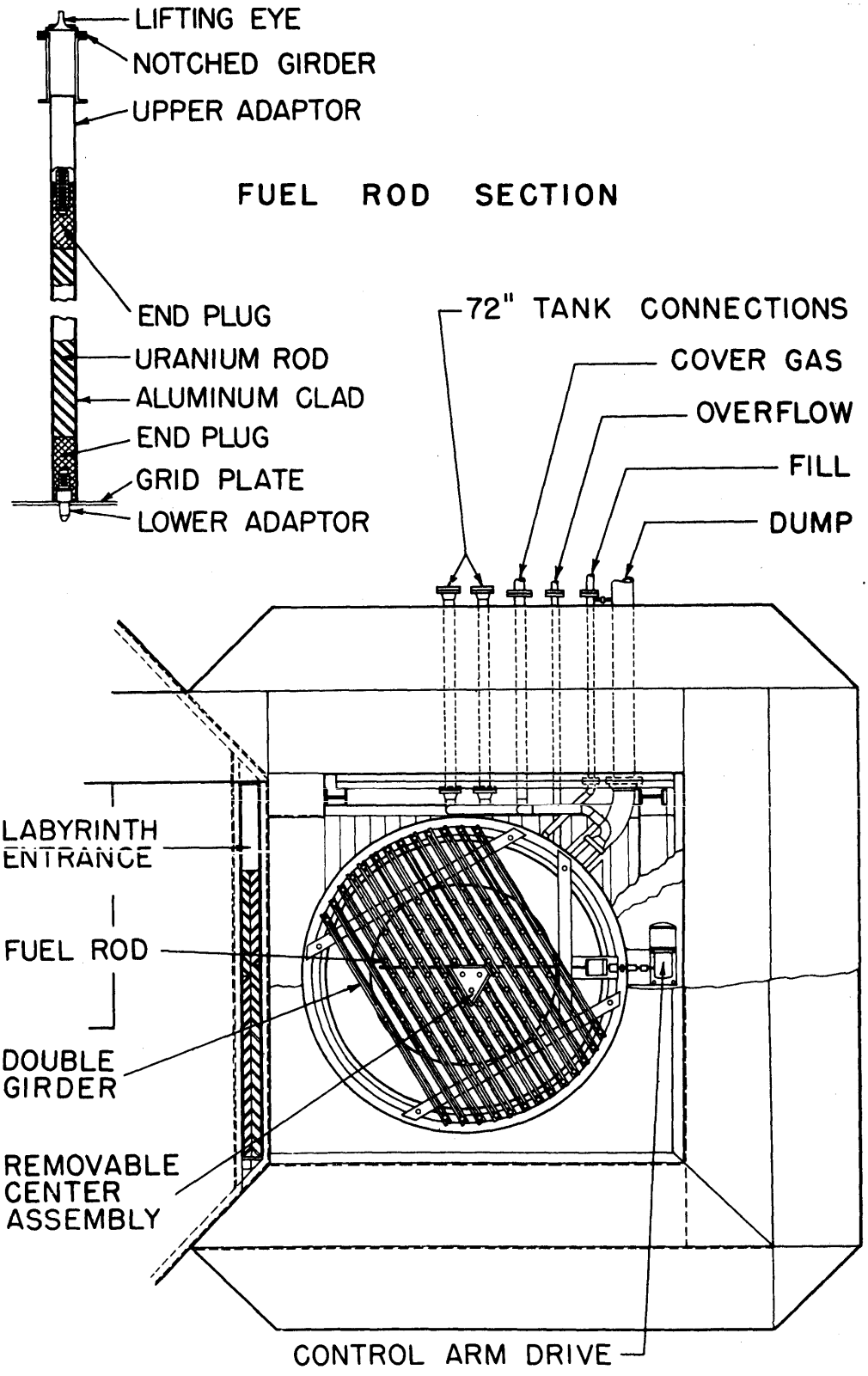

FIG. 3.3 PLAN VIEW OF THE SUBCRITICAL ASSEMBLY

adapters, screwed into the bottom of the rods, fit into positioning holes in a grid plate at the bottom of the exponential tank.

Before each run in the facility, a 1/16-inch-diameter, 0.010-inch-thick gold foil was placed in a 5/8-inch-diameter sample tube located in a fixed location in the graphite wall of the cavity opposite the thermal column. This foil was used to monitor the flux and irradiation time for each run. The foil was taped on the end of a 1/4-inch-diameter polyethylene rod which was fully inserted into the sample hole, thus ensuring a standard position for each monitor foil. The flux distribution in the sample tube is shown in Figure 3.4. It is seen that the flux shape is flat over several inches at the end of the tube which further lessens the chance of positioning errors.

3.2 Formation of Two Region Assemblies

The flexibility of the M. I. T. lattice facility and the availability of several types of fuel rods allows the formation of assemblies varying in center region size, fuel enrichment, fuel rod diameter, and lattice pitch or spacing.

The diameter of the center region was limited to about one-half the diameter of the exponential tank to ensure sufficient outer region for meaningful measurements. This restriction limited the number of cells in the center region, particularly for lattices of large pitch.

The fuel used in the assemblies was composed of metallic uranium of natural or low enrichment, clad in Type 1100 aluminum. These rods were arranged in triangular arrays with spacings corresponding to pitches previously studied in single region lattices. Thus,

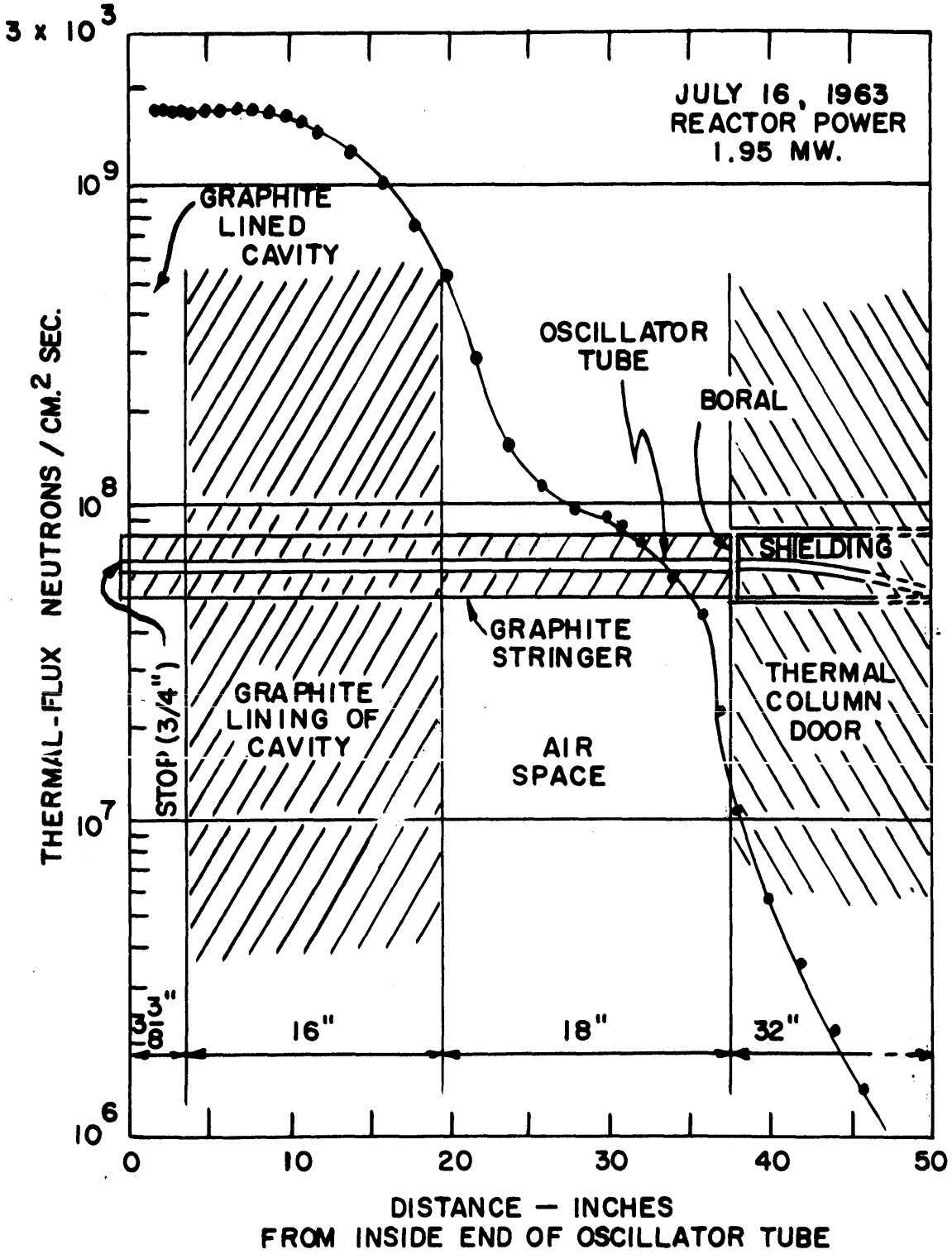

FIG. 3.4 VERTICAL SECTION OF THE CAVITY SAMPLE TUBE WITH THE NEUTRON FLUX DISTRIBUTION MEASURED BY CLARK (C1) SUPERIMPOSED

most of the results from two region assemblies can be compared directly with those made independently on single region lattices.

When the two regions of an assembly differ in pitch, they differ by a factor of two. Any other ratio would have required the additional expenditure of time and money for the fabrication of a new girder system, which was considered unnecessary. Instead, the second region is easily formed by the insertion (or removal) of alternate fuel rods from an existing single region lattice. The resulting difference in the fuel to moderator ratios of the two regions provides a wide variation in L^2, the thermal diffusion length, and such assemblies exhibit the greatest variation in the neutron spectra across the assembly. Other assemblies were formed by substituting rods of another enrichment or diameter into a single region lattice.

The word "assembly" in this report refers to a system of fuel rods and moderator containing two regions differing in fuel element pitch, enrichment or diameter, or some combination of the three. A list of the two region assemblies studied is given in Table 3.1. Roman numerals are applied to consecutively number the assemblies in the order in which they were studied. Table 3.1 also gives the number of "rings" in each region of an assembly. Rings are defined as hexagonals of fuel rods about the center rod as shown in Figure 3.5. Thus, a four-ring assembly such as assembly III has 61 fuel rods in the center region. The number of rings in the outer region is less well defined because of the circular shape of the tank. The number of complete rings in the outer region is given in the table.

Assemblies were chosen to allow the effects of rod size, spacing,

TABLE 3.1

Two Region Assemblies Tested in the M. I. T. Lattice Facility

Assembly Designation	Properties Common to Both Regions	Outer Region	Inner Region
I	0.25-in.-diameter, 1.027% U-235 fuel	9 rings – 1.25-in. spacing	2 rings* – 2.50-in. spacing**
II	0.25-in.-diameter, 1.027% U-235 fuel	7 rings – 1.25-in. spacing	3 rings – 2.50-in. spacing
III	0.25-in.-diameter, 1.027% U-235 fuel	5 rings – 1.25-in. spacing	4 rings – 2.50-in. spacing
IV	0.25-in.-diameter, 1.027% U-235 fuel	4 rings – 2.50-in. spacing	6 rings – 1.25-in. spacing
V	0.25-in.-diameter, 1.143% U-235 fuel	9 rings – 1.25-in. spacing	2 rings – 2.50-in. spacing
VI	0.25-in.-diameter, 1.143% U-235 fuel	5 rings – 1.25-in. spacing	4 rings – 2.50-in. spacing
VII	0.25-in.-diameter, 1.75-in. spacing	7 rings – 1.143% U-235 fuel	3 rings – 1.027% U-235 fuel
VIII	0.25-in.-diameter, 1.75-in. spacing	5 rings – 1.143% U-235 fuel	5 rings – 1.027% U-235 fuel
IX	2.50-in. spacing	3 rings – 0.75-in.-diameter, 0.947% U-235 fuel	4 rings – 0.25-in.-diameter, 1.027% U-235 fuel
X	2.50-in. spacing	5 rings – 0.75-in.-diameter, 0.947% U-235 fuel	2 rings – 0.25-in.-diameter, 1.027% U-235 fuel
XI	5.00-in. spacing	2 rings – 0.75-in.-diameter, 0.947% U-235 fuel	2 rings – 1.0-in.-diameter, natural uranium fuel

*Rings about the central rod.

**All spacings are the triangular lattice pitches used.

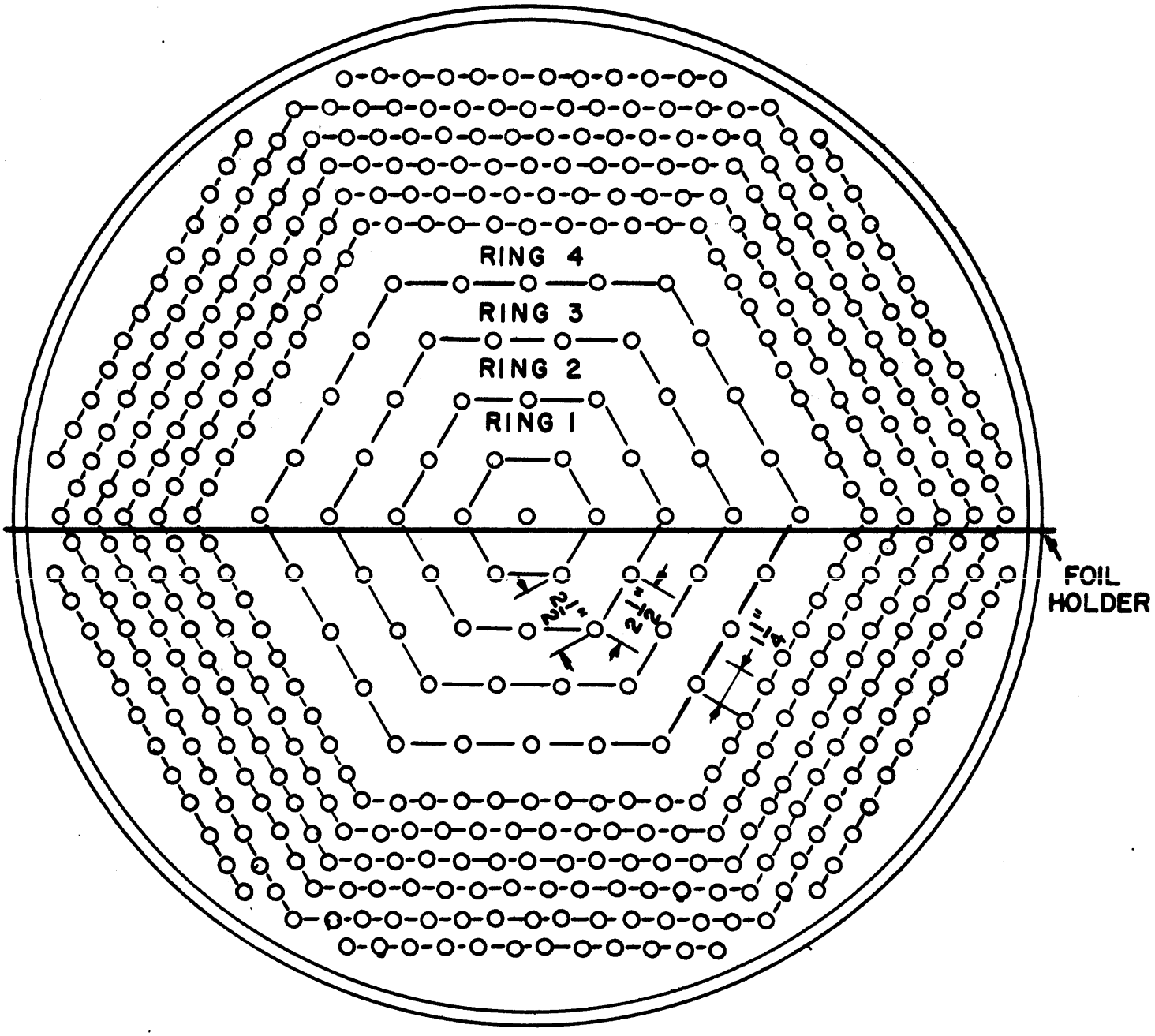

FIG. 3.5 PLAN VIEW OF ASSEMBLY III
(FOUR RING $2\frac{1}{2}$ INCH PITCH IN $1\frac{1}{4}$ INCH PITCH)

center region size and fuel enrichment to be examined in a systematic way. Assemblies I through VI have regions which differ only in rod spacing, while the center region size varies with each assembly. The regions of assemblies VII and VIII have slightly different enrichments, while in IX, X, and XI both rod size and enrichment differ in the two regions.

It should be noted that restrictions of space within the facility, ultimately determined by criticality considerations, made some of the regions quite small in comparison with the diffusion and slowing down lengths of the lattice materials.

The word "lattice" as used in this report refers to a system of fuel and moderator composing one region of an assembly. The lattice is specified by the fuel rod enrichment, diameter and pitch. Table 3.2 lists the lattices involved in the assemblies and the region in the assembly in which each lattice was used. The lattices are numbered with arabic numerals to distinguish them from assembly designations.

3.3 Measurements Made in the Assemblies

Neutron flux measurements made by means of foil detectors in a subcritical lattice may be roughly divided into traverses to determine the overall flux shape in the assembly, and determinations of neutron activation inside a fuel rod. Macroscopic traverses in a single region lattice are made to determine the material buckling. Such determinations have been made by the various investigators of the M. I. T. Lattice Project (P1, H2, K1). The usual detector foils used have been gold foils, although copper foils have also been employed.

TABLE 3.2

Lattices Studied in Two Region Assemblies

Lattice Number	Fuel Rod Diameter (Inch)	U-235 Concentration in Fuel (Percent)	Lattice Pitch (Inches)	Assembly	Region
1	0.25	1.027	1.25	I	Outer
				II	Outer
				III	Outer
				IV	Inner
2	0.25	1.027	1.75	VII	Inner
				VIII	Inner
3	0.25	1.027	2.50	I	Inner
				II	Inner
				III	Inner
				IV	Outer
				IX	Inner
				X	Inner
4	0.25	1.143	1.25	V	Outer
				VI	Outer
5	0.25	1.143	1.75	VII	Outer
				VIII	Outer
6	0.25	1.143	2.50	V	Inner
				VI	Inner
7	0.75	0.947	2.50	IX	Outer
				X	Outer
8	0.75	0.947	5.00	XI	Outer
9	1.0	0.71 (natural)	5.00	XI	Inner

In an effort to determine the constancy of the material buckling with neutron energy, cadmium-covered gold foils have also been used. The results of radial and axial traverses are individually fitted to the one-group diffusion expression for the flux distribution.

In the two region assemblies, gold traverses, both bare and cadmium-covered, were made in the radial direction and bare gold traverses in the axial direction. Previous Lattice Project experience gained from the buckling measurements in single region lattices was employed in determining the procedures used for this study. Details of the procedures are given below.

The value of integral parameter measurements made in the fuel rods of a two region assembly is directly related to the degree to which the spectrum in the area of the measurement simulates that of a critical lattice of the same composition. In order to determine the degree of spectral similarity in the assemblies, the cadmium ratio of gold in the moderator was obtained from the radial traverses, and also parameter measurements were made inside fuel rods at various radial distances from the assembly center. The parameters chosen for this purpose were δ_{28}, the ratio of fissions in U^{238} to fissions in U^{235}, and R_{28}, the cadmium ratio of U^{238} inside a fuel rod. The former parameter is related to the fast fission factor, ϵ (see section 2.4), and the latter to the resonance escape probability, p (see section 2.2.4). Both parameters have been measured in single region lattices for each of the lattices involved in the two region assemblies. Details of the experimental procedures used for these integral parameter measurements are also given below.

3.4 Gold Traverses

The following sections present the procedures used for the axial and radial gold foil traverses.

3.4.1 Gold Axial Traverses

During the course of the experimental program, several changes were made in the technique for positioning foils for axial traverses. For runs in Assembly I and for part of Assembly III runs, foil holders designed for 1/16-inch-diameter, 0.010-inch-thick gold foils were used. These holders were fabricated from aluminum extruded T-stock and were machined with a series of 1/16-inch-diameter depressions spaced 1-1/2 inches apart into which foils were placed and secured with mylar tape. The holder was suspended vertically from the top support girders of the facility into the moderator region between the fuel elements. Figure 3.6 shows the holder positioned in the assembly. In a 1-1/4-inch-pitch lattice, the top of the holder fit snugly between the upper adapters of two fuel elements and the support girders. With the 2-1/2-inch spacing, a dummy fuel adapter was placed in the support girder to mock the 1-1/4-inch spacing and thus ensure proper positioning of the holder. The use of this dummy adapter is illustrated in Figure 3.6. The bottom of the holder was inserted through a hole in the grid plate into which it was guided by thin aluminum strips permanently fastened to the grid plate with epoxy resin. Three positions in the grid plate were prepared in this fashion: at 3.0, 6.25 and 10.0 inches from the center of the assembly.

Although good results were obtained with this arrangement, it was

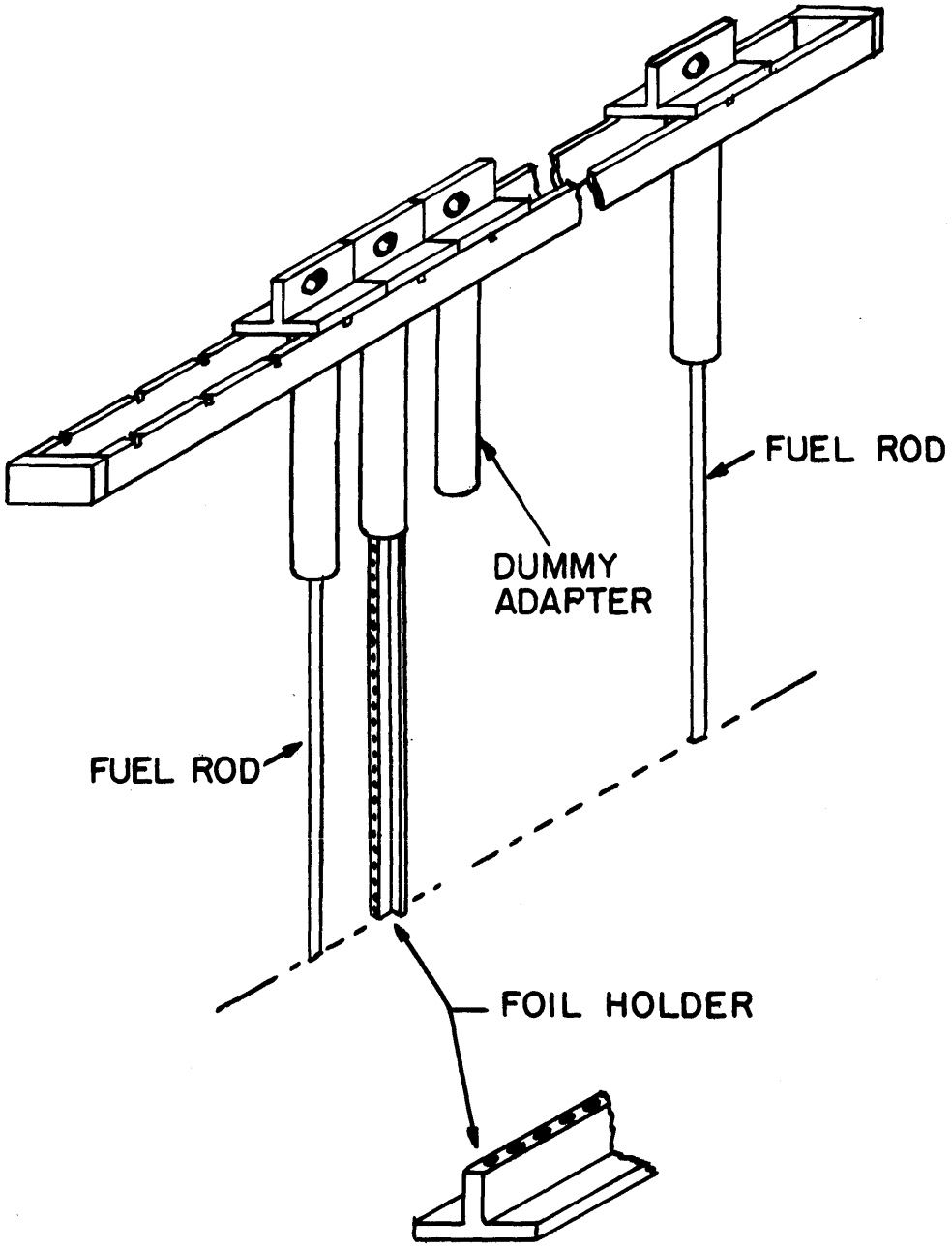

FIG. 3.6 AXIAL FOIL HOLDER USED IN ASSEMBLIES I AND III

concluded that better positioning with less effort and a greater choice of radial positions could be obtained by installing foils inside fuel rods. Although small positioning errors of the foils inside the rod might be expected to be magnified by the fuel disadvantage factor or variations of thermal neutron leakage into the foil position could prove to be a source of error, experiments performed with this foil arrangement proved to be more consistent than those with the previous foil holders. Uncertainty in the weights of the foils was reduced at the same time by employing larger foils of 1/8-inch diameter. This method was followed throughout the remaining assemblies and is described below.

Experimental rods in the Lattice Project consist of hollow aluminum tubes of the same inner diameter as the fuel rod fitted with threaded end caps which simulate the upper and lower adapters of a regular fuel rod. These rods can then be positioned in the lattice in the same fashion as the regular fuel rods.

For axial traverses, two-inch-long slugs of fuel, identical in diameter and enrichment to that of the lattice fuel, were inserted in an experimental rod. Aluminum planchettes, thirty-two mils thick, machined to hold 1/8-inch-diameter gold foils, were placed between the slugs to make up the foil detectors for the axial traverse. A typical rod contained seventeen foils which were more than sufficient to cover the exponential portion of the axial distribution.

The center fuel position of the assembly was the standard position for axial traverses done in this manner, although other fuel positions were also used. The length of the axial irradiations varied from one to four hours, depending on the multiplication of the lattice being studied.

3.4.2 Gold Radial Traverses

Gold foils were positioned in the moderator between rows of fuel by aluminum foil holders. As in the case of the axial traverses, two types of foil holders were used.

The first type, used for runs in Assembly I and in part of those in Assembly III, was machined with a series of concentric circular depressions of 1/16- and 1/8-inch diameter, which made the holder capable of accepting bare 1/16-inch-diameter gold foils or 1/8-inch-diameter cadmium covers. Foil positions were spaced 1-1/4 inches apart, making a total of twenty-six possible foil positions. The holder was lowered into the lattice tank using aluminum chains. A notch close to one end of the foil holder was inserted into a corresponding notch in a holder support previously attached to a lattice fuel rod. A second unnotched support on a second fuel rod held the other end of the holder in the horizontal position. These supports were situated twenty-four inches above the bottom of the fuel and positioned the holder parallel to the support girder next to the central fuel element.

The installation of this foil holder into the tank and positive latching into the support bracket was a difficult and uncertain task. The second type of holder made considerable improvement in positive positioning and ease of installation. This holder was also made of aluminum stock but was suspended from the top girders by aluminum chain attached to both ends of the holder. Hook-type adapters positively positioned the holders in the horizontal plane as shown in Figure 3.7. Several holders of this type were used, the spacing between foil positions varying with the lattice pitch. In all cases, 1/8-inch-diameter, 10-mil-thick gold foils were used.

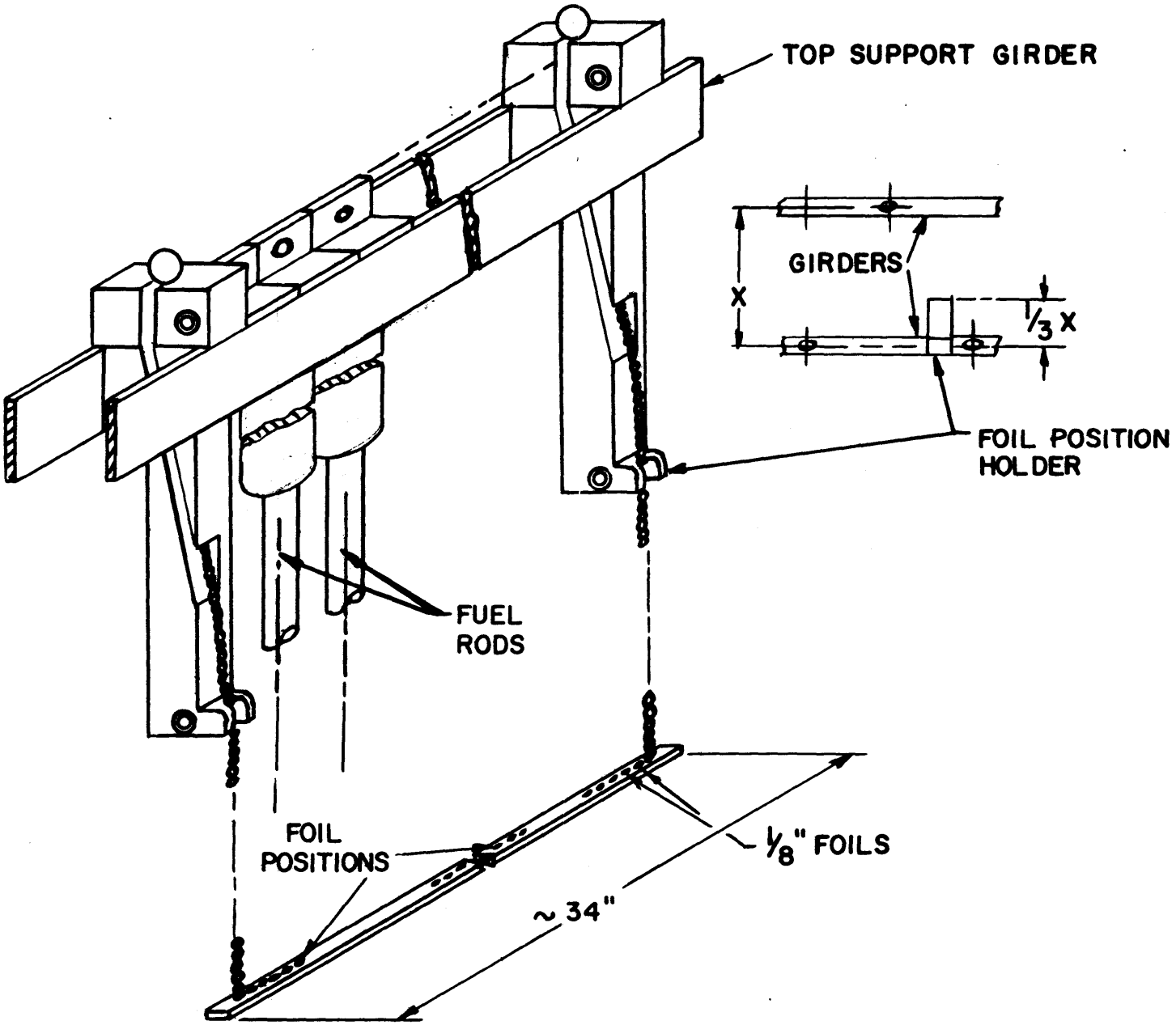

FIG. 3.7 RADIAL FOIL HOLDER ARRANGEMENT

3.4.3 Counting Method

Gold foils, activated in the above traverses, were counted with a NaI crystal scintillation counter. The counting technique was the same for both 1/8-inch and 1/16-inch gold foils. A single channel analyzer was used to restrict the gamma rays counted to those with energies above about 320 Kev. This energy corresponds to the minimum in the gamma-ray spectrum of Au^{198} immediately before the principle gamma-ray peak of 412 Kev (H7). This setting was chosen in an effort to minimize the effect of instrument drift on counting results. A typical counting system is shown in Figure 3.8.

Automatic sample changers facilitated the counting and allowed several counting passes (usually three) for each traverse. A preset count, which varied from 20,000 to 100,000 counts, was used for each foil in each pass. Since at least two such counting arrangements were available during most of the experiments, each traverse was usually counted on both systems. After preliminary data reduction, the output of the counting system with the smaller deviation between passes was selected for further treatment.

3.5 U^{238} Cadmium Ratio

The following sections describe the irradiation procedures and counting methods used in determining the cadmium ratio of U^{238} inside a fuel rod.

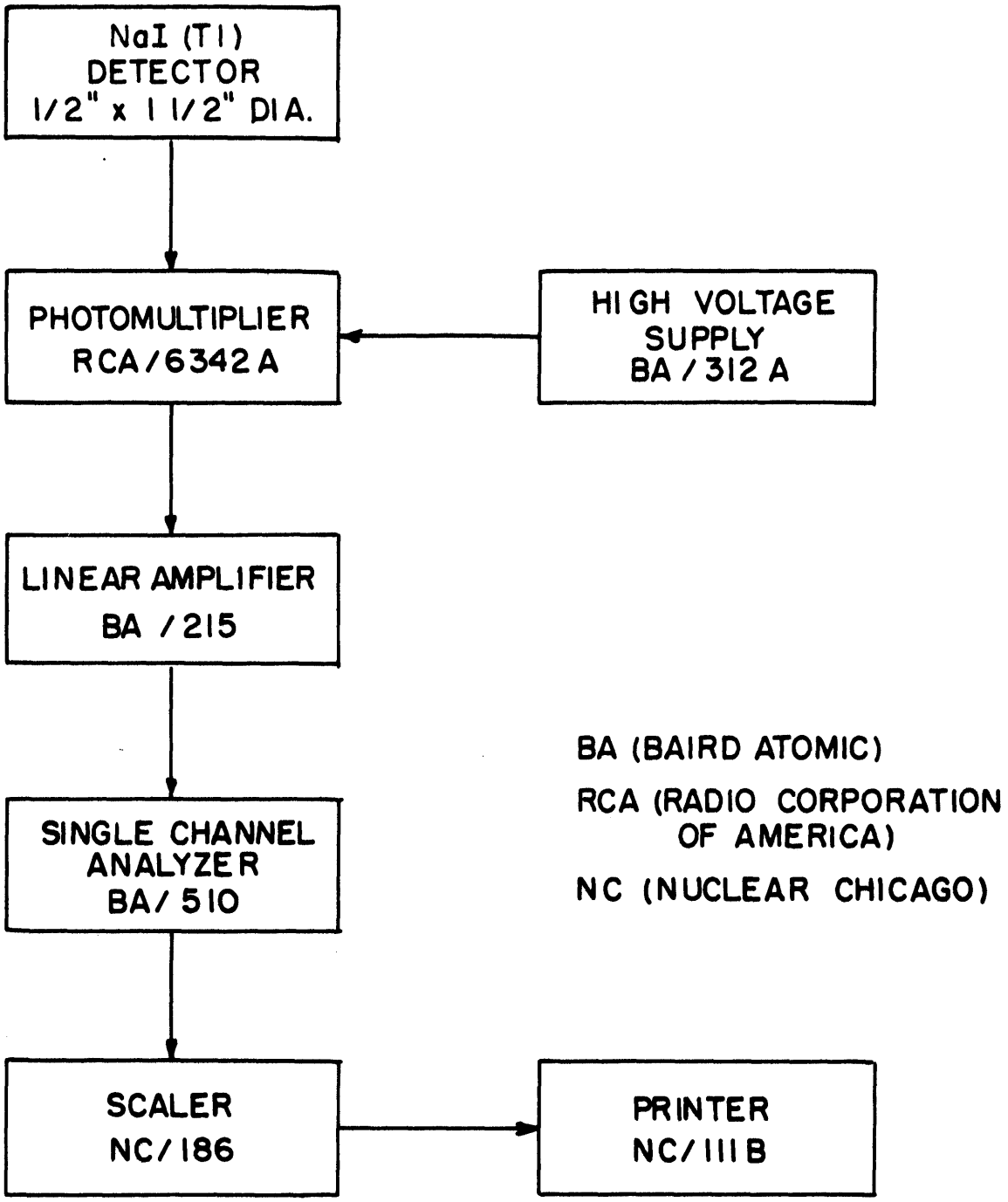

FIG. 3.8 BLOCK DIAGRAM OF TYPICAL GAMMA-COUNTING SYSTEM

3.5.1 Foil Arrangement

Figure 3.9 shows the foil packet arrangement used in the measurement of the U^{238}-cadmium ratio. The detector foils were uranium foils depleted in U^{235} content to 18 ppm, 0.005 inch thick and of the same diameter as the fuel rods. Each detector foil was sandwiched between two depleted uranium catcher foils and the three foils then placed between two 0.060-inch-thick fuel slugs. This packet of fuel and slugs was then secured by either a Teflon sleeve or mylar tape. Previous work (D1) has shown that the two types of sleeves produced no detectable difference in the results. At each end of the packet, a 0.020-inch-thick cover foil was placed. These foils were Type 1100 aluminum for the bare runs and cadmium for the cadmium-covered runs. The aluminum covers were used to preserve the positioning of the foils between bare and cadmium-covered runs. Their effect on the activity of the detector foils has been shown to be negligible (D1).

The foil packet, together with its cover foils, were placed between two fuel slugs in an experimental rod. For cadmium-covered runs, the rod was wrapped with 0.20 inch of cadmium for one-half inch on both sides of the detector foil position. The foils were irradiated at a height of 16 inches from the bottom of the fuel region. Irradiations of about 6 hours for the bare runs and 12 hours for the cadmium-covered runs produced sufficient activity in the lattices studied.

Bare runs and cadmium-covered runs were not made simultaneously. In order to ensure reproducibility of foil position for a cadmium ratio determination, the same fuel slugs were used to load the

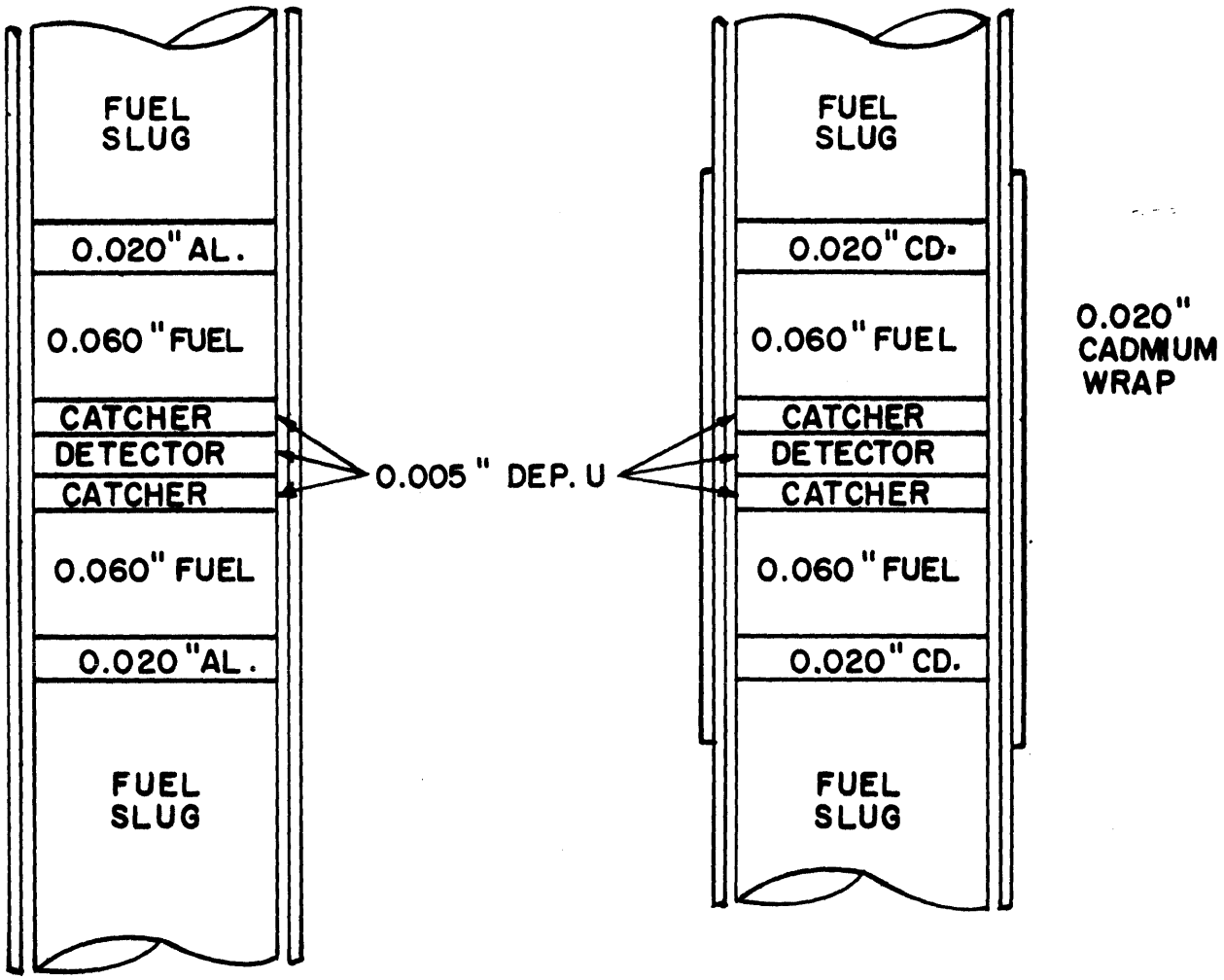

a. FUEL PACKET FOR BARE IRRADIATION

b. FUEL PACKET FOR CADMIUM COVERED IRRADIATION

FIG. 3.9 FOIL PACKET ARRANGEMENT FOR MEASUREMENT OF R_{28}

experimental rod in both cases. The activities were then normalized, using the activities of gold monitor foils described in section 3.1.

3.5.2 Counting Method

After irradiation, the U^{239} formed in the depleted uranium foils was allowed to decay to Np^{239} before counting. A minimum cooling time of four hours was required. The counting system consisted of an integral-counting probe unit containing a 1/2-inch-thick, 1-1/2-inch-diameter NaI(T1) crystal and an RCA 6342A photomultiplier; a pre-amplifier built for the Lattice Project, a Sturrup, Inc. Model 4201 high voltage supply and a Radiation Instrument Development Laboratory (RIDL) single-channel spectrometer. The spectrometer consisted of an RIDL Model 30-19 amplifier, an RIDL Model 33-10 single-channel analyzer and an RIDL Model 49-25 combination scaler-timer, all mounted in an RIDL Model 29-1 chassis. A diagram of the counting apparatus is shown in Figure 3.10. A differential gamma-ray counting method was used. The 103-Kev peak in the gamma- and X-ray spectrum of Np^{239} was straddled with a window width corresponding to 38 Kev. The 84-Kev gamma ray of Tm^{170} was used to set the lower limit of the window, and the 123-Kev gamma ray of Co^{57}, to set the upper limit. The calibration was made every time the system was used. At least five counting passes were made with each foil. The average of the corrected counts from all passes was taken as the desired foil activity.

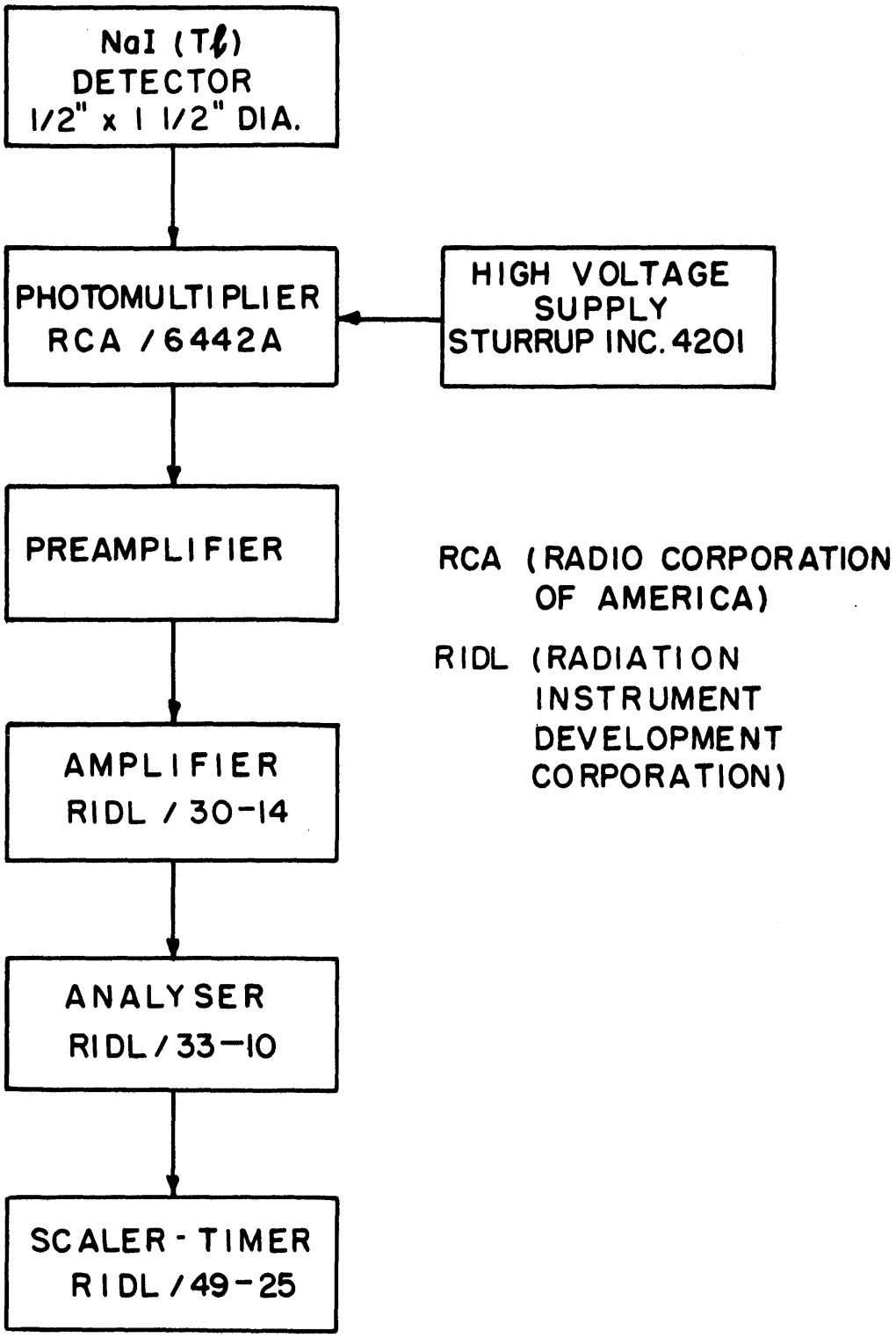

FIG. 3.10 COUNTING SYSTEM USED TO MEASURE THE Np^{239} ACTIVITY OF THE DEPLETED URANIUM FOILS

3.6 δ_{28} Measurements

The fast fission ratio, δ_{28}, is defined by the relationship (W1, B1):

$$\delta_{28} = \frac{\text{Average total } U^{238} \text{ fission rate in the foil}}{\text{Average total } U^{235} \text{ fission rate in the foil}} ,$$

which may be written as:

$$\delta_{28} = P(t) \frac{C_E \cdot a \cdot \Gamma(t) - S}{1 - a \cdot \Gamma(t)} , \qquad (3.1)$$

where

C_E is an enrichment correction given by $\left(\frac{N_N}{N_F}\right)^{25} \left(\frac{N_F}{N_N}\right)^{28}$, where the subscript F refers to the fuel material and N refers to the natural uranium;

a is given by

$$a = \left(\frac{W_N}{W_D}\right) \left(\frac{N_N}{N_D}\right)^{28} ,$$

where the subscript D refers to depleted uranium;

S is the ratio, $\left(\frac{N_D}{N_F}\right)^{25} \left(\frac{N_F}{N_D}\right)^{28}$;

P(t) is the ratio of the measured fission product activity per U^{235} fission to the measured fission product activity per U^{238} fission;

$\Gamma(t)$ is the ratio of the fission product activity measured in a foil depleted in U^{235} to the fission product activity measured in a foil of natural uranium, with both foils irradiated in the same neutron flux.

P(t) depends on both the fuel rod diameter and the irradiation time. However, extensive measurements of P(t) in the exponential facility at M. I. T. have shown very slight dependence on time or fuel

rod size (P2, B1). Therefore, P(t) has been taken to be a constant for each of the assemblies with a value of 1.14 ± 0.02 (S1). The method of determining $\Gamma(t)$ will be discussed in the next section.

3.6.1 Foil Arrangement

The quantity $\Gamma(t)$ was measured by irradiating two uranium foils, one depleted in U^{235}, the other a natural uranium foil. Both foils were 0.005 inch thick and of the same diameter as the fuel rod. Foil packets were composed of the two detector foils, each sandwiched between two uranium "catcher" foils, identical in size and composition with the corresponding detector foil. (In the case of the one-inch-diameter fuel, the catcher foils were 0.001-inch-thick aluminum foils.) The catcher foils prevent the contamination of the detector foils with fission products produced in uranium of a different U^{235} composition. The packet was completed by two 0.060-inch-thick fuel slugs at top and bottom, and the packet was secured with mylar tape. The packet is shown in Figure 3.11.

The packet was placed between two fuel slugs in an experimental fuel rod at about 16 inches from the bottom of the fuel. The foils were then irradiated for about 12 hours.

3.6.2 Counting Method

The irradiated foils were allowed to decay for four hours after irradiation to allow the 23-minute U^{239} to decay to Np^{239} and thus prevent the inclusion of the 1.2-Mev beta ray from U^{239} in the fission product count. The foils were then counted with a Baird Atomic

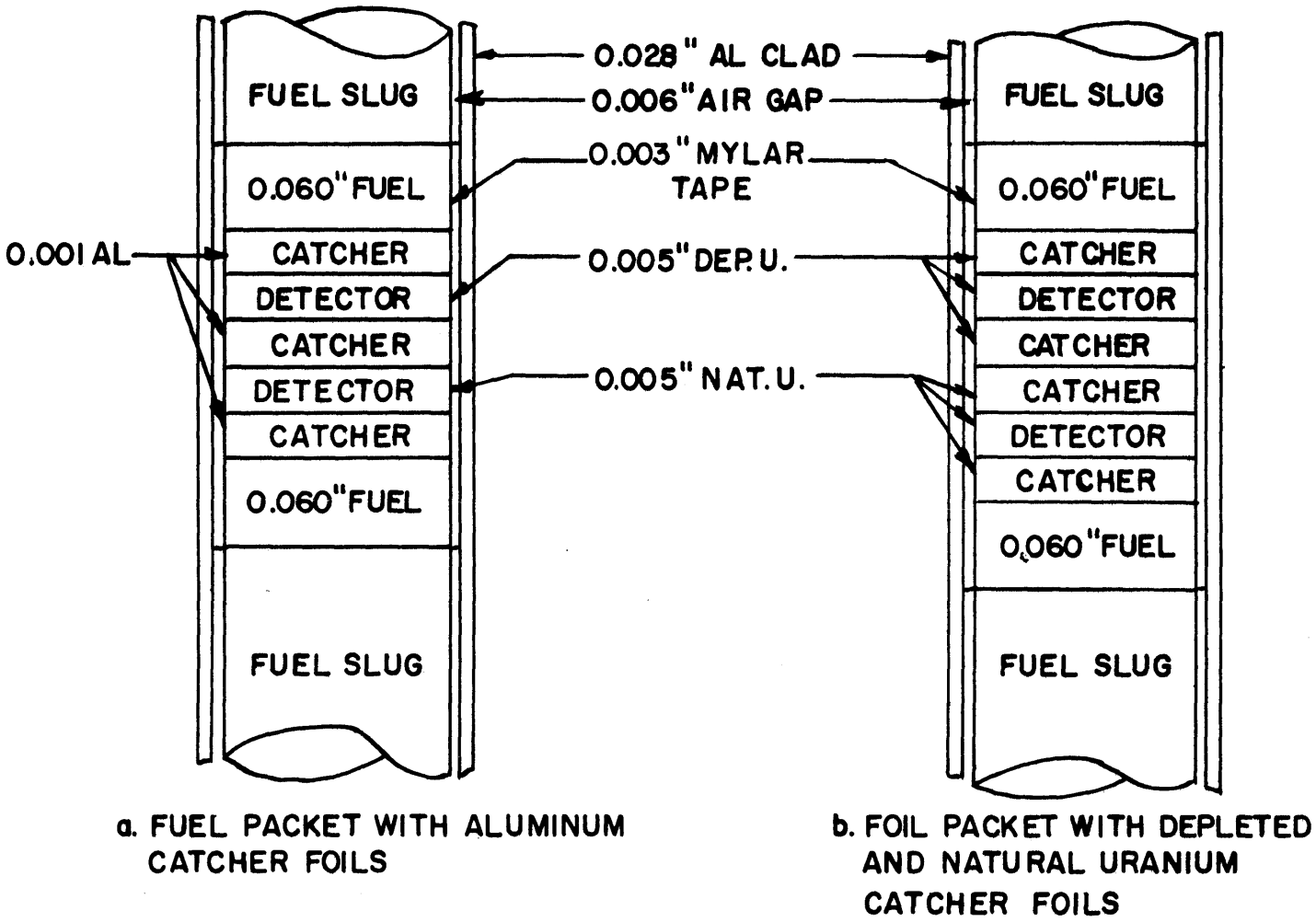

a. FUEL PACKET WITH ALUMINUM CATCHER FOILS

b. FOIL PACKET WITH DEPLETED AND NATURAL URANIUM CATCHER FOILS

FIG. 3.11 FOIL PACKET ARRANGEMENT FOR MEASUREMENT OF δ_{28}

Model 815BL scintillation detector, a Baird Atomic Model 215 linear amplifier, and a Baird Atomic Model 960 timer. The scintillation detector contained a 1-3/4-inch-thick, 2-inch-diameter NaI(T1) crystal, an RCA 6342A photomultiplier and a preamplifier. A schematic diagram is shown in Figure 3.12. The foils were counted for fission product activity by the integral gamma-ray counting technique with a baseline corresponding to 0.72 Mev. The 667-Kev and 840-Kev photopeaks of Cs^{137} and Mn^{54}, respectively, were used to calibrate the equipment. Each foil was counted a minimum of six times to define the time dependence of the activity.

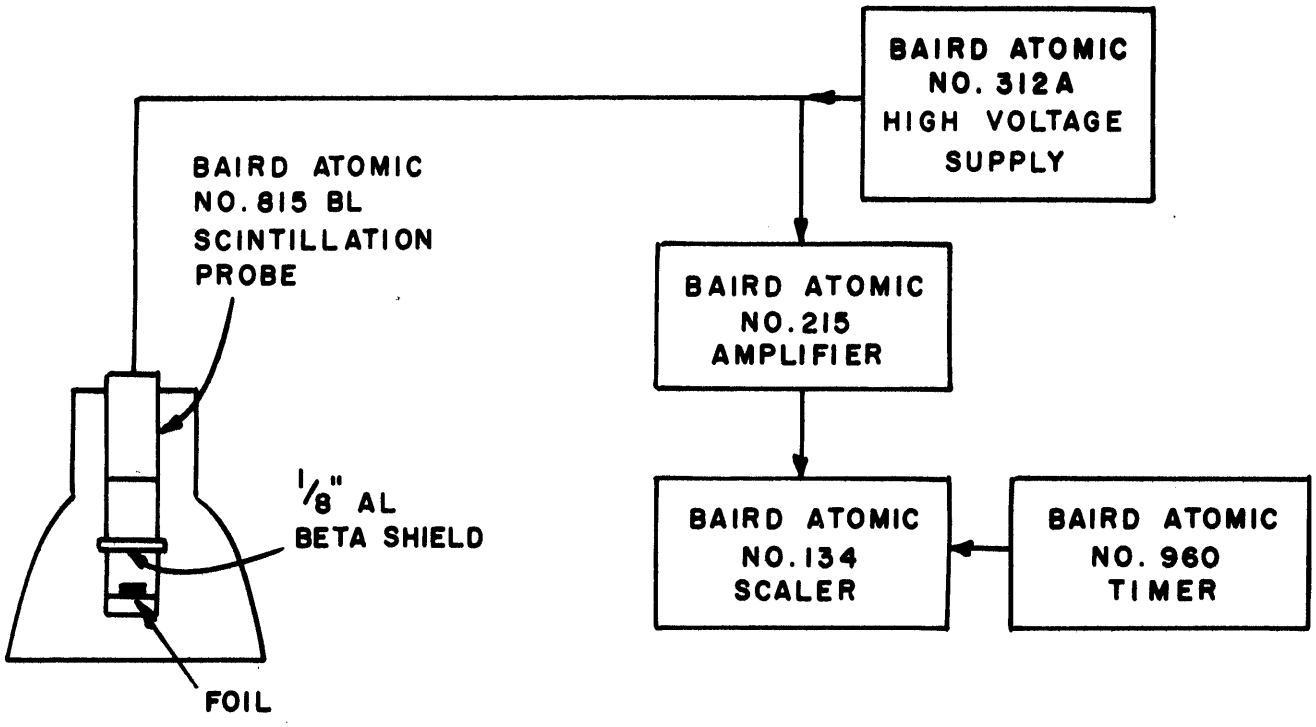

FIG. 3.12 COUNTING SYSTEM USED TO MEASURE THE GROSS FISSION PRODUCT ACTIVITY OF THE NATURAL AND DEPLETED URANIUM FOILS

Chapter IV

METHODS OF DATA REDUCTION AND EXPERIMENTAL RESULTS

4.1 Introduction

This chapter describes techniques used for analyses of the raw data obtained from the experiments described in the preceding chapter. As a result of these analyses, the data are presented in the form of commonly measured lattice quantities suitable for testing the theories developed in Chapter II. The analyses of this chapter include correction of the counting data, calculation of the axial buckling, gold-cadmium ratios, δ_{28} and the U^{238}-cadmium ratios. The results of these determinations will then be presented.

4.2 Techniques of Data Analyses

The methods used for data reduction have been developed by various workers on the Heavy Water Lattice Project (S2, D1, P1, W1).

4.2.1 Gold Foil Activation

The gold foil counting data were corrected with the ACT5 computer program written by Simms (S2) and subsequently modified by Clikeman (C2). This program processes the raw data obtained from the automatic counters described in section 3.4.3 for activity having a single half-life. Gold activity, having a half-life of 64.8 hours, is thus suitable input for the code.

The program corrects the raw data for:

1. Decay of activity from the time the irradiation ended to the time at which the counting of the foils begins.
2. Decay of activity during the time interval in which the foils are being counted.
3. Background.
4. Counter dead time.
5. Foil weight.

Corrections 2, 3, and 4 are applied to each counting pass; corrections 1 and 5 are applied to the average count rate over all the passes. The average is calculated by weighting the individual results with the number of pre-set counts for the pass.

The axial and radial bare and cadmium-covered foils used in the traverses of these lattices together with the monitor foils were analyzed in this manner. (In general, correction 1 was not applied to the monitor foils by ACT5 since monitors from several runs were commonly counted at the same time.)

4.2.2 Gold-Cadmium Ratios

The output from the computer code ACT5 includes punched cards containing the corrected activities and the statistical counting error for each foil counted. These cards for a bare and cadmium-covered set of foils comprising a single run, together with their respective monitor foils, are used as input to the program AGE described in Appendix B. The initial part of this program applies correction 1 to each monitor foil and proceeds to normalize the traverses to the monitor foil activities. A gold-cadmium ratio for

each traverse position is calculated from these normalized activities, together with the counting errors of the individual foils involved.

4.2.3 Axial Buckling

The corrected activities for the axial traverses obtained from ACT5 were analyzed for the axial buckling of each assembly with the computer program AXFIT, initially written by Palmedo (P1). The AXFIT code is basically a least squares fit of the activities to a hyperbolic sine function:

$$\phi(z) = A \sinh \gamma (H-z), \tag{4.1}$$

where H is the extrapolated height of the lattice core and γ^2 is the axial buckling. The code fits the activities to the expression for several values of the extrapolated height supplied as input to the code. Only points greater than 30 cm from the bottom of the tank were used and points at the top are successively dropped by the code. Each time the number of experimental points considered is decreased, a value of γ^2 is found for each value of the extrapolated height. Plots of γ^2 versus H for each point dropped have a common intersection, as shown in Figure 4.1. This intersection defines the required value of γ^2. Note that the intersection of the curves is rather poorly defined since the slopes of the intersecting lines are not greatly different.

4.2.4 Uranium Foil Activation

The Np^{239} counts from the activated depleted uranium foils described in section 3.5.1 were corrected for the same effects as the gold foils (section 4.2.1). The bare and cadmium-covered activities were normalized to the activities of the bare gold monitor foils

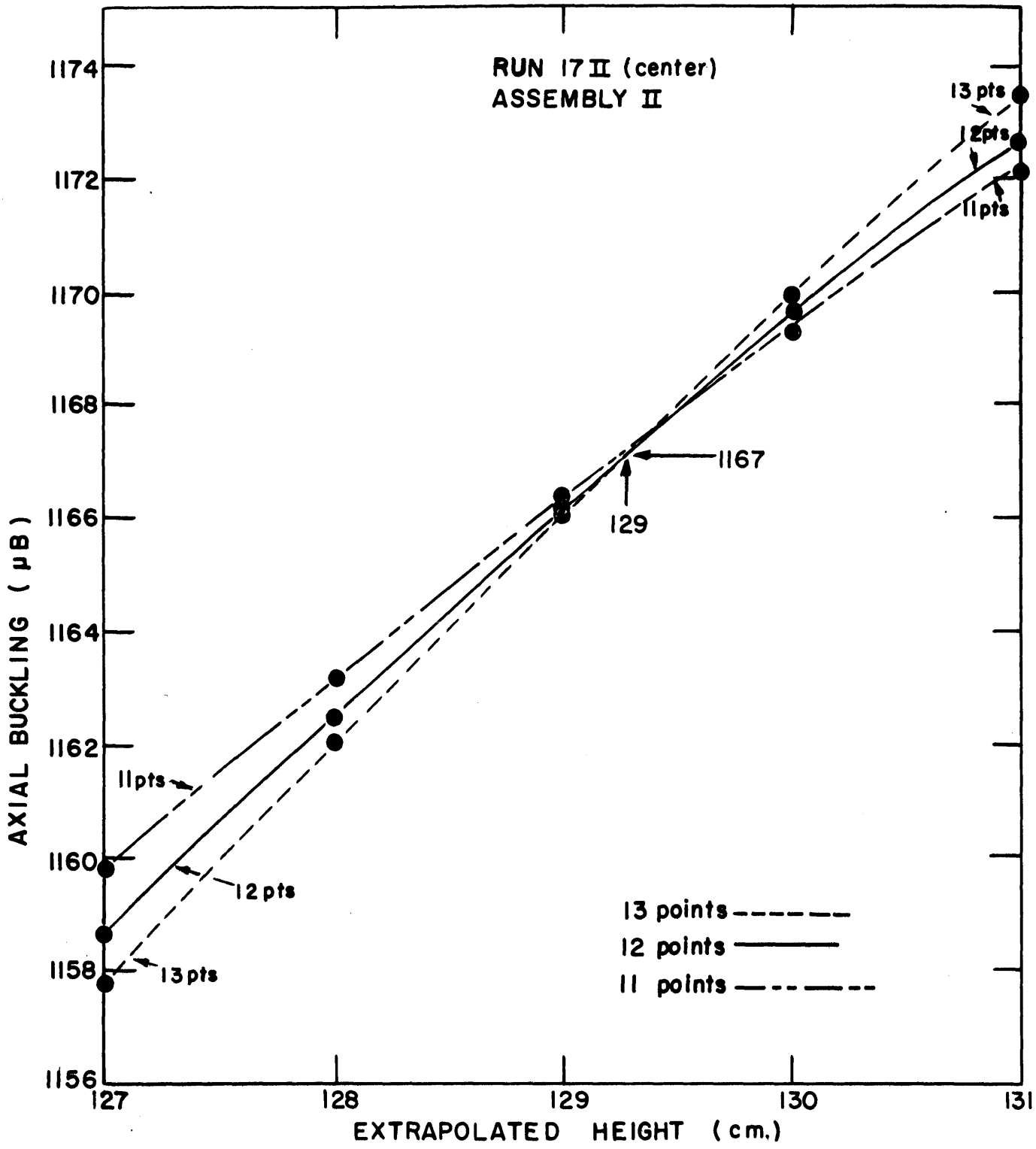

FIG. 4.1 AXIAL BUCKLING VERSUS EXTRAPOLATED HEIGHT

irradiated simultaneously in the hohlraum. A small correction to account for the different half-lives of Au^{198} and Np^{239} was also applied. The corrected neptunium activities were then used to calculate the U^{238}-cadmium ratio and ρ_{28}.

Since the decay of the fission product activity is not given by a simple exponential, but rather by a sum of exponentials, correction of the δ_{28} foils described in section 3.6.1 is not as straightforward. Use was made of the computer program designed for this purpose by Wolberg (W1). Input to the code includes the uncorrected counts and the times after irradiation for each count. The data for both depleted and natural foils are required. After corrections for background and foil weights are applied, a least squares fit is made to the natural uranium data to determine the time behavior of its activity. The natural foil activity at the times of the depleted foil counts is then estimated from the fitted polynomial. The ratio of depleted activity to natural activity $\Gamma(t)$ is found for each depleted foil pass. From other input data, including $P(t)$, the code uses Eq. 3.1 to compute δ_{28}.

4.3 Experimental Results

This section presents the results of the analyses of the data using the techniques described in the preceding section.

4.3.1 Axial Buckling

One of the prime assumptions made in the theory of Chapter II is the constancy of axial buckling with radial position in the assemblies. To test this assumption, axial traverses were made at several radial positions in assemblies II and V. If the assumption is true, then the

ratio of foil activities at equal heights for pairs of traverses should be a constant for each assembly and independent of radial position. However, if a small difference in axial buckling exists, and if an exponential shape is assumed in both radial positions, then the ratio of foil activities at equal heights would be:

$$\frac{Act_1(z)}{Act_2(z)} = A\ e^{\Delta\gamma z} \approx A(1+\Delta\gamma z)\ . \qquad (4.2)$$

Small differences of axial bucklings should then produce a straight line for the plot of activity ratio versus height.

Figures 4.2 and 4.3 show the plots of activity ratio versus axial position for experiments in Assemblies II and V. For the four cases shown, least squares fits to Eq. 4.2 gave values of $\Delta\gamma^2$ of $0.05 \pm .05\ \mu B$, $9 \pm 2\ \mu B$ (the first five points were dropped from the fit to produce a maximum buckling difference), $0.48 \pm 0.8\ \mu B$, and $0.52 \pm 1.5\ \mu B$, respectively. Of the four cases, only one produced a significant difference in buckling. No reason for this anomalous behavior is apparent and the traverse must therefore be suspect. In any case, the difference is within the uncertainty of axial buckling measurements (approximately 25 μB) and if such a difference did exist, it would not seriously affect the analyses of the two region assembly.

Axial bucklings for each of the assemblies are presented in Table 4.1. (The unit for buckling in this table and throughout this report is the microbuck (μB) equal to 10^{-6} inverse square centimeters.) The axial bucklings measured in full lattices for both the test and reference regions of each assembly are also given for purposes of

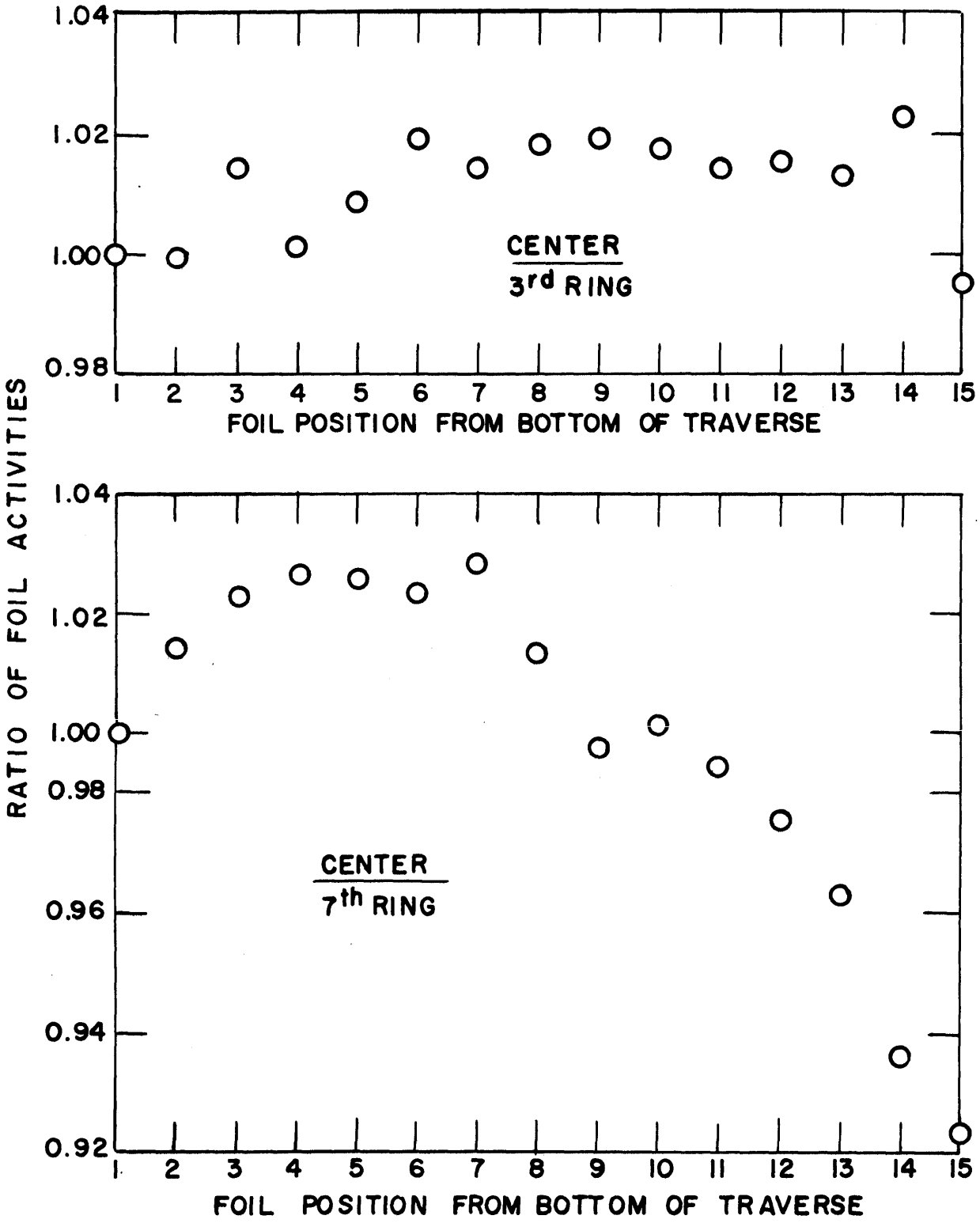

FIG. 4.2 RATIO OF AXIAL FOIL ACTIVITIES IN 3 RING ASSEMBLY-ASSEMBLY II (FIRST FOIL POSITION 32 cm. ABOVE BOTTOM OF FUEL; FOIL POSITIONS ARE 2.0 INCHES APART

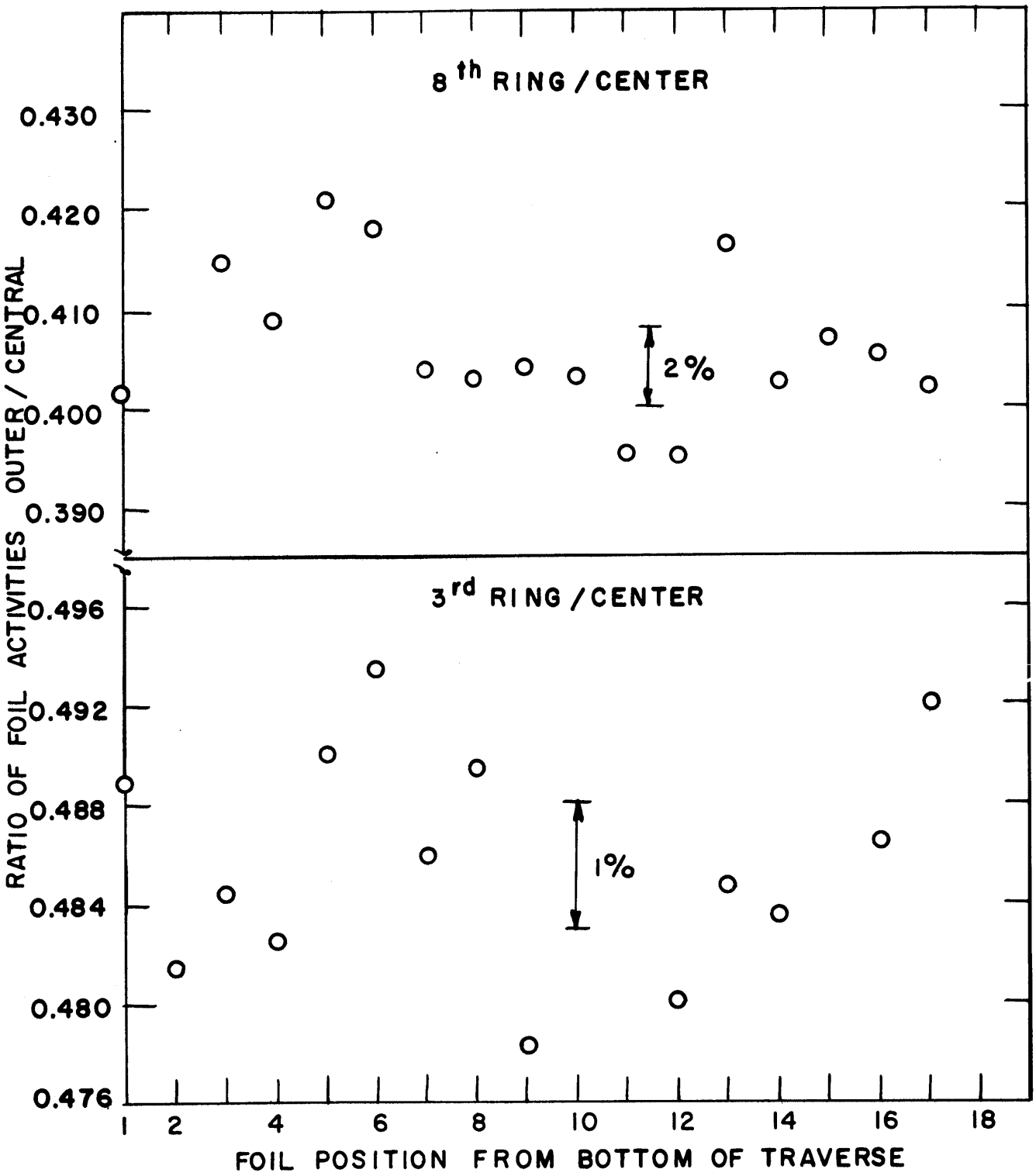

FIG. 4.3 RATIO OF AXIAL FOIL ACTIVITIES IN ASSEMBLY V AS A FUNCTION OF HEIGHT, (FIRST FOIL POSITION 22 cm. ABOVE BOTTOM OF FUEL; FOIL POSITIONS ARE 2.0 INCHES APART)

TABLE 4.1

Axial Bucklings in Two Region Assemblies

Assembly Designation	Full Lattice Values		Assembly Axial Buckling (μB)
	Test Region (μB)	Reference Region (μB)	
I	1525	1167	1192
II	1525	1167	1183
III	1525	1167	1281
IV	1167	1525	1299
V	1396	948	1051
VI	1396	948	1112
VII	1200	1013	1006
VIII	1200	1013	1074
IX	1525	1395	1204
X	1525	1395	1200
XI	547*	277*	380*

*Four-foot-diameter lattice tank

comparison. Uncertainties in the measured values are about 25 μB.

In general, the two region assembly value falls between those of the corresponding full lattices. Assemblies IX and X are notable exceptions. A qualitative explanation for this behavior may be obtained by considering Figure 4.4 which shows the variation of full lattice axial bucklings with lattice pitch for the 0.75-inch-diameter and 0.25-inch-diameter fuel rods. (The axial bucklings for this figure were taken from results of full lattice experiments. The experimental results were corrected where necessary to a three-foot-diameter lattice tank.) Since the effect of reducing the fraction of fuel by forming a two-region assembly should have the same qualitative effect as reducing the lattice pitch in a single region lattice, the assembly axial buckling should fall somewhere on a nonlinear curve joining the values of the lattices composing the assembly. A definite minimum is to be expected in such a curve, based on consideration of the single region curves of Figure 4.3. This same effect is not evident in the other assemblies because the individual lattices are either close to or on the same side of the inflection in the buckling curve.

4.3.2 Gold Radial Traverses

This section presents the results of bare and cadmium-covered gold foil traverses made in the radial direction in each of the eleven assemblies. The first figure for each assembly shows the cadmium ratio as a function of radial position, while the second figure gives the epicadmium and subcadmium foil activities on an arbitrary scale.

With the exception of Assembly I, the cadmium ratios for all the

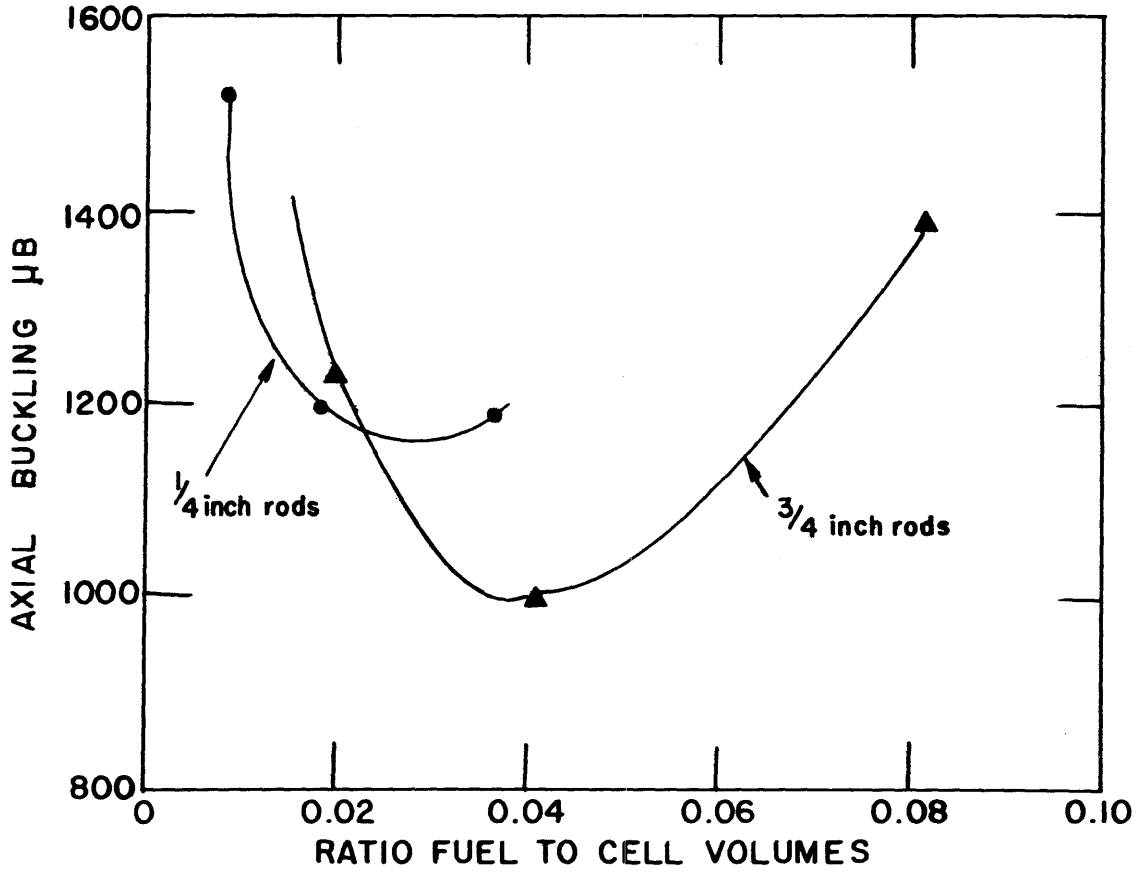

FIG.4.4 AXIAL BUCKLING FOR 0.25 INCH DIAM. 1.027 % ENRICHED RODS AND 0.75 INCH DIAM. 0.997 % ENRICHED RODS IN 3 FOOT DIAM. LATTICE TANK.

assemblies are for 1/4-inch-diameter, 0.010-inch-thick gold foils. In each of these assemblies, at least two traverses of each type were made and, since foil positions on the holder used were symmetrical about the holder center, each bare and cadmium-covered foil activity, with the exception of that for the center foil position, is the result of counting four foils. This procedure resulted in an average standard error of approximately one percent for the cadmium ratios.

In Assembly I, only one set of traverses was made with an unsymmetrical foil holder using 1/16-inch-diameter, 0.010-inch-thick gold foils. The uncertainty for these cadmium ratios is estimated to be about three percent. The effect of a slight horizontal misalignment of the foil holder in these runs is apparent from the oscillation in the resulting cadmium ratios shown in Figure 4.5. (Alternate cadmium ratios in the traverse were calculated from foils on one side of the foil holder center.) This uncertainty in positioning, the nonsymmetry of the foil holder, and the error introduced by weighing the smaller foils, led to the adoption of the foil holder used in subsequent assemblies.

In general, the shapes of the experimental curves are not unexpected from the composition of the assemblies. In Assembly I, where the center region has a larger pitch than the outer region, a flattening of the epicadmium flux in the center region is evident. Fast neutrons born in this region are relatively few and the contribution of the outer region to the epicadmium flux is considerable, especially near the boundary between regions. This tends to flatten the radial distribution. On the other hand, the greater diffusion length in the center region

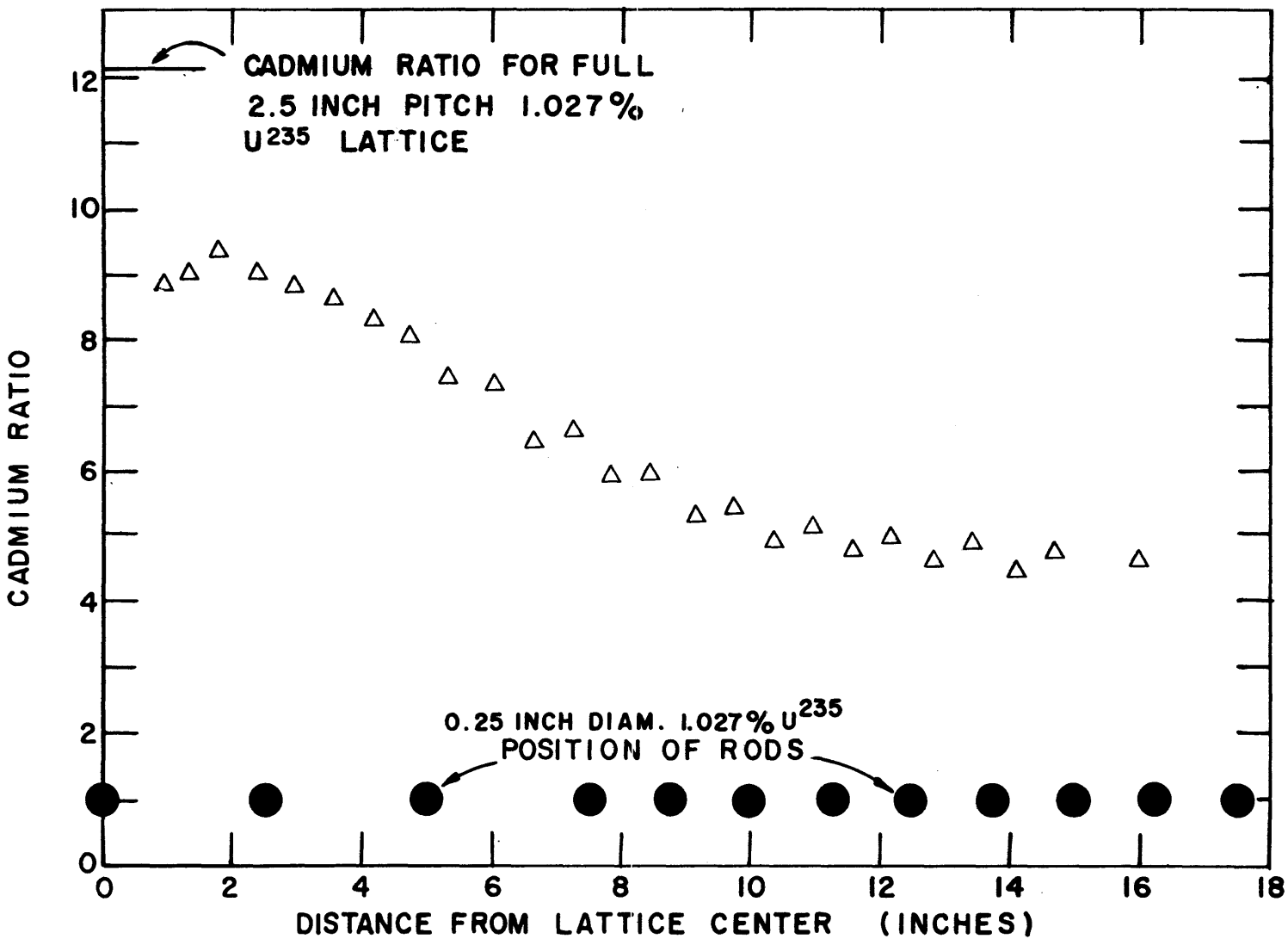

FIG. 4.5 GOLD CADMIUM RATIOS IN ASSEMBLY I

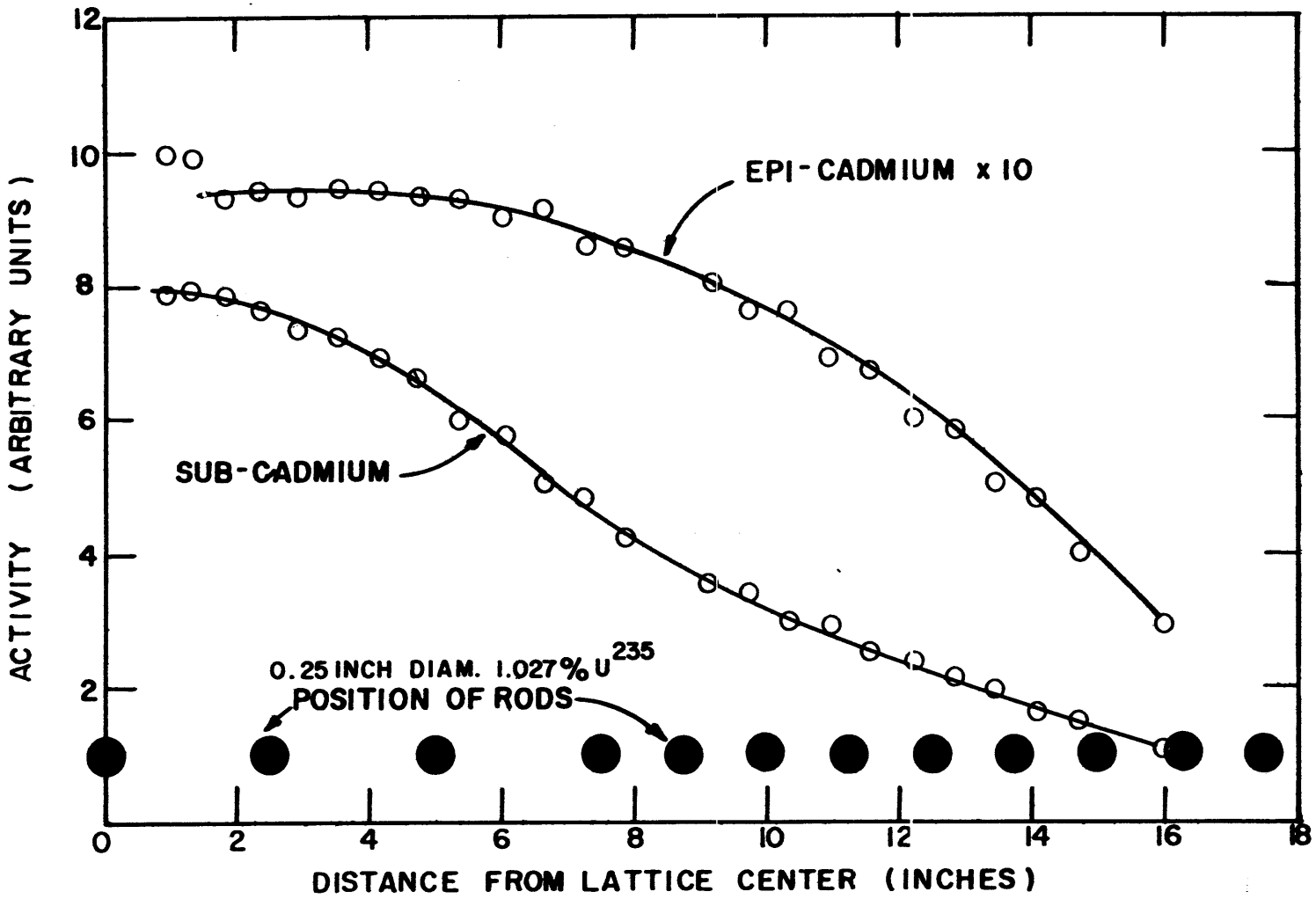

FIG. 4.6 GOLD FOIL ACTIVITIES IN ASSEMBLY I

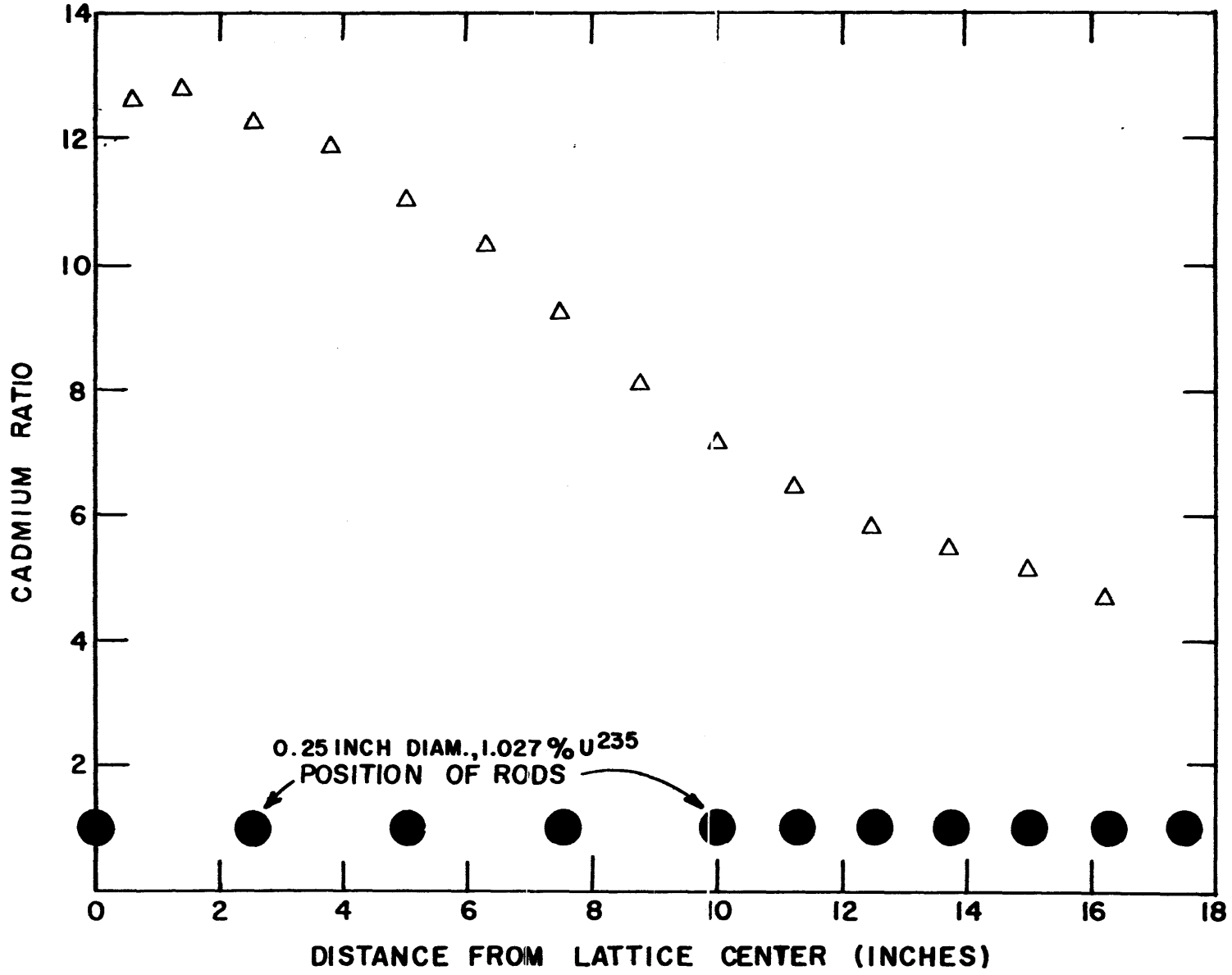

FIG. 4.7 GOLD CADMIUM RATIO IN ASSEMBLY II

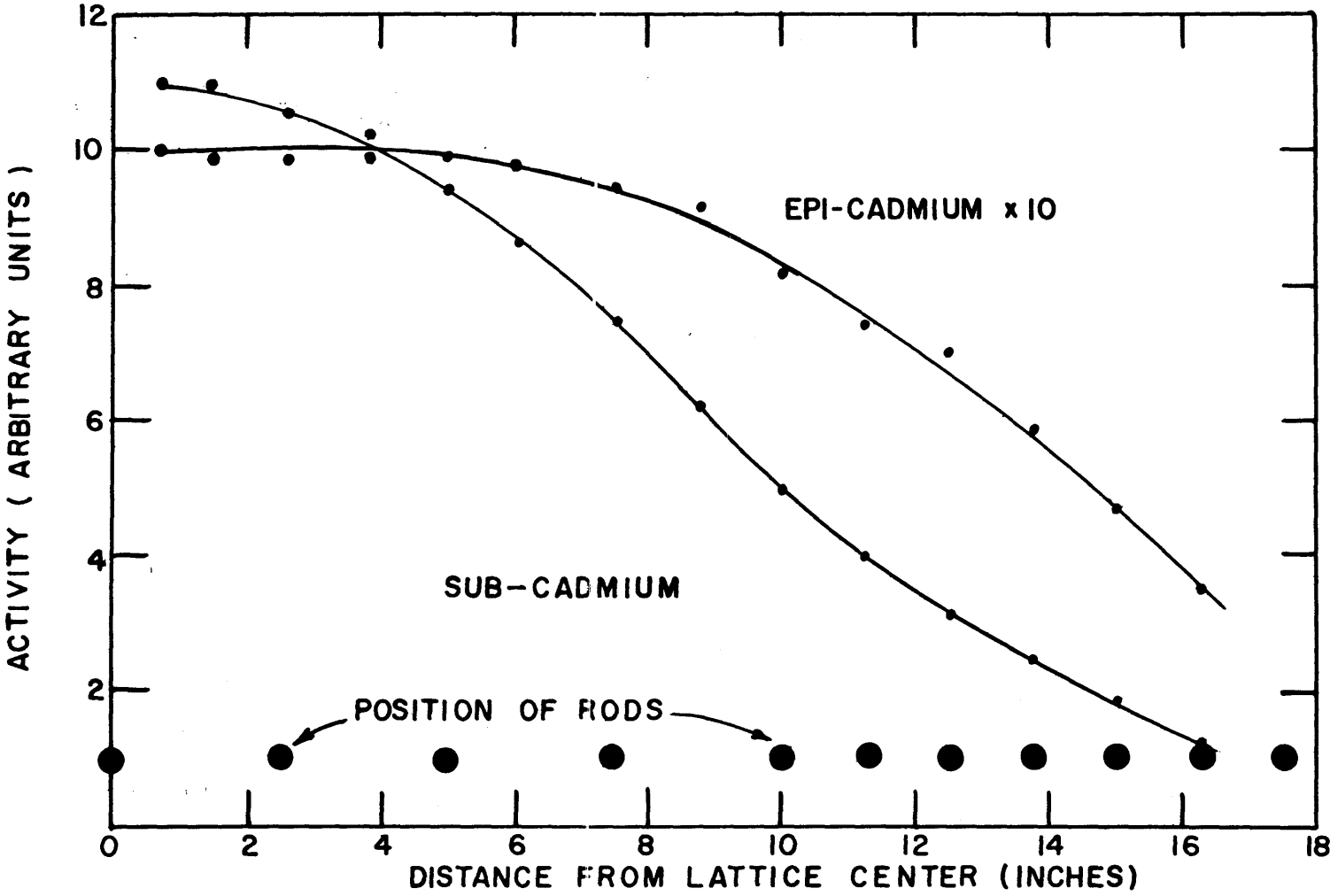

FIG. 4.8 GOLD FOIL ACTIVITIES IN ASSEMBLY II

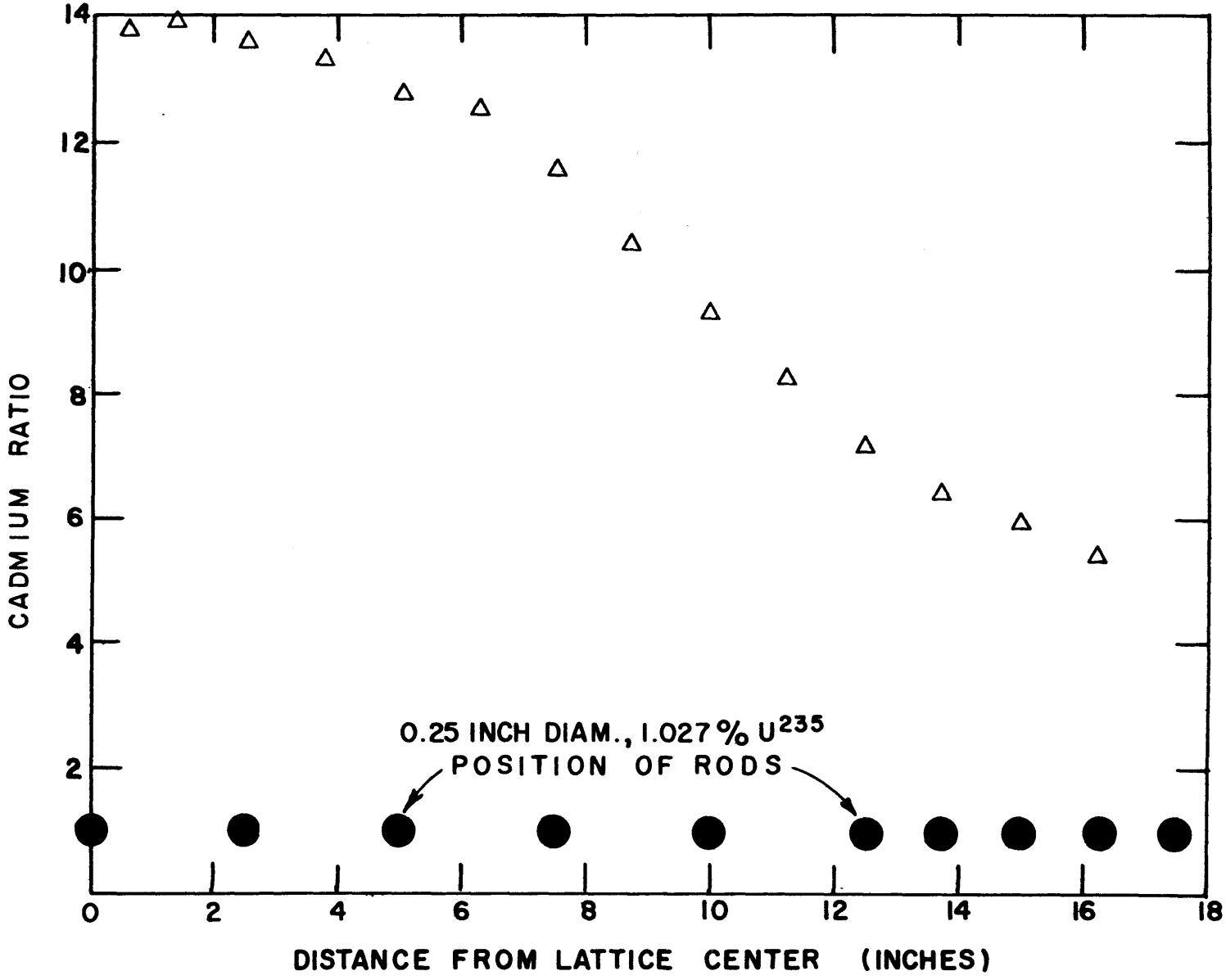

FIG. 4.9 GOLD CADMIUM RATIO IN ASSEMBLY III

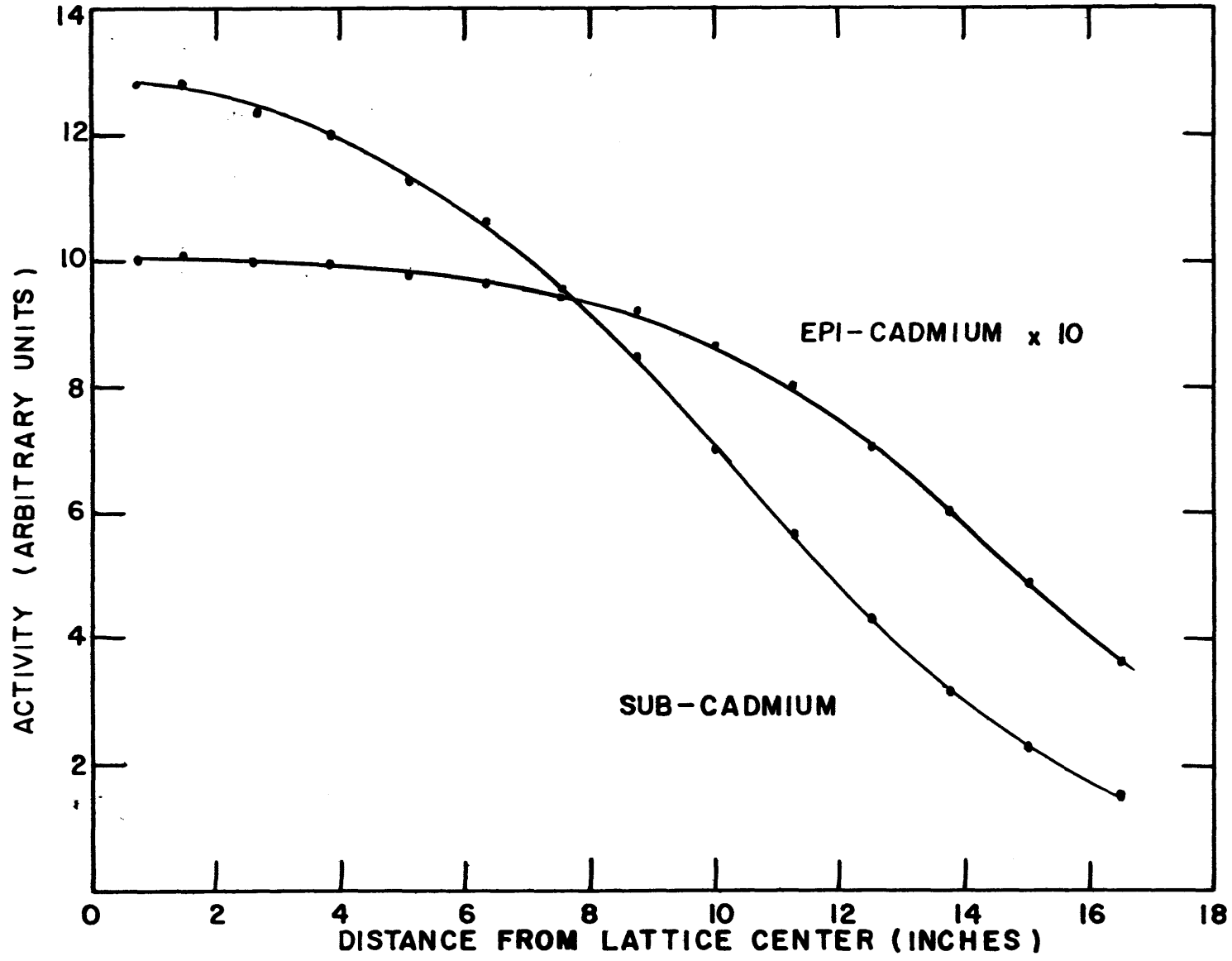

FIG. 4.10 GOLD FOIL ACTIVITIES IN ASSEMBLY III

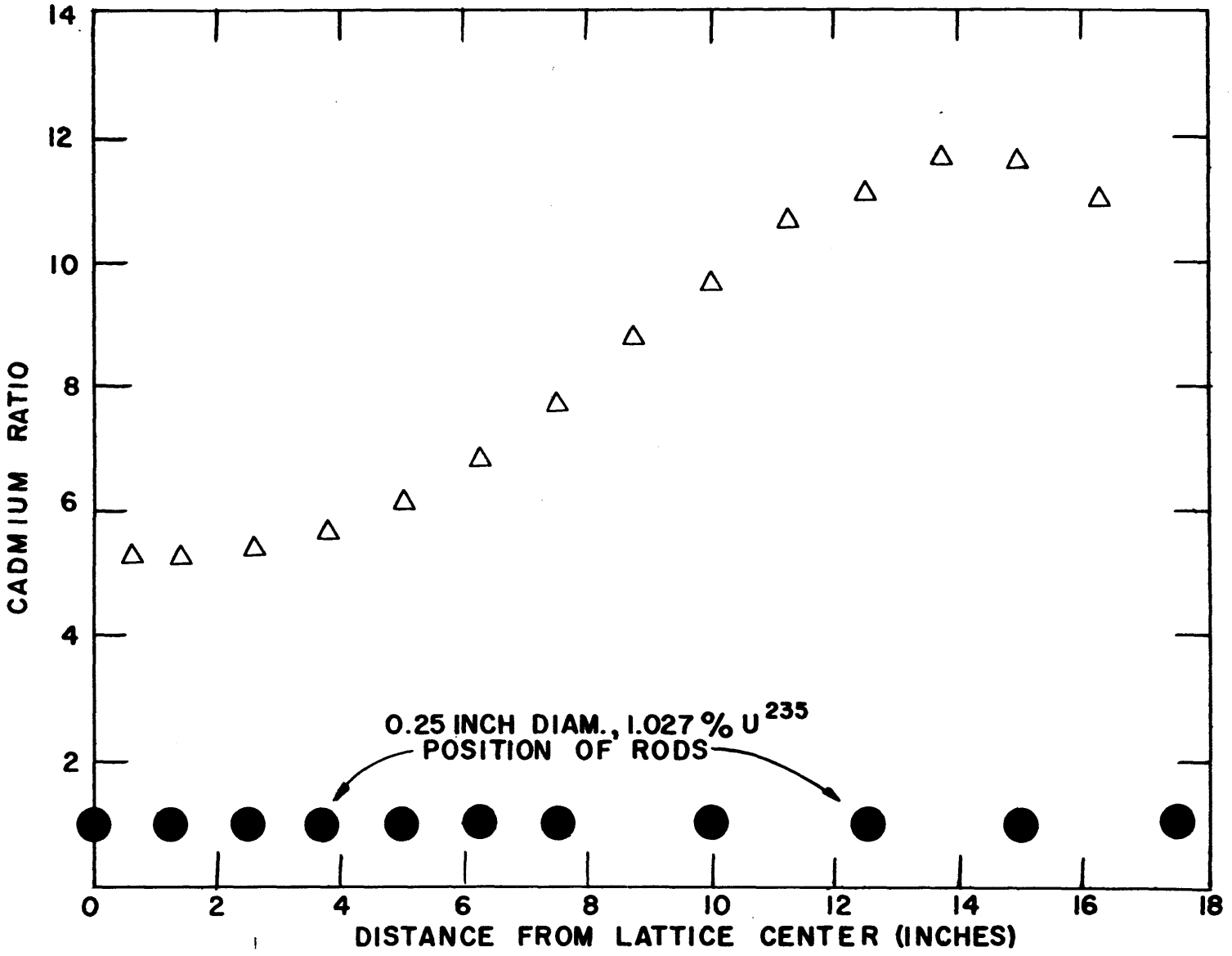

FIG. 4.11 GOLD CADMIUM RATIO IN ASSEMBLY IV

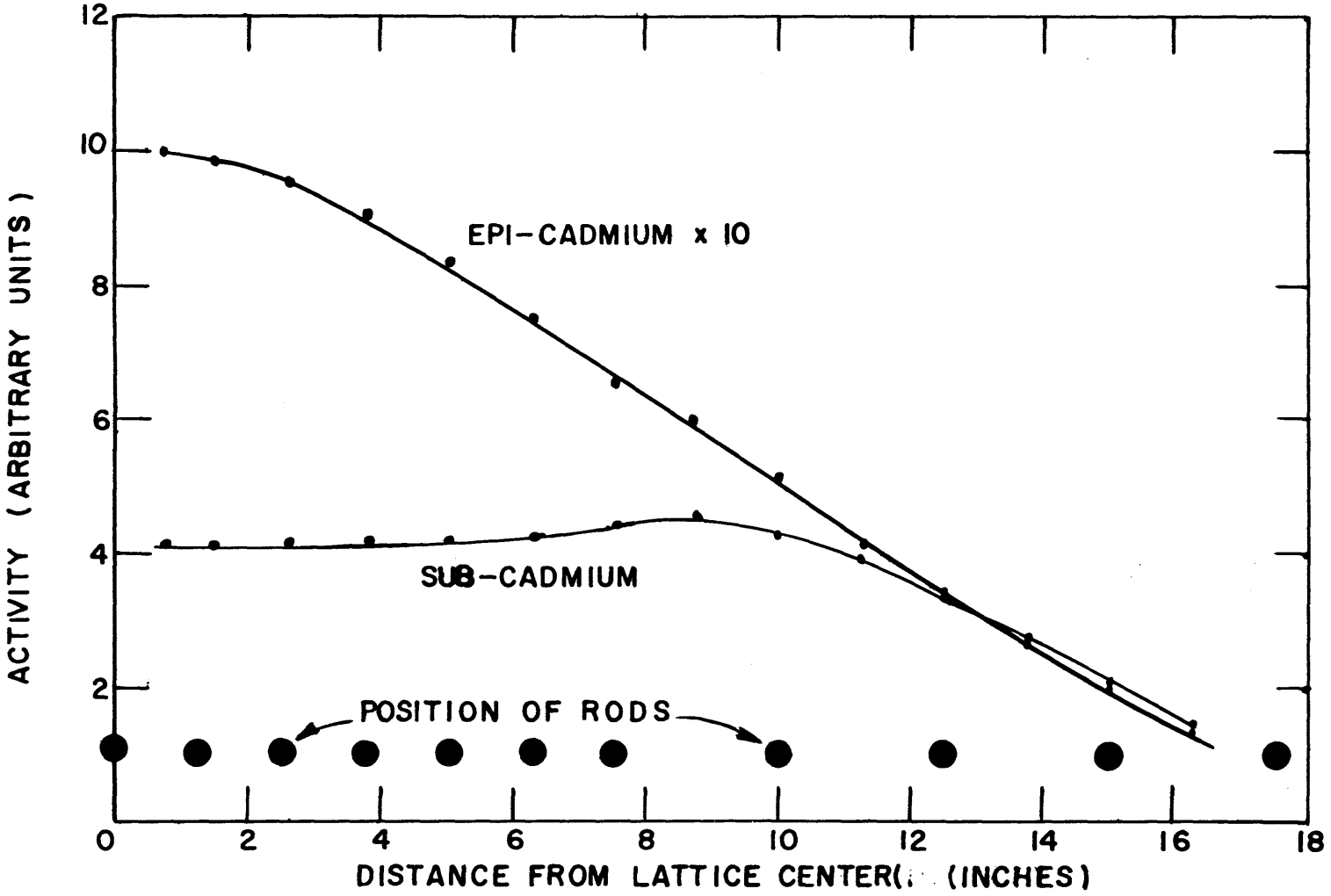

FIG. 4.12 GOLD FOIL ACTIVITIES IN ASSEMBLY IV

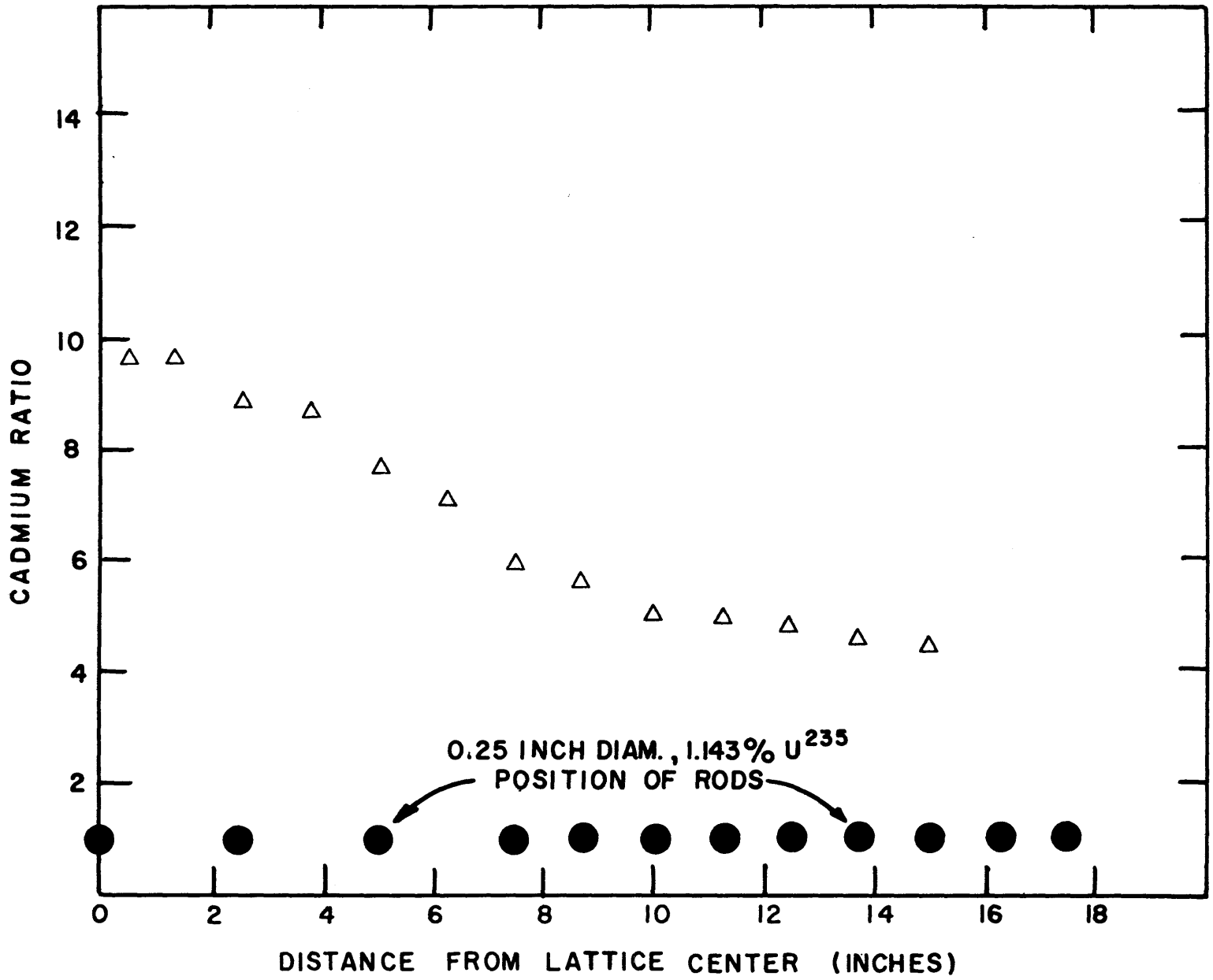

FIG. 4.13 GOLD CADMIUM RATIO IN ASSEMBLY V

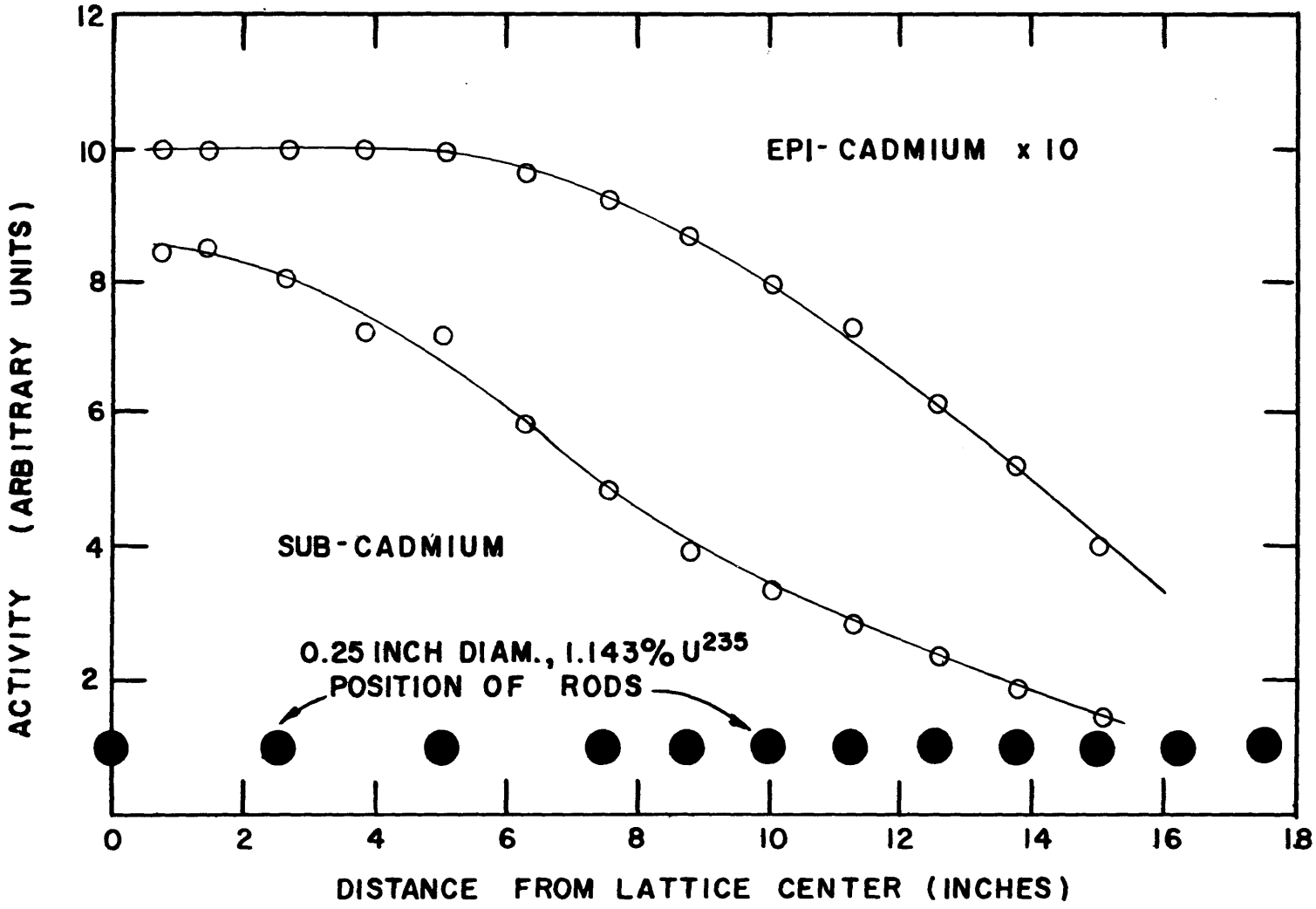

FIG. 4.14 GOLD FOIL ACTIVITIES IN ASSEMBLY V

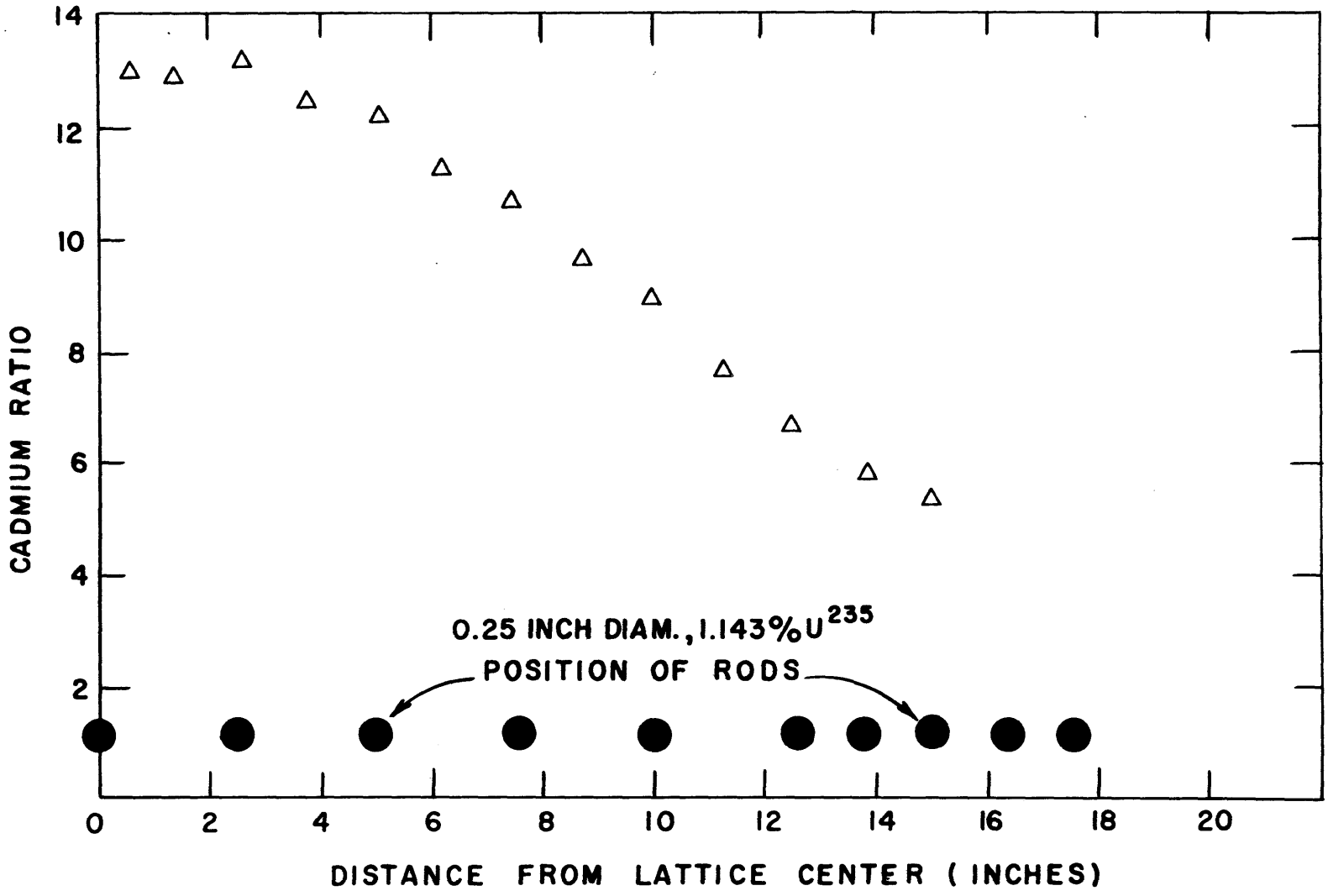

FIG. 4.15 GOLD CADMIUM RATIO IN ASSEMBLY VI

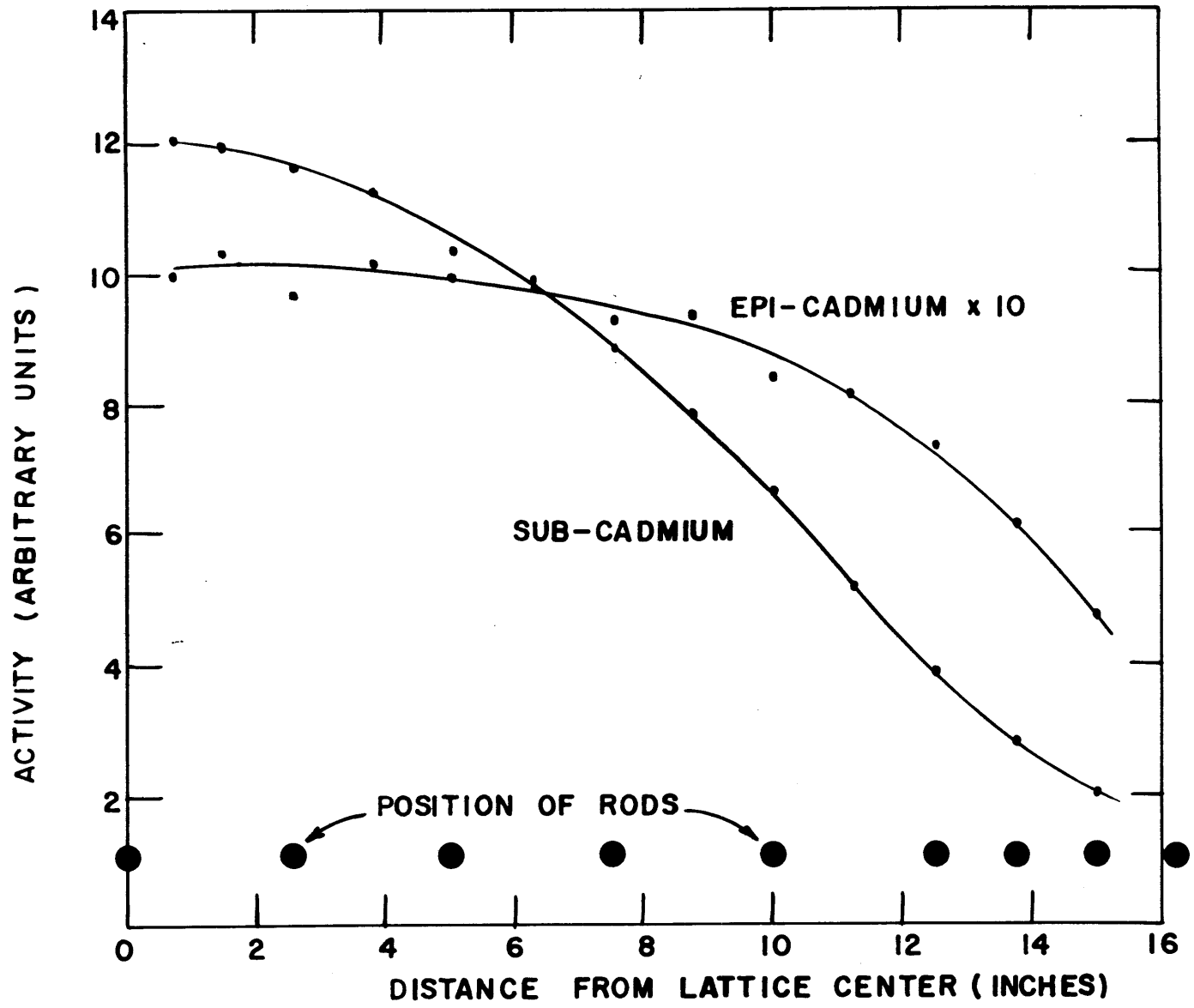

FIG. 4.16 GOLD FOIL ACTIVITIES IN ASSEMBLY VI

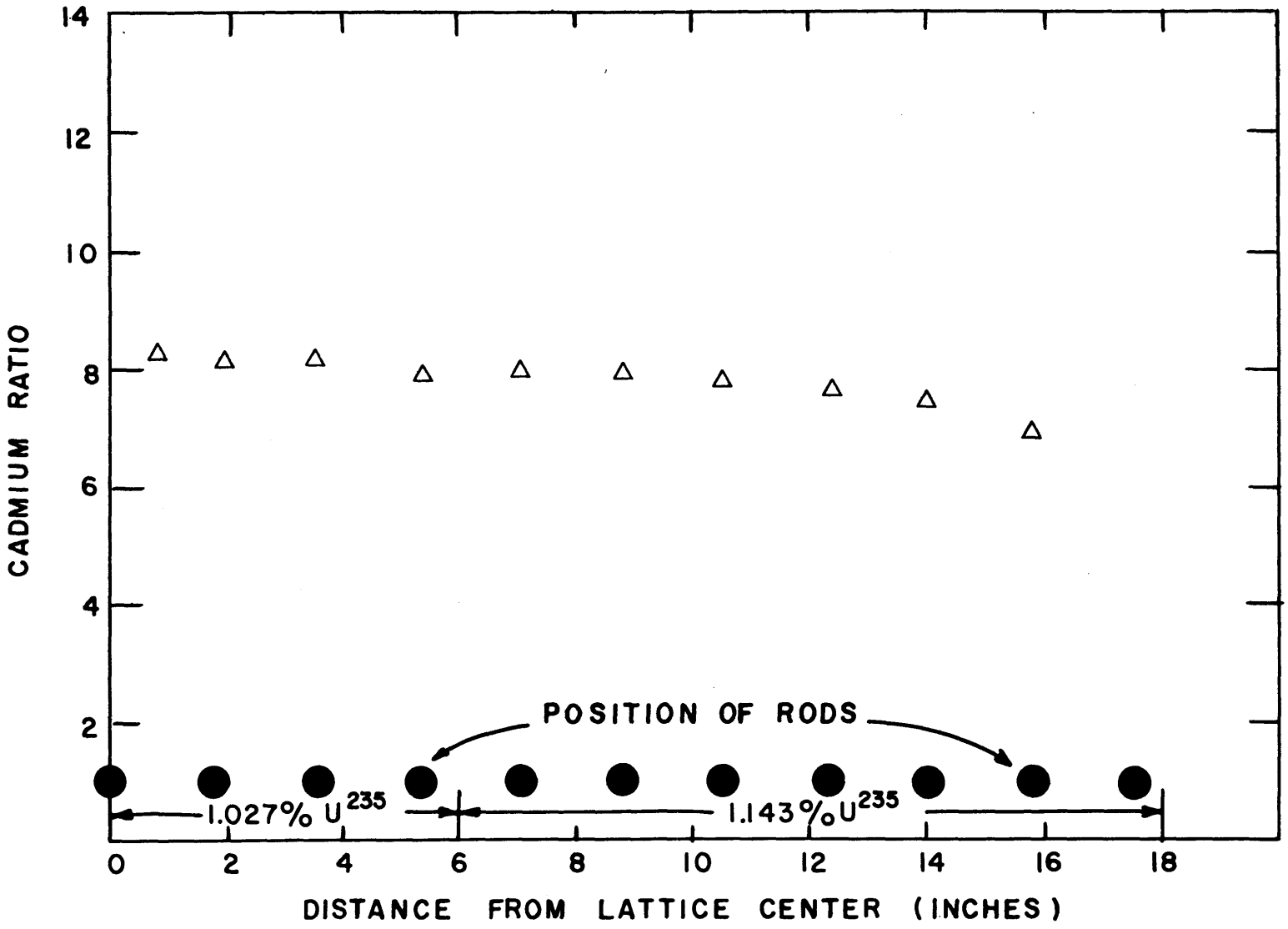

FIG. 4.17 GOLD CADMIUM RATIOS IN ASSEMBLY VII

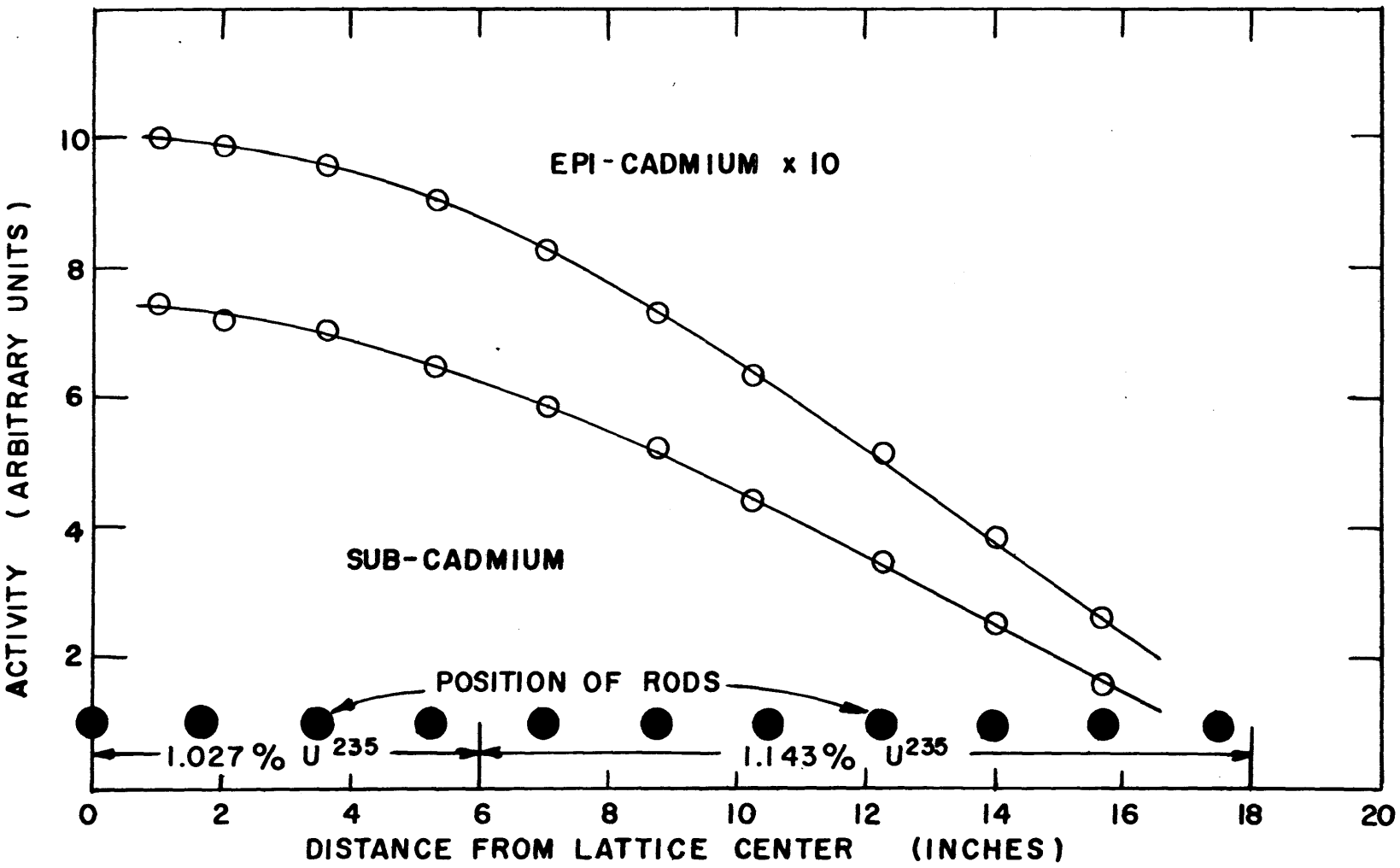

FIG. 4.18 GOLD FOIL ACTIVITIES IN ASSEMBLY VII

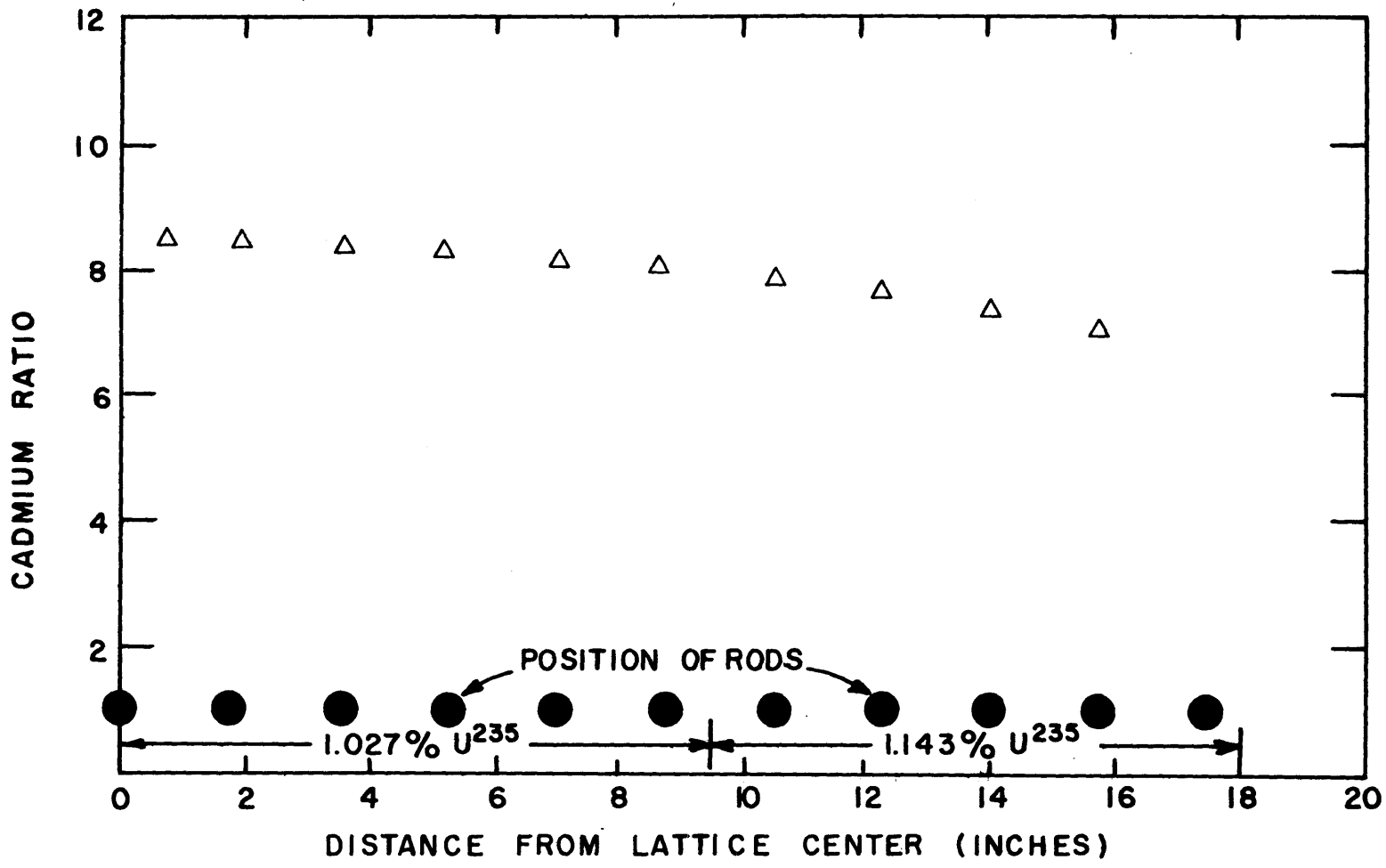

FIG. 4.19 GOLD CADMIUM RATIOS IN ASSEMBLY VIII

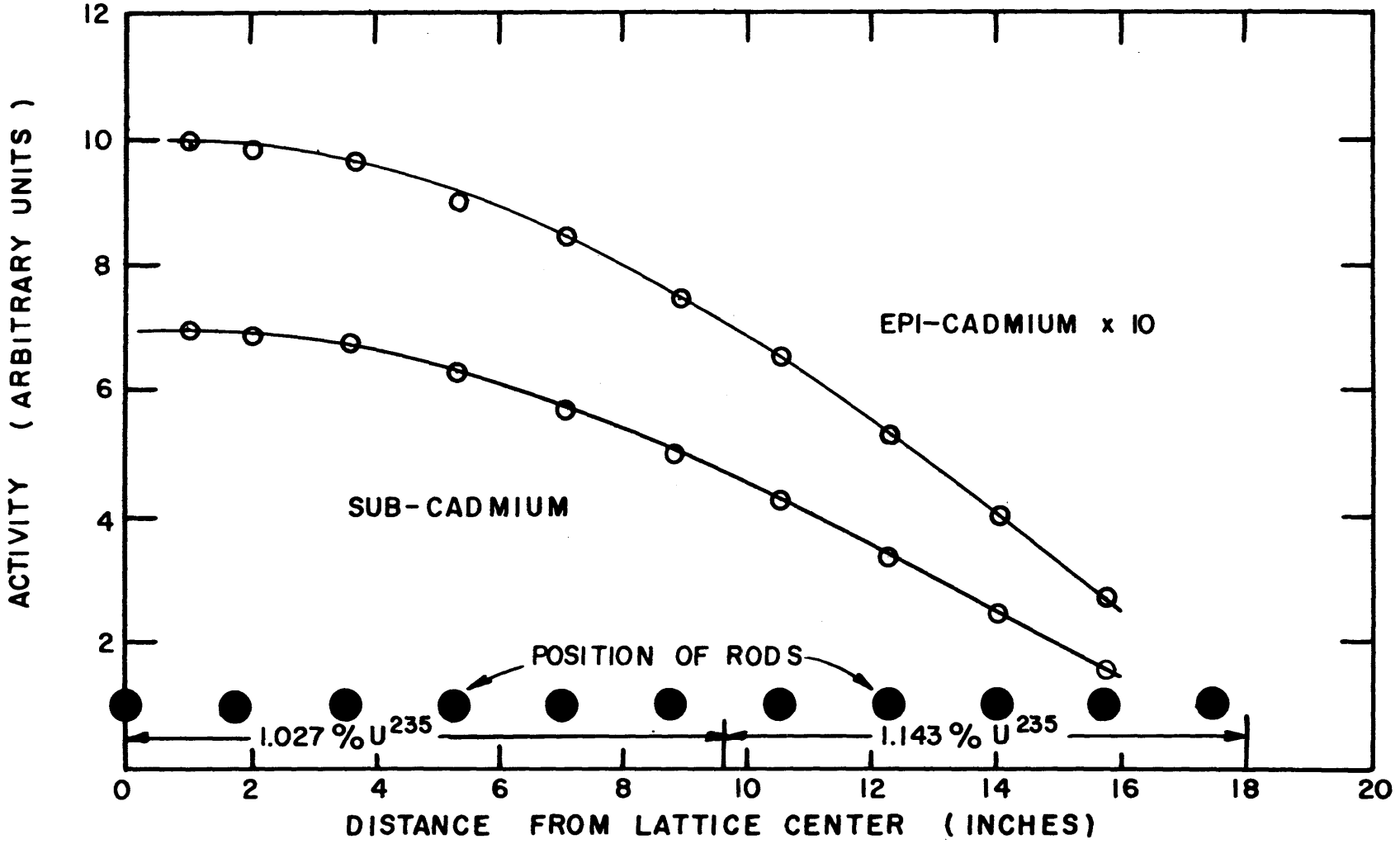

FIG. 4.20 GOLD FOIL ACTIVITIES IN ASSEMBLY VIII

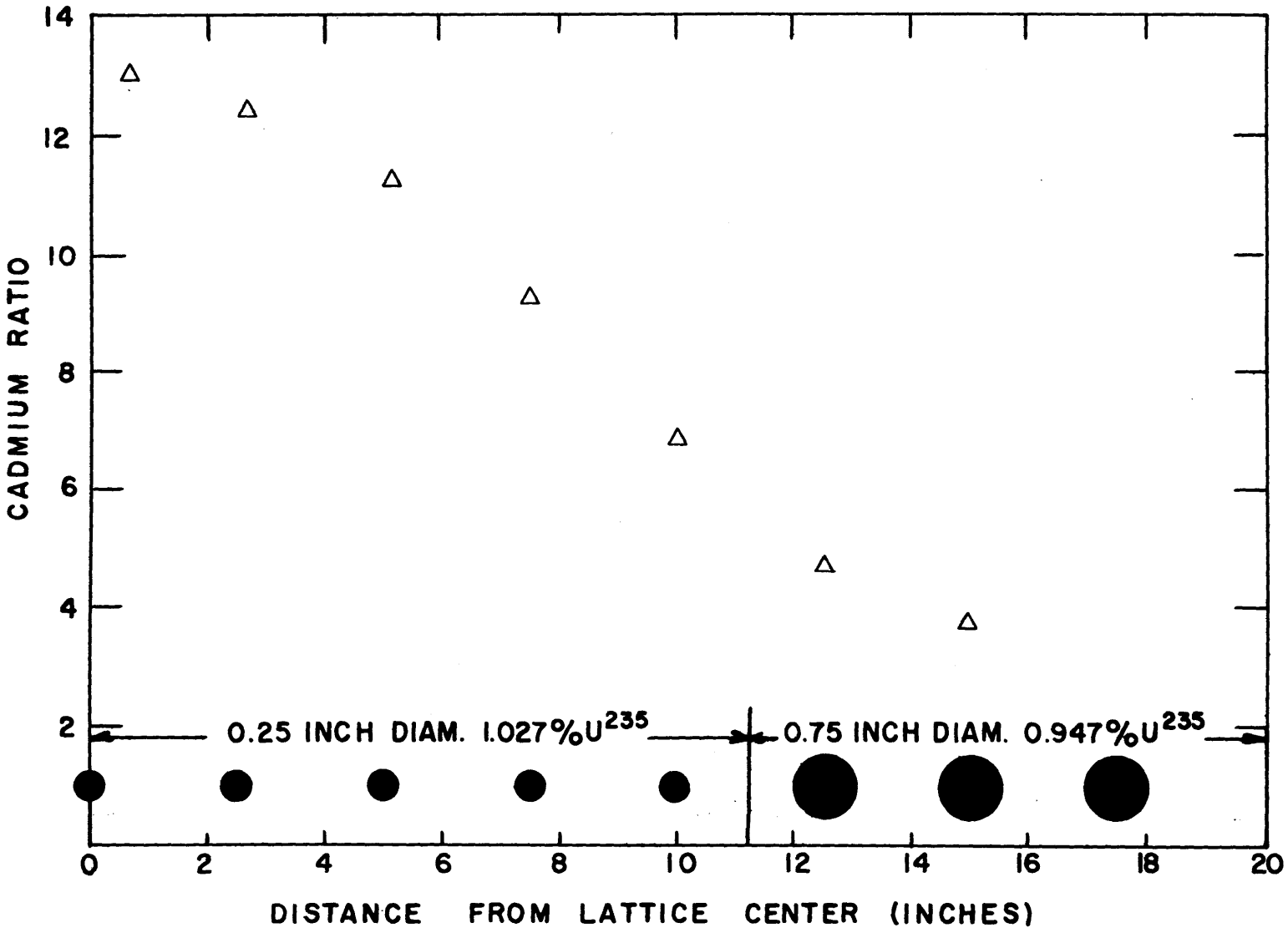

FIG. 4.21 GOLD CADMIUM RATIOS IN ASSEMBLY IX

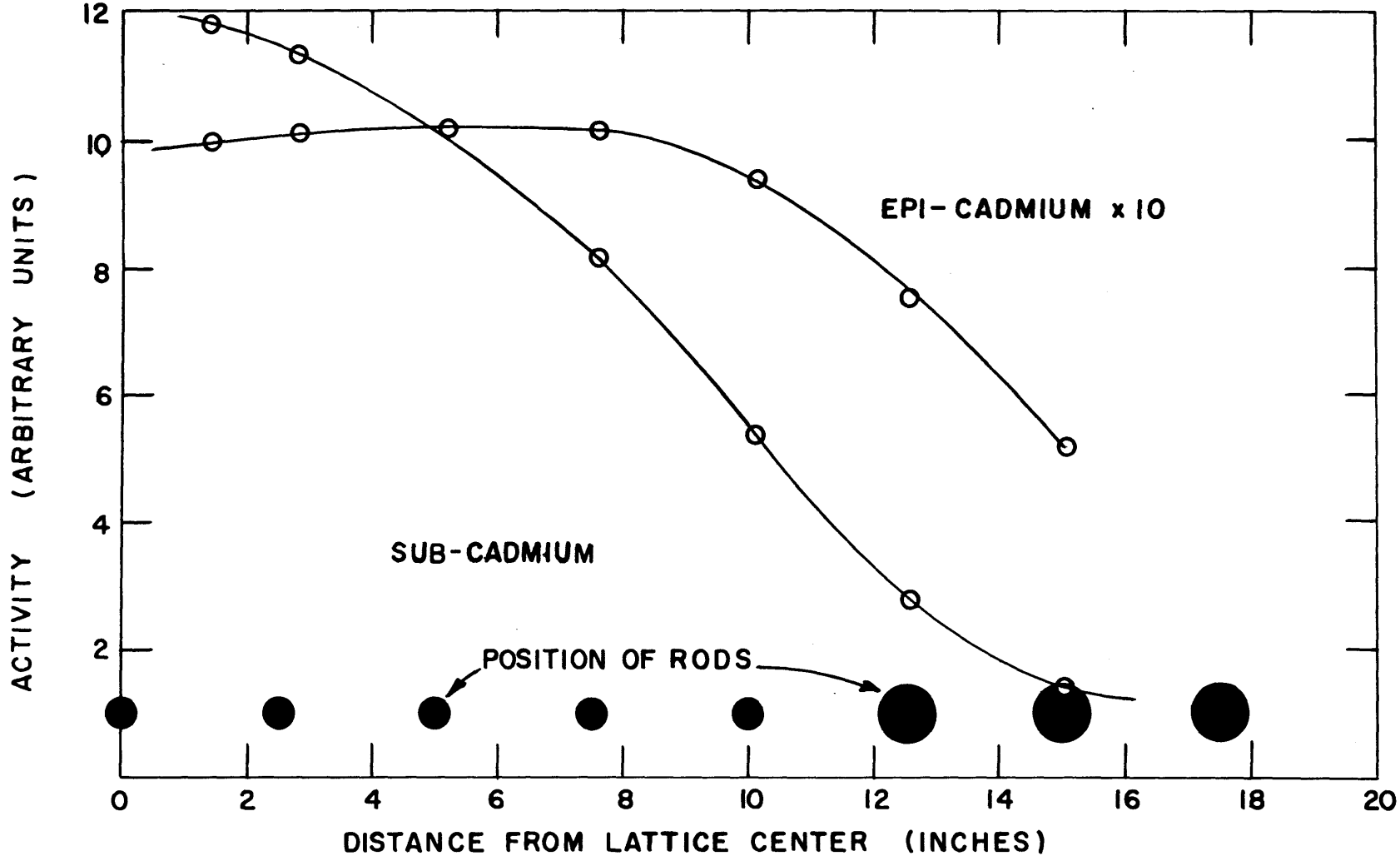

FIG. 4.22 GOLD FOIL ACTIVITIES IN ASSEMBLY IX

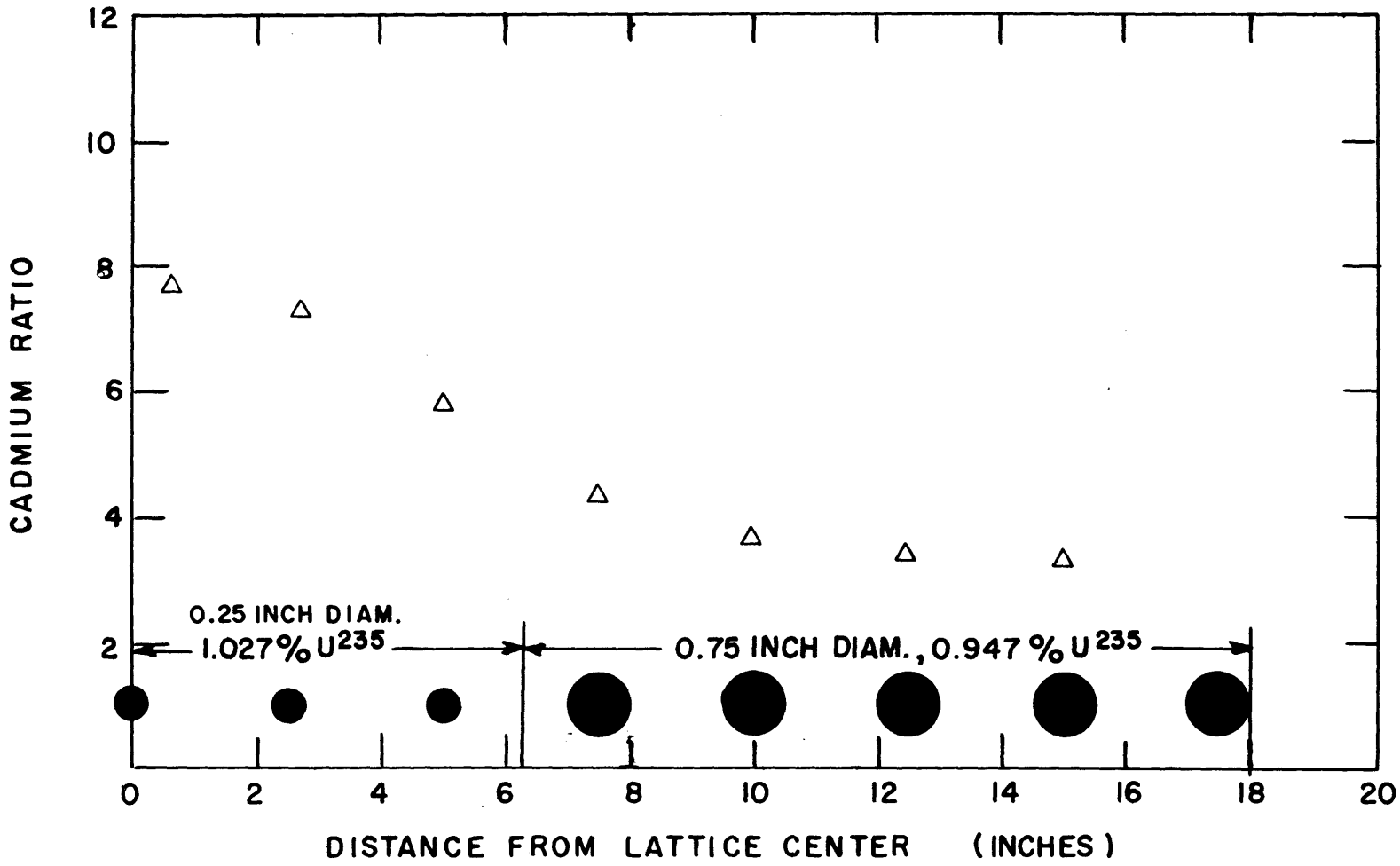

FIG. 4.23 GOLD CADMIUM RATIOS IN ASSEMBLY X

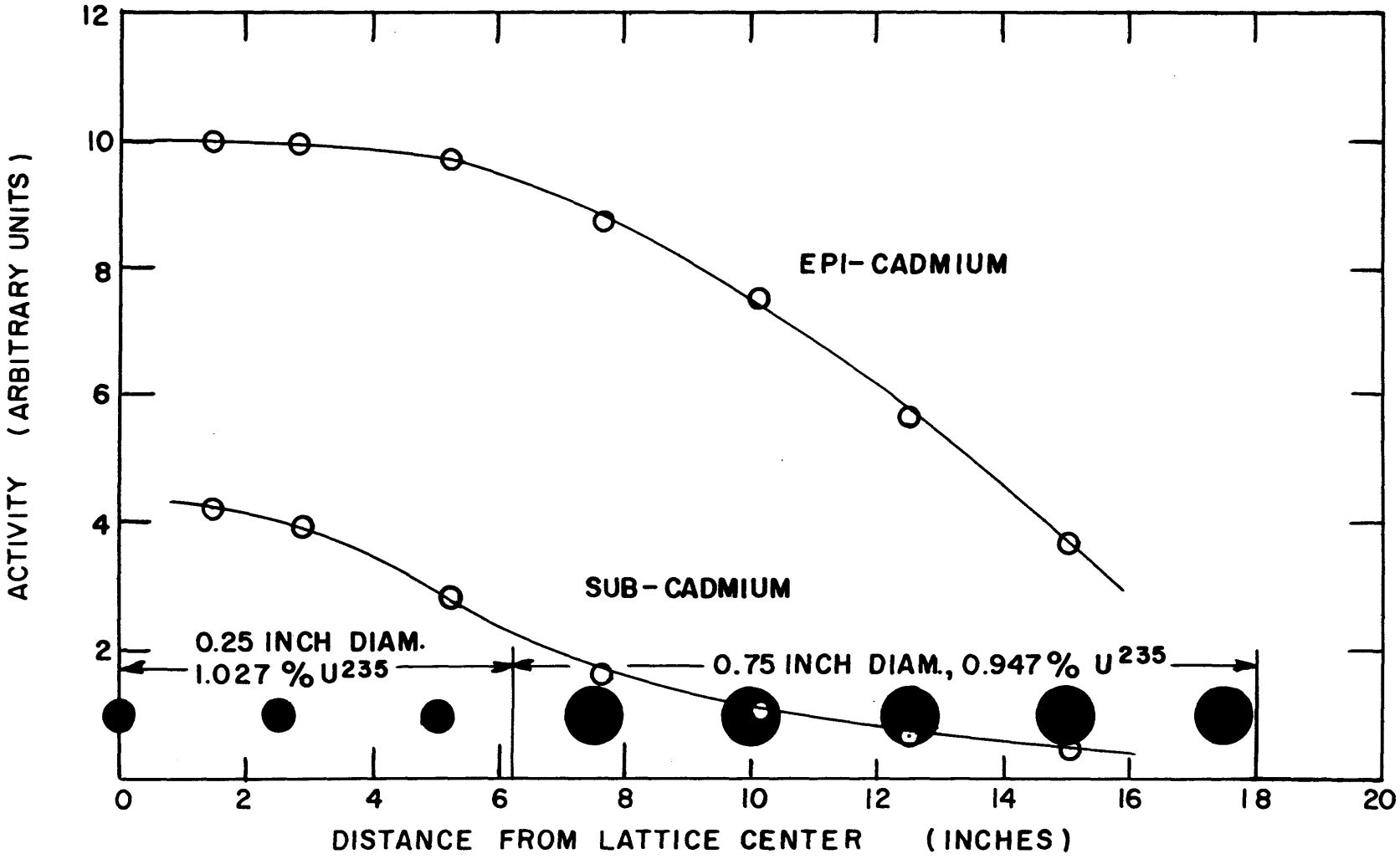

FIG. 4.24 GOLD FOIL ACTIVITIES IN ASSEMBLY X

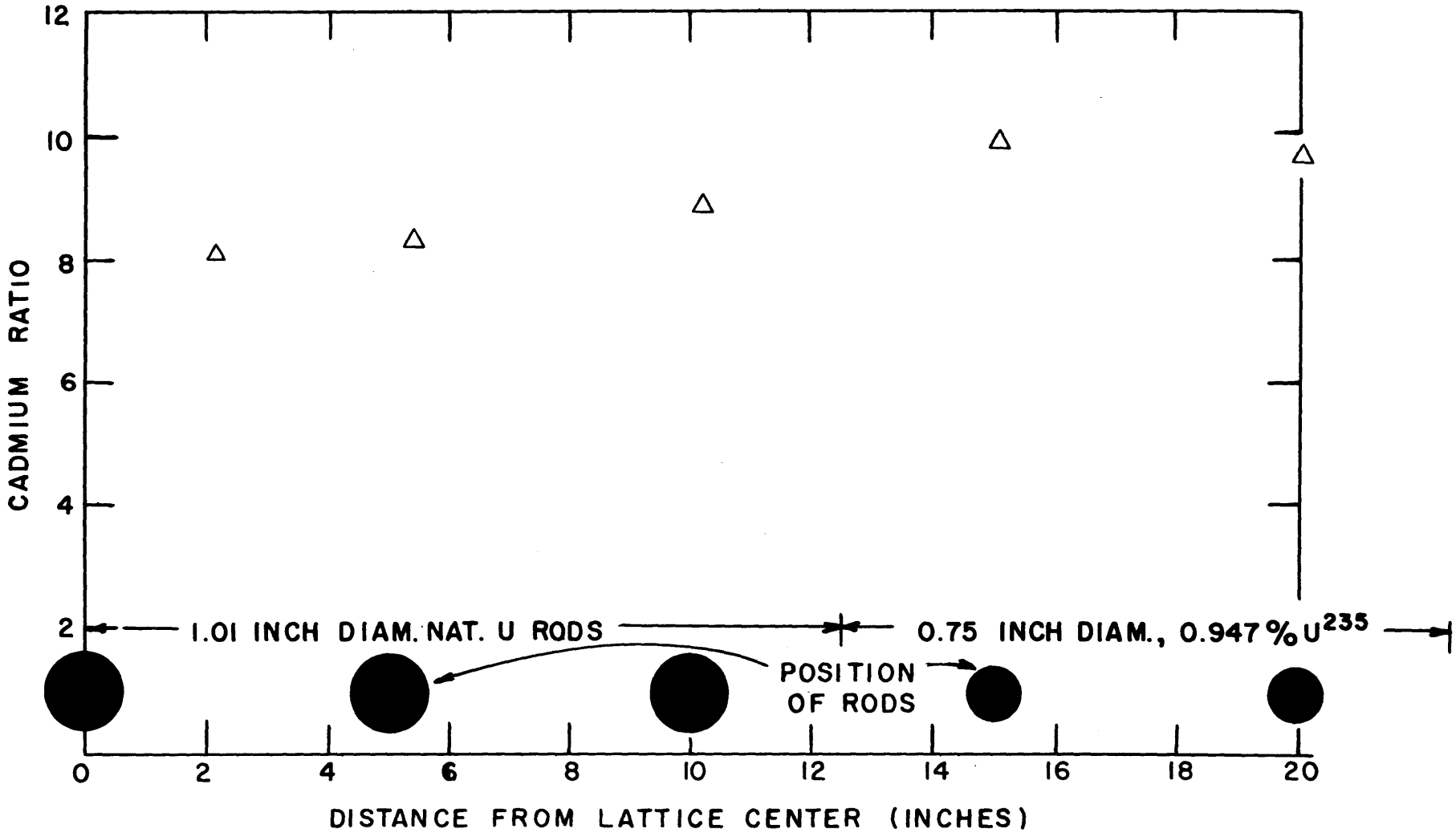

FIG. 4.25 GOLD CADMIUM RATIOS IN ASSEMBLY XI

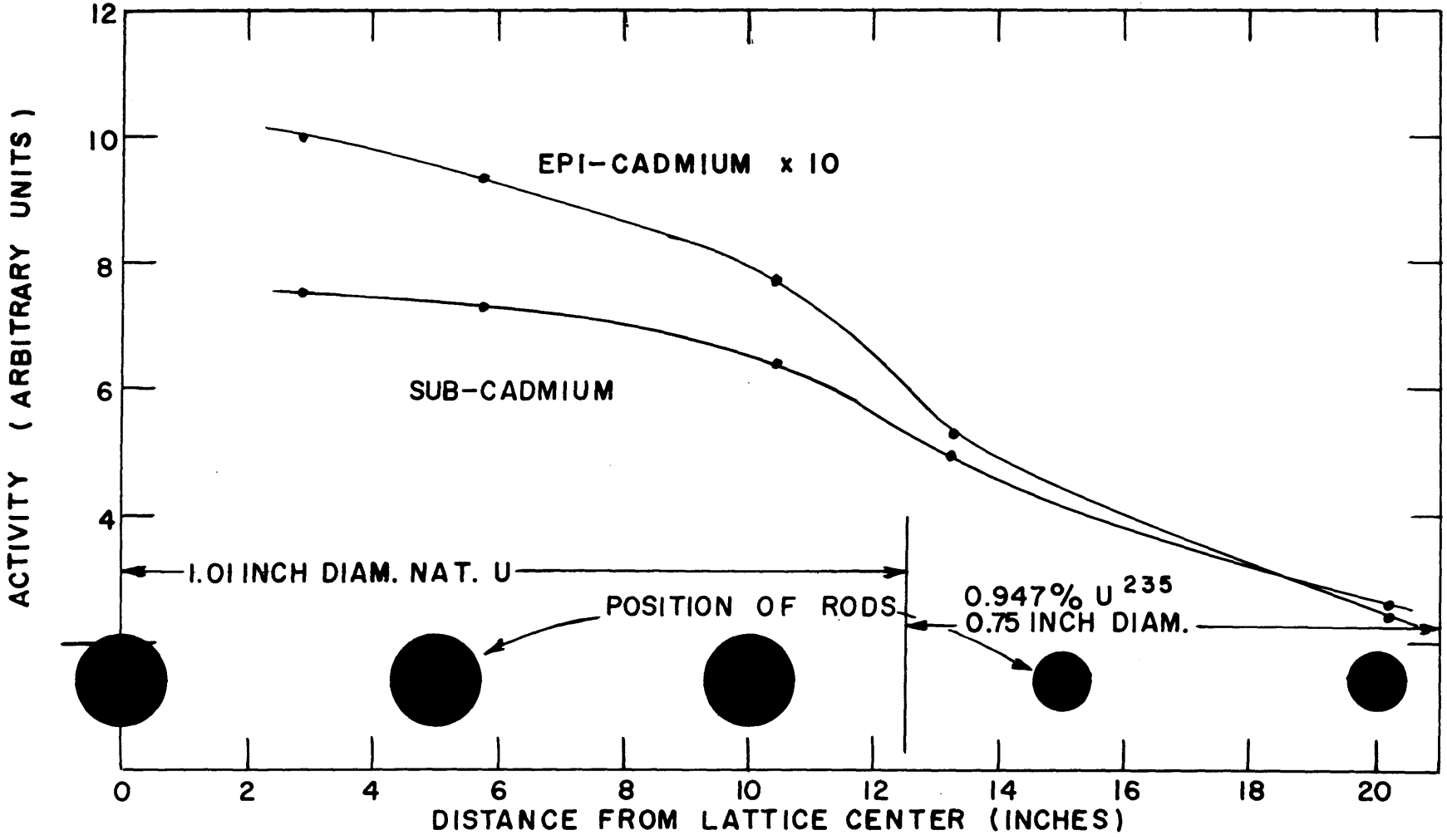

FIG. 4.26 GOLD FOIL ACTIVITIES IN ASSEMBLY XI

allows the thermal flux to peak. As the center region radius is increased in Assemblies II and III, the region of flattened epicadmium flux increases proportionately.

The regions of Assembly IV are reversed from those of the preceding assemblies. The subcadmium flux is now depleted in the center region due to higher thermal absorption, and evidence of a "reflector" peak formed by the greater moderating properties of the outer region can be seen just outside the boundary between the regions.

Assemblies V and VI are very similar to Assemblies I and III, differing only slightly in fuel enrichment. Flux shapes are therefore almost identical.

Very little difference exists between the properties of inner and outer regions of Assemblies VII and VIII. The traverses in these assemblies show little difference from those of a single region lattice.

The inner region of Assembly IX is poorer in fuel than the outer region. In this case, not only is the epicadmium flux flattened in the center region, but a definite increase is noticeable in Figure 4.22 as the outer region is approached. The smaller test region of Assembly X does not allow any similar increase to be observed in Figure 4.24.

The small differences in enrichment and in fuel size between the regions of Assembly XI are not sufficient to produce large perturbations in the flux distributions. The larger cadmium ratio in the outer region, however, is evidence of the lower fuel-to-moderator ratio.

4.3.3 U^{238}-Cadmium Ratios

Cadmium ratios of U^{238} inside the fuel rods were measured as a function of radial position in Assemblies III and IV. The results of these measurements are shown in Figures 4.27 and 4.28. In all other assemblies, with the exception of Assembly II, measurements were made in the center fuel rod only, and the results are given in Table 4.2. Each value shown is the average of two independent measurements, and the error quoted is the standard deviation. For comparison, the value in a full lattice of test region composition is also given. These single region values are from reference H5.

The same qualitative tendencies, evident in the gold-cadmium ratio results, are noticeable for the U^{238} values. (Compare Figure 4.27 with Figure 4.9 and Figure 4.28 with Figure 4.11.) As would be expected, the deviation from the single region values is smaller, the larger the test region, indicating a greater approach to the desired neutron spectrum.

4.3.4 δ_{28} Measured in Two Region Assemblies

Because of other research being done using the M. I. T. Lattice Facility, the time available for two region assemblies was usually limited to five days for each assembly. Occasionally, a complete set of measurements could not be obtained in this time. For this reason, δ_{28} was not measured in Assemblies I, V and VI. Measurements of δ_{28} were made in the central fuel element of all other assemblies. In most cases, two independent determinations were made for each assembly. The results are shown in Table 4.3 along with previously

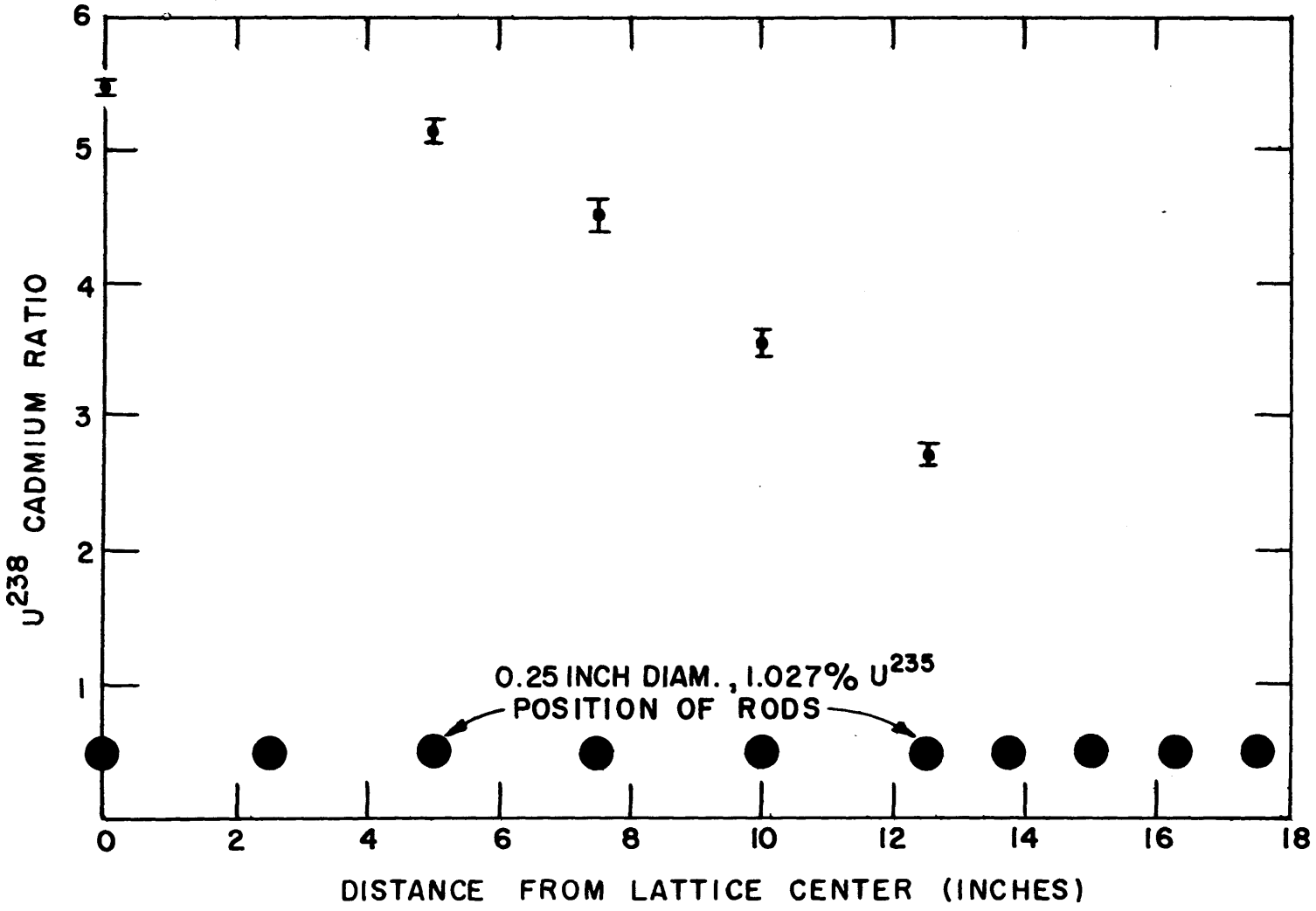

FIG. 4.27 U^{238} CADMIUM RATIO IN RODS OF ASSEMBLY III

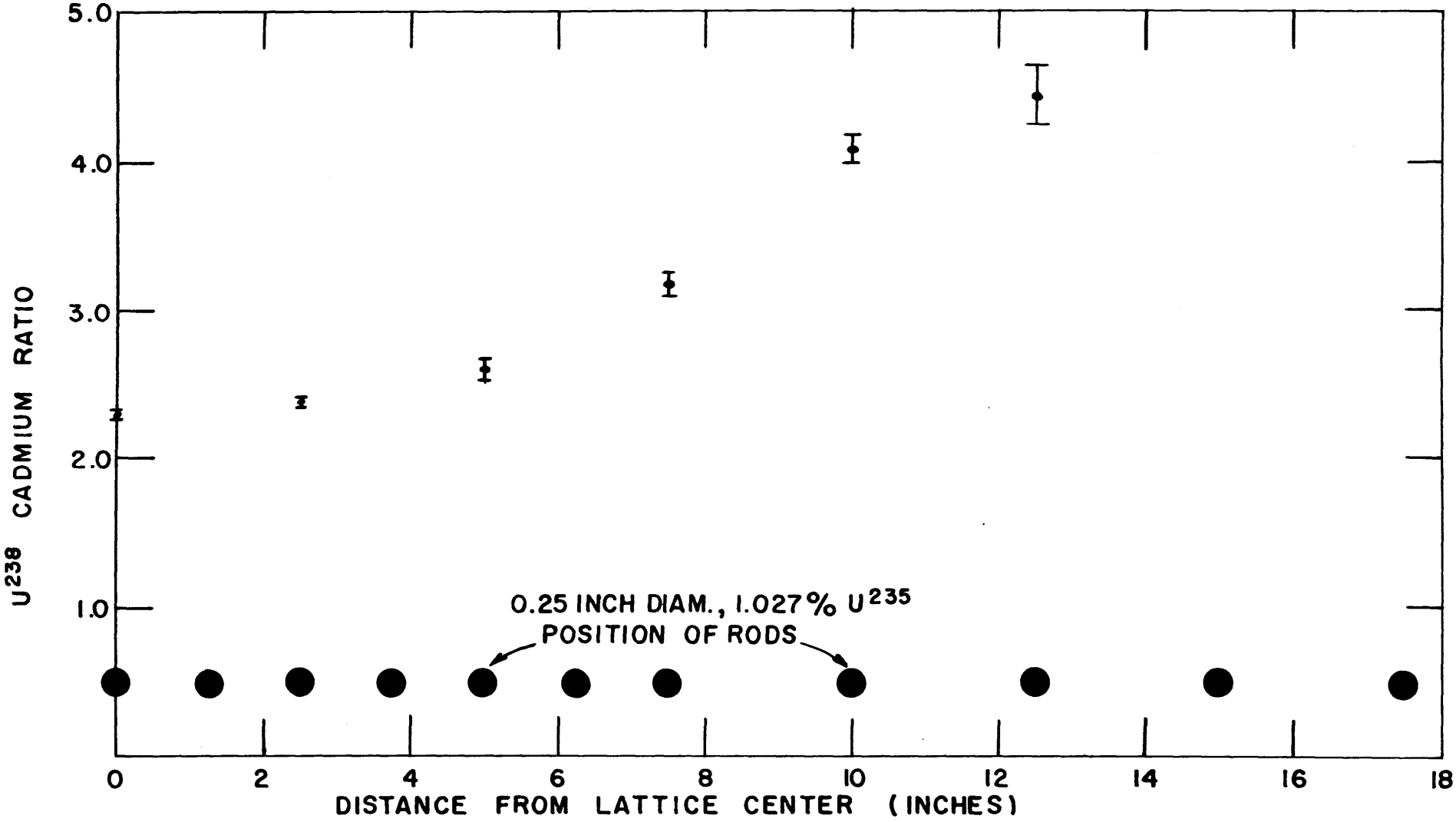

FIG. 4.28 U^{238} CADMIUM RATIO IN RODS OF ASSEMBLY IV

TABLE 4.2

R_{28} Measurements in Center Position of Two Region Assemblies

Assembly Designation	Center Lattice Designation	Two Region Value	Single Region Lattice
I	3	3.84 ± .04	5.40 ± .03
III	3	5.48 ± .06	5.40 ± .03
IV	1	2.28 ± .04	2.18 ± .01
V	6	4.07 ± .06	5.27 ± .10
VI	6	5.21 ± .08	5.27 ± .10
VII	2	3.08 ± .13	3.28 ± .02
VIII	2	3.43 ± .17	3.28 ± .02
IX	3	5.03 ± .10	5.40 ± .03
X	3	3.40 ± .07	5.40 ± .03
XI	9	3.30 ± .09	3.50 ± .01

TABLE 4.3

δ_{28} Measurements in Center Position of Two Region Assemblies

Assembly Designation	Center Lattice Designation		Assembly δ_{28}	Full Lattice Value
II	3		0.0192	
			0.0188	
		Average	0.0190	0.0183 ± .0007
III	3		0.02016	
			0.01870	
		Average	0.01943	0.0183 ± .0007
IV	1		0.0280	
			0.0272	
		Average	0.0276	0.0274 ± .0012
VII	2		0.0201	
			0.0201	
		Average	0.0201	0.0217 ± .0007
VIII	2	(One measurement)	0.0198	0.0217 ± .0007
IX	3	(One measurement)	0.0166	0.0183 ± .0007
X	3		0.0173	
			0.0193	
		Average	0.0183	0.0183 ± .0007
XI	9		0.0604	
			0.0595	
		Average	0.0600	0.0596 ± .0017

reported values for the full lattice corresponding to the test region of the assembly. It is immediately apparent that only small corrections will be necessary to obtain the full lattice values from the two region assembly measurements.

In Assemblies III and IX, δ_{28} measurements were made at various radial positions. The results are shown in Figures 4.29 and 4.30. In Assembly III, both regions were composed of 1/4-inch-diameter fuel rods. The variation in δ_{28} between regions is, therefore, completely due to differences in interaction with the neighboring rods. In Assembly IX, the abrupt change in δ_{28} as the region boundary is crossed is largely due to the difference in the single rod contributions of the 1/4-inch-diameter rods of the inner region and the 3/4-inch-diameter rods in the outer region.

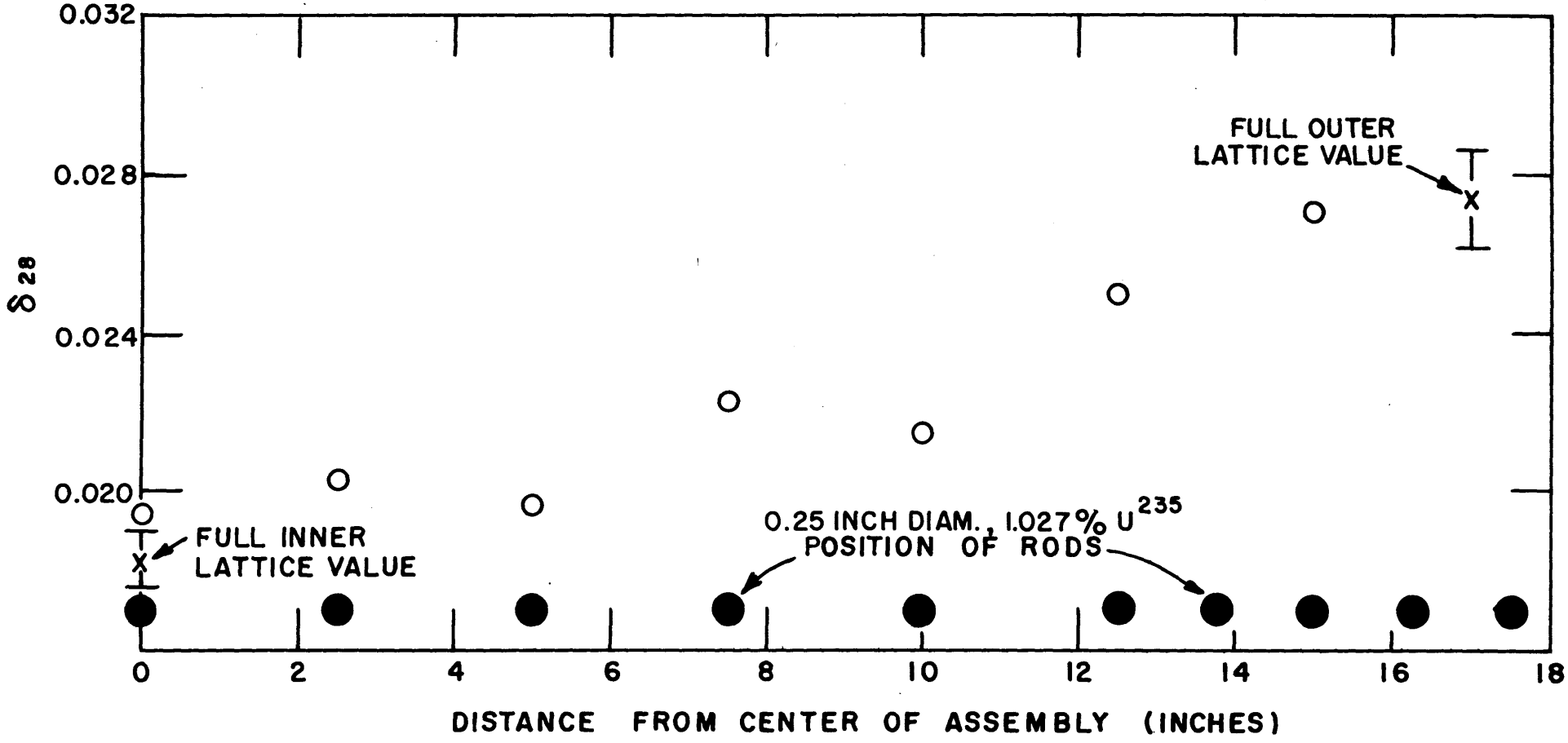

FIG. 4.29 δ_{28} IN ASSEMBLY III

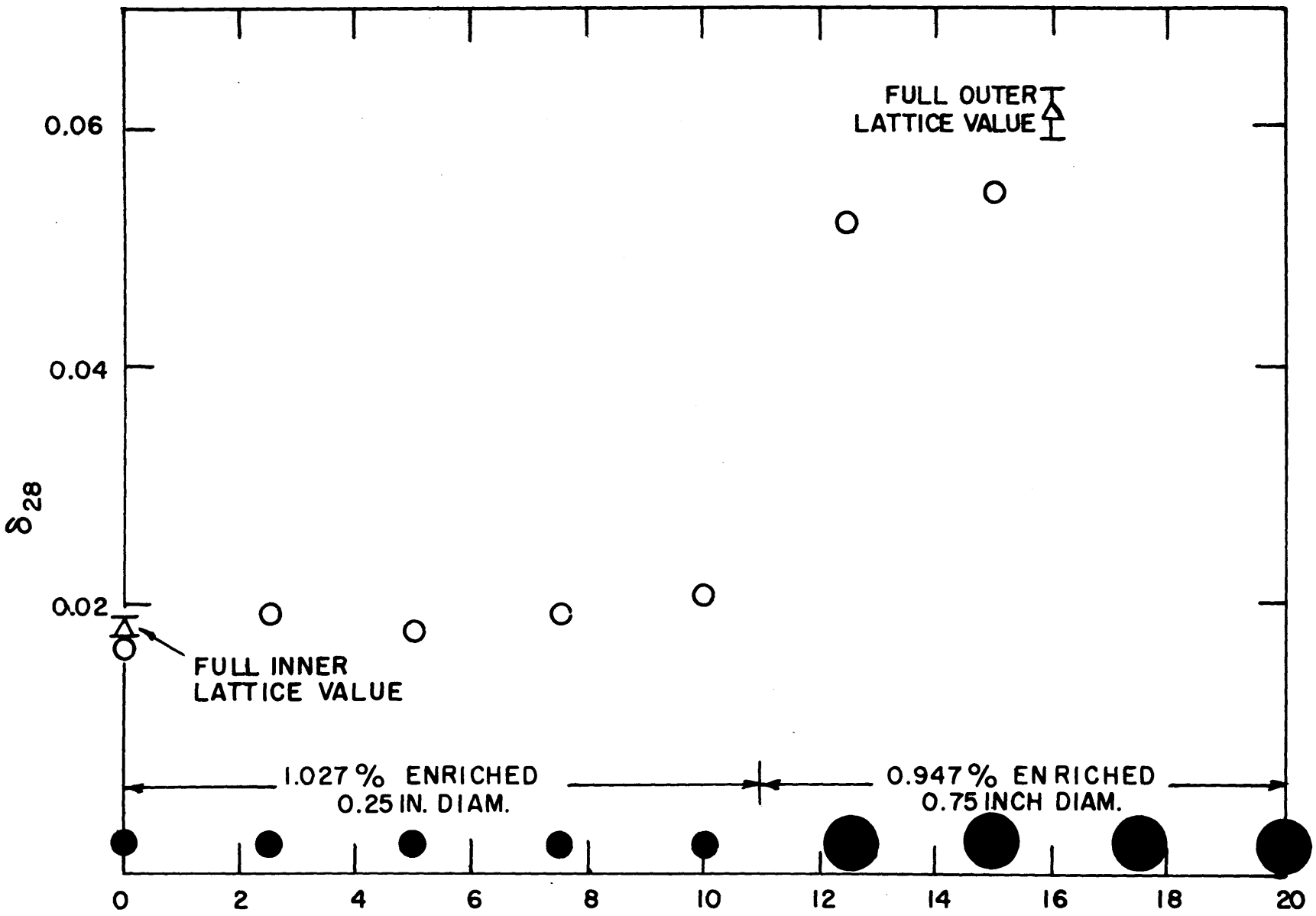

FIG. 4.30 δ_{28} IN ASSEMBLY IX 2 1/2 INCH SPACING

Chapter V

APPLICATION OF THEORY TO EXPERIMENTAL RESULTS

5.1 Introduction

The results of applying the theories presented in Chapter II to the experimental results of Chapter IV are presented in this chapter.

5.2 Application of Age Theory to Gold Foil Traverses

The experimental bare and cadmium-covered gold foil neutron flux traverses presented in section 4.3.2 were fitted to the theoretical expressions developed in section 2.2.2, using the computer program AGE described in Appendix B. Several simplifications were made beyond those necessary to the theory. These simplifications will be discussed before presenting the results of the analyses.

In determining the series representation of the source distribution using Eq. 2.6, some finite limit must be placed on the number of terms to be used. From preliminary trials, it was found that terms above the sixth contribute little to the slowing down density even at an age of 20 sq. cm. Their effect on the final flux distribution at the gold resonance is negligible. To be conservative, a total of ten terms is used in the computer program, both for the series expressing the source distribution (Eq. 2.6) and in those expressing the effect of resonance absorption (Eq. 2.17).

In Figures 5.1 to 5.11, the solid line labelled $\tau = 0$ is the source

distribution computed directly from the total thermal activation:

$$q(0, r) = \frac{k_\infty \Sigma_a}{p} \phi(r) \ . \qquad (2.4)$$

The dashed lines are the approximations given by the series expansion of Eq. 2.6. It can be seen that in assemblies having large differences in $\frac{k_\infty \Sigma_a}{p}$ between the regions, large oscillations are noticeable in the series approximation; while in assemblies with more alike regions, the approximation is considerably better. In all cases, the oscillations are suppressed in the theoretical distributions for neutrons of age 30 cm^2 and over, and the oscillations have no noticeable effect on the final gold resonance distributions.

As mentioned in section 2.2.2, actual U^{238} resonance absorption was simplified by two assumptions: (1) The resonance absorption in the statistical range was treated as a series of hypothetical resolved resonances, and (2) all resonances, whether actual or hypothetical, were subject to "lumping" to reduce the number of calculations required and consequently the computer time.

Adjacent resonances were combined if the sum of their fractional effective resonance integrals did not exceed approximately two percent. A weighted average energy was then assigned to the combined resonances. This process was limited by its nature to resonances with small contribution to the total absorption process. The statistical region was treated completely in this manner by assuming a 1/E dependence for the resonance integral in this region. The large resonances at low energies which have the largest effect on the slowing down density distribution at the gold resonance were unaffected by this

lumping procedure. Table 5.1 gives the resonance data actually used in the computer calculation. Values in the table were calculated from the output of the computer program RES, described in Appendix B, which uses the theory of Appendix A to calculate U^{238} effective resonance integrals for uranium rods. The uncombined resonance data are given in Table A.1.

The fractional effective resonance integrals are used in the program AGE to compute the partial resonance escape probabilities from the total resonance escape probabilities given in Table 5.2. If the simple exponential formula for resonance escape probability is assumed to hold, both for the total and each fractional probability, then (G3):

$$p_j = \exp\left[- \frac{N_U V_U \phi_U}{\xi \Sigma_s V_M \phi_M} \, ERI_j \right] , \tag{5.1}$$

or

$$\ln p_j = - \left[\frac{N_U V_U \phi_U}{\xi \Sigma_s V_M \phi_M} \, ERI_j \right] , \tag{5.2}$$

and

$$\ln p_j = f_j \ln p , \tag{5.3}$$

where f_j is the fractional effective resonance integral for the j^{th} resonance and p is the total resonance escape probability. To obtain Eq. 5.3 from Eq. 5.2 implies that the quantity $\frac{N_U V_U \phi_U}{\xi \Sigma_s V_M \phi_M}$ is constant over all resonances. The slowing down power, $\xi \Sigma_s$, is commonly assumed constant with energy throughout the resonance energy range, and although the resonance disadvantage factor, $\frac{\phi_U}{\phi_M}$, will vary with the strength of the particular resonance, the effect on the more important resonances is slight.

TABLE 5.1

Fractional U^{238} Effective Resonance Integrals
Used in Determination of Slowing Down Densities

Resonance Energy (Kev)	Age* (cm^2)	Fractional ERI		
		0.25-Inch Diameter	0.75-Inch Diameter	1.00-Inch Diameter
0.00668	97.6	0.30703	0.2680	0.2549
0.0210	89.9	0.13826	0.1191	0.1128
0.0368	86.2	0.11337	0.09807	0.09323
0.0663	82.2	0.04220	0.03491	0.03295
0.0811	80.8	0.01656	0.01589	0.01596
0.0900	80.1	0.00208	0.00280	0.00298
0.1025	79.3	0.03607	0.03028	0.02864
0.1165	78.4	0.01663	0.01705	0.01753
0.1176	76.4	0.01410	0.01467	0.01492
0.1896	75.1	0.02095	0.01758	0.01658
0.2085	74.5	0.01618	0.01780	0.01871
0.2811	72.5	0.01334	0.01400	0.01448
0.3618	70.8	0.01220	0.01315	0.01277
0.4413	69.4	0.01393	0.01450	0.01482
0.5501	68.0	0.01266	0.01416	0.01490
0.6600	66.7	0.01172	0.01338	0.01410
0.7795	65.6	0.01041	0.01214	0.01277
0.9207	64.5	0.00913	0.01082	0.01155
Statistical Region (20 resonances)		0.00966	0.01359	0.01477

*From Equation 5.4

TABLE 5.2

Properties of Lattices Forming Two Region Assemblies

Lattice Designation	$\xi\Sigma_s$ (cm^{-1})	Σ_a (cm^{-1})	D_{th} (cm^{-1})	$\left(\frac{ERI}{\sigma_o}\right)_{28}$	p	L^2 (cm^2)	τ (cm^2)
1	0.1724	0.01132	0.8251	6.24	0.8441	72.9	129.0
2	0.1775	0.006085	0.8217	6.24	0.9194	135.0	125.0
3	0.1802	0.003084	0.8011	6.24	0.9603	260.0	123.0
4	0.1724	0.01193	0.8494	6.24	0.8441	71.2	129.0
5	0.1775	0.006403	0.8229	6.24	0.9194	128.0	125.0
6	0.1802	0.003270	0.8042	6.24	0.9603	245.9	123.0
7	0.1655	0.017753	0.8547	4.10	0.7100	48.1	128.0
8	0.1784	0.004544	0.8046	4.10	0.9412	177.1	121.0
9	0.1754	0.006233	0.8340	3.73	0.9051	133.8	122.0

The age assigned to each U^{238} resonance of Table 5.1 requires a relationship between neutron energy and age in D_2O. Very little information is available for neutron ages at energies other than that of the indium resonance. Purity of the D_2O in the lattice assemblies during these investigations averaged 99.5%. The age to indium resonance in such a mixture has been measured as 108 ± 3 cm^2 (W5). The value of τ for other energies was obtained from the relation (W6):

$$\tau(E) = \tau(1.44 \text{ ev.}) - \left[\frac{D}{\xi \Sigma_s} \ln \left(\frac{E(\text{ev.})}{1.44} \right) \right]. \qquad (5.4)$$

Here again, use is made of the assumption of constant slowing down properties over the entire energy range. This is a good assumption in the region of the major resonances. The area in which it may not hold (close to fission energies) is also one of small resonance absorption and is therefore of lesser importance.

Fractional ERI's for Au^{197}, used to compute the non-1/v coefficients (Eq. 2.21), were calculated by the theory outlined in Appendix A. Table 5.3 gives values of the fractional ERI's for Au^{197} used in the computations. A value of 2.43 barns was taken to be the ratio of the total effective resonance integral (excluding the 1/v component) to the 2200 meter/sec absorption cross section. This value was used by Simms (S2) for 0.010-inch-thick gold foils and includes the resonance self-shielding effect in a 1/E flux.

Finally, the radius of the inner region, R, was computed by substituting for the actual hexagonal shape with a circular one of equal area, giving:

$$R = 0.52504\, b \left(1 + \sum_{k=1}^{N} 6k \right)^{1/2}, \qquad (5.5)$$

where b is the pitch of the center region in centimeters and N is the number of rings as defined in section 3.2. The radii used in the calculations are given in Table 5.4.

TABLE 5.3

Fractional Effective Resonance Integrals of Au^{197} for 0.010-Inch-Thick Gold Foils

Resonance Energy (ev)	Age* (cm^2)	Fractional ERI
4.90	99.71	0.8738
46.5	84.6	0.00080
58.1	83.1	0.01827
61.5	82.7	0.05954
80.2	80.9	0.01357
110.0	78.8	0.0059
153.0	76.6	0.0100
168.0	76.0	0.0120
194.0	75.0	0.0066

*From Equation 5.4

TABLE 5.4

Inner Region Equivalent Radii for Two Region Assemblies

Assembly Designation	Inner Region Radius (cm)	Assembly Designation	Inner Region Radius (cm)
I	14.53	VII	14.20
II	20.28	VIII	22.26
III	26.04	IX	26.04
IV	18.79	X	14.53
V	14.53	XI	29.06
VI	26.04		

5.2.1 Neutron Slowing Down Density Distributions

The results of the least squares fit of the experimental slowing down densities to the theory of Chapter II are presented in this section. Table 5.5 gives the values of $k_\infty \Sigma_a/p$ found for each assembly. Good agreement was obtained between assemblies of different region sizes except for those having a center region of only two rings (Assemblies I, V, and X). The values from experiments in these assemblies are bracketed in the table and were not used to compute the lattice averages.

The anomalous results found in the assemblies having a two-ring test region lead to the conclusion that a certain minimum size of test region is required for meaningful results. The equivalent radius of these test regions was 14.53 centimeters which is about $1.3\sqrt{\tau}$. However, Assembly VII, which had a smaller equivalent radius but a larger number of rings, agreed well with its corresponding Assembly VIII. It should be noted, however, that Assembly VII, unlike the other small test region assemblies, has equal values for the resonance escape probability and a small difference in $k_\infty \Sigma_a/p$ between the two regions. It is not unreasonable that the limit on test region size is a function of the difference in the neutron sources of the regions (i.e. $k_\infty \Sigma_a/p$) as well as the slowing down length. The present set of experiments does not offer a definitive answer but does indicate that a minimum size exists.

Figures 5.1 to 5.11 present the experimental points and fitted curves for the slowing down density at the gold resonance ($\tau = 99.7$ cm^2) for typical runs in each of the eleven assemblies. Also shown are the

TABLE 5.5

Values of $k_\infty \Sigma_a / p$ from Two Region Assembly Experiments

Assembly Designation	LATTICE DESIGNATION								
	1	2	3	4	5	6	7	8	9
I	(.01920)		(.00297)						
II	.01688 .01824		.00410 .00375						
III	.01744 .01586		.00431 .00420						
IV	.01898 .01826		.00466 .00447						
V				(.01998)		(.00236)			
VI				.01917		.00463			
VII		.00882 .00850			.01057 .00998				
VIII		.00869 .00942			.01077 .00915				
IX			.00443 .00429				.03171 .03012		
X			(.00254) (.00269)				(.06228) (.06355)		
XI								.00657 .00663	.00851 .00846
Average	.01761	.00885	.00427	.01917	.01011	.00463	.03091	.00660	.00848

distributions of the fission source ($\tau = 0$) and of densities at several intermediate values of the neutron age. The dashed lines indicate the series approximations to the source distributions (Eq. 2.6). As mentioned before, this approximation is best when the two regions are not greatly different. Assemblies VII (Fig. 5.7), VIII (Fig. 5.8), and XI (Fig. 5.11) illustrate this conclusion. The step changes in the source distributions, as indicated in the figures, do not actually exist. The assumption of a constant value of $k_\infty \Sigma_a/p$ throughout each region is ultimately based on consideration of properties of a unit cell. This concept is not strictly applicable in the neighborhood of a boundary, and the actual source distribution may be closer to the rounded curves produced by the series expansion at the boundary.

As would be expected, a large step change in the source across the region boundary is poorly represented by the series. In all cases, the oscillations in the distributions disappear very quickly as the slowing down process takes place, and the curves for the age of 30 cm^2 are smooth across the assemblies.

As can be implied from these distributions, the neutron energy spectrum as a function of radius in assemblies with large differences in $k_\infty \Sigma_a/p$ between regions varies greatly from a 1/E distribution. Figures 5.12 and 5.13 show the slowing down density versus neutron age in Assemblies III and IV at several radial positions. These curves are sections through the curves of Figures 5.3 and 5.4 taken at constant radial position. The radial positions chosen are foil positions on either side of the region boundary and those closest to the assemblies' center and outer radii. In these figures the quantities are presented as smooth

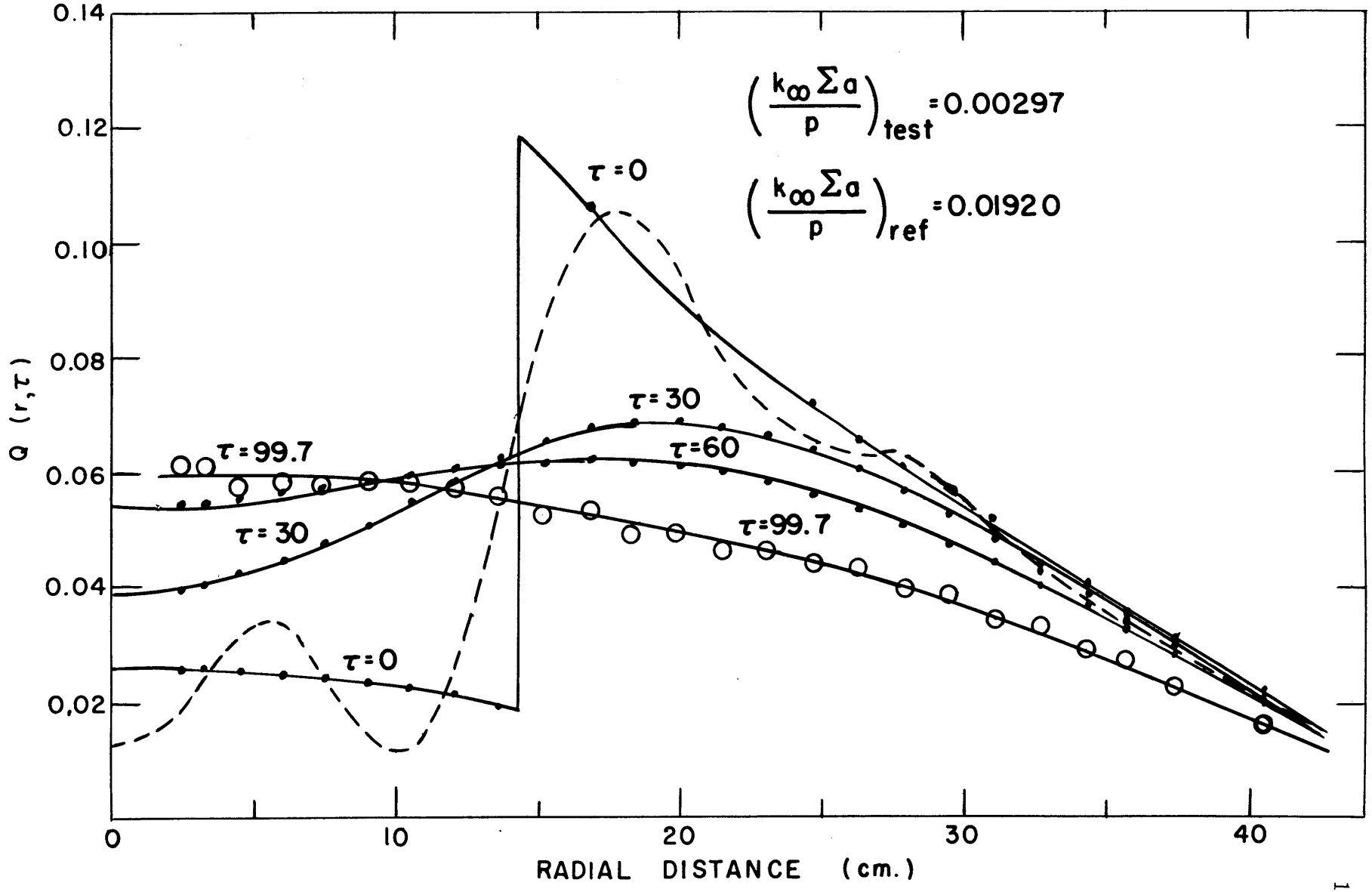

FIG. 5.1 SLOWING DOWN DENSITY DISTRIBUTIONS IN ASSEMBLY I

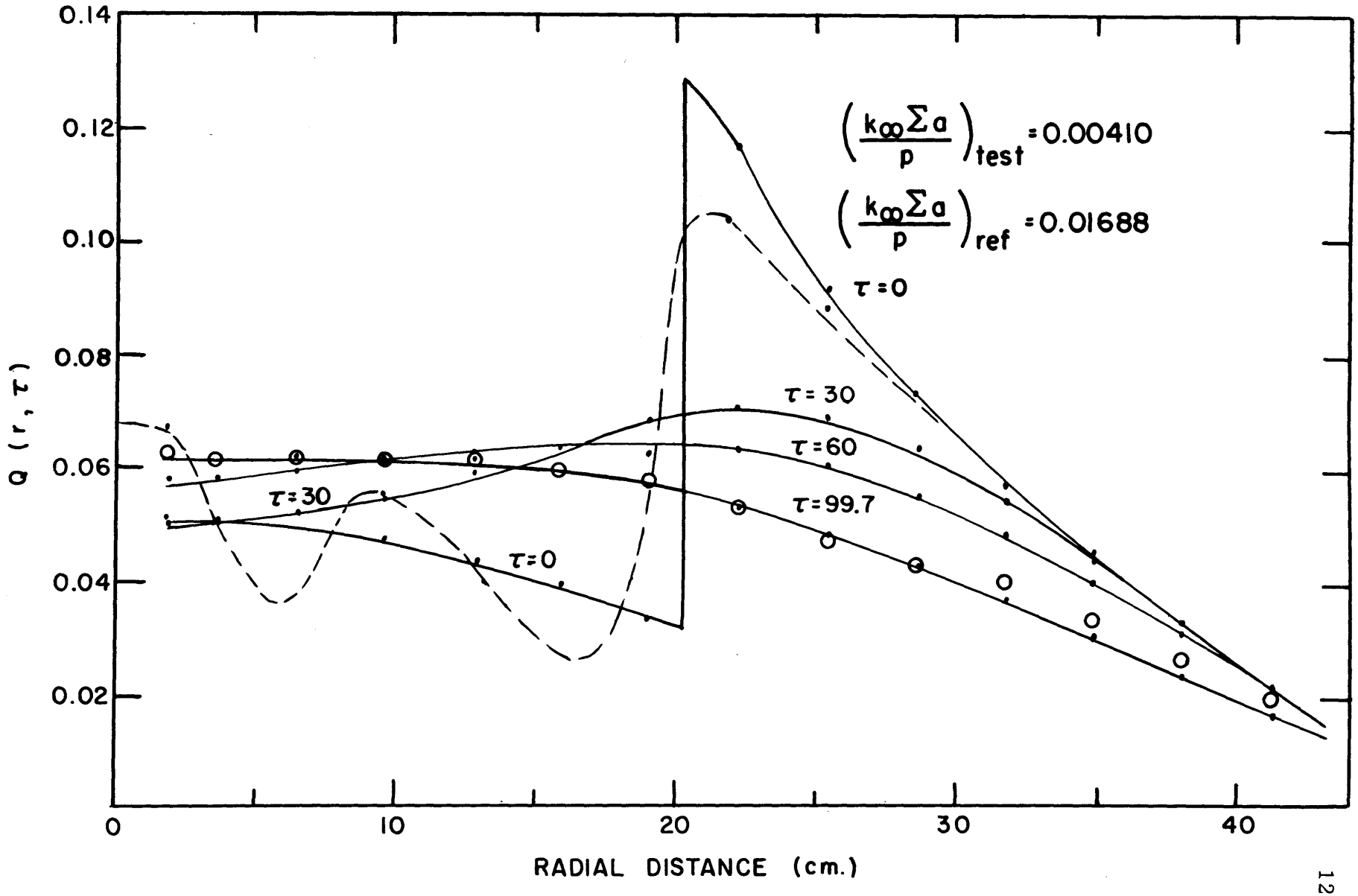

FIG. 5.2 SLOWING DOWN DENSITY DISTRIBUTIONS IN ASSEMBLY II

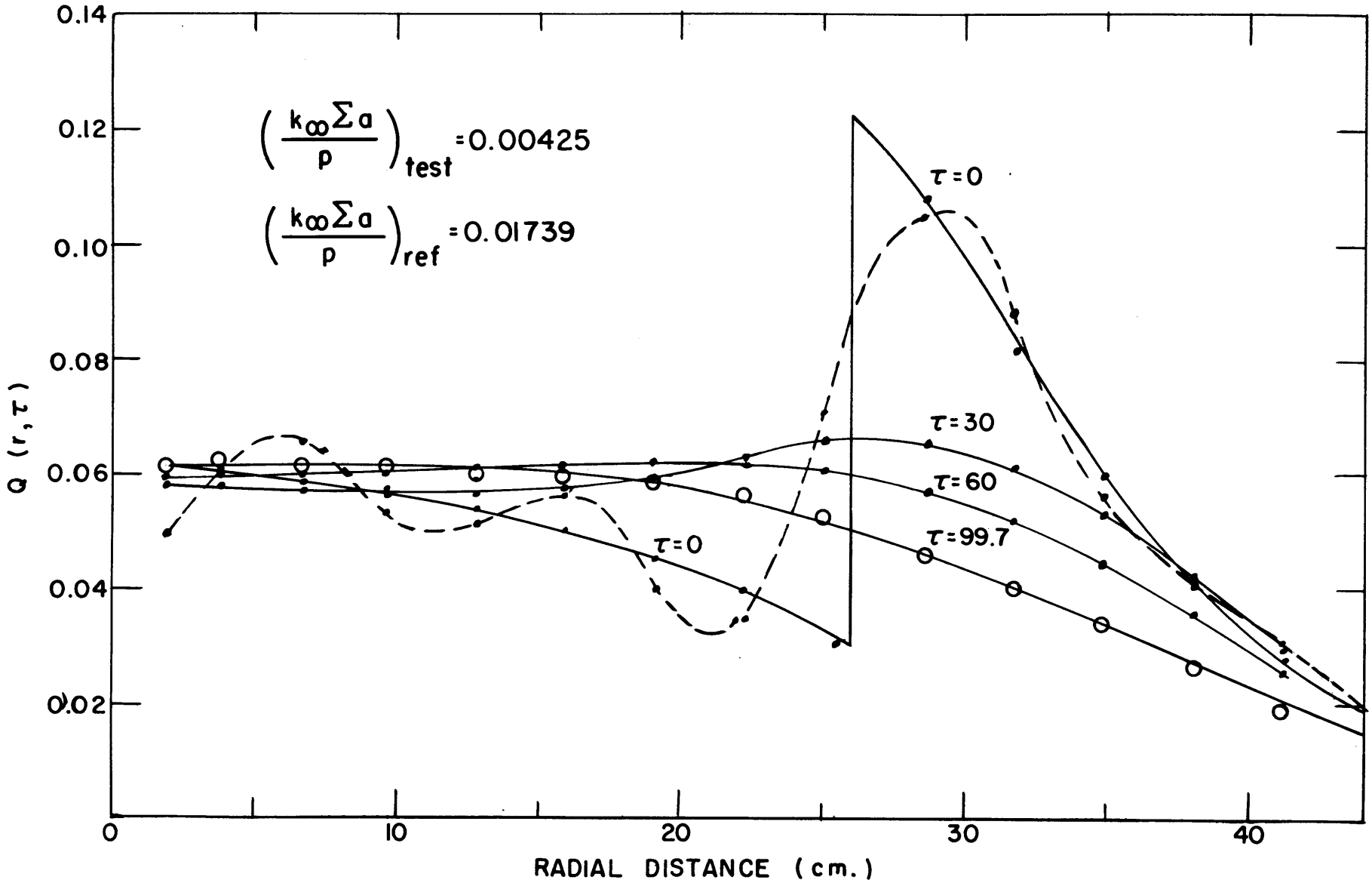

FIG. 5.3 SLOWING DOWN DENSITY DISTRIBUTIONS IN ASSEMBLY III

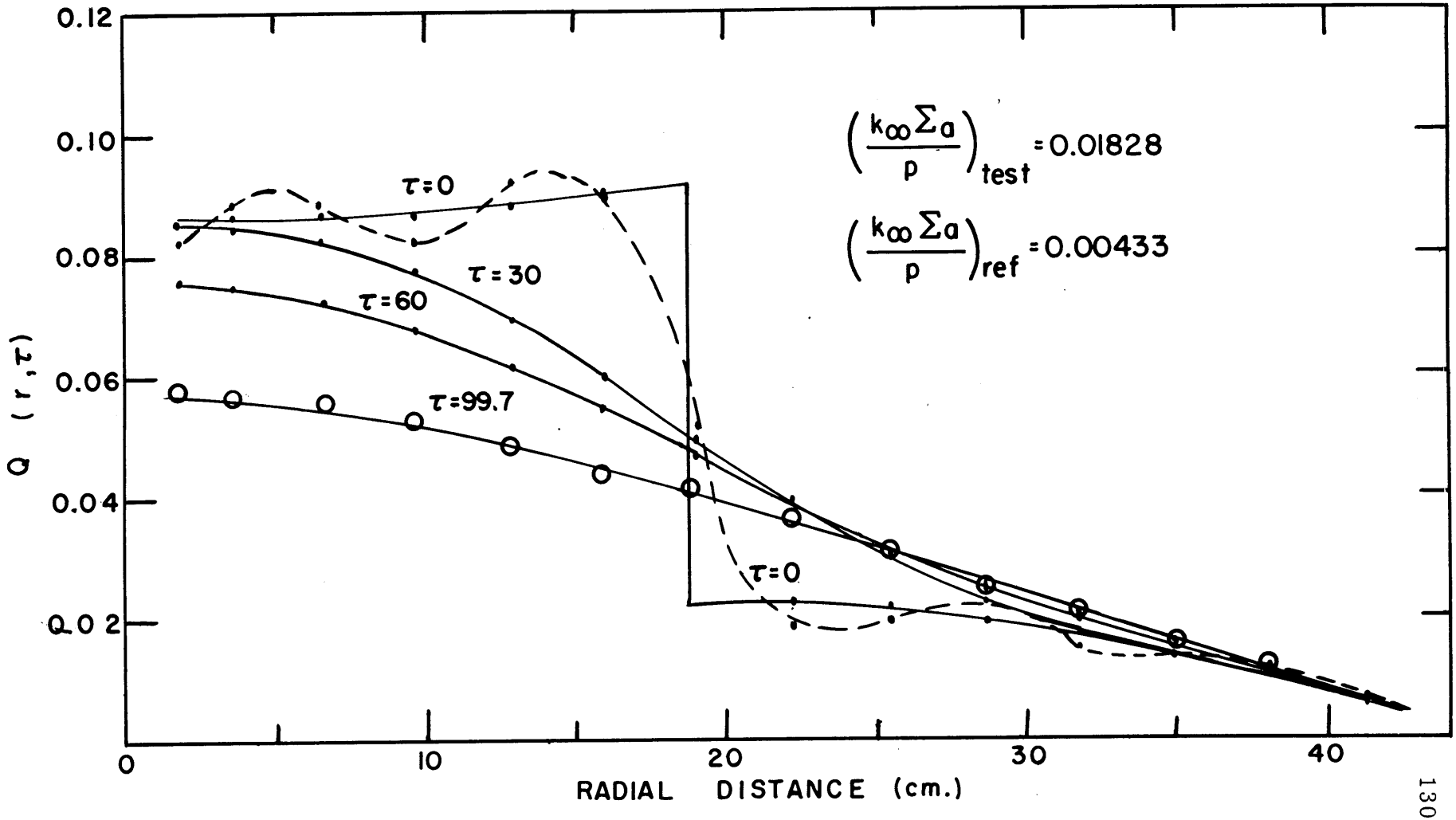

FIG. 5.4 SLOWING DOWN DENSITY DISTRIBUTIONS IN ASSEMBLY IV

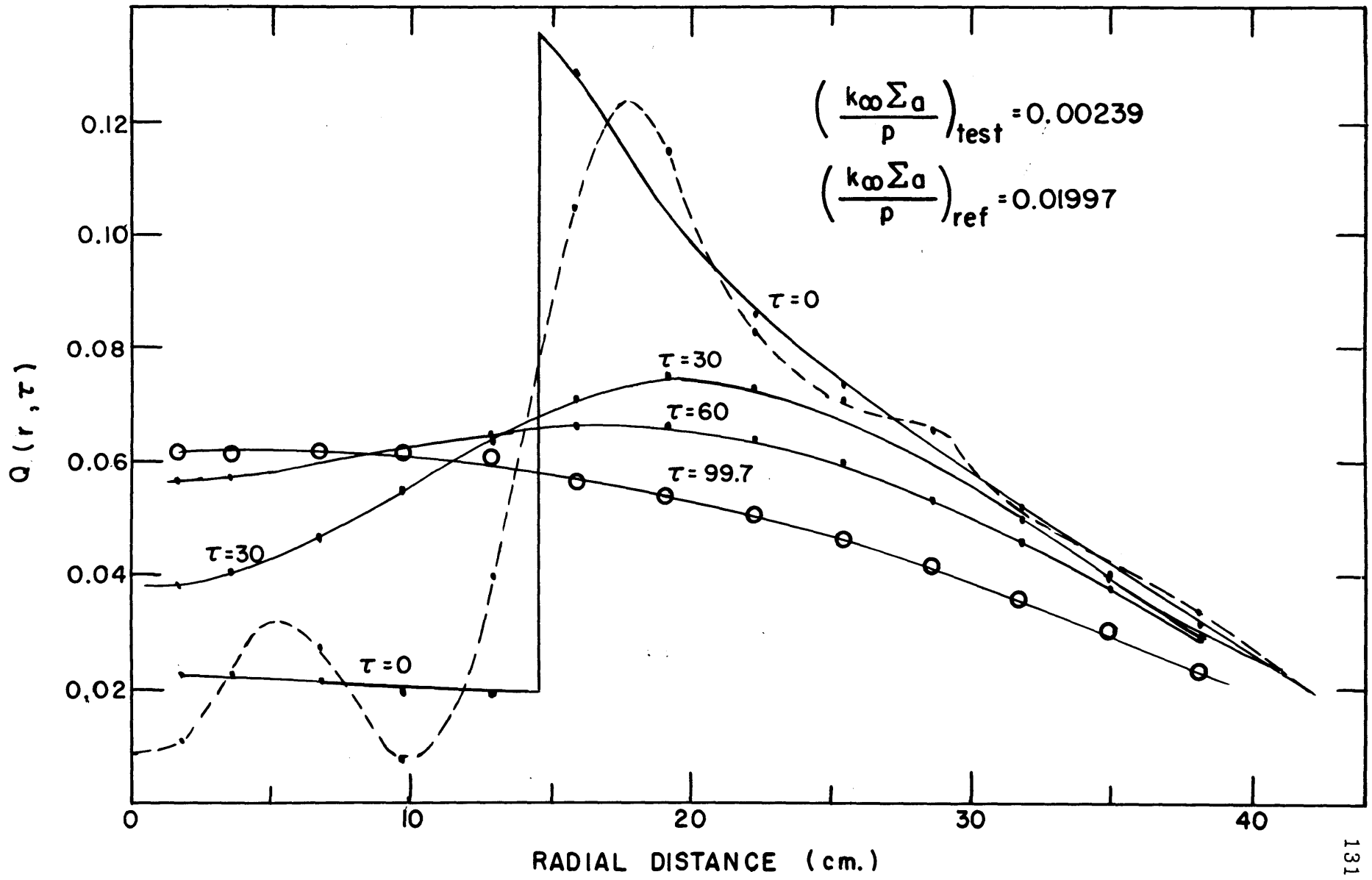

FIG. 5.5 SLOWING DOWN DENSITY DISTRIBUTIONS IN ASSEMBLY V

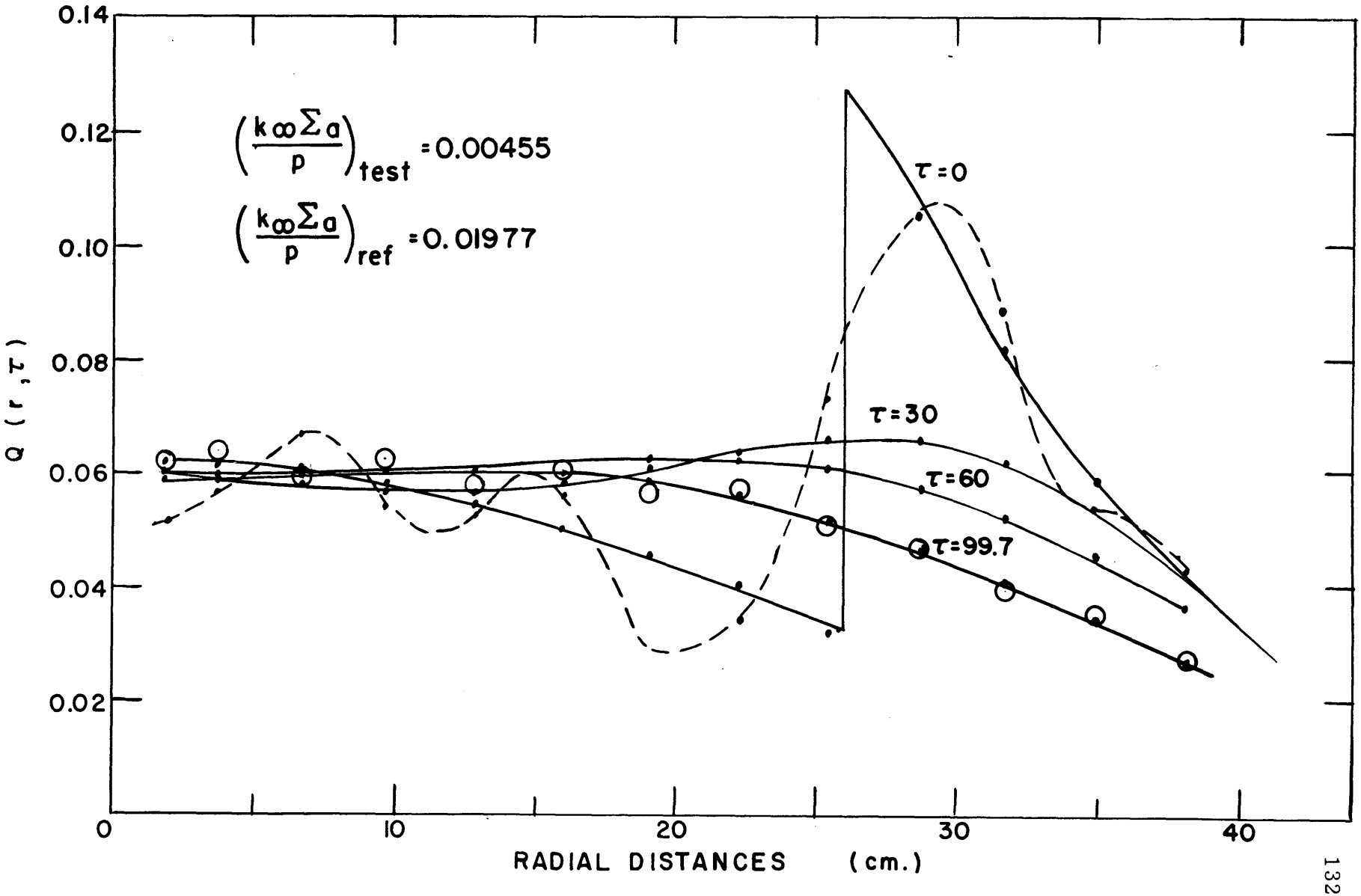

FIG. 5.6 SLOWING DOWN DENSITY DISTRIBUTIONS IN ASSEMBLY VI

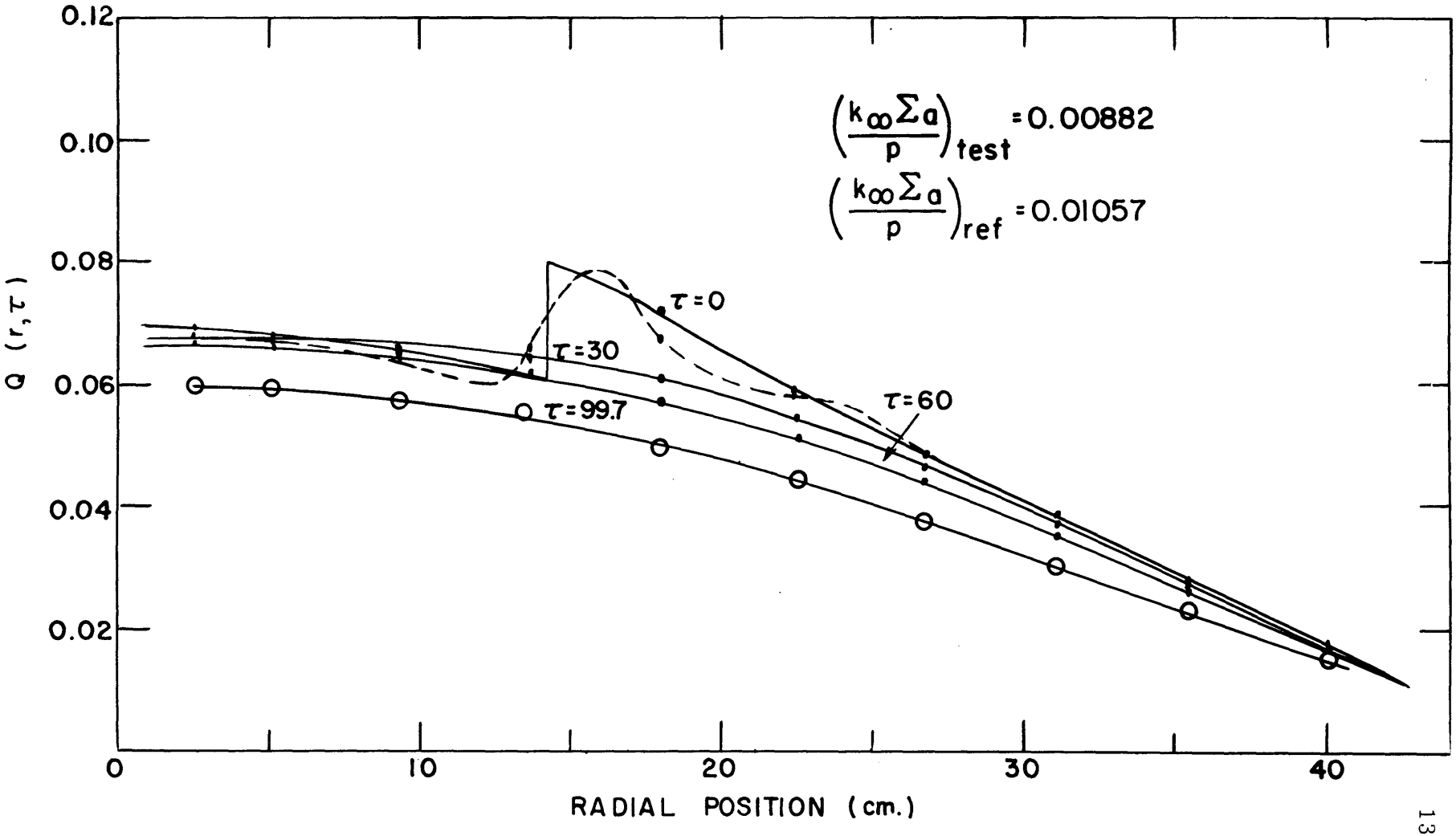

FIG. 5.7 SLOWING DOWN DENSITY DISTRIBUTIONS IN ASSEMBLY VII

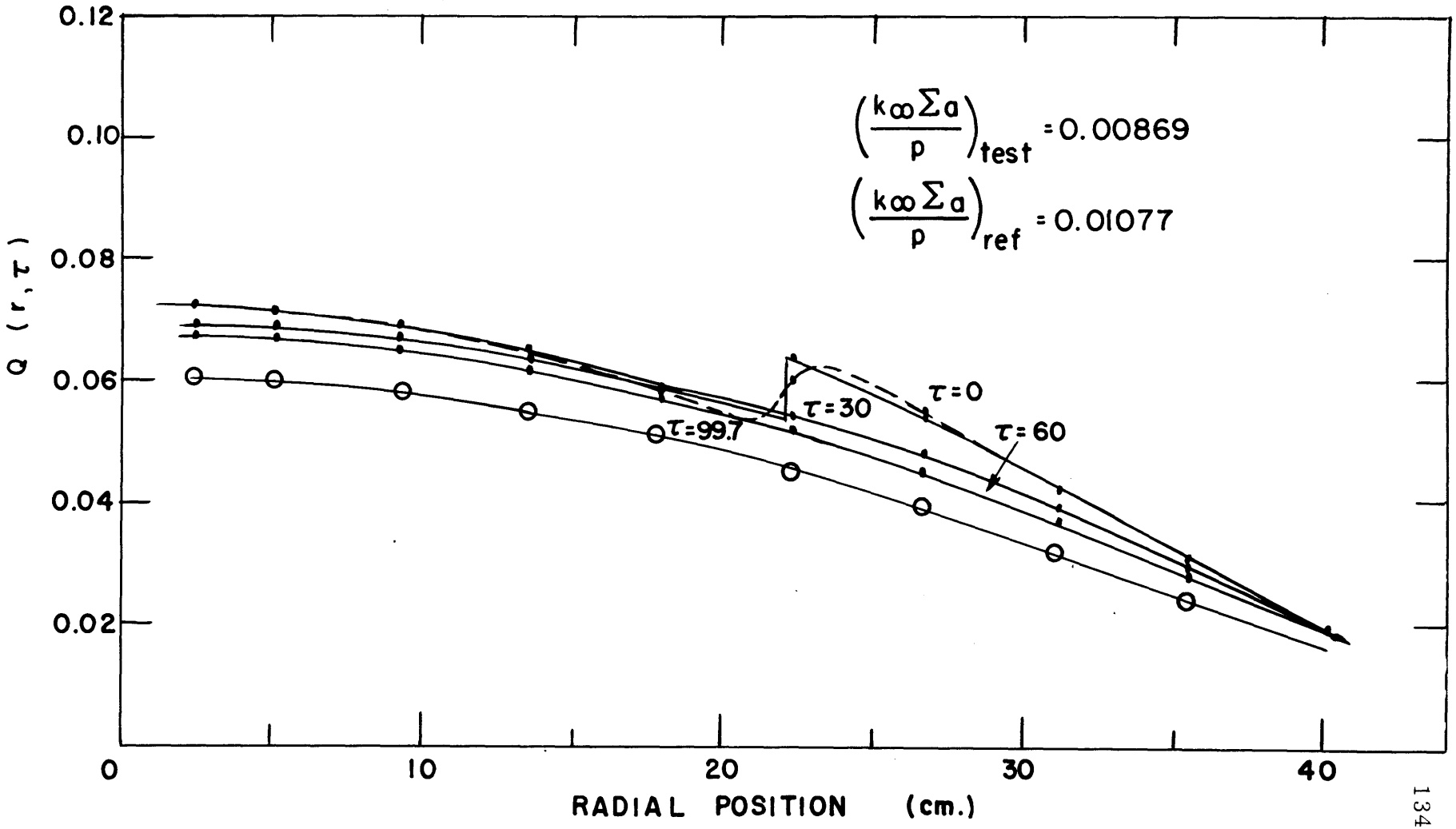

FIG. 5.8 SLOWING DOWN DENSITY DISTRIBUTIONS IN ASSEMBLY VIII

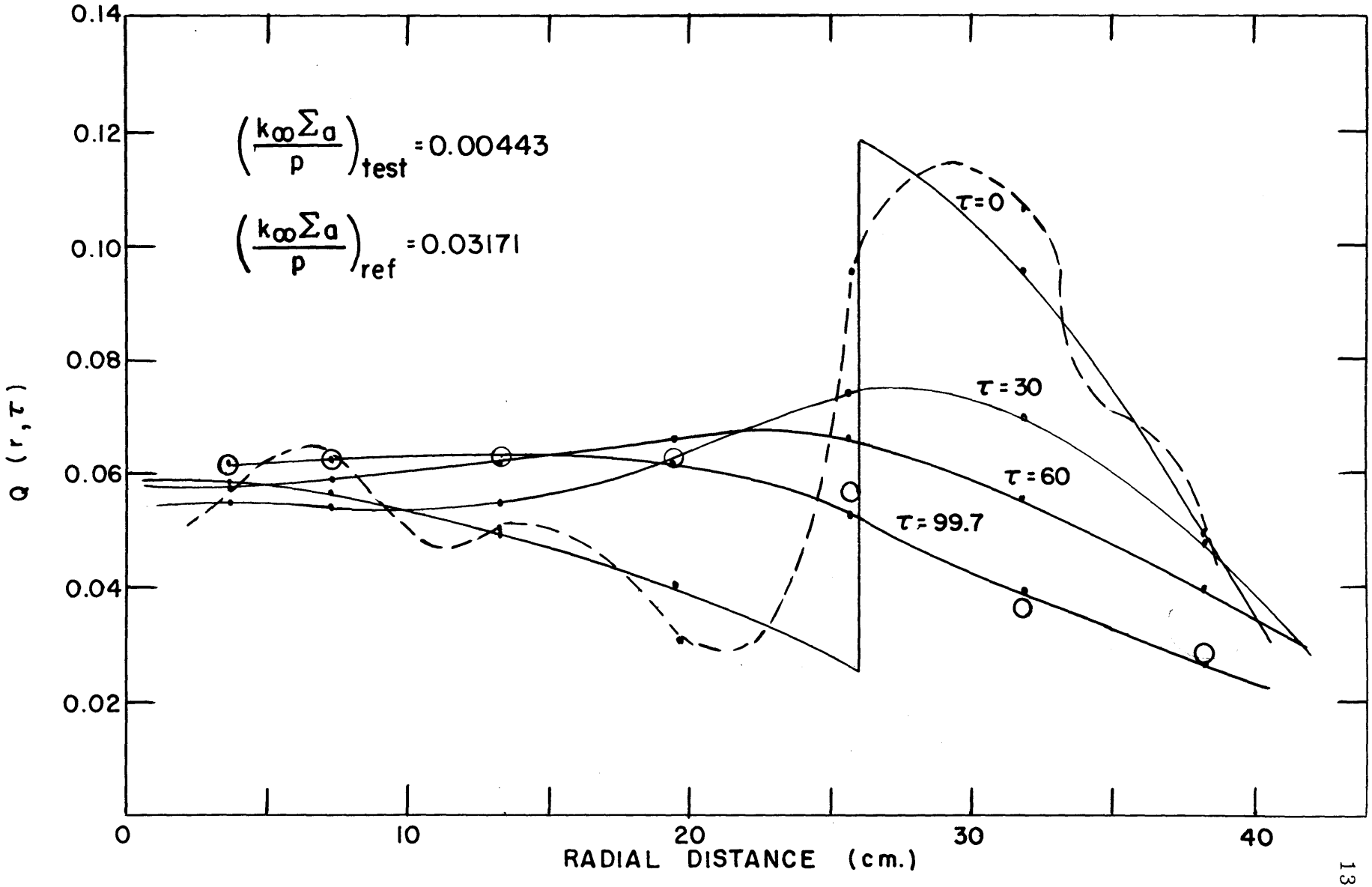

FIG. 5.9 SLOWING DOWN DENSITY DISTRIBUTIONS IN ASSEMBLY IX

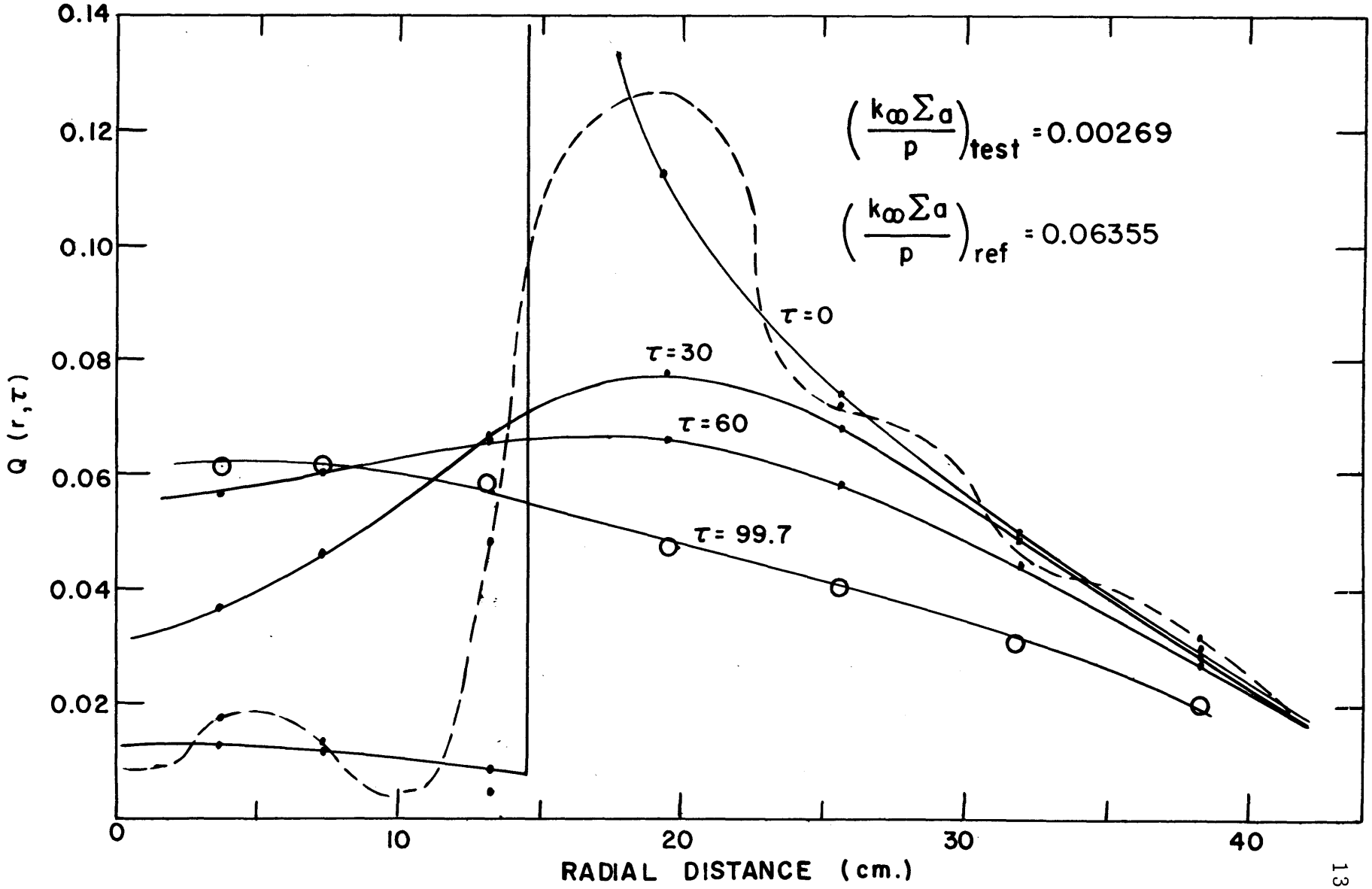

FIG. 5.10 SLOWING DOWN DENSITY DISTRIBUTIONS IN ASSEMBLY X

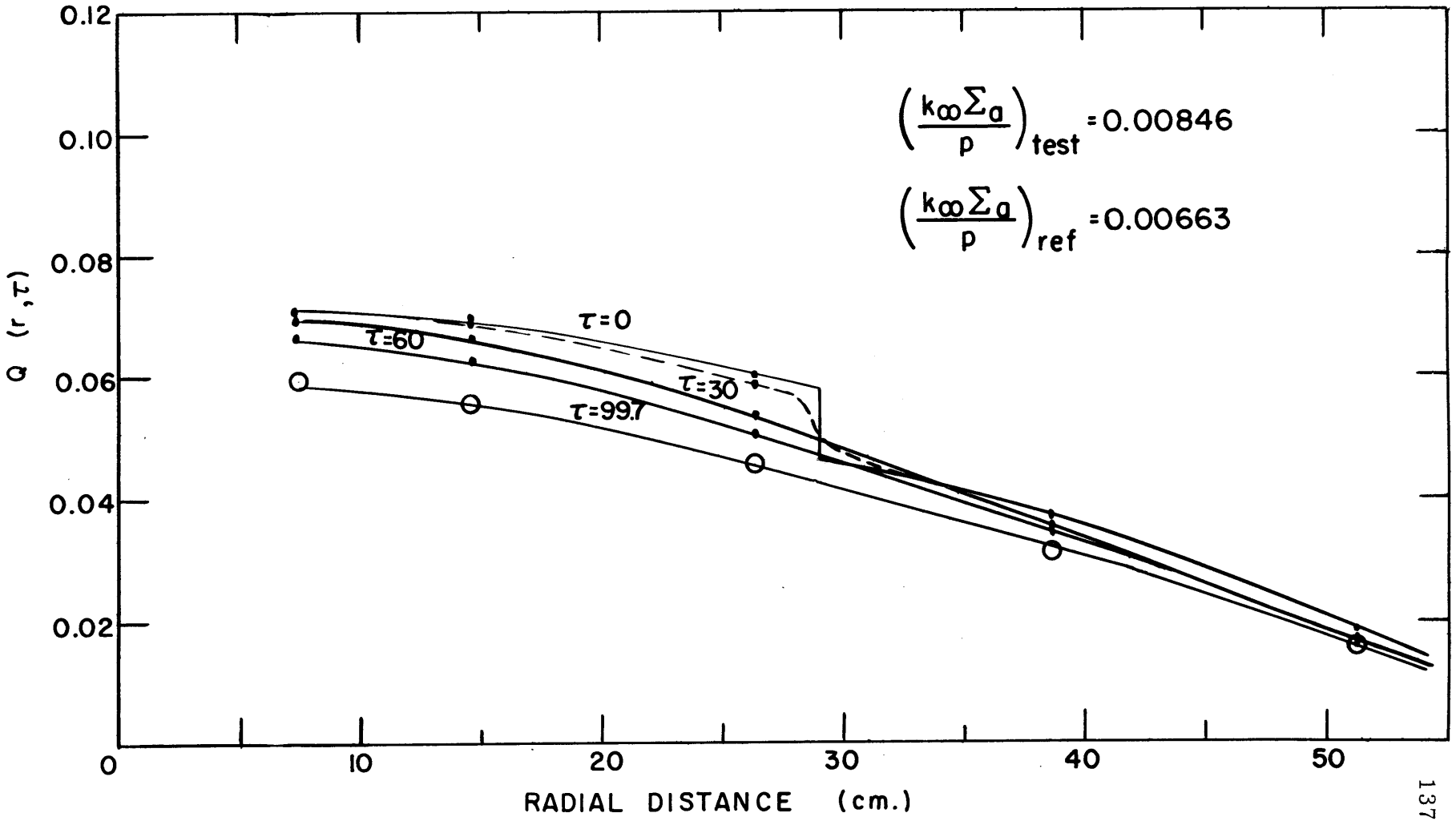

FIG. 5.11 SLOWING DOWN DENSITY DISTRIBUTIONS IN ASSEMBLY XI

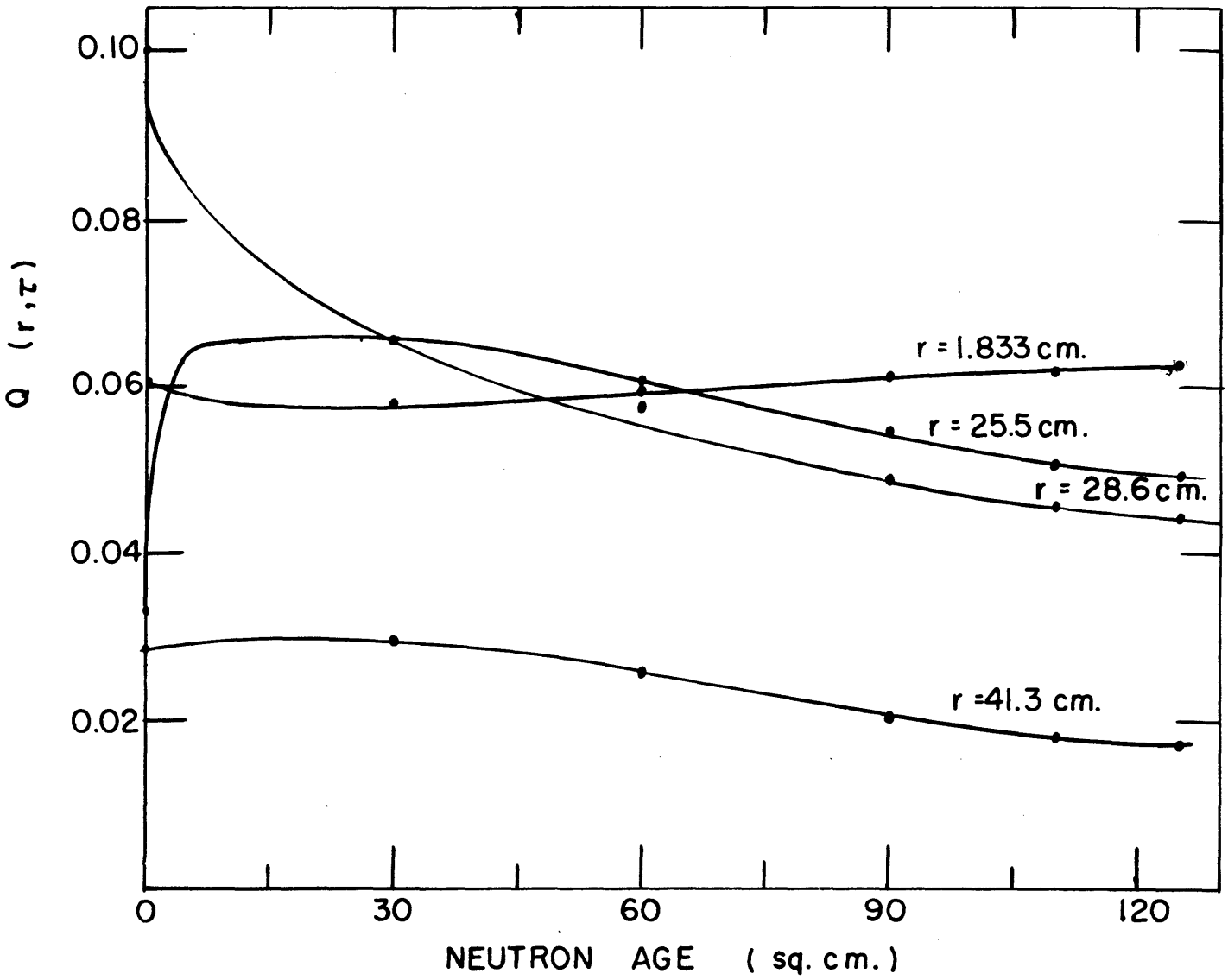

FIG. 5.12 APPROXIMATE SLOWING DOWN DENSITY VERSUS AGE FOR SEVERAL RADIAL POSITIONS IN ASSEMBLY III

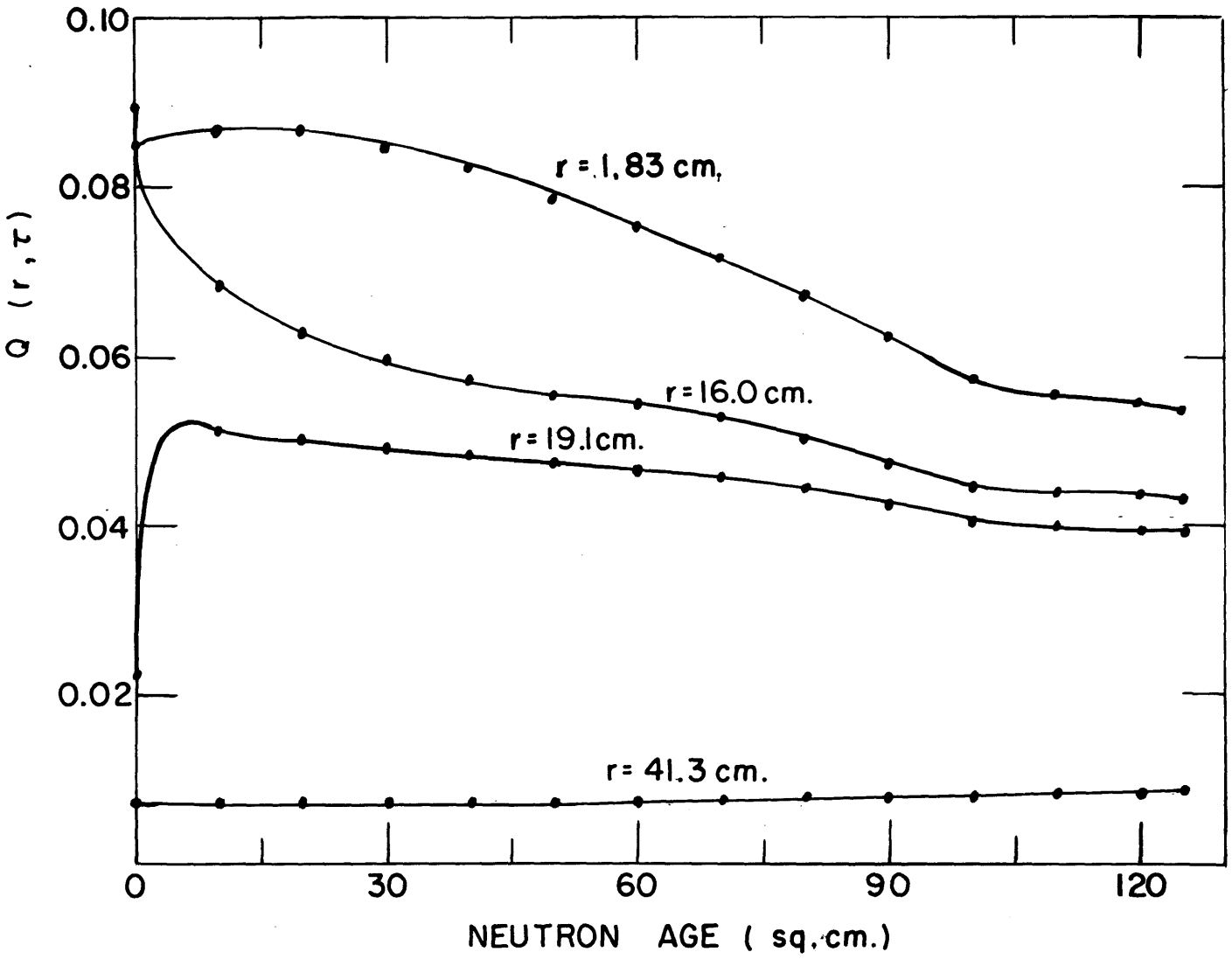

FIG. 5.13 APPROXIMATE SLOWING DOWN DENSITY VERSUS AGE FOR SEVERAL RADIAL POSITIONS IN ASSEMBLY IV

curves. In reality, discontinuities exist at neutron ages corresponding to U^{238} resonance energies. Also, the shape of the curves near the source energies has been estimated from only a few points. However, the general trend in the distributions can be seen, and the large changes in the neutron slowing down spectrum which occur across the assemblies are obvious. Because of the approximations necessary in the theory, the large variations at very low values of the age may be in error, but even at larger values of the age, a significant variation in the spectral shape can be observed as the assembly is traversed.

5.2.2 Infinite Multiplication Factor

Values of the macroscopic absorption cross section and resonance escape probability were computed for each lattice composing the two region assemblies. Details of these calculations are given in Appendix D and the values obtained in Table 5.2.

With these values of Σ_a and p, the infinite multiplication factor, k_∞, can be calculated from the measured values of $k_\infty \Sigma_a / p$, using the theoretically calculated values of the other two parameters. Table 5.6 presents the infinite multiplication factors derived from the two region assembly measurements. The individual determinations of $k_\infty \Sigma_a / p$ used for these average values of k_∞ are given in Table 5.5. Note that the experiments in two-ring assemblies, bracketed in Table 5.5, have not been used. The errors quoted in the table are the standard errors of the averages of independent determinations and do not include possible errors in the calculated quantities. Also given in Table 5.6 are the values of the infinite multiplication factor calculated from age-diffusion theory (G3):

TABLE 5.6

Values of the Infinite Multiplication Factor, k_∞, from Two Region Assembly Experiments

Lattice Designation	Assemblies Considered	Average k_∞	Age-Diffusion Theory (Eq. 5.6)	Previously Reported Values
1	II, III, IV	1.325 ± .08	1.250	1.304 ± .02 (S1)
2	VII, VIII	1.340 ± .07	1.336	1.375 ± .021 (D1)
3	II, III, IV, IX	1.332 ± .09	1.367	1.395 ± .021 (D1)
4	VI	1.360 (one measurement)	1.308	1.330 ± .027 (H6)
5	VII, VIII	1.453 ± .13	1.387	1.393 ± .011 (H6)
6	VI	1.360 (one measurement)	1.402	1.422 ± .007 (H6)
7	IX	1.236 ± .04	1.176	1.187 ± .027 (H6)
8	XI	1.367 ± .01	1.364	1.379 ± .021 (B2)
9	XI	1.232 ± .01	1.218	1.219 ± .014 (W1)

$$k_\infty = \frac{e^{-B_m^2 \tau}}{1 + L^2 B_m^2} . \qquad (5.6)$$

Calculation of the age, τ, and the diffusion length, L, is described in Appendix D. Material bucklings from single region measurements made by the Heavy Water Lattice Project (H5) were used.

The infinite multiplication factor for each of the lattices has been reported by previous workers on the project. These values, and corresponding references, are included in Table 5.6. In general, the agreement of the results of the present investigation with other experimental determinations is good within the experimental error. In the case of the last three lattices, only two determinations of $k_\infty \Sigma_a / p$ were made for each lattice. The errors quoted for these lattices were estimated by inefficient statistics and may be overly optimistic. Where k_∞ was found from more than one assembly (lattices 1, 2, 3, and 5), the error is considerably higher, although inspection of Table 5.5 shows, with the exception of the smallest test regions, no definite trend between assemblies of varying region sizes or composition. Because of the larger number of independent determinations, the errors quoted for lattices 1, 2, 3, and 5 are, perhaps, more indicative of the inherent error in the method. These errors range from five to nine percent of the value of k_∞ and are considerably higher than those quoted for other methods of evaluating k_∞.

5.2.3 Correction of ρ_{28} Measurements to Full Lattice Values

In full, single region lattices studied at M. I. T., the thermal flux distribution can be represented over most of the lattice volume by a

pure J_o function (P1, C5). Higher harmonics are not of sufficient strength to be detected in either the radial or axial directions. The Bessel function series in the equations of section 2.2 are no longer required to describe the slowing down density and the slowing down function of Eq. 2.23 becomes:

$$\psi(\tau) = \frac{p(\tau)}{\xi\Sigma_s} \frac{k_\infty \Sigma_a}{p} e^{-B_m^2 \tau} , \qquad (5.7)$$

which is identical with Eq. 2.32 for a critical system. Thus the absence of higher harmonics in the thermal flux distribution leads to the conclusion that the slowing down spectrum in the single region exponential facility closely approximates that of a critical system. Two region measurements of ρ_{28}, corrected by Eq. 2.33, can then be validly compared with previous measurements in the single region lattices.

The computer program AGE computes "relative" ρ_{28} values defined by Eq. 2.22 and Eq. 2.30 for each point in the gold foil traverses. Values at actual fuel rod positions are found by interpolation. The correction factor given by Eq. 2.33 can then be calculated, using the measured values of $k_\infty \Sigma_a / p$ listed in Table 5.5.

Table 5.7 gives the measured and corrected values of ρ_{28} from the two region assembly experiments. The corresponding results from single region lattices are also listed. The two region assembly values were taken from the measured R_{28}'s given in Table 4.2 and Figs. 4.26 and 4.27. Note the large corrections necessary for measurements in test regions of small size.

Table 5.8 consolidates the information from the previous table by

TABLE 5.7

Comparison of Corrected Two Region Assembly Measurements of ρ_{28} with Single Region Results

Assembly Designation	Size of Inner Region*	Assembly Ring**	Measured ρ_{28}	Corrected ρ_{28}	Single Region ρ_{28} (H5)
I	2	0	0.352 ± .005	0.210 ± .003	0.227 ± .001
III	4	0	0.223 ± .003	0.202 ± .003	0.227 ± .001
		2	0.242 ± .005	0.193 ± .003	0.227 ± .001
		3	0.283 ± .010	0.193 ± .006	0.227 ± .001
		4	0.391 ± .015	0.791 ± .031	0.845 ± .007
		5	0.585 ± .024	0.820 ± .050	0.845 ± .007
IV	6	0	0.781 ± .021	0.806 ± .021	0.845 ± .007
		2	0.719 ± .019	0.785 ± .019	0.845 ± .007
		4	0.621 ± .028	0.779 ± .035	0.845 ± .007
		6	0.459 ± .020	0.223 ± .009	0.227 ± .001
		7	0.324 ± .014	0.214 ± .009	0.227 ± .001
		8	0.291 ± .022	0.249 ± .019	0.227 ± .001
V	2	0	0.356 ± .007	0.221 ± .004	0.222 ± .026
VI	4	0	0.238 ± .005	0.216 ± .005	0.222 ± .026
VII	3	0	0.481 ± .036	0.475 ± .036	0.437 ± .003
VIII	5	0	0.412 ± .033	0.383 ± .033	0.437 ± .003
IX	3	0	0.248 ± .006	0.214 ± .005	0.227 ± .001
X	2	0	0.417 ± .012	0.270 ± .008	0.227 ± .001
XI	2	0	0.435 ± .017	0.415 ± .016	0.401 ± .002

*Given in terms of number of rings (see section 3.2).

**Ring "O" is center fuel rod.

TABLE 5.8

Full Lattice ρ_{28} from Two Region Assembly Measurements

Lattice Designation	Average Corrected ρ_{28}	Single Region ρ_{28} (H5)
1	0.796 ± .019	0.845 ± .007
2	0.429 ± .065	0.437 ± .003
3	0.220 ± .026	0.227 ± .001
6	0.218 ± .003	0.222 ± .026
9	0.415 ± .016	0.401 ± .002

listing the average values of the corrected ρ_{28} from two region assemblies for each of the lattices in which the quantity was measured. With the exception of lattice 1, the average values of ρ_{28} from the two region experiments agree within experimental error with the single region determinations.

5.3 Determination of δ_{28}^{SR} from Two Region Assembly Measurements

Values of δ_{28} measured in the two region assemblies and given in Table 4.3 and Figures 4.28 and 4.29 were reduced to values of δ_{28}^{SR} by the method developed in Chapter II.

Fuel rods are spaced about the center rod in a series of hexagonal "rings" as shown in Figure 3.5. The summation required for use of Eq. 2.43 was evaluated by considering the rods in these "rings" to be on a series of concentric circles centered on the subject rod. For example, Ring 4 of Figure 3.5 was represented by three circles as shown in Figure 5.14. The interaction kernel, K_{ij}, for each circle

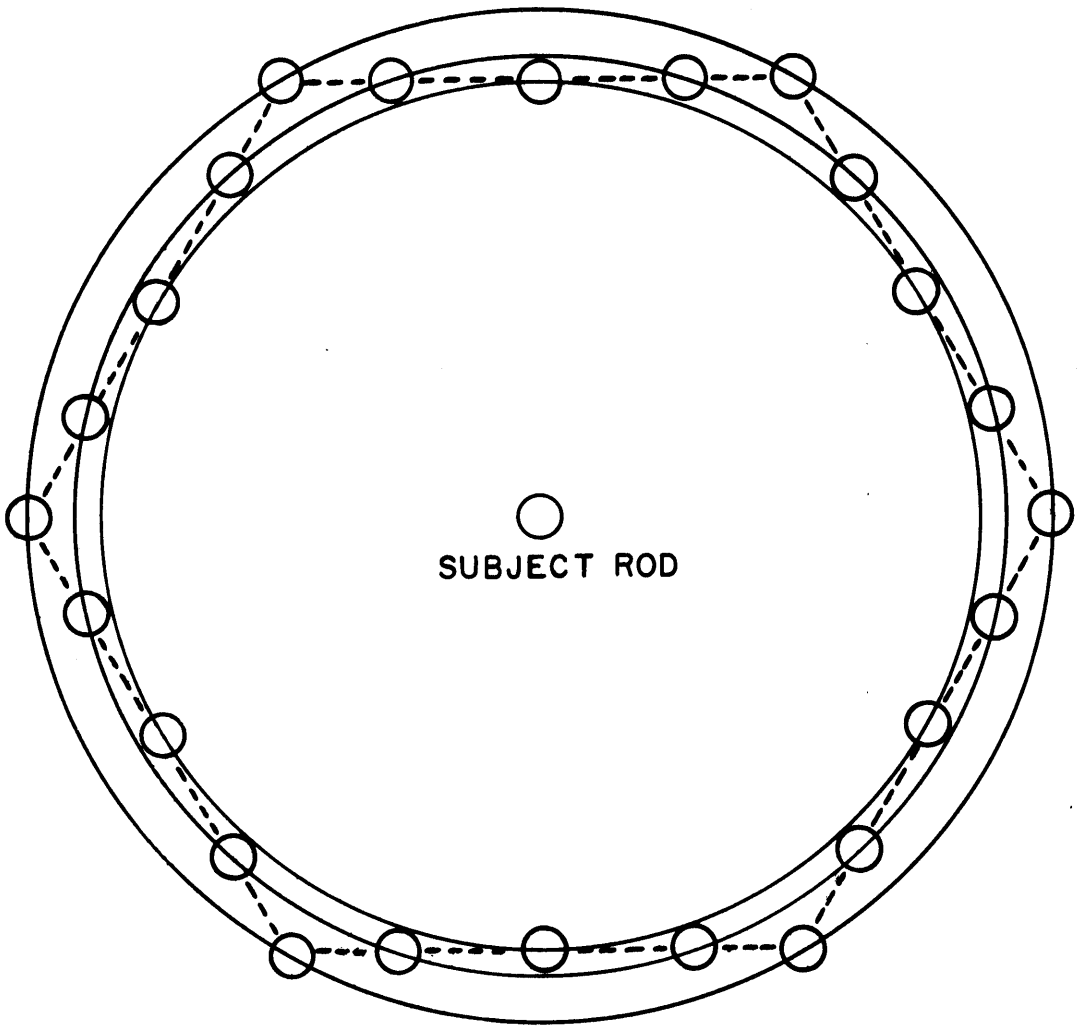

FIG. 5.14 DIVISION OF HEXAGONAL FUEL ARRAY INTO CONCENTRIC CIRCLES

in the assembly was approximated by the line source description given by Eq. 2.49. H^{SR} was evaluated by the computer program ROD described in Appendix B. Values of H^{SR} are given in Table 5.10.

The results of these computations are presented in Table 5.9 for each fuel rod position in which δ_{28} was measured. Also given are single rod measurements of δ_{28}^{SR} reported in reference H5. The average values of δ_{28}^{SR} from Table 5.9 are given in Table 5.10 for each type of fuel rod used in formation of the two region assemblies. Agreement of the two region assembly results with single rod experiments is good within the quoted experimental errors.

Another test of the theory is available by comparing values of δ_{28} for full lattices predicted by Eq. 2.43, using the average values of δ_{28}^{SR} from the two region measurements with the results of δ_{28} measurements in full single region lattices (H5). Such a comparison is presented in Table 5.11. The agreement is very good in all cases except for lattice 8. This lattice, together with lattice 7, was composed of 0.75-inch-diameter rods. From Table 5.10, it is seen that the two region value of δ_{28}^{SR} for this type fuel rod is in poorest agreement with the single rod experiment. If the single rod experimental results for δ_{28}^{SR} are used, Eq. 2.43 predicts values of δ_{28} for lattices 7 and 8 of $0.0634 \pm .0025$ and $0.0450 \pm .0018$, respectively, which are in better agreement with single region values, indicating that experimental rather than theoretical error is responsible for the poor agreement.

TABLE 5.9

δ_{28}^{SR} Calculated from δ_{28} Measurements in Two Region Assemblies

Assembly Designation	Assembly Ring*	Measured δ_{28}	Two Region δ_{28}^{SR}	Single Rod δ_{28}^{SR}
II	0	0.0190	0.0163	0.0163
III	0	0.0194	0.0168	0.0163
	1	0.0206	0.0178	0.0163
	2	0.0197	0.0169	0.0163
	3	0.0222	0.0188	0.0163
	4	0.0214	0.0172	0.0163
	5	0.0250	0.0164	0.0163
	7	0.0271	0.0164	0.0163
IV	0	0.0276	0.0161	0.0163
VII	0	0.0201	0.0148	0.0147
VIII	0	0.0198	0.0146	0.0147
IX	0	0.0166	0.0142	0.0163
	1	0.0194	0.0164	0.0163
	2	0.0178	0.0148	0.0163
	3	0.0194	0.0152	0.0163
	4	0.0209	0.0133	0.0163
	5	0.0523	0.0393	0.0426
	6	0.0548	0.0362	0.0426
X	0	0.0183	0.0146	0.0163
XI	0	0.0600	0.0559	0.0577
	2	0.0601	0.0564	0.0577
	4	0.0430	0.0393	0.0426

*Ring "O" is the central fuel rod.

TABLE 5.10

Average Values of δ_{28}^{SR} from Two Region Assembly Measurements

Rod Diameter (Inches)	Percent U^{235}	H^{SR} *	Average Two Region δ_{28}^{SR}	Single Rod δ_{28}^{SR}
0.250	1.027	0.3677	0.0162 ± .0015	0.0163 ± .0012
0.250	1.143	0.3677	0.0147 ± .0013	0.0145 ± .0015
0.750	0.947	0.9428	0.0383 ± .0026	0.0426 ± .0017
1.01	0.71	1.9916	0.0562 ± .0005	0.0577 ± .0022

*Equation 2.40

TABLE 5.11

δ_{28} for Full Lattices Predicted from Two Region Experiments

Lattice Designation	Predicted δ_{28} (Eq. 2.43)	Single Region Measurement (H5)
1	0.0289 ± .0027	0.0274 ± .0012
2	0.0212 ± .0020	0.0217 ± .0007
3	0.0186 ± .0017	0.0183 ± .0007
4	0.0262 ± .0023	0.0264 ± .0040
5	0.0199 ± .0018	0.0204 ± .0030
6	0.0169 ± .0015	0.0164 ± .0010
7	0.0584 ± .0039	0.0615 ± .0021
8	0.0415 ± .0027	0.0489 ± .0017
9	0.0603 ± .0005	0.0596 ± .0017

5.4 Determination of the Test Region Material Buckling

To determine the test region material buckling, B_m^2, by the methods presented in Chapter II, the only experimental quantity required is γ^2, the axial buckling of the assembly. This quantity is determined from analysis of the axial gold foil traverses as discussed in section 4.2.3 and the results of measurements in each of the two region assemblies as presented in Table 4.1.

The one group diffusion theory analysis of section 2.4.1 requires the equivalent radius of the test region, the material buckling of the outer region and the ratio of diffusion coefficients to define the parameters of Eq. 2.60. The equivalent radius of each assembly is given in Table 5.3, and Table 5.2 lists the thermal diffusion coefficients evaluated by the method discussed in Appendix D. Equation 2.60 can then be solved by iteration for the material buckling.

The two group approach of section 2.4.2 requires considerably more input. Calculation of the thermal diffusion length, L, and the resonance escape probability, p, is described in Appendix D, and the values used in the computations are given in Table 5.2. The fast diffusion length, L_f^2, is taken as equal to the age to thermal energy, τ, given in Table 5.2. The use of the Fermi age for the fast diffusion length is a common assumption of two group theory (W6, G3). In some applications, it is found necessary to adjust its value to attain agreement with experimental flux distributions. However, applications of similar two group diffusion treatments to critical two region assemblies have shown the final result to be only weakly influenced by the value used for L_f^2 (G4, L1), and the value of the age to thermal

energies has normally been employed.

The average diffusion coefficient for the fast group is defined as (E1):

$$D_{f,n} = \frac{\int_{E_{th}}^{E_o} D_n(E)\,\phi(E)\,dE}{\int_{E_{th}}^{E_o} \phi(E)\,dE} \quad . \tag{5.8}$$

If the energy distribution of flux can be represented by a 1/E distribution, the expression becomes:

$$D_{f,n} = \frac{\int_{E_{th}}^{E_o} D(E)\,dE/E}{\ln E_o/E_{th}} \quad , \tag{5.9}$$

where E_{th} is thermal energy and E_o an average neutron source energy. The expression for the Fermi age with an energy-independent slowing down power, $\xi\Sigma_s$, is:

$$\tau_{th} = \frac{1}{\xi\Sigma_s} \int_{E_{th}}^{E_o} D(E)\,dE/E \quad . \tag{5.10}$$

The ratio of fast neutron diffusion coefficients for the two regions is then:

$$D_f = \frac{D_{f,2}}{D_{f,1}} = \frac{\tau_2(\xi\Sigma_s)_1}{\tau_1(\xi\Sigma_s)_2} \quad . \tag{5.11}$$

The assumptions of a 1/E spectrum and constant slowing down power introduce error into Eq. 5.11. The spectra obtained from age theory analysis (Figs. 5.12 and 5.13) show that the actual coefficient must vary over each region and the calculation of a more accurate average

coefficient would be quite difficult. The actual parameter in Eq. 2.73 which involves D_f is z, defined as D_s/D_f. The quantity z is used as a correction factor to the right-hand side of the equation, its effect being proportional to $|z-1|$. The largest value of the quantity $|z-1|$ for the assemblies considered was 0.06 which affected the test region buckling by a maximum of 25 μB from the case of equal diffusion coefficients. Further refinements of the calculation of D_f would affect the bucklings even less and, in view of the results to be presented, it was concluded that further correction to D_f was not warranted.

Table 5.12 presents the results of both the one- and two-group analyses for the material buckling of the test region. The results of single region measurements of the material buckling for each region of each assembly are also given in the table. The values are taken from Ref. H5.

The poor agreement of most of the two region assembly results with those of single region experiments is obvious. The best agreement occurs with Assemblies VII, VIII, and XI. Assembly VIII differed from VII only in having a larger test region and gave a result closer to the full lattice value. All three of these assemblies had little difference in resonance escape probability between regions. Inspection of the table shows that the greater the difference in resonance escape probabilities between the two regions, the poorer the agreement of the two group result with the single region value.

This conclusion agrees with experience of other workers on two region assemblies (G4, N1, C4). The factor S given by Eq. 2.76 cannot be accurately calculated using the infinite lattice values for the

TABLE 5.12

Test Region Material Bucklings from Two Region Assembly Experiments

Assembly Designation	Test Region Lattice	Resonance Escape Probability Ratio p_2/p_1	Reference Region Buckling* (μB)	Test Region Material Buckling (μB)		
				One Group Analysis (Eq. 2.60)	Two Group Analysis (Eq. 2.73)	Single Region*
I	3	0.879	1195	1138	1025	891
II	3	0.879	1195	1183	910	891
III	3	0.879	1195	1037	1013	891
IV	1	1.14	891	1300	1349	1199
V	6	0.879	1444	1159	880	1000
VI	6	0.879	1444	1260	1211	1000
VII	2	1.00	1405	1398	1259	1200
VIII	2	1.00	1405	1250	1224	1200
IX	3	0.739	969	1316	1171	891
X	3	0.739	969	1777	1378	891
XI	9	1.040	1130	872	907	865

* From Ref. H5

resonance escape probabilities. In an infinite lattice, the resonance absorption in a fuel rod can be considered the sum of the absorption of neutrons born in the rod itself plus the absorption of neutrons born in surrounding rods. All these absorptions do not depend on the intensity of the fission source since the lattice is infinite. However, with two connected lattices, some rods of one lattice are partially surrounded by rods of the other lattice and, if the fast source differs between lattices, the absorption of the boundary rods will be different from that of an infinite lattice. This is particularly true for test regions of small size.

The progressive substitution method attempts to evade this problem by treating S as an experimental unknown. At least two assemblies of different test region size must then be studied and analyzed to yield the material buckling. But S is not entirely independent of test region size (N1), the deviations from a constant value being greater for small size test regions.

The present set of assemblies was analyzed as progressive substitution experiments by plotting the right-hand side of Eq. 2.74 versus material buckling for each of the assemblies. The curves for Assemblies II and III intersected at 875 μB. However, Assembly I, which had a small test region of the same composition, failed to intersect with the curves for either of the other assemblies. The curve for Assembly V, which also had a small test region, failed to intersect with that of Assembly VI. Assemblies VII and VIII, where troubles with resonance escape are least, intersected at a value of 1175 μB for the test region buckling. The full lattice value is 1200 μB. Finally,

Assemblies IX and X gave a common value of 1010 μB for the test region buckling, which is somewhat better than analyses of the separate assemblies (Table 5.12) but still quite far from the single region value of 891 μB.

From these results, it is concluded that the combination of large differences in resonance escape probabilities between lattices composing most of the assemblies and small test region sizes prevents meaningful buckling determinations for the majority of the lattices involved in these particular assemblies. This conclusion is in agreement with experience at Saclay (N1): "It is really necessary to know the details of the resonance capture in the two lattices exactly in order to be able to interpret the measurement very correctly. This is why we think there is an important difficulty, at least in the case of heavy water lattices . . . . It is this difficulty which makes it necessary not to limit the experiment to replacing only a small number of rods. In summary, there is always interest in proceeding so that the pertinent parameters should not be too different between the lattices compared."

Chapter VI

CONCLUSIONS AND RECOMMENDATIONS

6.1 Conclusions on the Results of the Present Study

In order to examine the usefulness of two region subcritical facilities for lattice parameter measurements, theories which describe the behavior of the neutron population in the assemblies were required. Several attempts to apply two group diffusion equations to the experimental flux distributions were made, including direct fit to the theoretical solutions and a moments method of extracting bucklings, similar to that used in single region lattices (C5). Because of boundary problems present in the assemblies and the interaction between regions during the slowing down process, none of these attempts was successful. The theory which proved most valuable for describing the behavior of neutrons in the slowing down region was age theory, which has also been successfully applied to D_2O miniature lattices at M. I. T. (P4, S1). Interaction between the regions of the assemblies during the slowing down process was satisfactorily described by this theory. The variety of the assemblies studied provided a rather severe test of this result. The lattices which were used to form the assemblies offered a considerable range of resonance and thermal absorption properties (see Table 5.2). Further, these lattices were combined to produce assemblies with the full range of differences between regions possible with the lattices

available. These differences in region properties are visually evident in the source distributions of Figures 5.1 through 5.11. The discontinuities in these curves are proportional to the ratios of $k_\infty \Sigma_a / p$ for the two regions. These ratios varied from 1.1 for Assemblies VII and VIII to 7.2 for Assemblies IX and X.

The ratio ρ_{28} of epicadmium to subcadmium capture rates in U^{238} was used to test the validity of the age theory's spectral predictions. These spectra were used to correct ρ_{28} measurements made at various radial positions in the two region assemblies to critical lattice values. The corrected ρ_{28}'s were then compared with full, single region results. The success of this comparison provides a considerable confidence that the slowing down density distributions resulting from the age theory analysis are correct.

Similar corrections for ρ_{28} have been developed by Sefchovich (S1) for heavy water moderated miniature lattice assemblies, using age-diffusion theory. In addition, Sefchovich applied corrections to the parameter C^*, defined by the relation:

$$C^* = \frac{\text{average total } U^{238} \text{ capture rate in the fuel}}{\text{average total } U^{235} \text{ fission rate in the fuel}} . \qquad (6.1)$$

Again, a ratio of resonance to thermal reaction rates is required. Although the application of basic age theory differed from the present study in many respects, the success of the ρ_{28} and C^* corrections in the miniature lattices and of the ρ_{28} corrections in the two region assemblies would imply that similar corrections for C^* from two region assemblies would lead to valid C^* values.

The parameter directly determined from the age theory analysis of the experimental traverses is $k_\infty \Sigma_a / p$. By using calculated values of Σ_a and p, the infinite multiplication factor, k_∞, can be determined. Comparison of the two region results with values from other sources shows that two region assemblies can be used to evaluate this parameter if the size of the inner region is larger than some minimum value. For the present set of experiments, inner regions of at least seven cells in diameter were required. This minimum size appears to be a function of the properties of the lattices composing the assembly. The present set of experiments is insufficient to determine the nature of this dependence, but it is not unreasonable to suppose that it is a function of the age to thermal energies in the assembly as well as the difference in $k_\infty \Sigma_a / p$ between regions.

Table 6.1 lists previously reported values of k_∞ determined experimentally by a variety of methods during the course of the M.I.T. Heavy Water Lattice Project (D1, W1, H2, B2). Details of the methods are given in the referenced reports. The results of the present study are included in the table for comparison. It can be seen that the uncertainties of the present work are comparable with those of pulsed source techniques, but are considerably higher than the four-factor formula or the added absorber methods. Both of these methods, however, require considerable fuel inventory and experiment assembly time.

The assumptions inherent in age theory make its application to fast neutron phenomena doubtful. Instead, a heterogeneous approach was used to describe the fast neutron distribution. Predictions by this theory of δ_{28}^{SR} and δ_{28} for critical lattices using experimental

TABLE 6.1

Values of the Infinite Multiplication Factor, k_∞

Lattice Designation	SOURCE OF VALUES FOR k_∞				
	Two-Region Assembly	Four-Factor Formula	Pulsed Source (Age-Diffusion)	Pulsed Source (Two-Group)	Added Absorber
1	1.325 ± 0.08	1.304 ± 0.020			
2	1.340 ± 0.07	1.375 ± 0.021			
3	1.332 ± 0.09	1.395 ± 0.021			
4	1.360 (one meas.)	1.330 ± 0.027	1.330 ± 0.035	1.315 ± 0.03	
5	1.453 ± 0.13	1.393 ± 0.026	1.437 ± 0.070	1.389 ± 0.054	1.416 ± 0.011
6	1.360 (one meas.)	1.422 ± 0.028	1.445 ± 0.077	1.389 ± 0.054	1.429 ± 0.007
7	1.236 ± 0.04	1.154 ± 0.023	1.097 ± 0.036	1.151 ± 0.036	1.187 ± 0.027
8	1.367 ± 0.01		1.427 ± 0.021	1.379 ± 0.020	
9	1.232 ± 0.01	1.219 ± 0.014			

measurements of δ_{28} in the two region assemblies proved very successful even when the corrections required were large.

It may be mentioned that the agreement of the two region assembly values of δ_{28} and ρ_{28} with single region measurements has given additional confidence to the accuracy of the single region lattice results.

As mentioned before, the two region assemblies used for this present study were purposely formed to provide a severe test of theoretical models. In the case of the test region material buckling determinations, this test criterion proved to be too strict. Although age theory can satisfactorily treat the interaction of the regions during the slowing down process, diffusion theory, used for the buckling analyses, apparently fails to do so in most cases. Therefore, the present study can only re-enforce conclusions of previous investigators: Satisfactory buckling measurements can only be made in two region assemblies which have sufficiently large test regions whose properties do not differ drastically from those of the reference region.

It should be noted that the success of age theory to describe the present assemblies is dependent on a close similarity of the two regions' slowing down properties. If an assembly were formed from lattices with different moderators, the present analysis could not be applied.

6.2 General Conclusions on Two Region Assemblies

The results of this study have shown that two region subcritical assemblies can be used to obtain rod integral parameters, such as δ_{28}, ρ_{28}, and C^*, characteristic of the lattice material. These values can

be obtained with an accuracy comparable with that of measurements in full subcritical lattices. In addition, values of the infinite multiplication factor, k_∞, can be found, but with considerably higher uncertainty than achieved by alternate procedures such as individual determination of the four factors η, ϵ, p and f, or the method of added absorbers.

In common with both the miniature lattice and single rod measurements, the determination of the material buckling from the two region lattices presents serious difficulties. However, unlike the other two methods, previous workers have found that the material buckling is attainable if the regions of the assembly are sufficiently similar in their nuclear properties.

There is no inherent reason why the treatment presented here could not be applied to lattices composed of U^{233} or plutonium isotopes. For such cases, where the fuel supply is limited, the use of a two region assembly with an outer region composed of fuel of the more abundant isotope, U^{235}, may offer an attractive method of determining lattice characteristics, especially if an outer neutronically similar region could be formed which would allow a material buckling determination. These outer regions could be selected from a series of well-calibrated lattices on the basis of spectral indices which would assure a sufficient degree of matching with the test core. This type of approach could be particularly useful in evaluating the nuclear effects of small changes in core or fuel design. Since the two region assembly yields rod integral parameters of validity and accuracy equal to those of the miniature lattice or the single rod measurement, the added advantages

of buckling measurements and its particular suitability for design variation studies would increase its relative attractiveness.

6.3 Recommendations for Future Work

Although the present application of age theory to the two region assemblies considered in this report has produced valid results in most cases, the failure of the theory to completely describe assemblies with small test regions requires additional investigation. Future work could be centered on the nature of this limitation.

The area of buckling measurements in two region subcritical assemblies could not be adequately covered by the present investigation. Experiments similar to those made on the present assemblies could be applied to assemblies restricted to lattices of similar properties. Methods of correcting calculated values of S (Eq. 2.76) might be developed possibly by heterogeneous theory, or progressive substitution techniques might be applied. If the latter course is used, care should be taken to avoid test regions of small size.

Appendix A

EFFECTIVE RESONANCE INTEGRAL FOR U^{238}

A.1 Theory

As mentioned in section 2.2.2, a lumped resonance energy for U^{238} is not sufficient for the application of age theory to two region assemblies. Fractional resonance escape probabilities must be used for at least the more important resonances and for this fractional effective resonance integrals must be available.

Calculation of the resonance integrals for the various sized rods used in the assemblies was performed by the computer program RES described in Appendix B. This code uses the technique first developed by Wigner (W4) and modified by Chernick and Vernon (C1).

Two approximations to the resonance structure have been commonly adopted. The first one considers very narrow resonances widely spaced apart and is known as the Narrow Resonance (NR) approximation. Under this assumption, the resonance integral over a single Breit-Wigner resonance is given by (V1):

$$I(NR) = \frac{I_\infty}{\left[1 + \beta \frac{\sigma_o}{\sigma_p}\left(1 - \frac{\Gamma_n}{\Gamma}\frac{\sigma_o}{\sigma_p}\right)\right]^{1/2}}, \qquad (A.1)$$

where

$I_\infty = \pi/2\,(\Gamma_n/E_r)\,\beta\sigma_o$ is the infinitely dilute resonance integral;

σ_p is the moderator cross section per fuel atom;

Γ_n is the neutron width at half resonance;

Γ is the total width at half resonance, $= \Gamma_n + \Gamma_\gamma$;

Γ_γ is the gamma width at half resonance;

E_r is the resonance energy;

β is the ratio of peak resonance cross section to potential scattering cross section in the fuel given by:

$$\beta = 4\pi \lambda\!\!\!^{-}_o \, \Gamma_n / \Gamma \sigma_o$$

where: $\lambda\!\!\!^{-}_o$ is the DeBroglie wavelength of the neutron with energy E_r;

and σ_o is the potential scattering cross section in the fuel taken to be 10 barns.

The NR approximation is poor for the lower energy resonances of the heavy absorbers. For these it is better to assume an infinitely heavy absorber leading to the NRIA (narrow resonance, infinitely heavy absorber) formula:

$$I(\text{NRIA}) = \frac{I_\infty}{\left[1 + \beta \frac{\Gamma_\gamma}{\Gamma} \frac{\sigma_o}{\sigma_p}\right]^{1/2}} . \qquad \text{(A.2)}$$

Chernick and Vernon (C1) show that the above equations for homogeneous systems become identical to those for heterogeneous systems if the moderator cross section per fuel atom is replaced by $S/4N_fV_f$ where N_f is the atomic density of U^{238} in the fuel and V_f is the fuel volume. Further, if the Breit-Wigner resonance is allowed to have a Doppler broadening, temperature effects can also be included. The modifications lead to:

$$I(\text{NR}) = \frac{I_\infty}{\pi} \int_{-\infty}^{\infty} \frac{\psi(x,\theta)\, dx}{1 + \frac{\beta}{\lambda+1}\left(1 + \frac{\Gamma_n/\Gamma}{\lambda+1}\right)\psi(x,\theta)} \qquad \text{(A.3)}$$

and

$$I(\mathrm{NRIA}) = \frac{I_\infty}{\pi} \int_{-\infty}^{\infty} \frac{\psi(x,\theta)\, dx}{1 + \frac{\Gamma_\gamma}{\Gamma} \frac{\beta}{\lambda} \psi(x,\theta)} , \tag{A.4}$$

where $\lambda = 4V_f/S$ is the mean chord length in the fuel rod in units of mean free path at the resonance, and ψ is the Doppler-broadened Breit-Wigner shape which is a function of $\theta = 4E_o kT/A\Gamma^2$. In ref. A1, the integral

$$J(\theta^{-1/2}, \Delta) = \frac{1}{2\Delta} \int_{-\infty}^{\infty} \frac{\psi(\theta,x)}{1 + \frac{\psi(\theta,x)}{\Delta}} dx \tag{A.5}$$

is tabulated. The resonance integrals can then be written in terms of the tabulated function as:

$$I(\mathrm{NR}) = \frac{2I_\infty(\lambda+1)}{\beta\left(1 + \frac{\Gamma_n/\Gamma}{\lambda+1}\right)} J\left[\theta^{-1/2}, \frac{\lambda+1}{\beta\left(1 + \frac{\Gamma_n/\Gamma}{\lambda+1}\right)}\right] , \tag{A.6}$$

$$I(\mathrm{NRIA}) = \frac{2I_\infty \lambda\Gamma}{\beta\Gamma_\gamma} J\left[\theta^{-1/2}, \frac{\lambda\Gamma}{\beta\Gamma_\gamma}\right] . \tag{A.7}$$

To calculate the contribution of each resolved resonance to the resonance integral, a choice must be made between the two models above. A more recent approach (G2) has been to use the Intermediate Resonance (IR) model which uses a linear combination of the two earlier approximations. The accuracy required for the present application did not warrant the added complications introduced by the use of this modification. Consequently, previous workers' choice of models was followed by using the NRIA model for six prominent resonances and considering all other resonances to be narrow and widely spaced (NR).

The region of unresolved resonances (E > ~1 Kev) must also be treated. Vernon (V1) found the total resonance integral above 30 Kev and the p-wave interactions down to one Kev are negligibly different from infinite dilution. His recommendation of a constant contribution of 1.6 barns to the effective resonance integral from these effects was adopted.

Contributions from the s-wave interactions are estimated by:

$$I = \frac{0.82}{D} \int_{1\ \text{Kev}}^{30\ \text{Kev}} I_{NR}(E)\, dE \ , \qquad (A.8)$$

using the average values of Γ_n and Γ_γ in the resolved resonance range. D is the spacing between resonances in the statistical range, and the correction factor of 0.82 is applied to account for statistical fluctuations in Γ_n, Γ_γ and D.

Data for the U^{238} resonances used in the calculations were obtained from ref. V1.

A.2 Effective Resonance Integrals Calculated by Computer Code RES

The results of the computation outlined above for the fuel rod types used in the two region assemblies are given in Table A.1.

It is of interest to compare the total effective integrals thus obtained with a standard recipe for resonance integrals. Table A.2 shows this comparison with the well-known formula of Hellstrand (H4):

$$ERI = 2.81 + 24.7\,(S/M)^{1/2} \ . \qquad (A.9)$$

The agreement is quite good, leading to considerable confidence in the use of the fractional ERI's computed from the program's output.

TABLE A.1

Effective Resonance Integrals for Uranium Rods

Resonance Energy (ev)	Neutron Width (ev)	Peak Cross Section (barns)	Infinite Dilution ERI (barns)	Fuel Rod ERI (barns)		
				0.25-Inch Diameter	0.75-Inch Diameter	1.0-Inch Diameter
6.68	0.00148	22119	127.95	5.1702	2.9693	2.5676
21.0	0.009	33210	61.108	2.3283	1.3193	1.1364
36.8	0.033	40535	42.563	1.9091	1.0867	0.9392
66.3	0.023	18975	11.059	0.7107	0.3868	0.3320
81.1	0.0021	2525	1.2031	0.2789	0.1761	0.1608
90.0	0.00008	94	0.04026	0.0350	0.0310	0.0300
102.5	0.065	18427	6.9469	0.6074	0.3355	0.2886
116.5	0.015	8466	2.8079	0.2800	0.1889	0.1766
145.6	0.0008	563	0.14948	0.0887	0.0648	0.0604
165.2	0.0035	1963	0.45917	0.1488	0.0978	0.0899
189.6	0.135	11616	2.3673	0.3528	0.1948	0.1670
208.5	0.055	8628	1.5991	0.1453	0.1082	0.1042
237.5	0.032	6198	1.0084	0.1272	0.0890	0.0843
264.5	0.00023	91	0.01332	0.0118	0.0108	0.0105
274	0.027	4972	0.70121	0.1097	0.0753	0.0709
291	0.019	3899	0.51775	0.1032	0.0691	0.0645
311.5	0.001	326	0.04050	0.0298	0.0242	0.0231
348	0.045	4837	0.53713	0.0803	0.0574	0.0547
377	0.0015	397	0.04068	0.0293	0.0236	0.0224
398.5	0.010	1888	0.18311	0.0660	0.0405	0.0284
411	0.017	2589	0.24339	0.0709	0.0479	0.0447
435	0.014	2171	0.19284	0.0640	0.0371	0.0326
455	0.0007	158	0.01345	0.0117	0.0105	0.0102
464	0.007	1243	0.10352	0.0490	0.0358	0.0341
479	0.0045	840	0.06781	0.0392	0.0294	0.0276
490	0.001	208	0.01637	0.0138	0.0122	0.0118
519	0.037	3013	0.22435	0.0528	0.0372	0.0353

TABLE A.1 (concluded)

Effective Resonance Integrals for Uranium Rods

Resonance Energy (ev)	Neutron Width (ev)	Peak Cross Section (barns)	Infinite Dilution ERI (barns)	Fuel Rod ERI (barns)		
				0.25-Inch Diameter	0.75-Inch Diameter	1.0-Inch Diameter
536	0.054	3337	0.24059	0.0483	0.0348	0.0333
557	0.001	182	0.01267	0.0111	0.0099	0.0096
581	0.042	2826	0.18796	0.0459	0.0326	0.0310
596	0.066	3182	0.20633	0.0412	0.0302	0.0290
605	0.0006	102	0.00654	0.0061	0.0057	0.0056
621	0.039	2571	0.15998	0.0430	0.0306	0.0290
629	0.009	1109	0.06811	0.0356	0.0264	0.0249
662	0.125	3286	0.19182	0.0317	0.0244	0.0238
680	0.0013	192	0.01092	0.0096	0.00867	0.0084
695	0.053	2559	0.14226	0.0362	0.0262	0.0251
710	0.017	1499	0.08156	0.0351	0.0263	0.0251
723	0.0147	1347	0.07199	0.0335	0.0250	0.0240
732	0.00425	524	0.02766	0.0202	0.0164	0.0156
766	0.009	910	0.04593	0.0272	0.0207	0.0196
782	0.003	362	0.01788	0.0145	0.0123	0.0118
792	0.011	1016	0.04956	0.0277	0.0210	0.0198
825	0.06	2238	0.10484	0.0291	0.0213	0.0205
855	0.13	2561	0.11573	0.0232	0.0178	0.0174
859	0.06	2150	0.09670	0.0277	0.0204	0.0196
867	0.0022	246	0.01099	0.0096	0.0085	0.0082
896	0.0013	146	0.00629	0.0058	0.0054	0.0053
909	0.09	2249	0.09562	0.0237	0.0178	0.0173
928	0.037	1685	0.07017	0.0270	0.0199	0.0190
940	0.195	2460	0.10111	0.0188	0.0148	0.0146
960	0.09	2130	0.08573	0.0223	0.0167	0.0162
983	0.001	1035	0.00407	0.0038	0.0036	0.0036
995	0.4	2465	0.09574	0.0150	0.0127	0.0298
Stat. region greater than 1 Kev				3.2527	3.0115	

TABLE A.2

Effective Resonance Integrals of U^{238}

Fuel Rod Diameter (Inch)	Effective Resonance Integral (Barns)	
	From Eq. A.9	Computer Program
0.25	17.07	16.84
0.75	11.04	11.08
1.00	9.94	10.07

Appendix B

COMPUTER PROGRAMS

B.1 Introduction

The programs described in this appendix have been written to perform the calculations required for the two region assembly analyses. All programs have been written in the FORTRAN IV language for use on the MIT IBM-360 computer.

B.2 Description of the Computer Program RES

The computer program RES, written for the calculation of the U^{238} effective resonance integral, uses the theory outlined in Appendix A. The program consists of a main section and four function subroutines. Input data are read into the main program which calls the function XNR to compute the partial effective resonance integrals for the narrow resonances and the function XNRIM for the infinite mass resonances. The integration of the narrow resonances over the statistical region is performed by Gaussian numerical integration with QG10, a subroutine supplied with the IBM-360 computer. The function subroutine FXNR supplies QG10 with the partial resonance integrals required for the integration as calculated by the subroutine XNR. Values of the Doppler-broadened Breit-Wigner function are supplied by XINT which interpolates between values in a table from Ref. A1 given as input to the program. (The subroutines ATSM, ALI and ATSE

are part of the IBM Scientific Subroutine Package and are described in Ref. S3.)

It should be noted that the program was specifically designed for cylindrical fuel rods of low enrichment. (The rods are assumed to be pure U^{238}.) Slight modification would allow a variable density to be employed.

B.2.1 Input Specification for RES

The input data are given below in the order required. The names of the variables for each FORMAT statement are given, followed by the required FORMAT in parentheses, and then by a brief description of the variable.

1. DIAM (E12.5)

   DIAM is the diameter of the fuel rod in inches.

2. NRIM, GG, D (I2, 2E12.5)

   NRIM is the total number of infinite mass resonances.

   GG is the gamma width at half resonance corresponding to Γ_γ in section A.1. This is assumed constant over the resonance region.

   D is the average spacing between resonances in the statistical region.

3. F(I), H(I) I=1, NRIM (6E12.5)

   F(I) is the energy of the i^{th} infinite mass resonance (ev).

   H(I) is the neutron width at half resonance for this resonance corresponding to Γ_n in Eq. A.4 (ev).

4. NR (I5)

   NR is the total number of resolved narrow resonances.

5. E(I), G(I), I=1, NR

   E(I) is the energy of the i^{th} resolved narrow resonance.

   G(I) is the neutron width at half resonance for this resonance corresponding to Γ_n in Eq. A.3 (ev).

6. B(J), J=1, 13 (6E12.5)

   The array B is composed of values of $\theta^{-1/2}$ taken in ascending order from the table of Ref. A1.

7. (A(I,J) J=1, 13), I=1, 28 (6E12.5)

   The array A contains the values of $k = \ln \Delta / \ln 2$ taken in order from the table of Ref. A1.

B.2.2 FORTRAN Listing

The FORTRAN listing of the program RES is given below.

```
CRES
C      CALCULATES PARTIAL EFFECTIVE RESONANCE INTEGRALS FOR U-238 IN
C      METAL RODS
C      REF-VERNON,'RESONANCE INTEGRALS OF U-238', NUCL. SCI. AND ENG.-7,
C                                                          252-259(1960)
C
       DIMENSION A(28,13),E(100),G(100),F(100),H(100),B(13)
       COMMON A,GG,SQ,NCOND,GAVE,B
C
C      INPUT  -- FUEL SPECIFICATION
       READ(5,1) DIAM
     1 FORMAT(6E12.5)
       WRITE(6,2) DIAM
     2 FORMAT(1H1,'  EFFECTIVE RESONANCE INTEGRAL FOR ',F10.5,' INCH DIAM
      1ETER RODS')
C
C      INPUT  U-238 RESONANCE PARAMETERS
C      INFINITE MASS RESONANCES
       READ(5,3) NRIM,GG,D
       READ(5,1) (F(I),H(I),I=1,NRIM)
C      NARROW RESONANCES
       READ(5,3) NR
     3 FORMAT(I2,2E12.5)
       READ(5,1) (E(I),G(I),I=1,NR)
       READ(5,1) (B(J),J=1,13)
       READ(5,1) ((A(I,J),J=1,13),I=1,28)
       WRITE(6,4)
     4 FORMAT('    ENERGY      NEUTRON         PEAK           ERI          ERI'/
      1'                  WIDTH        SIGMA     INF. DIL.      LATTICE')
C
       SUM=0.0
       ERI=0.0
       SQ=1.0/(20.0*0.0473*DIAM*1.27)
C      CALCULATION OF INFINITE MASS RESONANCES
       DO 6 I=1,NRIM
       ERI=ERI+XNRIM(F(I),H(I))
     6 SUM =SUM+H(I)
C      CALCULATION OF NARROW RESONANCES
       NCOND=1
       DO 5 I=1,NR
       ERI=ERI+XNR(E(I),G(I))
     5 SUM=SUM+G(I)
C
       NCOND=2
C
C      CALCULATION OF STATISTICAL REGION
       EXTERNAL FXNR
       X=NR*NRIM
       GAVE=SUM/X
       CALL QG10(1.0E+03,3.0E+04,FXNR,X)
C      AN AVERAGE CORRECTION FACTOR OF 0.82 IS APPLIED TO THE
C      CONTRIBUTION OF THE STATISTICAL REGION
       X=0.82*X/D+1.6
       WRITE(6,7) X
     7 FORMAT(' STAT. REGION  GREATER THAN 1KEV',17X,E12.5)
       ERI=ERI+X
       WRITE(6,8) ERI
```

```
8 FORMAT(1HO,'  TOTAL EFFECTIVE RESONANCE INTEGRAL = ',F10.5)
  STOP
  END

  FUNCTION XNR(E,G)
  DIMENSION A(28,13),B(13)
  COMMON A,GG,SQ,NCOND,GAVE,B
  GAMMA=GG*G
  SQIG=SQRT(2317.18/E)*GAMMA
  SIGO=2603640.0*G/(E*GAMMA)
  XINF=3.14159*GG*SIGO/(2.0*E)
  BETA=SIGO/10.0
  XK=BETA*(1.0-G/(GAMMA*(SQ+1.0)))/(SQ+1.0)
  XNR=XINF*XINT(SQIG,1.0/XK)
  GO TO(1,2),NCOND
1 WRITE(6,3) E,G,SIGO,XINF,XNR
2 RETURN
3 FORMAT(1X,5E12.5)
  END

  FUNCTION XNRIM(E,G)
  DIMENSION A(28,13),B(13)
  COMMON A,GG,SQ,NCOND,GAVE,B
  GAMMA=GG*G
  SQIG=SQRT(2317.18/E)*GAMMA
  SIGO=2603640.0*G/(E*GAMMA)
  XINF=3.14159*GG*SIGO/(2.0*E)
  BETA=SIGO/10.0
  XK=GG*BETA/(GAMMA*SQ)
  XNRIM=XINF*XINT(SQIG,1.0/XK)
  WRITE(6,3) E,G,SIGO,XINF,XNRIM
3 FORMAT(1X,5E12.5)
  RETURN
  END

  FUNCTION FXNR(E)
  DIMENSION A(28,13),B(13)
  COMMON A,GG,SQ,NCOND,GAVE,B
  FXNR=XNR(E,GAVE)
  RETURN
  END

  FUNCTION XINT(X,Y)
  DIMENSION A(28,13),ARG(28),VAL(28),D(28),E(13),B(13),T(28)
  COMMON A,GG,SQ,NCOND,GAVE,B
  W =ALOG(Y*1.0E+05)/ALOG(2.0)
  DO 1 I=1,28
  DO 2 L=1,13
2 E(L)=A(I,L)
  CALL ATSM(X,B,E,13,1,ARG,VAL,13)
1 CALL ALI(X,ARG,VAL,T(I),13,0.01,IER)
  CALL ATSE(W,4.0,0.5,T,28,1,ARG,VAL,28)
  CALL ALI(W,ARG,VAL,XINT,28,0.01,IER)
  XINT=2.0*Y*XINT/3.14159
  RETURN
  END
```

B.3 Description of Computer Program AGE

The application of age theory to two region assemblies is described in section 2.2. The code AGE was written to perform these calculations. The workings of the code may be divided into several steps:

1. Parameters describing the materials and geometry of the assembly are read in together with the axial buckling and the results of bare and cadmium-covered gold foil radial traverses together with their corresponding monitor foils. The axial buckling is determined from axial traverses by the code AXFIT (see section 4.2.3). The gold foil activities are submitted in the form of output from the code ACTIVE (see section 4.2.1). A more complete description of the input quantities and the required formats is given in the next section.

2. The subroutine RATIO corrects the monitor foils for decay during the period between the end of irradiation and the start of counting. The gold-cadmium ratio for each point in the traverse is calculated together with the standard error derived from the errors of the traverse foils and the monitors. (The subroutine DELAY, originally written by R. Simms and modified by F. Clikeman, is used to compute the number of hours between the end of irradiation and the start of monitor foil counting.) The radial foil position from the center of the foil holder, bare and cadmium-covered activities, the cadmium ratio and its error are printed for each foil position.

3. For symmetrical foil holders, the activity at each radial point is taken as the average of the activities on each half of the holder.

This procedure minimizes any error due to deviation of the holder from the horizontal position. If the holder is not symmetrical, each foil is considered separately. In either case, the activities are normalized to unity for the epicadmium activity of the center foil. Distances from the assembly center are calculated from the foil positions on the foil holder and the perpendicular distance of the holder from the assembly center.

4. Using the effective resonance integral for the gold foils and the slowing down power, Σ_s, for each region, which are supplied as input to the code, the slowing down function, ψ, and total thermal flux are calculated by Eqs. 2.24 and 2.27.

5. Fractional effective resonance integrals for U^{238} for each resonance and the total resonance escape probability are read in for each of the regions of the assembly. The neutron ages corresponding to the U^{238} resonances are also supplied.

6. Expansion coefficients defined by Eqs. 2.10 and 2.11 are computed for the first ten terms of the series. The necessary integration is performed by ten-point Gaussian integration using the subroutine QG10, a scientific subroutine supplied with the IBM-360 computer (S3). The function PRODUT supplies the product of the appropriate Bessel function and the thermal activation to QG10, the thermal activations being found by Lagrange interpolation among the measured values. The resulting coefficients are printed as output.

7. Resonance absorption is included by modifying the expansion coefficients at each resonance energy as described in section 2.2.2.

The integrals of Bessel function products are computed by the function subprogram BESS, using IBM-360 subroutines to compute the necessary Bessel functions.

8. The slowing down from the lowest U^{238} resonance to the principal gold resonance is included in the expansion coefficients. (I. e., the j^{th} coefficient is multiplied by $\exp(\gamma^2-\alpha_j^2)\Delta\tau$, where $\Delta\tau$ is the difference between the ages of the U^{238} resonance and that of gold.) The coefficients of $\left(\frac{k_\infty\Sigma_a}{p}\right)_1$ and $\left(\frac{k_\infty\Sigma_a}{p}\right)_2$ given in Eq. 2.17 are determined for each point in the traverse by summing the first ten terms in the series involved. (The summation is performed by the subroutine MATRIX.)

9. The quantity $\frac{k_\infty\Sigma_a}{p}$ for each region is found by a least squares fit to Eq. 2.17. This fit is performed by the subroutine FITZ, which was originally written to do a fit of experimental data to an n-dimensional straight line. This subroutine also evaluates the standard error in the fit of the data to the straight line and the error in each of the coefficients.

10. Using the results of the least squares fit, non-1/v parameters, C_{SC} and C_{EC}, are calculated by Eq. 2.21. Because of the discontinuities in the slowing down density at the U^{238} resonances, the total integral in this equation is the sum of integrals evaluated analytically between each pair of U^{238} resonances.

11. The new values of C_{SC} and C_{EC} are used to recalculate the slowing down function, ψ_{Au}, and the total thermal activation . Steps 9, 10 and 11 are repeated until the fractional change in the $\frac{k_\infty\Sigma_a}{p}$ values is less than 0.1%.

12. If desired, slowing down densities are calculated for neutron ages defined by the input to the code. The subroutine DENS does these calculations using the final values of $\frac{k_\infty \Sigma_a}{p}$ for each region. The results are printed.

13. The results of the analysis are used to compute relative values of ρ_{28} at each point in the traverse from Eq. 2.23. The absorption in each resonance is computed separately using the fractional ERI's supplied as input to the program. Equation 2.23 becomes:

$$\rho_{28}(r) = \frac{\psi(r, \tau_{Au}) \left[\left(\sum_k f_k \frac{Q(r, \tau_k)}{Q(r, \tau_{Au})} \right) \left(\frac{ERI}{\sigma_o} \right)_{28} + C_{EC} \right]}{0.886 + \psi(r, \tau_{Au}) C_{SC}} , \quad (B.1)$$

where f_k is the fractional ERI at age τ_k and the indicated summation is over all resonances of U^{238}. The value of $\left(\frac{ERI}{\sigma}\right)_{28}$ is supplied as input and is assumed the same as that of an infinite lattice. The values of the relative ρ_{28}'s are printed as output.

14. The input to the code specifies the maximum number of traverse points to be dropped. Points at the outer boundary of the assembly are dropped successively and steps 9 through 13 are repeated.

B.3.1 Input Specification for AGE

The input specifications are given below in the order required. The names of the variables for each format statement are given, followed by the required FORMAT in parentheses, and then by a brief description of the variable.

1. NFOIL, IBOUND, NDROP, DIST, GAMMA2, OUT (3I5, 3E12.5)

   NFOIL is the number of foils in each traverse. The program will not accept traverses which differ in the number or position of the foils. The maximum number of foils is 50.

   IBOUND is the serial number of the first foil in the outer region, counted from the center foil outward.

   NDROP is the maximum number of points to be dropped for a least squares fit.

   DIST is the perpendicular distance in centimeters of the foil holder from the assembly center.

   GAMMA2 is the axial buckling in inverse square centimeters as determined by AXFIT from axial traverses in the assembly.

   OUT is the physical outer radius of the assembly in centimeters.

2. NTRES, NTAU, RAD, REXT (2I5, 2E12.5)

   NTRES is the number of U^{238} resonances to be included in the analysis. Maximum value is 100.

   NTAU is the number of neutron ages for which neutron densities are to be calculated. Maximum value is 20.

   RAD is the radius of the inner region in centimeters.

   REXT is the extrapolated radius of the assembly in centimeters.

3. TA(I), I=1,NTAU (7E10.5)

   The array TA contains the neutron ages at which slowing down densities are to be calculated.

4. G(I), I=1,18 (18A4)

   Identification in alphanumeric characters of the cadmium-covered traverse. A 1 is placed in column 1 for carriage control. Columns 2 to 72 may contain any alphanumeric characters. These will be printed with the output from the code.

5. AV(J), Z(J), ERR(J), J=1,NFOIL (E12.5, F12.4, E12.5)

   AV(J) is the counts of the j^{th} foil corrected to the end of the irradiation. Foil positions are assumed to be consecutively numbered from one end of the foil holder to the other.

   Z(J) is the distance in centimeters of the j^{th} foil from the foil holder center.

   ERR(J) is the counting error of the j^{th} foil.

   The format of this card type is compatible with the punched output of the code ACTIVE (see section 4.2.1).

6. TM2 (E12.5)

   TM2 is the half-life of gold-198 in hours.

7. IDATE(2, I), IDATE(1, I), (IDATE(J, I), J=3, 5), I=1, 2 (2(5I5, 5X))

   IDATE(2, 1), IDATE(1, 1), IDATE(3, 1), IDATE(4, 1), and IDATE(5, 1) are the day, month, year, hour, and minute at the time of the end of the irradiation. When I=2, the same quantities are given to define the start of counting the monitor foil.

8. XMON, ERRM (E12.5, 12X, E12.5)

   XMON is the monitor counts corrected to the beginning of counting.

   ERRM is the counting error of the monitor foil.

9. Card types 4 to 8 are repeated for the bare gold traverse. The 1 in column 1 of card type 4 is omitted.

10. RES, SL1, SL2, TAU, ERI1, ERI2 (6E12.5)

    RES is ERI/σ_o for the gold foils. No 1/v component is included.

    SL1 and SL2 are the slowing down powers, $\xi\Sigma_s$, for the inner and outer regions, respectively.

ERI1 and ERI2 are ERI/σ_o for U^{238} in the rods of the inner and outer regions, respectively.

11. EO1 and EO2 (2E12.5)

EO1 and EO2 are the energies of the thermal neutrons in ev. in the inner and outer regions, respectively.

12. P1, P2 (2E12.5)

P1 and P2 are the total resonance escape probabilities in the inner and outer regions, respectively.

13. F1(I) I=1,NTRES (6E12.5)

F2(I) I=1,NTRES (6E12.5)

F1 and F2 are the fractional effective resonance integrals for U^{238} in the rods of the inner and outer regions, respectively. This resonance information must be supplied in order of decreasing resonance energy.

14. TRES(I), I=1,NTRES (6E12.5)

TRES(I) is the neutron age to the i^{th} resonance of U^{238} as defined in card type 13.

15. AU(I) I=1,9 (6E12.5)

AU(I) is the fractional effective resonance integral for the i^{th} resonance of Gold-198.

16. TAUR(I) I=1,9 (6E12.5)

TAUR(I) is the neutron age to the i^{th} resonance of Gold-198 as defined in card type 15.

B.3.2 FORTRAN Listing of AGE

The FORTRAN listing of the program AGE is given below.

```
CAGE
CAPPLICATION OF AGE THEORY TO TWO REGION LATTICES
C
      DIMENSION G(18),RO(50),PHI(50,2),Y(50),X(50),F1(100),F2(100),   TA
     1(20),XINT(50,50),BC(10),DC(10),VA(50),T(50),U(50),V(10,50),
     2DD(10),DRES(10),XRAD(10,10),XREX(10,10),RR(50),SS(50),HP(10),AU(9)
     3,TAUR(9),C1(50),C2(50),RA(50)
      DIMENSION AV(50),ERR(50),AVC(50),Z(50),AT(50),R(50),ALPHA(50),
     1TRES(100),B(10,100),D(10,100),BES(50,10),BB(2)
      COMMON AV,ERR,INDEX,AVC,NFOIL,Z,VA,T,IBESS,MT,ALPHA,GAMMA2,BES,
     1TRES,B,D,BB,MX,R,NTRES
C     INPUT
      EFUNF(T)=EXP(16.11810*(2.0-T)/6.726)
  602 INDEX=0
      READ(5,1) NFOIL,IBOUND,NDROP,DIST,GAMMA2,OUT
      IF(NFOIL)114,603,114
  114 READ(5,2030) NTRES,NTAU,RAD,REXT
      READ(5,2031) (TA(I),I=1,NTAU)
 2030 FORMAT(2I5,3E10.5)
 2031 FORMAT(7E10.5)
    1 FORMAT(3I5,4E12.5)
   14 INDEX=INDEX+1
      READ (5,103) (G(I),I=1,18)
      WRITE(6,103) (G(I),I=1,18)
      READ(5,2) (AV(J),Z(J),ERR(J),J=1,NFOIL)
    2 FORMAT(E12.5,F12.4,E12.5)
      CALL RATIO
      DO 22  I=1,NFOIL
   22 RO(I)= SQRT(DIST**2+(Z(I))**2)
      IF(Z(1)-Z(NFOIL))32,31,32
   32 MX=NFOIL
      DO 38 I=1,MX
      PHI(I,INDEX)=AVC(I)
      X(I)=Z(I)
   38 R(I)=RO(I)
      GO TO (43,44),INDEX
   31 MX=(NFOIL+1)/2
      DO 18 I=1,MX
      MI=NFOIL-I+1
      J1=MX-I+1
      PHI(J1,INDEX)=0.5*(AVC(I)+AVC(MI))
      X(J1)=Z(I)
   18 R(J1)=RO(I)
      GO TO (43,44),INDEX
   43 XNORM=PHI(1,1)
   44 DO 42 I=1,MX
   42 PHI(I,INDEX)=PHI(I,INDEX)/XNORM
      GO TO (14,15),INDEX
C
C CALCULATION OF SLOWING DOWN FUNCTIONS AND TOTAL THERMAL ACTIVITIES
   15 READ(5,400) RES,SL1,SL2,TAU,ERI1,ERI2
      READ(5,400) E01,E02
      E01=SQRT(E01)
      E02=SQRT(E02)
      WRITE(6,105)
  105 FORMAT(1HO,10X,21HNORMALIZED ACTIVITIES/3X,6HRADIUS,8X,7HEPI-CAD,
     17X,7H TOTAL )
```

```
      WRITE(6,106) (R(I),PHI(I,1),PHI(I,2),I=1,MX)
  106 FORMAT(1X,3F12.5)
  400 FORMAT(6E12.5)
      DO 30 I=1,MX
      RAT=PHI(I,2)/PHI(I,1)-1.0
      Y(I)=0.886/(RAT*(RES+0.5)-0.414)
   30 AT(I)=(PHI(I,2)-PHI(I,1))/(0.886+0.414*Y(I))
      WRITE(6,107)GAMMA2,OUT,RES, TAU,SL1,SL2
  107 FORMAT(1X,'MEASURED AXIAL RELAXATION LENGTH =',E12.5,/' ASSEMBLY R
     1ADIUS =',F12.5,/' GOLD RESONANCE INTEGRAL =',F12.5,/' AGE TO GOLD
     2 RESONANCE =',F12.5,/' SL1 =',E12.5,'  SL2 =',E12.5)
      READ(5,400) P1,P2
      READ(5,400) (F1(I),I=1,NTRES)
      READ(5,400) (F2(I),I=1,NTRES)
      READ(5,400)(TRES(I),I=1,NTRES)
      READ(5,400) (AU(I),I=1,9)
      READ(5,400) (TAUR(I),I=1,9)
      WRITE(6,80) P1,P2
   80 FORMAT(1X,' RESONANCE ESCAPE PROBABILITIES'/' INNER REGION =',F12.
     15,'  OUTER REGION =',F12.5)
      ALP1=ALOG(P1)
      ALP2=ALOG(P2)
  401 FORMAT(F12.5,E12.5)
      WRITE(6,404)
  404 FORMAT(9HO  RADIUS,2X,18HTHERMAL ACTIVATION,5X,21HSLOWING DOWN FUN
     1CTION)
      WRITE (7,401) (R(I),AT(I),I=1,MX)
      WRITE(6,425) (R(I),AT(I),Y(I),I=1,MX)
  425 FORMAT(F10.5,3X,E12.5,5X,E12.5)
  405 FORMAT(F10.5,3X,E12.5,5X,E12.5,5X,F10.5)
      MT=MX+2
      VA(1)=AT(2)
      T(1)=-R(2)
      DO 70 I=1,MX
      K=I+1
      VA(K)=AT(I)
   70 T(K)=R(I)
      VA(MT)=0.0
      T(MT)=REXT
C
C EXPANSION OF ZERO AGE SLOWING DOWN DENSITY IN TERMS OF J-0 FUNCTIONS
      EXTERNAL  PROD
      WRITE(6,502) REXT
  502 FORMAT(23H1EXTRAPOLATED RADIUS IS,F12.5)
      ALPHA(1)=2.404825/REXT
      ALPHA(2)=5.520078/REXT
      ALPHA(3)=8.653727/REXT
      ALPHA(4)=11.79153/REXT
      ALPHA(5)=14.93091/REXT
      ALPHA(6)=18.07106/REXT
      ALPHA( 7)=21.21164/REXT
      ALPHA( 8)=24.35247/REXT
      ALPHA( 9)=27.49348/REXT
      ALPHA(10)=30.63460/REXT
      WRITE(6,503) RAD
  503 FORMAT(19HOBOUNDARY RADIUS IS,F12.5)
      DO 33 J=1,10
```

```
      IBESS=J
      CALL QG10(0.0, RAD,PROD,XIN)
      XINT(J,1)=XIN
      CALL QG10(0.0,REXT,PROD,XIN)
      XINT(J,3)=XIN
      CALL QG10(RAD, OUT,PROD,XIN)
   33 XINT(J,2)=XIN
      WRITE(6,410)
      DO 60 J=1,10
      CALL BESJ(ALPHA(J)*REXT,1,RJ,0.1E-05,IER)
      HP(J)=2.0/(REXT*RJ)**2
      B(J,1)=XINT(J,1)*HP(J)
      D(J,1)=XINT(J,2)*HP(J)
      Z(J)=XINT(J,3)*HP(J)
   60 WRITE(6,400) ALPHA(J),B(J,1),D(J,1),Z(J)
  410 FORMAT(42HOCOEFFICIENTS OF BESSEL FUNCTION EXPANSION/6H ALPHA,8X,
     1 1HB,10X,1HD)
C
C    CALCULATION OF BESSEL FUNCTIONS
      DO 2012 I=1,MX
      DO 2013 J=1,10
      CALL BESJ(R(I)*ALPHA(J),0,RJ,0.1E-05,IER)
 2013 BES(I,J)=RJ
 2012 CONTINUE
C
C CALCULATION OF INTEGRALS OF BESSEL FUNCTION PRODUCTS
      DO 2000 I=1,10
      CALL BESJ(RAD*ALPHA(I),0,RJ,0.1E-05,IER)
      CALL BESJ(RAD*ALPHA(I),1,BJ,0.1E-05,IER)
      XRAD(I,I)=RAD**2*(RJ**2+BJ**2)/2.0
 2000 XREX(I,I)=1.0/HP(I)-XRAD(I,I)
      DO 2001 I=1,9
      K=I+1
      DO 2001 J=K,10
      XRAD(I,J)=BESS(ALPHA(I),ALPHA(J),RAD)
      XREX(I,J)=-XRAD(I,J)
      XRAD(J,I)=XRAD(I,J)
 2001 XREX(J,I)=XREX(I,J)
      DO 2002 I=1,10
      DO 2002 J=1,10
      XRAD(I,J)=XRAD(I,J)*HP(I)
 2002 XREX(I,J)=XREX(I,J)*HP(I)
      DTAU=TRES(1)
      DO 2111 K=1,NTRES
      DO 2003 I=1,10
      BC(I)=B(I,K)*EXP((GAMMA2-ALPHA(I)**2)*DTAU)
 2003 DC(I)=D(I,K)*EXP((GAMMA2-ALPHA(I)**2)*DTAU)
      PP=EXP(F1(K)*ALP1)
      QQ=EXP(F2(K)*ALP2)
      DO 34 I=1,10
      B(I,K+1)=0.0
      D(I,K+1)=0.0
      DO 34 N=1,10
      B(I,K+1)=B(I,K+1)+BC(N)*(PP*XRAD(I,N)+QQ*XREX(I,N))
      D(I,K+1)=D(I,K+1)+DC(N)*(PP*XRAD(I,N)+QQ*XREX(I,N))
   34 CONTINUE
 2111 DTAU=TRES(K+1)-TRES(K)
```

```
C
C  CALCULATION OF EXPANSION COEFFIENTS AT GOLD RESONANCE
      DTAU=TAU-TRES(NTRES)
      M=NTRES+1
      DO 82 I=1,10
   82 AV(I)=B(I,M)*EXP((GAMMA2-ALPHA(I)**2)*DTAU)
      CALL MATRIX(AV,RR)
      DO 83 I=1,10
   83 AV(I)=D(I,M)*EXP((GAMMA2-ALPHA(I)**2)*DTAU)
      CALL MATRIX(AV,SS)
C
C   LEAST SQUARES FIT TO SLOWING DOWN FUNCTION
      DO 2004 I=1,MX
      V(1,I)=RR(I)
 2004 V(2,I)=SS(I)
      WRITE(6,84)
   84 FORMAT(1HO,' SERIES SUMMATIONS')
      WRITE(6,400)(V(1,I),V(2,I),I=1,MX)
      AO=0.0
      BO=0.0
      NDROP=NDROP+1
      DO 85 NR=1,NDROP
      MA=MX-NR+1
      NP=NR-1
      DTAU=TAU-TRES(NTRES)
      WRITE(6,86) NP
   86 FORMAT(1H1,I5,' POINTS DROPPED')
 3007 DO 2017 I=1,MX
      IF(I-IBOUND)2015,2016,2016
 2015 SL=SL1
      GO TO 2017
 2016 SL=SL2
 2017 U(I)=Y(I)*AT(I)*SL
      CALL FITZ(V,U,2,MA,BB,DD)
      WRITE(6,87)  (BB(I),DD(I),I=1,2)
   87 FORMAT('  (K*SIGMA/P)1 =',F10.5,1H(,E12.5,1H),'  (K*SIGMA/P) =',
     1F10.5,1H(,E12.5,1H))
      EPS1=ABS(BB(1)-AO)/BB(1)
      EPS2=ABS(BB(2)-BO)/BB(2)
      AO=BB(1)
      BO=BB(2)
C SPECTRAL  CORRECTION OF EPI CADMIUM ABSORPTION
      DO 3001 I=1,10
      CA=6.726*(GAMMA2-ALPHA(I)**2)
      BS=0.0
      DO 3002 J=1,NTRES
      AS=BB(1)*B(I,J)+BB(2)*D(I,J)
      XLL=EFUNF(TRES(J))
      IF(J-1) 3003,3003,3004
 3003 UL=EFUNF(0.0)
      GO TO 3002
 3004 UL=EFUNF(TRES(J-1))
 3002 BS=BS+UL**CA*(AS/XLL**(.5*CA)-AS/UL**(.5*CA))
      AS=BB(1)*B(I,M)+BB(2)*D(I,M)
      UL=EFUNF(TRES(NTRES))
      UI=UL
      XLL=0.4
```

```
      BS=BS*UL**CA*(AS/XLL**(.5*CA)-AS/UL**(.5*CA))
      Z(I)=BS*E01/(.5*CA)
      UL=0.12
      HP(I)=UI**CA*(AS/UL**(.5*CA)-AS/XLL**(.5*CA))*E01/(.5*CA)
 3001 BC(I)=AS*EXP((GAMMA2-ALPHA(I)**2)*DTAU)
      CALL MATRIX(BC,AV)
      DO 303 I=1,MX
  303 AVC(I)=0.0
      DO 302 I=1,9
      CALL DENS(TAUR(I),RR)
      DO 302 J=1,MX
  302 AVC(J)=RES*AU(I)*RR(J)/AV(J)*AVC(J)
      CALL MATRIX(Z,RR)
      CALL MATRIX(HP,SS)
      WRITE(6,3008)
 3008 FORMAT(' RATIOS OF 1/V ABSORPTIONS TO GOLD RESONANCE ABSOPTIONS')
      DO 3005 I=1,MX
      IF(I-IBOUND)300,301,301
  301 RR(I)=E02*RR(I)/E01
      SS(I)=E02*SS(I)/E01
  300 C1(I)=RR(I)/AV(I)
      C2(I)=SS(I)/AV(I)
      WRITE(6,405) R(I),C1(I),C2(I),AVC(I)
      RAT=PHI(I,2)/PHI(I,1)-1.0
      Y(I)=0.886/(RAT*(AVC(I)*C1(I))-C2(I))
 3005 AT(I)=(PHI(I,2)-PHI(I,1))/(0.886*C2(I)*Y(I))
      WRITE(6,404)
      WRITE(6,425) (R(I),AT(I),Y(I),I=1,MX)
      IF(EPS1.LE.0.001.AND.EPS2.LE.0.001) GO TO 3006
      GO TO 3007
 3006 DO 2010 N=1,NTAU
      CALL DENS(TA(N),AV)
      WRITE(6,7) TA(N)
    7 FORMAT(1HO,'  SLOWING DOWN DENSITY AT',F10.5,' SQ. CM.')
 2010 WRITE(6,807) (R(I),AV(I),I=1,MX)
C
C  CALCULATION  OF RELATIVE RHO-28
      WRITE(6,806)
  806 FORMAT(1HO,'RELATIVE VALUES OF RHO-28')
      DO 801 I=1,10
      Z(I)=0.0
      DO 801 L=2,M
  801 Z(I)=(BB(1)*B(I,L)*BB(2)*D(I,L))*F1(L-1)*Z(I)
      CALL MATRIX(Z,RR)
      IB=IBOUND-1
      DO 802 I=1,IB
      RHO=(C1(I)*AV(I)*ER11*RR(I))/(0.886*AT(I)*SL1*C2(I)*AV(I))
  802 WRITE(6,807) R(I),RHO
      DO 803 I=1,10
      Z(I)=0.0
      DO 803 L=2,M
  803 Z(I)=(BB(1)*B(I,L)*BB(2)*D(I,L))*F2(L-1)*Z(I)
      CALL MATRIX(Z,RR)
      DO 804 I=IBOUND,MX
      RHO=(C1(I)*AV(I)*ER12*RR(I))/(0.886*AT(I)*SL2*C2(I)*AV(I))
  804 WRITE(6,807) R(I),RHO
   85 CONTINUE
```

```
  807 FORMAT(1X,F12.5,E12.5)
      GO TO 602
  603 STOP
  103 FORMAT(18A4)
      END

      SUBROUTINE RATIO
CRATIO   CALCULATION OF CADMIUM RATIOS - J. GOSNELL
      DIMENSION ERAV(50),RAT(50),ERA(50),RATIO(50),ERRAT(50),IDATE(5,2)
      DIMENSION AV(50),ERR(50),AVC(50),Z(50)
      COMMON AV,ERR,INDEX,AVC,NFOIL,Z
      READ(5,1)TM2
      READ(5,2) ((IDATE(2,I),IDATE(1,I),(IDATE(J,I),J=3,5),I=1,2)
      WRITE(6,12) ((IDATE(2,I),IDATE(1,I),(IDATE(J,I),J=3,5),I=1,2)
   12 FORMAT('  END OF RUN',I10,'/',I2,'/',I2,I10,'.',I2/'  MONITOR FOIL
     1 COUNTED',I10,'/',I2,'/',I2,I10,'.',I2)
      CALL DELAY(IDATE,DLAYTM)
      READ(5,3) XMON,ERRM
      DEKAY=ALOG(2.0)/TM2
      CORR=XMON* EXP(DEKAY*DLAYTM)
      WRITE(6,103) CORR
  103 FORMAT('  MONITOR FOIL CORRECTED COUNTS',2X,E12.5)
      ERRC=ERRM* EXP(DEKAY*DLAYTM)
      DO 4 I=1,NFOIL
      AVC(I)=AV(I)/CORR
      ERAV(I)= SQRT((ERR(I)/AV(I))**2+(ERRC/CORR)**2)
      GO TO (5,4),INDEX
    5 RAT(I)=AVC(I)
      ERA(I)=ERAV(I)
    4 CONTINUE
      GO TO (8,9),INDEX
    9 WRITE(6,100)
      DO 10 I=1,NFOIL
      F=RAT(I)
      IF(F)20,21,20
   21 RATIO(I)=0.0
      ERRAT(I)=0.0
      GO TO 10
   20 RATIO(I)=AVC(I)/RAT(I)
      ERRAT(I)=RATIO(I)* SQRT(ERAV(I)**2+ERA(I)**2)
   10 WRITE(6,101) Z(I),RAT(I),AVC(I),RATIO(I),ERRAT(I)
    8 RETURN
    1 FORMAT(E12.5)
    2 FORMAT(2(5I5,5X))
    3 FORMAT(E12.5,12X,E12.5)
  100 FORMAT(13HOHOLDER POSIT,5X,7HEPI-CAD,7X,7H TOTAL ,5X,9HCAD RATIO,8
     1X,5HSIGMA)
  101 FORMAT(1X,F12.5,4(2X,E12.5))
      END

      SUBROUTINE DELAY ( IDATE, DLAYTM )                                DELAY 1
C     DELAY
      DIMENSION M(12), IDATE(5,2), IDAY(2)                              DELAY 2
C                                                                       DELAY 3
C     IDATE(I,K)  I=MONTH, DAY, YEAR, HOUR, MINUTE  K=1=END OF IRRAD.   DELAY 4
C     TIME    K=2=START OF COUNT TIME                                   DELAY 5
C                                                                       DELAY 6
```

```
C     DERTERMINATION OF THE NUMBER OF DAYS FROM THE BEGINNING OF THE    DELAY 7
C     YEAR TO (1) THE END OF IRRADIATION TIME AND (2) THE START OF THE  DELAY 8
C     COUNT TIME.   A CHECK FOR LEAP YEAR IS ALSO INCLUDED.             DELAY 9
C                                                                       DELAY10
      M( 1) =  00                                                       DELAY11
      M( 2) =  31                                                       DELAY12
      M( 3) =  59                                                       DELAY13
      M( 4) =  90                                                       DELAY14
      M( 5) = 120                                                       DELAY15
      M( 6) = 151                                                       DELAY16
      M( 7) = 181                                                       DELAY17
      M( 8) = 212                                                       DELAY18
      M( 9) = 243                                                       DELAY19
      M(10) = 273                                                       DELAY20
      M(11) = 304                                                       DELAY21
      M(12) = 334                                                       DELAY22
      DO 550 K=1,2                                                      DELAY23
      J = IDATE(1,K)                                                    DELAY24
      IDAY(K) = M(J) + IDATE(2,K)                                       DELAY25
      YEAR =  FLOAT( IDATE(3,K)) / 4.0
      XYEAR=INT(YEAR)
      IF ( XYEAR - YEAR ) 550, 510, 550                                 DELAY28
  510 IF ( IDAY(K) - 60 ) 550, 520, 540                                 DELAY29
  520 IF (IDATE(1,K) - 2)550, 550, 540                                  DELAY30
  540 IDAY(K) = IDAY(K) + 1                                             DELAY31
  550 CONTINUE                                                          DELAY32
      IF ( IDAY(2) - IDAY(1) ) 1, 5, 5                                  DELAY33
    1 YEAR =  FLOAT( IDATE(3,1) ) / 4.0
      XYEAR=INT(YEAR)
      IF ( XYEAR - YEAR ) 3, 4, 3                                       DELAY36
    3 IDAY(2) = IDAY(2) + 365                                           DELAY37
      GO TO 5                                                           DELAY38
    4 IDAY(2) = IDAY(2) + 366                                           DELAY39
    5 DIFDAY = ( IDAY(2) - IDAY(1) - 1 ) * 24                           DELAY40
      TOTOUR = ( 24.0 -  FLOAT(IDATE(4,1)) -  FLOAT(IDATE(5,1)) / 60.0 )DELAY41
     1  +  FLOAT(IDATE(4,2)) +  FLOAT(IDATE(5,2)) / 60.0               DELAY42
      DLAYTM = DIFDAY + TOTOUR                                          DELAY43
C                                                                       DELAY44
C     DLAYTM IS THE TIME DIFFERENCE BETWEEN THE STOPPING OF THE         DELAY45
C     IRRADIATION AND THE START OF THE FOIL COUNTING.  THE TIME IS IN   DELAY46
C     HOURS                                                             DELAY47
C                                                                       DELAY48
      RETURN                                                            DELAY49
      END                                                               DELAY50

      FUNCTION BESS(A,B,R)
C
C  CALCULATES INTEGRAL OF BESSEL FUNCTION PRODUCT
C
      CALL BESJ(A*R,0,AJ0,0.1E-05,IER)
      CALL BESJ(B*R,0,BJ0,0.1E-05,IER)
      CALL BESJ(A*R,1,AJ1,0.1E-05,IER)
      CALL BESJ(B*R,1,BJ1,0.1E-05,IER)
      BESS=R*(A*AJ1*BJ0-B*BJ1*AJ0)/(A**2-B**2)
      RETURN
      END
```

```
      FUNCTION PROD(X)
C     DEFINES FUNCTION TO BE INTEGRATED FOR BESSEL FUNCTION EXPANSION
C
      DIMENSION VAL(50),T(50)
      DIMENSION AV(50),ERR(50),AVC(50),Z(50),AT(50),R(50),ALPHA(50)
      COMMON AV,ERR,INDEX,AVC,NFOIL,Z,AT,R,IBESS,MX,ALPHA
C
      CALL ATSM(X,R,AT,MX,1,T,VAL,MX)
      CALL ALI(X,T,VAL,Y,MX,0.1E-04,IER)
      CALL BESJ(ALPHA(IBESS)*X,0,RJ,0.1E-05,IER)
      PROD=Y*RJ*X
      RETURN
      END

      SUBROUTINE DENS(TAU,Q)
      DIMENSION A(10),Q(50)
      DIMENSION AV(50),ERR(50),AVC(50),Z(50),AT(50),R(50),ALPHA(50),
     1TRES(100),B(10,100),D(10,100),BES(50,10),BB(2),VA(50),T(50)
      COMMON AV,ERR,INDEX,AVC,NFOIL,Z,VA,T,IBESS,MT,ALPHA,GAMMA2,BES,
     1TRES,B,D,BB,MX,R,NTRES
      DO 1 K=1,NTRES
      IF(TAU-TRES(K))11,11,1
    1 CONTINUE
      K=NTRES+1
   11 IF(K-1)4,4,5
    4 TB=0.0
      GO TO 12
    5 TB=TRES(K-1)
   12 DO 3 J=1,10
    3 A(J)=(BB(1)*B(J,K)+BB(2)*D(J,K))*EXP((GAMMA2-ALPHA(J)**2)*(TAU-TB)
     1)
      CALL MATRIX(A,Q)
      RETURN
      END

      SUBROUTINE MATRIX(A,C)
      DIMENSION A(10),C(50)
      DIMENSION AV(50),ERR(50),AVC(50),Z(50),AT(50),R(50),ALPHA(50),
     1TRES(100),B(10,100),D(10,100),BES(50,10),BB(2),T(50),VA(50)
      COMMON AV,ERR,INDEX,AVC,NFOIL,Z,VA,T,IBESS,MT,ALPHA,GAMMA2,BES,
     1TRES,B,D,BB,MX,R,NTRES
      DO 1 I=1,MX
    1 C(I)=0.0
      DO 2 I=1,MX
      DO 2 J=1,10
    2 C(I)=C(I)+A(J)*BES(I,J)
      RETURN
      END

      SUBROUTINE FITZ(X,Y,N,MT,A,SIGMA)
      DIMENSION X(10,50),Y(50),A(10),SIGMA(10),B(10),C(10,10),Z(50),R(10),
     1),CC(10,10)
C     DOES A LEAST SQUARES FIT TO A STRAIGHT LINE
C     Y(I)=A(1)X(1,I)+A(2)X(2,I)+.....+A(N)X(N,I)
C     THE A'S ARE THE CONSTANTS TO BE EVALUATED FROM EXPERIMENTAL VALUES
C OF THE VARIABLES Y AND X'S.
C     MAXIMUM OF 50 SETS OF EXPERIMENTAL POINTS IN 10 DIMENSIONS
```

```
C
      M=MT
      WRITE(6,200)
   16 DO 1 J=1,N
      R(J)=0.0
      B(J)=0.0
      DO 1 K=1,N
    1 C(J,K)=0.0
      CC(J,K)=0.0
      DO 2 J=1,N
      DO 2 I=1,M
      B(J)=Y(I)*X(J,I)+B(J)
      DO 2 K=1,N
      CC(J,K)=X(J,I)*X(K,I)+C(J,K)
    2 C(J,K)=X(J,I)*X(K,I)+C(J,K)
      KS=0
      CALL SIMQ(C,B,N,KS,10)
C
C     DETERMINATION OF GOODNESS OF FIT
      DO 8 J=1,N
    8 A(J)=B(J)
      SUM =0.0
      DO 5 I=1,M
      Z(I)=0.0
      DO 6 J=1,N
    6 Z(I)=A(J)*X(J,I)+Z(I)
      ERR=Y(I)-Z(I)
      WRITE(6,100) Y(I),Z(I),ERR
    5 SUM=SUM+ERR**2
      XM=FLOAT(M)
      SIGMAY=SQRT(SUM/(XM-2.0))
      WRITE(6,101)SIGMAY
  100 FORMAT(1X,3E12.5)
C
C     ESTIMATION OF ERROR FOR EACH CONSTANT
   17 DO 3 I=1,M
      DO 4 J=1,N
      DO 4 K=1,N
      B(J)=X(J,I)
    4 C(J,K)=CC(J,K)
      KS=0
      CALL SIMQ(C,B,N,KS,10)
      DO 3 K=1,N
    3 R(K)=B(K)**2+R(K)
      DO 7 K=1,N
    7 SIGMA(K)=SIGMAY*SQRT(R(K))
      RETURN
  200 FORMAT(18HOLEAST SQUARES FIT)
  101 FORMAT(44H DEVIATION OF POINTS FROM A STRAIGHT LINE = ,E12.5)
      END
C                                                                      SIMQ 001
C     ..................................................................SIMQ 002
C                                                                      SIMQ 003
C        SUBROUTINE SIMQ - OBTAINED FROM THE MIT COMPUTATION CENTER     SIMQ 004
C                                                                      SIMQ 005
C        PURPOSE                                                       SIMQ 006
C           OBTAIN SOLUTION OF A SET OF SIMULTANEOUS LINEAR EQUATIONS,  SIMQ 007
```

```
C            AX=B                                                          SIMQ 008
C                                                                          SIMQ 009
C         USAGE                                                            SIMQ 010
C              CALL SIMQ(A,B,N,KS,M)                                       SIMQ 011
C                                                                          SIMQ 012
C         DESCRIPTION OF PARAMETERS                                        SIMQ 013
C            A - MATRIX OF COEFFICIENTS STORED COLUMNWISE.  THESE ARE      SIMQ 014
C                DESTROYED IN THE COMPUTATION.  THE SIZE OF MATRIX A IS    SIMQ 015
C              M BY M.                                                     SIMQ 016
C         B - VECTOR OF ORIGINAL CONSTANTS (AT LEAST OF LENGTH N). THE     SIMQ 017
C              FIRST N PLACES ARE REPLACED BY FINAL SOLUTION VALUES,       SIMQ 018
C              VECTOR X.                                                   SIMQ A18
C            N - NUMBER OF EQUATIONS AND VARIABLES                         SIMQ 019
C            KS - OUTPUT DIGIT                                             SIMQ 020
C                 0 FOR A NORMAL SOLUTION                                  SIMQ 021
C                 1 FOR A SINGULAR SET OF EQUATIONS                        SIMQ 022
C         M - NUMBER OF ROWS AND COLUMNS FOR A AS DIMENSIONED IN THE       SIMQ A22
C              CALLING PROGRAM.                                            SIMQ B22
C                                                                          SIMQ 023
C         REMARKS                                                          SIMQ 024
C            MATRIX A MUST BE GENERAL.                                     SIMQ 025
C            IF MATRIX IS SINGULAR , SOLUTION VALUES ARE MEANINGLESS.      SIMQ 026
C            AN ALTERNATIVE SOLUTION MAY BE OBTAINED BY USING MATRIX       SIMQ 027
C            INVERSION (MINV) AND MATRIX PRODUCT (GMPRD).                  SIMQ 028
C                                                                          SIMQ 029
C         SUBROUTINES AND FUNCTION SUBPROGRAMS REQUIRED                    SIMQ 030
C            NONE                                                          SIMQ 031
C                                                                          SIMQ 032
C         METHOD                                                           SIMQ 033
C            METHOD OF SOLUTION IS BY ELIMINATION USING LARGEST PIVOTAL    SIMQ 034
C            DIVISOR. EACH STAGE OF ELIMINATION CONSISTS OF INTERCHANGINGSIMQ 035
C            ROWS WHEN NECESSARY TO AVOID DIVISION BY ZERO OR SMALL        SIMQ 036
C            ELEMENTS.                                                     SIMQ 037
C            THE FORWARD SOLUTION TO OBTAIN VARIABLE N IS DONE IN          SIMQ 038
C            N STAGES. THE BACK SOLUTION FOR THE OTHER VARIABLES IS        SIMQ 039
C            CALCULATED BY SUCCESSIVE SUBSTITUTIONS. FINAL SOLUTION        SIMQ 040
C            VALUES ARE DEVELOPED IN VECTOR B, WITH VARIABLE 1 IN B(1),    SIMQ 041
C            VARIABLE 2 IN B(2),.....,  VARIABLE N IN B(N).                SIMQ 042
C            IF NO PIVOT CAN BE FOUND EXCEEDING A TOLERANCE OF 0.0,        SIMQ 043
C            THE MATRIX IS CONSIDERED SINGULAR AND KS IS SET TO 1. THIS    SIMQ 044
C            TOLERANCE CAN BE MODIFIED BY REPLACING THE FIRST STATEMENT.   SIMQ 045
C                                                                          SIMQ A45
C              THIS PROGRAM IS AN ADAPTATION OF THE VERSION IN THE S/360   SIMQ B45
C              SCIENTIFIC SUBROUTINE PACKAGE.  THIS PROGRAM PERMITS THE    SIMQ C45
C              PROGRAMMER TO DIMENSION THE MATRIX A GREATER THAN N BY N-   SIMQ D45
C              A CONDITION IMPOSED BY THE SIMQ IN SSPLIB--HENCE SEVERAL    SIMQ E45
C              VALUES OF N MAY BE USED IN THE CALLING PROGRAM WITHOUT      SIMQ F45
C              CHANGING THE DIMENSIONS OF A.                               SIMQ G45
C                                                                          SIMQ 046
C     ..................................................................SIMQ 047
C                                                                          SIMQ 048
      SUBROUTINE SIMQ(A,B,N,KS,M)
      DIMENSION A(M,M),B(1)
C                                                                          SIMQ 051
C        FORWARD SOLUTION                                                  SIMQ 052
C                                                                          SIMQ 053
      TOL=0.0                                                              SIMQ 054
```

```
      KS=0                                                              SIMQ 055
      DO 65 J=1,N
      JY=J+1                                                            SIMQ 058
      BIGA=0                                                            SIMQ 060
      DO 30 I=J,N
C                                                                       SIMQ 063
C        SEARCH FOR MAXIMUM COEFFICIENT IN COLUMN                       SIMQ 064
C                                                                       SIMQ 065
      IF (ABS(BIGA)-ABS(A(I,J)))20,30,30
20    BIGA=A(I,J)
      IMAX=I
30    CONTINUE
C                                                                       SIMQ 071
C        TEST FOR PIVOT LESS THAN TOLERANCE (SINGULAR MATRIX)           SIMQ 072
C                                                                       SIMQ 073
      IF(ABS(BIGA)-TOL) 35,35,40                                        SIMQ 074
   35 KS=1                                                              SIMQ 075
      RETURN                                                            SIMQ 076
C                                                                       SIMQ 077
C        INTERCHANGE ROWS IF NECESSARY                                  SIMQ 078
C                                                                       SIMQ 079
40    DO 50 K=J,N
      SAVE=A(J,K)
      A(J,K)=A(IMAX,K)
      A(IMAX,K)=SAVE
C                                                                       SIMQ 088
C        DIVIDE EQUATION BY LEADING COEFFICIENT                         SIMQ 089
C                                                                       SIMQ 090
50    A(J,K)=A(J,K)/BIGA
      SAVE=B(IMAX)                                                      SIMQ 092
      B(IMAX)=B(J)                                                      SIMQ 093
      B(J)=SAVE/BIGA                                                    SIMQ 094
C                                                                       SIMQ 095
C        ELIMINATE NEXT VARIABLE                                        SIMQ 096
C                                                                       SIMQ 097
      IF(J-N) 55,70,55                                                  SIMQ 098
55    DO 65 IX=JY,N                                                     SIMQ 100
      IT=J-IX                                                           SIMQ 102
      DO 60 JX=JY,N                                                     SIMQ 103
60    A(IX,JX)=A(IX,JX)-(A(IX,IX+IT)*A(IX+IT,JX))
65    B(IX)=B(IX)-(B(J)*A(IX,IX+IT))
C                                                                       SIMQ 108
C        BACK SOLUTION                                                  SIMQ 109
C                                                                       SIMQ 110
   70 NY=N-1                                                            SIMQ 111
      IT=N*N                                                            SIMQ 112
      DO 80 J=1,NY                                                      SIMQ 113
      IB=N-J                                                            SIMQ 115
      IC=N                                                              SIMQ 116
      DO 80 K=1,J                                                       SIMQ 117
      B(IB)=B(IB)-A(IB,IC)*B(IC)
   80 IC=IC-1                                                           SIMQ 120
      RETURN                                                            SIMQ 121
      END                                                               SIMQ 122
```

B.4 Description of the Computer Program ROD

This program computes the ratio of the total uncollided flux to the total fission source within a fuel rod in an infinite sea of moderator. This ratio, H^{SR}, is:

$$H^{SR} = \frac{\int_0^{R_o} 2\pi \phi_{SR}^{f}(r)\, r\, dr}{\int_0^{R_o} 2\pi\, S(r)\, r\, dr} = \frac{\int_0^{R_o} \left[\phi_{SR}^{A}(r, r, \Sigma_R) + \phi_{SR}^{C}(r, R_o, \Sigma_R\right] r\, dr}{\int_0^{R_o} S(r)\, r\, dr}, \tag{B.2}$$

where ϕ_{SR}^{A} and ϕ_{SR}^{C} are defined by Eqs. 2.44 and 2.50. Output from the program also presents the values of the uncollided flux at various points within the fuel rod.

The various integrals and functions required for the calculation of the uncollided flux are evaluated by the methods described in Appendix C.

B.4.1 Description of the Main Program

The main program does the following steps:

1. The first ten binomial coefficients, A(n,m), are calculated for future use by the formula (A2):

$$A(n,m) = \frac{n!}{m!\,(n-m)!}\,. \tag{B.3}$$

The necessary factorials are calculated by the function subroutine FAC.

2. The following input is supplied to the program:

   a. 26 values of the integral $\int_x^{\infty} K_o(t)\, dt$, taken from the tabulation of reference A2 covering values of x from 0.0 to 0.25. (This is a sufficient range to include all rod sizes involved in the two-region assemblies.)

b. The fuel rod radius, the coefficient b of the parabolic source distribution (Eq. 2.44), and the macroscopic removal cross section for the uncollided flux in the fuel.

3. The C_n functions (Eq. 2.46) at the rod radius are calculated for values of n from 2 to 12. $C_2(\Sigma R_o)$ is found by interpolation in the supplied table. The remaining functions are generated by the equations of Appendix C, using the IBM-360 subroutines (S3) to compute the required Bessel functions.

4. Integration across the rod is performed by eight-point Gaussian numerical integration, using IBM subroutine QG8 (S3). The required products of radius and flux within the fuel rod are supplied by the function subroutine FASPHI, described in the next section.

5. The integral of the parabolic source distribution is evaluated and the program prints the total uncollided flux, the total fission source, and the ratio H^{SR} as output.

B.4.2 Description of the Subroutine FASPHI

For each point within the rod stipulated by the Gaussian integration, FASPHI computes the uncollided flux and supplies the product of the flux and radius to QG8. The steps in the calculation are:

1. $I_{11}(\Sigma r)$ is assumed zero and $I_{10}(\Sigma r)$ is taken to be unity. Lower order Bessel functions are calculated by backward recurrence:

$$I_{n-1}(x) = I_{n+1}(x) + \frac{2n}{n} I_n(x) . \qquad (B.4)$$

The results are normalized to the true values by using the relationship (A2):

$$e^x = I_o(x) + 2I_1(x) + 2I_2(x) + \ldots 2I_{10}(x) + \ldots \qquad (B.5)$$

2. The derivatives of the Bessel functions are found from (A2):

$$I_n^{(k)}(x) = \frac{1}{2k} I_{n-k}(x) + A(k,1)I_{n-k+2}(x) + A(k,2)I_{n-k+4}(x) + \ldots I_{n+k}(x), \qquad (B.6)$$

where $k = 0, 1, 2, \ldots$,

and the A array is composed of the binomial coefficients calculated in the main program.

3. The C_n, S_j, and f_k functions are evaluated by the formulae derived in Appendix C.

4. $\phi^A_{SR}(r, r, \Sigma_R)$ and $\phi^C_{SR}(r, R, \Sigma_R)$ are evaluated by Eq. 2.45 and Eq. 2.51 and their sum, equal to the uncollided flux at the required radius, is printed as output.

5. The flux is multiplied by the radius and the product returned to program QG8.

B.4.3 Input Specification for ROD

The input data specifications are given below in the order required. The names of the variables for each format statement are given, followed by the required FORMAT in parentheses, and then by a brief description of the variable.

1. CC(I), I=1, 26 (6E12.5)

The array CC contains values of the integral $\int_x^\infty K_o(t)\,dt$ with x increasing from 0.0 in increments of 0.01.

2. RO, B, SIGMA (3E12.5)

RO is the radius of the fuel rod in centimeters.

B is the coefficient of the parabolic fission source distribution, Eq. 2.44.

SIGMA is the macroscopic removal cross section of the fuel for uncollided flux.

B.4.4 Fortran Listing of ROD

The Fortran listing of the program ROD is given below.

```
CROD
C CALCULATES TOTAL UNCOLLIDED FLUX IN A SINGLE ROD
      DIMENSION A(11,10),D(12),CC(26),ARG(26),VAL(26)
      COMMON SIGMA,B,RO,A,CC,D,DO
C
C     CALCULATION OF BINOMIAL COEFFICIENTS
      DO 1 N=1,10
      NN=N+1
      DO 1 KK=1,NN
      K=KK-1
    1 A(KK,N)=FAC(N)/(FAC(N-K)*FAC(K))
C
C     INPUT
      READ(5,100) (CC(I),I=1,26)
      READ(5,102) NRUN
      DO 85 IRUN=1,NRUN
      READ(5,100) RO,B,SIGMA
      WRITE(6,101) RO,B,SIGMA
C
C     CALCULATION OF C FUNCTIONS AT ROD RADIUS
      Z=SIGMA*RO
      CALL BESK(Z,0,D(1),IER)
      CALL BESK(Z,1,DO,IER)
      CALL ATSE(Z,0.0,0.005,CC,26,1,ARG,VAL,26)
      CALL ALI(Z,ARG,VAL,D(2),26,1.0E-06,IER)
      D(3)=Z*(DO-D(2))
      DO 2 N=4,12
      XN=N
    2 D(N)=(XN-3.0)*D(N-2)/(XN-2.0)+Z*(D(N-3)-D(N-1))/(XN-2.0)
C
      EXTERNAL FASPHI
      CALL QG8(0.0,RO,FASPHI,Y)
      X=FASPHI(RO)
      WRITE(6,103) Y
      S=RO**2/2.0+B*RO**4/4.0
      WRITE(6,104) S
      R=Y/S
      WRITE(6,105) R
  100 FORMAT(6E12.5)
  101  FORMAT(1H1,' FUEL ROD RADIUS IS',F10.5/'  DISTRIBUTION OF FISSION
     1S IN ROD GIVEN BY 1.0 + ',F10.5,'*R**2'/'  FAST NEUTRON REMOVAL CR
     2OSS-SECTION IS',F10.5)
  102 FORMAT(I5)
  103 FORMAT(1HO,'TOTAL UNCOLLIDED FLUX IN ROD =',E12.5)
  104 FORMAT(1HO,'TOTAL FISSIONS IN ROD =',E12.5)
  105 FORMAT(1HO,'RATIO OF TOTAL UNCOLLIDED FLUX TO FISSIONS =',F10.5)
   85 CONTINUE
      STOP
      END

      FUNCTION  FAC(N)
C     COMPUTES N FACTORIAL
C
      FAC=1.0
      IF(N) 1,2,1
    1 DO 3 I=1,N
```

```
      XI=I
    3 FAC=FAC*XI
    2 RETURN
      END

      FUNCTION FASPHI(X)
      DIMENSION XI(11),A(11,10),C(12),CC(26),ARG(26),VAL(26),V(12),U(12)
     1,S(12),G(12),H(12),F(12),D(12),DI(10)
      COMMON SIGMA,B,R0,A,CC,D,D0
C
C     CALCULATION OF FIRST TEN MODIFIED BESSEL FUNCTIONS OF FIRST
C     KIND BY BACKWARD RECURRANCE
      Z=X*SIGMA
      XI(10)=1.0
      XI(11)=0.0
      DO 1 J=1,9
      K=9-J+1
      XK=K
    1 XI(K)=2.0*XK*XI(K+1)/Z+XI(K+2)
      SUM=XI(1)
      DO 2 J=2,10
    2 SUM=SUM+2.0*XI(J)
      XNORM=EXP(Z)/SUM
      DO 3 J=1,11
    3 XI(J)=XNORM*XI(J)
      WRITE(6,100)  X
      WRITE(6,101) (XI(J),J=1,10)
C
C     CALCULATION OF BESSEL FUNCTION DERIVITIVES
      DO 6 J=1,10
      DI(J)=0.0
      N=J+1
      K=-J-2
      DO 4 L=1,N
      K=K+2
      IF(K)5,7,7
    5 LL=-K+1
      GO TO 4
    7 LL=K+1
    4 DI(J)=DI(J)+A(L,J)*XI(LL)
    6 DI(J)=DI(J)/(2.0**J)
      WRITE(6,103) (DI(J),J=1,10)
C
C     CALCULATION OF C INTEGRALS
      CALL BESK(Z,0,C(1),IER)
      CALL BESK(Z,1,C0,IER)
      CALL ATSE(Z,0.0,0.005,CC,26,1,ARG,VAL,26)
      CALL ALI(Z,ARG,VAL,C(2),26,1.0E-06,IER)
      C(3)=Z*(C0-C(2))
      DO 8 N=4,12
      XN=N
    8 C(N)=(XN-3.0)*C(N-2)/(XN-2.0)+Z*(C(N-3)-C(N-1))/(XN-2.0)
      WRITE(6,102) (C(N),N=1,12)
C
C      CALCULATION OF V INTEGRALS
      V(12)=0.0
      DO 9 J=1,9
```

```
      K=12-J
    9 V(K)=Z*(DI(K-2)-V(K+1))/FLOAT(K)
      V(2)=Z*(XI(1)-V(3))/2.0
      XNORM=XI(2)/V(2)
      DO 10 J=2,10
   10 V(J)=V(J)*XNORM
      WRITE(6,106) (V(I),I=2,10)
C
C     CALCULATION OF U INTEGRALS
      U(12)=0.0
      DO 11 J=1,9
      K=12-J
   11 U(K)=Z*(DI(K-2)-U(K+1))/FLOAT(K+2)
      U(2)=Z*(XI(1)-U(3))/5.0
      XNORM=(XI(2)-2.0*XI(3)/Z)/U(2)
      DO 12 J=2,10
      U(J)=U(J)*XNORM
C
C     CALCULATION OF S INTEGRALS
   12 S(J)=(V(J)*X**(J-1)+B*X**(J+1)*U(J))/SIGMA
      WRITE(6,107) (U(J),J=2,10)
      WRITE(6,108) (S(J),J=2,10)
C
C     CALCULATION OF G FUNCTIONS
      G(1)=(X*C0-R0*D0)/SIGMA
      G(2)=R0*D(2)-X*C(2)-SIGMA*G(1)
      G(3)=C(1)-D(1)-SIGMA*G(2)
      DO 13 J=4,12
   13 G(J)=(C(J)/X**(J-3)-D(J)/R0**(J-3)-SIGMA*G(J-1))/FLOAT(J-3)
      WRITE(6,105) (G(J),J=1,12)
C
C     CALCULATION OF H INTEGRALS
      H(5)=2.0*(C(1)-D(1))/3.0+C(3)-D(3)+(C(5)-D(5))/3.0
      DO 14 I=1,5
      K=6-I
   14 H(K-1)=(C(K)/X**(K-5)-D(K)/R0**(K-5)-H(K)*FLOAT(K-5))/SIGMA
      DO 15 I=6,12
   15  H(I)=(C(I)/X**(I-5)-D(I)/R0**(I-5)-SIGMA*H(I-1))/FLOAT(I-5)
      WRITE(6,109) (H(I),I=1,12)
C
C     CALCULATION OF F INTEGRALS
      DO 16 I=1,12
   16 F(I)=G(I)+B*H(I)
      WRITE(6,110) (F(I),I=1,12)
C
C     CALCULATION OF PHIA
      PHIA=0.0
      DO 17 J=2,10
   17 PHIA=PHIA+C(J)*S(J)/X**(J-1)
C
C     CALCULATION OF PHIC
      PHIC=XI(1)*F(2)
      DO 18 J=3,12
   18 PHIC=PHIC+DI(J-2)*F(J)*X**(J-2)
      FASPHI=PHIA+PHIC
      WRITE(6,111) PHIA,PHIC,FASPHI
      FASPHI=FASPHI*X
```

```
      RETURN
  100 FORMAT(1H0,F10.5,4H CM.)
  101 FORMAT(2H I,8E12.5/5X,4E12.5)
  103 FORMAT(3H DI,8E12.5/5X,2E12.5)
  102  FORMAT(2H C,8E12.5/5X,4E12.5)
  106  FORMAT(2H V,9E12.5)
  107  FORMAT(2H U,9E12.5)
  108  FORMAT(2H S,9E12.5)
  105  FORMAT(2H G,8E12.5/5X,4E12.5)
  109  FORMAT(2H H,8E12.5/5X,4E12.5)
  110  FORMAT(2H F,8E12.5/5X,4E12.5)
  111 FORMAT(1X,'FLUX',3E12.5)
      END
```

Appendix C

EVALUATION OF UNCOLLIDED FLUX INTEGRATED KERNELS

C.1 Introduction

Pilat (P3) has derived the following semi-analytic expressions for the uncollided flux arising from fissions in an infinitely long cylindrical source of radius R_o:

$$\phi^{A}_{SR}(r, R_o, \Sigma) = \frac{1}{r}\left\{ C_2(\Sigma r) S_2(\Sigma, R_o) + \frac{C_3(\Sigma r) S_3(\Sigma, R_o)}{r} + \frac{C_4(\Sigma r) S_4(\Sigma, R_o)}{r^2} + \frac{C_5(\Sigma r) S_5(\Sigma, R_o)}{r^3} + \ldots \right\},$$

$$r \geq R_o , \qquad (C.1)$$

and

$$\phi^{B}_{SR}(r, R_o, \Sigma) = \phi^{A}_{SR}(r, r, \Sigma) + \phi^{C}_{SR}(r, R_o, \Sigma), \quad r \leq R_o , \qquad (C.2)$$

where

$$\phi^{C}_{SR}(r, R_o, \Sigma) = I_o(\Sigma r) f_2(r, R_o) + r I^{(1)}_o(\Sigma r) f_3(r, R_o) + \frac{r^2}{2} I^{(2)}_o(\Sigma r) f_4(r, R_o) + \ldots , \qquad (C.3)$$

$$C_n(z) \equiv \int_1^{\infty} \frac{dt\, e^{-zt}}{t^{n-1}\sqrt{t^2 - 1}} , \qquad (C.4)$$

$$S_j(\Sigma, u) \equiv \int_0^{u} R^{j-1} I^{(j-2)}_o(\Sigma R) S(R)\, dR , \qquad (C.5)$$

$$f_k(r, R_o) \equiv \int_r^{R_o} C_k(\Sigma R)\, S(R) \frac{dR}{R^{k-2}}\,, \tag{C.6}$$

$I_o^{(i)}(x) \equiv i^{th}$ derivative of $I_o(x)$,

and S(R) is the source distribution within the cylinder of radius R_o.

The purpose of this appendix is to present some mathematical properties of these integrals which can be used to facilitate their numerical evaluation.

C.2 The C_n Functions

The C_n functions have been evaluated by Pilat, using an infinite series representation in terms of exponential integrals. Because of the slow convergence of the series, 5000 terms of the series were found to be necessary to produce sufficient accuracy.

A more convenient method is developed here by deriving a recurrence relationship. To do this, the defining relationship, Eq. C.4, is integrated by parts:

$$C_n(z) = \left[\frac{e^{-zt\sqrt{t^2-1}}}{t^n} \right]_1^\infty + z \int_1^\infty \frac{e^{-zt\sqrt{t^2-1}}}{t^n} + n \int_1^\infty \frac{e^{-zt\sqrt{t^2-1}}}{t^{n+1}}\,.$$

The first term vanishes at both limits of integration and rearrangement of the remaining terms gives:

$$C_n(z) = z\left[\int_1^\infty \frac{e^{-zt}}{t^{n-2}\sqrt{t^2-1}} - \int_1^\infty \frac{e^{-zt}}{t^n\sqrt{t^2-1}} \right]$$

$$+ n\left[\int_1^\infty \frac{e^{-zt}}{t^{n-1}\sqrt{t^2-1}} - \int_1^\infty \frac{e^{-zt}}{t^{n+1}\sqrt{t^2-1}} \right].$$

Using the definition of the C_n function, Eq. C.4, and the substitution, $j = n+2$, gives:

$$(j-2)C_j(z) = z[C_{j-3}(z) - C_{j-1}(z)] + (j-3)C_{j-2}(z), \qquad (C.7)$$

which is the required recurrence relationship.

It remains to define the first three C_n functions:

$$C_1(z) = \int_1^\infty \frac{dt\, e^{-zt}}{\sqrt{t^2-1}} = K_o(z), \qquad (C.8)$$

$$C_2(z) = \int_1^\infty \frac{dt\, e^{-zt}}{t\sqrt{t^2-1}} = \int_0^{\pi/2} e^{-z \sec\theta}\, d\theta = \int_z^\infty K_o(t)\, dt, \qquad (C.9)$$

and

$$C_3(z) = \int_1^\infty \frac{dt\, e^{-zt}}{t^2\sqrt{t^2-1}} = \int_1^\infty \frac{e^{-zt}}{(t^2-1)^{-3/2}} - z\int_1^\infty \frac{e^{-zt}}{t(t^2-1)^{1/2}}$$

$$= zK_1(z) - zC_2(z), \qquad (C.10)$$

where $K_o(z)$ and $K_1(z)$ are modified Bessel Functions of the Second Kind which, along with the integral of K_o, are tabulated functions (A1).

Values of the C_n functions, calculated by the above method, are given in Table C.1.

C.3 The S_j Functions

In order to define relationships for these functions, it is necessary to stipulate the source distribution, S(R). Following Woodruff (W3), a parabolic fission source in the rod is assumed.

$$S(r) = 1 + br^2 = 1 + b\frac{z^2}{\Sigma^2}, \qquad (C.11)$$

TABLE C.1

Values of the C_n Functions

x	$C_2(x)$	$C_3(x)$	$C_4(x)$	$C_5(x)$	$C_6(x)$
0.00	1.57080	1.00000	0.78540	0.66667	0.58905
0.02	1.47024	0.96969	0.76570	0.65116	0.57587
0.04	1.39738	0.94100	0.74660	0.63601	0.56300
0.06	1.33496	0.91373	0.72806	0.62129	0.55043
0.08	1.27029	0.88760	0.71004	0.60691	0.53814
0.10	1.22863	0.86252	0.69254	0.59288	0.52615
0.12	1.18194	0.83842	0.67554	0.57920	0.51443
0.14	1.13853	0.81522	0.65900	0.56586	0.50298
0.16	1.09791	0.79286	0.64292	0.55284	0.49179
0.18	1.05972	0.77129	0.62728	0.54014	0.48086
0.20	1.02368	0.75046	0.61206	0.52775	0.47018
0.22	0.98955	0.73033	0.59726	0.51565	0.45975
0.24	0.95714	0.71086	0.58285	0.50385	0.44956
0.26	0.92631	0.69203	0.56882	0.49234	0.43959
0.28	0.89691	0.67380	0.55516	0.48110	0.42986
0.30	0.86883	0.65615	0.54186	0.47013	0.42035
0.32	0.84169	0.64002	0.52861	0.46007	0.41086
0.34	0.81626	0.62246	0.51630	0.44897	0.40197
0.36	0.78889	0.60736	0.50378	0.43912	0.39297
0.38	0.76794	0.59079	0.49204	0.42881	0.38442
0.40	0.74520	0.57566	0.48038	0.41908	0.37594
0.42	0.72334	0.56098	0.46901	0.40959	0.36765
0.44	0.70230	0.54672	0.45793	0.40032	0.35955
0.46	0.68204	0.53288	0.44714	0.39127	0.35164
0.48	0.66252	0.51943	0.43662	0.38291	0.34384
0.50	0.64369	0.50637	0.42636	0.37380	0.33634

where $z = \Sigma r$. The parameter b depends on the character of the fuel rod and has been determined experimentally by Woodruff for the various rods used in the assemblies.

Use of the source distribution given by Eq. C.11 in the definition of the S_j functions, Eq. C.5, yields:

$$S_j(u) = \frac{u^{j-1}}{\Sigma} V_j(u) + \frac{bu^{j+1}}{\Sigma} U_j(u) , \tag{C.12}$$

where:

$$V_j(u) = \frac{1}{(\Sigma u)^{j-1}} \int_0^{\Sigma u} z^{j-1} I_o^{(j-2)}(z)\, dz ,$$

and

$$U_j(u) = \frac{1}{(\Sigma u)^{j+1}} \int_0^{\Sigma u} z^{j+1} I_o^{(j-2)}\, dz .$$

Again, integration by parts gives easily calculated relationships for the new functions:

$$V_j = I_o^{(j-3)}(u) - (j-1)V_{j-1}/\Sigma u , \tag{C.13}$$

and

$$U_j(u) = I_o^{(j-3)}(u) - (j+1)U_{j-1}(u)/\Sigma u . \tag{C.14}$$

Direct integration is used to define the starting functions:

$$V_2(u) = I_1(u) \quad \text{and} \quad U_2(u) = I_1(u) - 2\, I_2(u)/\Sigma u , \tag{C.15}$$

which, together with Eqs. C.13 and C.14, define the set of functions needed to evaluate $S_j(u)$.

C.4 The f_k Functions

The f_k function is treated in the same fashion as the S_j function above. Insertion of the same source distribution, Eq. C.11, into the defining equation, Eq. C.6, generates two auxilliary functions:

$$f_k(r, R_o) = g_k(r, R_o) + b h_k(r, R_o), \tag{C.16}$$

where

$$g_k(r, R_o) = \int_r^{R_o} \frac{C_k(\Sigma r)}{r^{k-2}}\, dr,$$

and

$$h_k(r, R_o) = \int_r^{R_o} \frac{C_k(\Sigma r)}{r^{k-1}}\, dr.$$

Since $C_k'(z) = -C_{k-1}(z)$, integration by parts gives:

$$(k-3) g_k(r, R_o) = \frac{C_n(\Sigma r)}{r^{k-3}} - \frac{C_n(\Sigma R_o)}{R_o^{k-3}} - \Sigma_k g_{n-1}(r, R_o), \tag{C.17}$$

$$(k-5) h_k(r, R_o) = \frac{C_n(\Sigma r)}{r^{k-5}} - \frac{C_n(\Sigma R_o)}{R_o^{k-5}} - \Sigma_k h_{k-1}(r, R_o). \tag{C.18}$$

The initial functions are found by direct integration to be:

$$g_3(r, R_o) = K_o(\Sigma r) - K_o(\Sigma R_o) + C_3(\Sigma r) - C_3(\Sigma R_o), \tag{C.19}$$

$$h_5(r, R_o) = \tfrac{2}{3} K_o(\Sigma r) - \tfrac{2}{3} K_o(\Sigma R_o) + C_3(\Sigma r) - C_3(\Sigma R_o) + \tfrac{1}{3} C_5(\Sigma r) - \tfrac{1}{3} C_5(\Sigma R_o). \tag{C.20}$$

With these functions as starting points, the relationships, Eqs. C.17 and C.18, will generate the other functions needed to evaluate the f_k functions.

Appendix D

CALCULATION OF LATTICE PARAMETERS

D.1 Introduction

Use of either the age theory or diffusion theory analyses presented in Chapter II requires calculation of several parameters which are properties of the lattice composition. This appendix presents the methods used to numerically evaluate these parameters. The values of the parameters, calculated by these methods and used in the two region assembly analyses, are listed in Table 5.2.

D.2 Age to Thermal Energies, τ

The procedure used to calculate the age to thermal energies is given by Galanin (G1). This method accounts for the increase in age over that of a pure moderator due to the moderator displacement by fuel and cladding. The inelastic scattering by uranium, which partially compensates for this increase, is also included.

Ignoring for the moment the inelastic scattering by uranium, the age to thermal energy may be defined as:

$$\tau_o = \int_{E_{th}}^{E_o} \frac{1}{3\xi\Sigma_s\Sigma_{tr}} \frac{dE}{E} , \qquad (D.1)$$

where E_{th} and E_o denote thermal and source energies, respectively, and Σ_{tr} is the transport cross section. The slowing down power, $\xi\Sigma_s$, for a mixture is:

$$\xi\Sigma_s = \sum_i \xi_i \Sigma_{s_i} u_i \,, \tag{D.2}$$

and the transport cross section is:

$$\Sigma_{tr} = \sum_i \Sigma_{tr_i} u_i \,, \tag{D.3}$$

where u_i is the volume fraction of the i^{th} material. Substitution of Eq. D.2 and Eq. D.3 into Eq. D.1 gives:

$$\tau_o = \frac{1}{\sum_j \sum_{k \geq j}} u_j u_k \int_{E_{th}}^{E_o} \frac{1}{3\xi_k \Sigma_{s_k} \Sigma_{tr_j}} \frac{dE}{E} \,, \tag{D.4}$$

or

$$\frac{1}{\tau_o} = \sum_j \sum_{k \geq j} u_j u_k A_{jk} \,, \tag{D.5}$$

where

$$A_{jk} = \frac{1}{\int_{E_{th}}^{E_o} \frac{1}{3\xi_k \Sigma_{s_k} \Sigma_{tr_j}} \frac{dE}{E}} \,. \tag{D.6}$$

The parameters A_{jk} have been determined by Galanin (G1), and a table of their values for materials of interest is given in Ref. A1.

Finally, the formula of Weinberg and Wigner (W6) is used to account for inelastic scattering in the fuel:

$$\tau = \tau_o \left[1 - \left(1 - \frac{\tau_1}{\tau_o} \right) \frac{\sigma_i}{\sigma_e + \sigma_i} P \right] \,, \tag{D.7}$$

where τ_1 is the age of neutrons that have undergone one collision; σ_i and σ_e are the inelastic and elastic scattering cross sections for

virgin neutrons, respectively; and P is the probability that a virgin neutron will undergo its first collision in the fuel. Values for all these parameters are given in Ref. W6.

D.3 Slowing Down Power, $\xi\Sigma_s$

The cell-averaged slowing down power, $\xi\Sigma_s$, is given by (A1):

$$\xi\Sigma_s = \frac{(\xi\Sigma_s)_F V_F + (\xi\Sigma_s)_C V_C + (\xi\Sigma_s)_M V_M}{V_F + V_C + V_M} , \qquad (D.8)$$

where

$$(\xi\Sigma_s)_M = (\xi\Sigma_s)_O + 2y(\xi\Sigma_s)_D + 2(1-y)(\xi\Sigma_s)_H . \qquad (D.9)$$

The subscripts F, C, and M refer to the fuel, clad and moderator, respectively. The subscripts O, D, and H stand for oxygen, deuterium, and hydrogen, respectively, and y is the mole fraction of D_2O in the moderator. The average concentration of D_2O in the moderator was 99.5 mole percent during the course of the experiments. Values of the slowing down power for pure materials were taken from Ref. E1.

D.4 Thermal Neutron Cell Properties, Σ_a, D_{th}, L^2

The parameters for thermal neutrons listed in Table 5.2 were were calculated from the output of the computer code THERMØS (H8, H9). This code has been successfully applied to D_2O-moderated lattices studied at M. I. T. Details of the application to these lattices are given in Ref. S2.

The code solves for the intracellular neutron density distribution in both space and energy, using integral transport theory. The cell,

which is assumed to be in an infinite medium, is divided into concentric regions. These regions are assigned compositions corresponding to the fuel, air-gap, clad and moderator. The source of thermal neutrons is assumed to be a spacially constant, 1/E distribution above 0.78 ev. Scattering is assumed to be isotropic but the scattering kernel is arbitrary. Since it has been shown (S2) that the best results are obtained with the extension of the Nelkin kernel to D_2O made by Honeck (H10), this kernel was used for the present work.

The output of the code of interest for the present application consists of total reaction rates, R_x, and volume-integrated-flux, Φ, for each region of the cell. The definitions of these quantities for the i^{th} region are:

$$R_x^i = \bar{\Sigma}_x^i V_i \bar{\phi}_i = \int_i d\underline{r} \int_0^{v^*} vN(\underline{r}, v)\, \Sigma_x^i(v)\, dv\,, \tag{D.10}$$

$$\Phi_i = V_i \bar{\phi}_i = \int_i d\underline{r} \int_0^{v^*} vN(r, v)\, dv\,. \tag{D.11}$$

In these equations, Σ_x^i represents the cross section for the reaction of interest; V_i is the volume of the i^{th} region; $\bar{\phi}_i$ is the average flux in the region; $N(\underline{r}, v)$ denotes the neutron density as a function of position and neutron velocity; v^* represents the upper limit of the velocity range considered.

In terms of these output quantities, the lattice parameters required for the present analyses become:

$$\Sigma_a = \frac{\sum_i R_a^i}{\sum_i \Phi_i}\,, \tag{D.12}$$

$$D_{th} = \frac{1}{3\bar{\Sigma}_{tr}} = \frac{\sum_i \Phi_i}{3 \sum_i R^i_{tr}}, \tag{D.13}$$

$$L^2 = \frac{1}{3\bar{\Sigma}_a \bar{\Sigma}_{tr}} = \frac{\left(\sum_i \Phi_i\right)^2}{3 \sum_i R_a \sum_i R_{tr}}. \tag{D.14}$$

D.5 Total Resonance Escape Probability, p

The resonance escape probability for the lattices was calculated by the exponential formula (E1):

$$p = \exp\left[- \frac{1}{\frac{V_M \xi_M \Sigma_{sM}}{N_F V_F \, ERI} F + (E-1)} \right], \tag{D.15}$$

where the subscripts F and M refer to the fuel and moderator, respectively, and the functions F and E are given by:

$$F = \frac{\kappa_F R_F}{2} \frac{I_0(\kappa_F R_F)}{I_1(\kappa_F R_F)}, \tag{D.16}$$

and

$$E = \frac{\kappa_M \left(R_M^2 - R_F^2\right)}{2R_F} \left[\frac{I_0(\kappa_M R_F) K_1(\kappa_M R_M) + K_0(\kappa_M R_F) I_1(\kappa_M R_M)}{I_1(\kappa_M R_M) K_1(\kappa_M R_F) - K_1(\kappa_M R_M) I_1(\kappa_M R_F)} \right]. \tag{D.17}$$

R_F is the radius of the fuel rod and R_M is the cylindricalized radius of the fuel cell, equal to 0.52504 b, where b is the triangular pitch of the lattice. Values for κ_F and κ_M were taken from Ref. E1. Effective resonance integrals were calculated by Eq. A.9 and are given in Table A.2.

Appendix E

REFERENCES

A1 Argonne National Laboratory, "Reactor Physics Constants," ANL 5800 (1963).

A2 Abramowitz, M., and I. A. Stegun, editors, Handbook of Mathematical Functions, National Bureau of Standards, USGPO, Washington, D. C. (1964)

B1 Bliss, H. E., "Measurements of the Fast Effect in Heavy Water, Partially Enriched Uranium Lattices," S.M. Thesis, M.I.T. Nucl. Eng. Dept. (1964).

B2 Bliss, H. E., I. Kaplan, and T. J. Thompson, "Use of a Pulsed Neutron Source to Determine Nuclear Parameters of Lattices of Partially Enriched Uranium Rods in Heavy Water," MIT-2344-7, MITNE-73 (1966).

B3 Bacher, P., et R. Naudet, "Mesures de Laplaciens par la Methode du Remplacement Progressif," J. Nucl. Energy, Part A: Reactor Science, 13, 112 (1961).

C1 Clark, L., "Prompt Activation Analysis for Boron and Lithium," S.M. Thesis, M.I.T. Nucl. Eng. Dept. (1963).

C2 Clikeman, F. M., Private communication.

C3 Chernic, J., and R. Vernon, "Some Refinements in the Calculation of Resonance Integrals," Nuclear Sci. Eng., 4, 649 (1958).

C4 Casini, G., and J. Mégier, "Critical Analysis of the Progressive Substitution Method for Material Buckling Measurements," Proceedings of the Symposium on Exponential and Critical Experiments, Amsterdam, September 2-6, 1963, Vol. III, p. 423, IAEA, Vienna (1964).

C5 Cheng, H. S., I. Kaplan, T. J. Thompson, and M. J. Driscoll, "Use of a Moments Method for the Analysis of Flux Distributions in Subcritical Assemblies," MIT-2344-11, MITNE-84 (1968).

E1 Etherington, H., editor, Nuclear Engineering Handbook, McGraw-Hill, New York (1958).

D1 D'Ardenne, W. H., T. J. Thompson, D. D. Lanning, and I. Kaplan, "Studies of Epithermal Neutrons in Uranium, Heavy Water Lattices," MIT-2344-2, MITNE-53 (1964).

G1 Galanin, A. D., Thermal Reactor Theory, Pergamon Press, New York (1960).

G2 Goldstein, R., and E. R. Cohen, "Theory of Resonance Absorption of Neutrons," Nuclear Sci. and Eng., 13, 132 (1962).

G3 Glasstone, S., and M. C. Edlund, The Elements of Nuclear Reactor Theory, D. Van Nostrand Co., Princeton, N. J. (1952).

G4 Graves, W. E., "Analysis of the Substitution Technique for the Determination of D_2O Lattice Bucklings," DP-832 (1963).

H1 Thompson, T. J., I. Kaplan, and A. E. Profio, "Heavy Water Lattice Project Annual Report," NYO-9658 (1961).

H2 Harrington, J., "Measurement of the Material Buckling of a Lattice of Slightly Enriched Uranium Rods in Heavy Water," S.M. Thesis, M.I.T. Nucl. Eng. Dept. (1963).

H3 Higgins, M. J., "Determination of Reactor Lattice Parameters Using Experimentally Measured Kernels," S.M. Thesis, M.I.T. Nucl. Eng. Dept. (1968).

H4 Hellstrand, E., "Measurements of Effective Resonance Integral in Uranium Metal and Oxide in Different Geometries," Jour. Appl. Phys., 28, 1493 (1957).

H5 Thompson, T. J., I. Kaplan, and M. J. Driscoll, "Heavy Water Lattice Project Final Report," MIT-2344-12, MITNE-86 (1967).

H6 Harrington, J., D. D. Lanning, I. Kaplan, and T. J. Thompson, "Use of Neutron Absorbers for Experimental Determination of Lattice Parameters in Subcritical Assemblies," MIT-2344-6, MITNE-69 (1966).

H7 Heath, R. L., "Scintillation Spectrometry, Gamma-Ray Spectrum Catalogue," IDO-16880-2, TID-4500 (1964).

H8 Honeck, H. C., "The Distribution of Thermal Neutrons in Space and Energy in Reactor Lattices. Part I: Theory," Nuclear Sci. Eng., 8, 193 (1960).

Honeck, H. C., and I. Kaplan, "The Distribution of Thermal Neutrons in Space and Energy in Reactor Lattices. Part II: Comparison of Theory and Experiment," Nuclear Sci. and Eng., 8, 203 (1960).

H9 Honeck, H. C., "THERMOS, a Thermalization Transport Theory Code for Reactor Lattice Calculations," BNL-5826 (1961).

H10 Honeck, H. C., "An Incoherent Thermal Scattering Model for Heavy Water," Trans. Am. Nucl. Soc., 5, No. 1, 47 (1962).

K1 Kim, H., "Measurements of the Material Buckling of Lattices of Enriched Uranium Rods in Heavy Water," S.M. Thesis, M.I.T. Nucl. Eng. Dept. (1963).

K2 Kouts, H., and R. Sher, "Experimental Studies of Slightly Enriched Uranium, Water Moderated Lattices, Part I: 0.600-Inch-Diameter Rods," BNL-486 (1957).

L1 Lutz, H. R., T. Auerbach, W. Heer, and R. W. Meier, "Two-Region Heavy Water Natural Uranium Lattice Studies in the Subcritical Assembly MINOR," Proceedings of the Symposium on Exponential and Critical Experiments, Amsterdam, September 2-6, 1963, Vol. II, p. 85, IAEA, Vienna (1964).

N1 Naudet, R., "Critical Examination of Substitution Methods," (Trans., J. L. Crancell), Paper presented to the European-American Committee on Reactor Physics, Idaho Falls, Idaho (1963).

P1 Palmedo, P. F., I. Kaplan, and T. J. Thompson, "Measurements of the Material Buckling of Lattices of Natural Uranium Rods in D_2O," NYO-9660, MITNE-13 (1962).

P2 Papay, L. T., "Fast Neutron Fission Effect for Single Slightly Enriched Uranium Rods in Air and Heavy Water," S.M. Thesis, M.I.T. Nucl. Eng. Dept. (1965).

P3 Pilat, E. E., M. J. Driscoll, I. Kaplan, and T. J. Thompson, "The Use of Experiments on a Single Fuel Element to Determine the Nuclear Parameters of Reactor Lattices," MIT-2344-10, MITNE-81 (1967).

P4 Peak, J. C., I. Kaplan, and T. J. Thompson, "Theory and Use of Small Subcritical Assemblies for the Measurement of Reactor Parameters," NYO-10204, MITNE-16 (1962).

P5 Persson, R., "Perturbation Method of Analysis Applied to Substitution Measurements of Buckling," AE-256 (1966).

S1 Sefchovich, E., I. Kaplan, and T. J. Thompson, "The Measurement of Reactor Parameters in Slightly Enriched Heavy Water Moderated Miniature Lattices," MIT-2344-8, MITNE-76 (1966).

S2 Simms, R. I., I. Kaplan, T. J. Thompson, and D. D. Lanning, "Analytical and Experimental Investigations of the Behavior of Thermal Neutrons in Lattices of Uranium Metal Rods in Heavy Water," NYO-10211, MITNE-33 (1963).

S3 "System/360 Scientific Subroutine Package, (360A-CM-03X), Version II, Programmer's Manual," IBM Corp. (1967).

V1 Vernon, R., "Resonance Integral of U^{238}," Nuclear Sci. Eng., 7, 252 (1960).

V2 Volpe, J. J., G. G. Smith, D. Klein, F. S. Frantz, and J. C. Andrews, "Two Region Studies in Slightly Enriched Water-Moderated Uranium and Uranium Dioxide Lattices," Nuclear Sci. Eng., 5, 360 (1959).

W1 Wolberg, J. R., T. J. Thompson, and I. Kaplan, "A Study of the Fast Fission Effect in Lattices of Uranium Rods in Heavy Water," NYO-9661, MITNE-15 (1962).

W2 Weitzberg, A., I. Kaplan, and T. J. Thompson, "Measurements of Neutron Capture in U-238 in Lattices of Uranium Rods in Heavy Water," NYO-9659, MITNE-11 (1962).

W3 Woodruff, G. L., I. Kaplan, and T. J. Thompson, "A Study of the Spatial Distributions of Fast Neutrons in Lattices of Slightly Enriched Uranium Rods Moderated by Heavy Water," MIT-2344-5, MITNE-67 (1965).

W4 Wigner, E. P., "Resonance Absorption of Neutrons by Spheres," CP-4 (1942).

W5 Wade, J. W., "Neutron Age in Mixtures of D_2O and H_2O," Nuclear Sci. and Eng., 4, 12 (1958).

W6 Weinberg, A. M., and E. P. Wigner, The Physical Theory of Neutron Chain Reactors, University of Chicago Press, Chicago (1958).